Modulation of radiosensitivity of human tumor and normal cells by inhibition of heat shock proteins Hsp90 and Hsp70

Modulation der Strahlenempfindlichkeit humaner maligner und nicht-maligner Zellen mittels Inhibition der Hitzeschockproteine Hsp90 und Hsp70

**Doctoral thesis for a doctoral degree
at Julius-Maximilians-Universität Würzburg**

**submitted by
Natalia Niewidok
from Warsaw, Poland**

Würzburg 2013

Submitted on: …………………………………………………………….......................

Members of the *Promotionskomitee*:

Chairperson: ………………………………………………………….......................…

Primary supervisor: …………………………………………………….......................

Second supervisor: …………………………………………………….......................

Date of public defense: …………………………………………………...................

Date of receipt of certificate: ……………………………………………...................

Contents

Abbreviations

γH2AX	phosphorylated form of histone variant H2AX
14-3-3σ	protein regulated by p53, contributes to G2/M arrest
7-AAD	7-amino-actinomycin D, fluorescent dye
17-AAG	17-N-allylamino -17-demethoxygeldanamycin, Hsp90 inhibitor
17-DMAG	17-dimethylaminoethylamino-17-demethoxygeldanamycin, Hsp90 inhibitor
a. u.	arbitrary units
Aha1	activator of heat shock protein 90
AIF	apoptosis-inducing factor
Akt	also known as protein kinase B (PKB), serine/threonine-specific protein kinase, key regulator of PI3K-Akt-mTOR pathway
ALK	anaplastic lymphoma kinase
Apaf1	apoptotic protease activating factor 1
ATM	ataxia telangiectasia mutated, serine/threonine kinase, activated by DNA damage
ATP	adenosine-5'-triphosphate
ATR	ataxia telangiectasia and Rad-3 related kinase, activated by DNA damage
Bad	Bcl-2 associated death promoter, initiates apoptosis
Bag-1	molecular chaperone regulator 1
Bak	Bcl-2 homologous antagonist/killer, pro-apoptotic protein
Bax	Bcl-2 associated X protein, regulator of apoptosis
Bcl-2	family of proteins regulating apoptosis
Bcl-xL	B-cell lymphoma 2-extra large, pro-survival protein
BIIB021	Hsp90 inhibitor, based on purine scaffold
bp	base pair(s)
BRCA2	breast cancer type 2 susceptibility protein, involved in DNA repair
BrdU	5-bromo-2'-deoxyuridine, synthetic nucleoside, analogue of thymidin
BSA	bovine serum albumine
Cdk(s)	cyclin-dependent kinase(s), proteins regulating cell cycle progression
CDKN2A	cyclin-dependent kinase inhibitor 2A, gene encoding inhibitors of Cdk4
CGM	complete growth medium
Chk1, Chk2	checkpoint kinases, regulators of cell cycle
CKI	cyclin-dependent kinase inhibitor
c-MET	proto-oncogene, Hsp90 client protein
CML	chronic myelogenous leukemia
CYP40	cyclophilin 40, Hsp90 co-chaperone
D_{10}	radiation dose yielding 10% survival
DDR	DNA damage response

Debio-0932	Hsp90 inhibitor, based on purine scaffold
DMSO	dimethyl sulfoxide
DNA	deoxyribonucleic acid
DNA-PK	DNA dependent protein kinase, required for DNA damage repair
DNase	deoxyribonuclease, catalyzes cleavage of DNA
DSB(s)	DNA double strand break(s)
DTT	dithiothreitol
E2F	family of transcription factors, builds complexes with Rb to control the cell cycle progression
ECL	enhanced chemiluminescence
EDTA	ethylenediaminetetraacetic acid
EGFR	epidermal growth factor receptor family
ErbB2/Her-2	human epidermal growth factor receptor 2
ERK/MAPK	extracellular signal-regulated kinase/mitogen-activated protein kinase, protein of Ras-Raf-MEK-ERK pathway
FACS	fluorescence activated cell sorting
FAK	focal adhesion kinase, Hsp90 client protein
FCS	fetal calf serum
FITC	fluorescein isothiocyanate, fluorescent dye
Flt-3	cell surface receptor kinase, Hsp90 client protein
GADD45a	growth arrest and DNA damage inducible protein, regulated by p53
GAPDH	glyceraldehyde 3-phosphate dehydrogenase
Grp94	member of Hsp90 family present in endoplasmic reticulum
Gy	Gray, unit of absorbed dose of energy
h	hour
H_2O_2	hydrogen peroxide
Hip	Hsp70 interacting protein
Hop	Hsp70/Hsp90 organizing protein
HR	homologous recombination
Hsc70	heat shock cognate 70
Hsf1	heat shock factor 1
Hsp(s)	heat shock protein(s)
HSR	heat shock response
hTERT	human telomerase reverse transcriptase
IF_{10}	growth inhibition factor calculated as follows D_{10} of control sample/D_{10} of tested sample
INK4	family of cell cycle inhibitors, including p16 and p19[ARF]
IR	ionizing radiation
kDa	kilodalton, atomic mass unit
KNK437	N-formyl-3,4-methylenedioxy-benzylidene-gamma-butyrolactam, inhibitor of heat shock response
KRAS	Kirsten rat sarcoma viral oncogene homologue, gene encoding k-RAS protein

Ku70, Ku80	proteins required for the non-homologous DNA end joining, together build a heterodimer
MAL3-101	Hsp70 inhibitor
MDM2	murine double minute protein, negative regulator of the p53
MEK	kinase that phosphorylates and activates ERK/MAPK
min	minute(s)
MRE11	meiotic recombination homologue, DNA damage repair protein, member of MRN complex
MRN	protein complex consisting of Mre11, Rad50 and Nbs1; important for DNA double strand break repair
mRNA	messenger ribonucleic acid
mut	mutated form
Myc	family of transcription factors
n.d.	not detected
NBS1	Nijmegen Breakage Syndrome 1 protein, DNA damage repair protein, member of MRN complex
NHEJ	non-homologous end joining
NSCLC	non-small cell lung carcinoma
NVP-AUY922	5-(2,4-dihydroxy-5-isopropyl-phenyl)-N-ethyl-4-[4(morpholinomethyl)phenyl]isoxazole 3-carboxamide, Hsp90 inhibitor
NVP-BEP800	2-amino-4-(2,4-dichloro-5-(2-(pyrrolidin-1-yl)ethoxy)phenyl)-N-ethylthieno[2,3-d]pyrimidine-6-carboxamide, Hsp90 inhibitor
p16	cyclin-dependent kinase inhibitor
$p19^{ARF}$	cell cycle inhibitor, disrupts MDM2-p53 complex
$p21^{Waf1}$	cyclin-dependent kinase inhibitor
p23	Hsp90 co-chaperone
p53	tumor suppressor, regulating cell cycle arrest and cell death
PAGE	polyacrylamide gel electrophoresis
PARP	poly (ADP-ribose) polymerase, involved in DNA repair , cleaved form indicates late apoptosis
PBS	phosphate buffered saline
PCR	polymerase chain reaction
PE	plating efficiency, the number of colonies observed/the number of cells plated
PES	2-phenylethynesulfonamide, Hsp70 inhibitor
PI	propidium iodide, fluorescent dye
PI3K	phosphatidylinositol 3-kinase
PLK	Polo-like kinase, plays role in G2/M arrest
PMSF	phenylmethanesulfonylfluoride
pRb	phosphorylated retinoblastoma protein

PTEN	phosphatase and tensin homologue, negative regulator of PI3K-Akt-mTOR pathway
PUMA	p53 up-regulated modulator of apoptosis, member of Bcl-2 family
RAD50	DNA damage repair protein, member of MRN complex
RAD51	plays major role in DNA homologous recombination
Raf-1	also known as c-RAF, protein kinase in Ras-Raf-MEK-ERK pathway
Ras	family of GTPases, involved in cellular signal transduction
Rb	retinoblastoma protein, tumor suppressor , builds complexes with E2F
RNA	ribonucleic acid
RNase	ribonuclease, catalyzes cleavage of RNA
rpm	revolutions per minute, measure of the frequency of rotation
RT	radiation therapy
RT-PCR	reverse transcriptase polymerase chain reaction
SCLC	small-cell lung carcinoma
SDS	sodium dodecyl sulfate
SF2	surviving fraction at 2 Gy
shRNA	small hairpin RNA
siRNA	small interfering RNA
SMARCA4	gene encoding ATP-dependent helicase Smarca4 (also known as Brg1)
SNX-5422	Hsp90 inhibitor
Src	gene encoding Sarcoma (Src) kinase
SSB(s)	DNA single strand break(s)
STK11	gene encoding serine/threonine kinase Stk11 (also known as Lkb1)
TAE	buffer containing Tris, acetic acid and EDTA
TBS	Tris-buffered saline buffer
TP53	gene encoding p53 protein
TRAP1	member of Hsp90 family, found in mitochondria
Tris	tris(hydroxymethyl)aminomethane
U	unit is defined as the amount of the enzyme that catalyzes the conversion of 1 µmol of substrate per minute
Wee1	nuclear kinase, inhibitor of Cdk1
WT	wild type
VEGFR	vascular endothelial growth factor receptor
VER-155008	Hsp70 inhibitor

1. Introduction

In 2008 approximately 12.7 million cases of cancer were diagnosed and 7.6 million patients died because of this disease worldwide (http: //globocan.iarc.fr. 2010). This makes malignant neoplasm the leading cause of death in economically developed countries and the second leading in developing countries. Global cancer rates have been increasing due to the aging of the population and lifestyle change, for example fatty diets, smoking or physical inactivity (Jemal et al. 2011). Depending on the grade of the cancer, tumor location and general patient condition therapy options include surgery, chemotherapy, radiation therapy (RT) and palliative care.

The development of radiation therapy has been driven by constant technological and medical advances since the discovery of X-rays by Wilhelm Conrad Röntgen in 1895. Ionizing radiation (IR) is currently utilized in ~50% of patients with solid tumors at some stage of their treatment (Bernier et al. 2004). The objective of such therapy is to deliver the optimal radiation dose to kill the tumor cells while sparing the non-tumorigenic tissue. Benefits of radiotherapy are patient cure, organ preservation and cost efficiency. Recent improvements, including intensity-modulated and image-guided RT, have increased the precision of irradiation, but there are still some limitations and side effects that can lead to treatment failure (Bischoff et al. 2009). Therefore, radiation therapy is usually combined with surgery and chemotherapeutics in a personalized strategy against cancer.

1.1 Cellular response to radiation-induced damage

Radiation leads to the disruption of chemical bonds in all basic components of the cell such as membranes, lipids, proteins and, most importantly, DNA (Ward et al. 1981). DNA lesions arise as a consequence of direct and indirect effects of IR. Radiation-induced, charged particles cause direct breaks in the phosphodiester backbone of nucleic acid (van der Schans et al. 1973). Indirect damage is caused by the ionization of water molecules, which leads to the building of hydrated electrons, hydrogen atoms and hydroxyl radicals that interact with DNA (von Sonntag et al. 1987). These direct and indirect interactions result in base and sugar-derived products, single and double strand breaks (SSBs and DSBs) as well as

DNA-protein crosslinks. Moreover, the radiation-induced DNA damage is not uniformly distributed throughout the genome, but the lesions cluster on the DNA within 0-20 bp (Burdak-Rothkamm et al. 2009).

It is commonly known that DNA lesions, and particularly double strand breaks, have the greatest potential for cell killing (Ward et al. 1975). Therefore, counteracting mechanisms evolved to repair these DNA DSBs and to protect the cells from genomic instability. Generally, DNA damage response (DDR) involves DNA repair and cell cycle checkpoint pathways. Failure to repair the damage, or its misrepair, may result in chromosomal rearrangements, including deletions and translocations, and/or lead to cell death (Fig. 1).
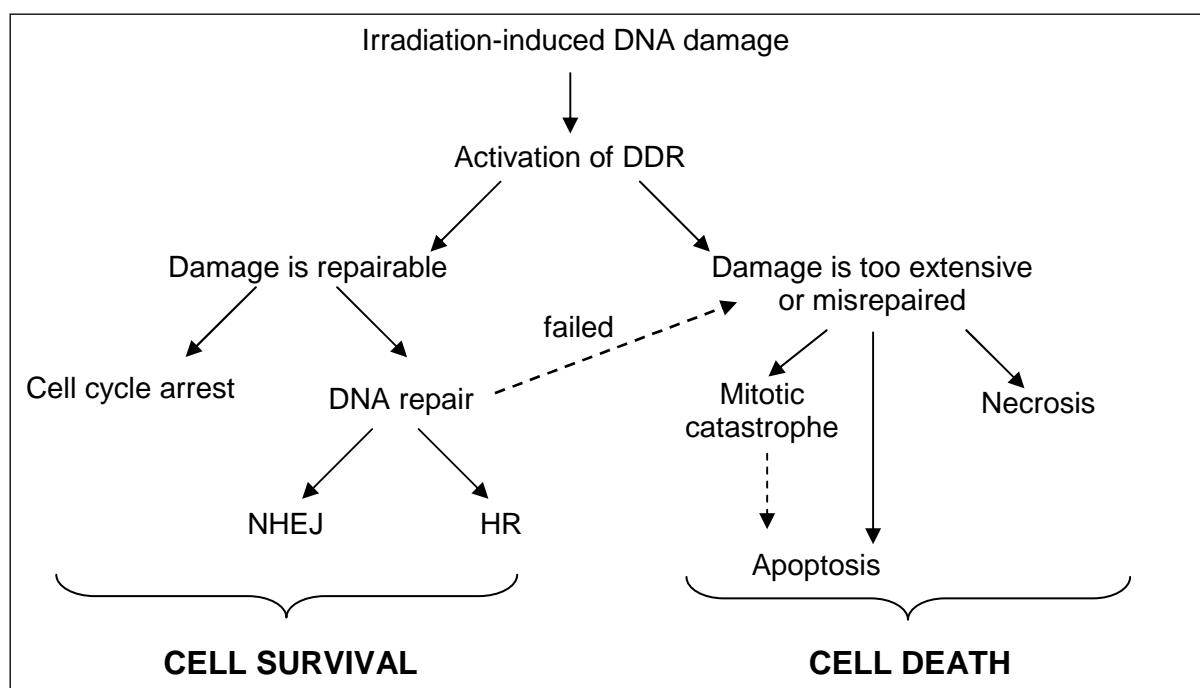
Figure 1. Cellular response to irradiation-induced DNA damage. When DNA lesion occurs, the cell activates DNA damage response (DDR) pathways. Cells can stop the cell cycle progression to enable initiation of DNA repair pathways, leading to the cell survival. For restoration of DNA DSBs there are two possible repair pathways: non-homologous end joining (NHEJ) and homologous recombination (HR). If the damage is too big or cannot be restored, the accumulation of genetic aberrations follows and the cells dies (see details in text).

The appearance of DNA DSB activates a signal transduction process that can initiate, depending on the scale of damage, the repair of the lesion, cell cycle arrest or programmed cell death (Fig. 1). One of the earliest events after DNA double strand break is the phosphorylation of serine 139 of the C-terminal tail of histone H2AX (phosphorylated form known as γH2AX, Rogakou et al. 1998). Next, multiple

proteins of DDR, such as transcription factors, cell-cycle regulation proteins and DSB repair proteins, are recruited to the site of the damage. Among them, the mammalian transducer kinases ATM (ataxia telangiectasia-mutated) and ATR (ataxia telangiectasia and Rad-3 related), together with DNA-PKcs (DNA-dependent protein kinase catalytic subunit), play a central role in damage repair initiation (Van Attikum et al. 2005). ATM and ATR phosphorylate proteins that activate cell cycle checkpoints and DNA repair pathways. Another important factor is the MRN complex, composed of Mre11, Rad50 and Nbs1, that is rapidly localized to nuclear foci at sites of DNA damage in response to radiation (Maser et al. 1997). Further H2AX become phosphorylated and the signal spreads to larger chromatin domains on either side of DSB (Rogakou et al. 1998). Then, depending on the amount of damage and cell cycle phase the lesion can be repaired. Two DNA double strand break repair pathways exist in human cells: non-homologous end joining and homologous recombination (Fig. 2). Non-homologous end joining (NHEJ) is considered to be the major pathway for the restoration of IR-induced DSBs, although it is error prone due to the lack of template strand (Burdak-Rothkamm et al. 2009). The first stage of NHEJ involves binding of the Ku70/Ku80 heterodimer to DSB ends and recruitment of DNA-PKcs. When the DNA-PK complex is assembled, it is responsible for DNA end processing and rejoining. If no further processing of the ends is necessary, DNA ligase IV completes the rejoining reaction. Alternatively, end processing may require the activities of other proteins, for instance the nuclease Artemis (Wyman et al. 2006). NHEJ is predominant in the G0/G1 phase, but it can also occur throughout other phases of the cell cycle.
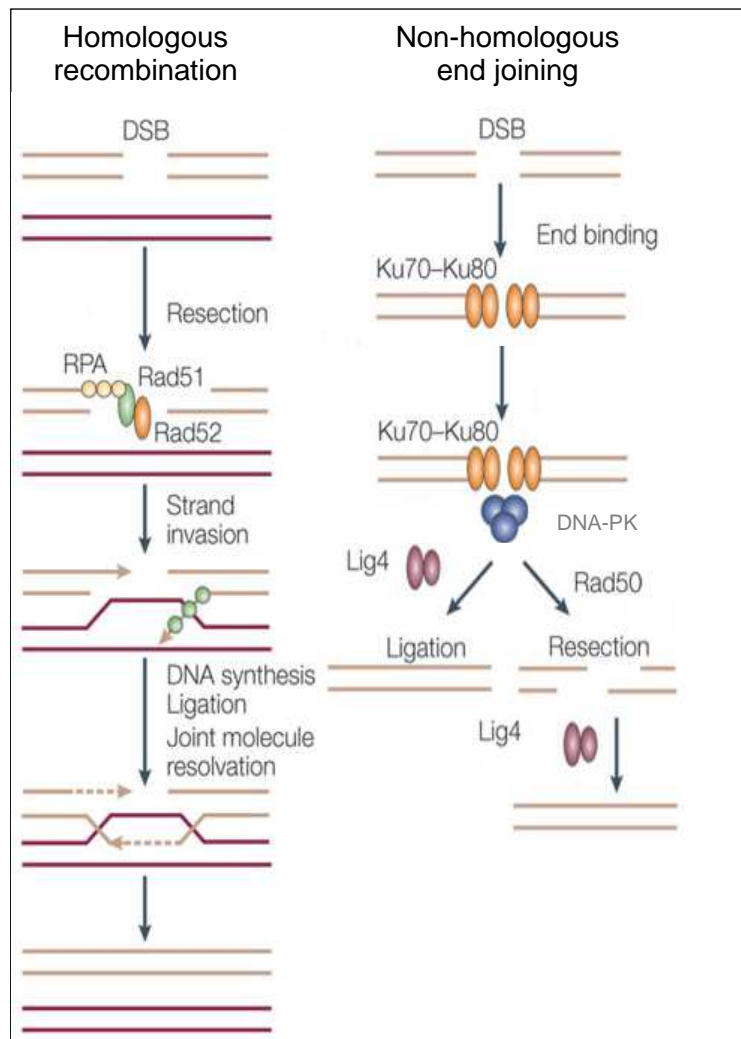
Figure 2. Homologous recombination and non-homologous end joining pathways. HR takes place in the S and G2 phases of the cell cycle and requires a template strand. The resection of the DNA strands is performed by the protein complex containing RAD51 recombinase. Then, the DNA synthesis of the lacking fragment and the rejoining of DNA ends follows. NHEJ can be initiated throughout every cell cycle phase and restores DNA DSBs without the template strand. DNA processing is controlled by Ku70/Ku80, together with DNA-PK. Ligase IV (Lig4) joins the DNA ends (adapted from Van Attikum et al. 2005).

Alternatively, DNA DSBs can be restored by homologous recombination (HR) pathway (Fig. 2). It is active mainly in the S and G2 phases of the cell cycle and allows error-free repair using the information from the undamaged sister chromatid or homologous chromosome. Recent evidence showed that HR can only repair a fraction of DSBs, which localize to heterochromatic DNA regions (Jeggo et al. 2011). After a DSB occurs, sections of DNA around the 5' ends are resected and one of the 3' single-stranded ends can invade an intact template strand. It results in the formation of a hybrid DNA molecule called displacement-loop (D-loop). This reaction

is performed by a nucleoprotein filament composed of the 3' single-stranded DSB-end coated with RAD51 recombinase. Then, DNA polymerase can extend the end of 3' invading strand by synthesizing new DNA and the lesion is restored (Li et al. 2008).

The irradiation-induced DNA damage can activate checkpoint pathways that inhibit the cell cycle progression at G1/S or G2/M checkpoint and induce a transient delay of the S phase. The phase of the cell cycle where the cycle arrests after IR depends on the p53 status; cells with wild type p53 arrest predominantly in the G1 phase, while cells with mutant p53 fail to arrest in G1, but rather accumulate in the S and G2 phases (Eastman et al. 2004). p53 is a tumor suppressor protein that induces the expression of multiple genes including cell cycle inhibitors (i.e. p21^{Waf1}, GADD45a, 14-3-3σ) and apoptosis promoting genes (i.e. PUMA, Bax, Bak). In tumors, the activity of p53 is frequently abrogated or altered by mutations enabling them to proliferate uncontrolled and evade cell death (Reinhardt et al. 2012). The activity of p53 is regulated by interactions with MDM2 protein (Haupt et al. 1997). MDM2 binds to p53 and thereby blocks its ability to regulate target genes and keeps it in unstable form. On the other hand, p53 activates the expression of the *mdm2* gene in an autoregulatory feedback loop (Haupt et al. 1997). In addition, MDM2 acts as ubiquitin ligase, thus targeting p53 for proteasome-mediated degradation.

Checkpoint pathways are coordinated with DNA damage repair and apoptosis, together determining the final cell response to DNA lesion. When DNA damage occurs in the G1 phase, ATM and ATR kinases phosphorylate and activate checkpoint kinases Chk2 and Chk1 respectively (Fig. 3). Chk2 and Chk1 phosphorylate and in this way inhibit the functioning of phosphatase CDC25, preventing the activation of Cdk4-cyclin D and arresting the cell cycle at the G1/S checkpoint (Iliakis et al. 2003). This response is initiated rapidly after DNA damage and is independent from p53 status. Additionally, the activated cell cycle inhibitor p16 can suppress Cdk4- and Cdk6-mediated phosphorylation of Rb, contributing to the G1/S arrest.

Figure 3. Induction of the cell cycle checkpoint pathway after DNA damage in the G1 phase. DNA DSB activates ATR and ATM kinases, which phosphorylate checkpoint kinases Chk1 and Chk2 to initiate p53-dependent and independent pathways that lead to the cell cycle arrest at G1/S transition point (adapted from Iliakis et al. 2003).

The G1/S arrest can also be induced by a p53-dependent mechanism. ATM and ATR kinases phosphorylate the p53 protein and disrupt its interaction with MDM2, which in turn leads to the increase of p53 transcriptional activity. Among the transcribed genes is p21^{Waf1}, which binds to and inactivates Cdk-cyclin complex, which results in pRb hypophosphorylation and sustained cell cycle arrest at the G1/S transition (Stewart et al. 2001, Kastan et al. 2004). MDM2 itself is also a target of ATM and ATR kinases after DNA damage resulting in the disruption of the complex with p53 (Fig. 3).

The G2/M arrest prevents the cells from initiating mitosis when they experience DNA damage during the G2 phase (Fig. 4). The general mechanism of the G2/M checkpoint involves activation of Chk1 and Chk2, which phosphorylate CDC25 to block its functions, which in turns inhibits the Cdk1-cyclin B activity and arrests the cell cycle (Iliakis et al. 2003). CDC25 can be also deactivated by members of Polo-like kinases (PLK) family (Kastan et al. 2004). Apart from down-regulating CDC25,

Chk1 and Chk2 phosphorylate and activate Wee1 kinase that inhibits Cdk1-cyclin B activity. DNA damage can influence the subcellular localization of cyclin B, disabling its translocation from cytoplasm to the nucleus, which is the other possibility of stopping the cell cycle before entering mitosis (Pines et al. 1991, Jin et al. 1998). The maintenance of G2/M checkpoint relies on the activity of proteins transcriptionally regulated by p53 and BRCA1. Their activation leads to the up-regulation of p21^{Waf1}, GADD45a and 14-3-3σ proteins that can inhibit the progression into mitosis (Taylor et al. 2001).
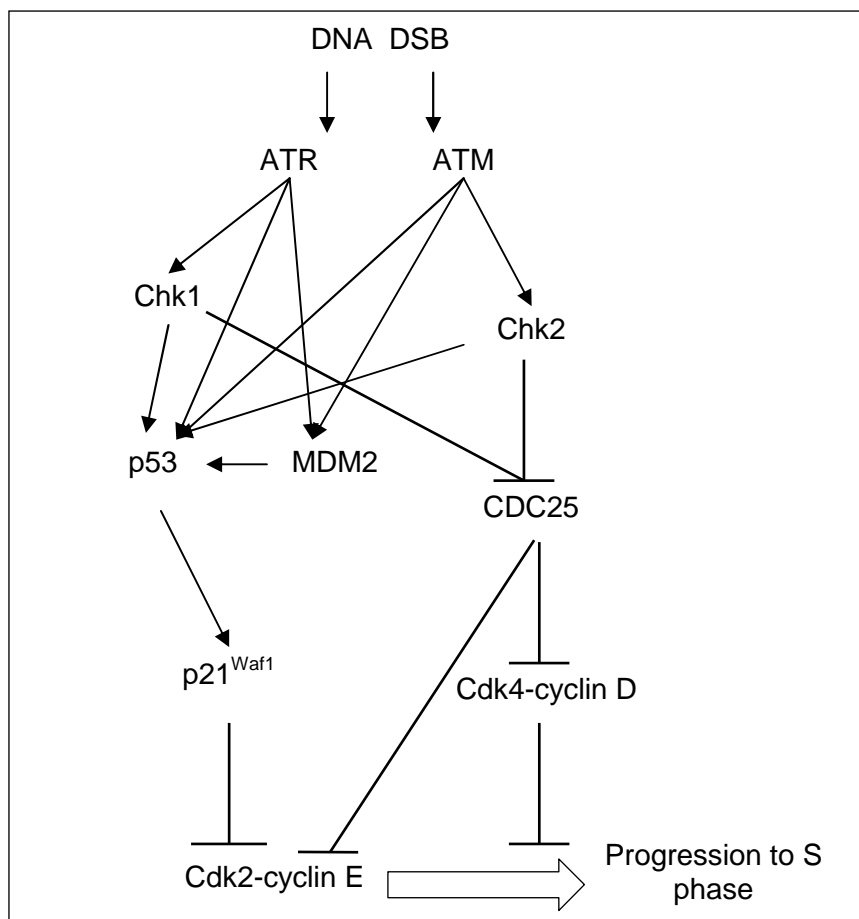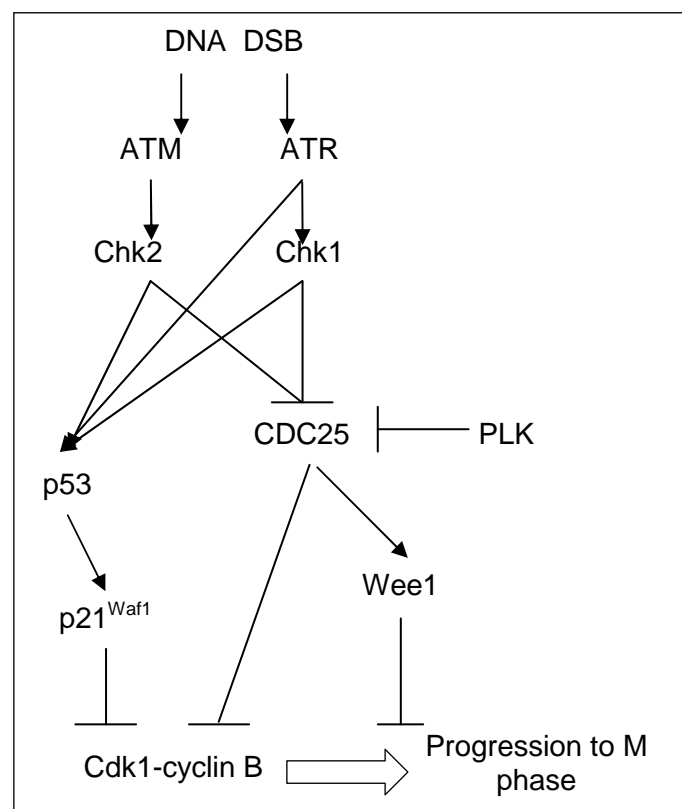

Figure 4. Induction of the cell cycle checkpoint pathway after DNA damage in the G2 phase. DNA DSB activates ATR and ATM kinases that phosphorylate checkpoint kinases Chk1 and Chk2. This initiates p53-dependent and independent pathways that lead to the cell cycle arrest at the G2/M transition point (adapted from Iliakis et al. 2003).

Depending on the extent of DNA damage, the cell can activate pro-survival pathways (DNA repair and cell cycle arrest) or can eliminate damaged cells by cell death programs (Fig. 1). There are several mechanisms leading to cell killing following exposure to irradiation, but it is mainly a result of a mitotic catastrophe or an apoptosis (Eriksson et al. 2010). Mitotic catastrophe occurs when cells proceed through mitosis with unrepaired or misrepaired DNA damage that prevents error-free

replication and separation of the genetic material (Portugal et al. 2010). This is associated with the accumulation of multinucleated, giant cells containing uncondensed chromosomes, chromosome aberrations and micronuclei. It is suggested that mitotic catastrophe is a pre-stage for other cell death pathways like apoptosis and necrosis (Vakifahmetoglu et al. 2008).
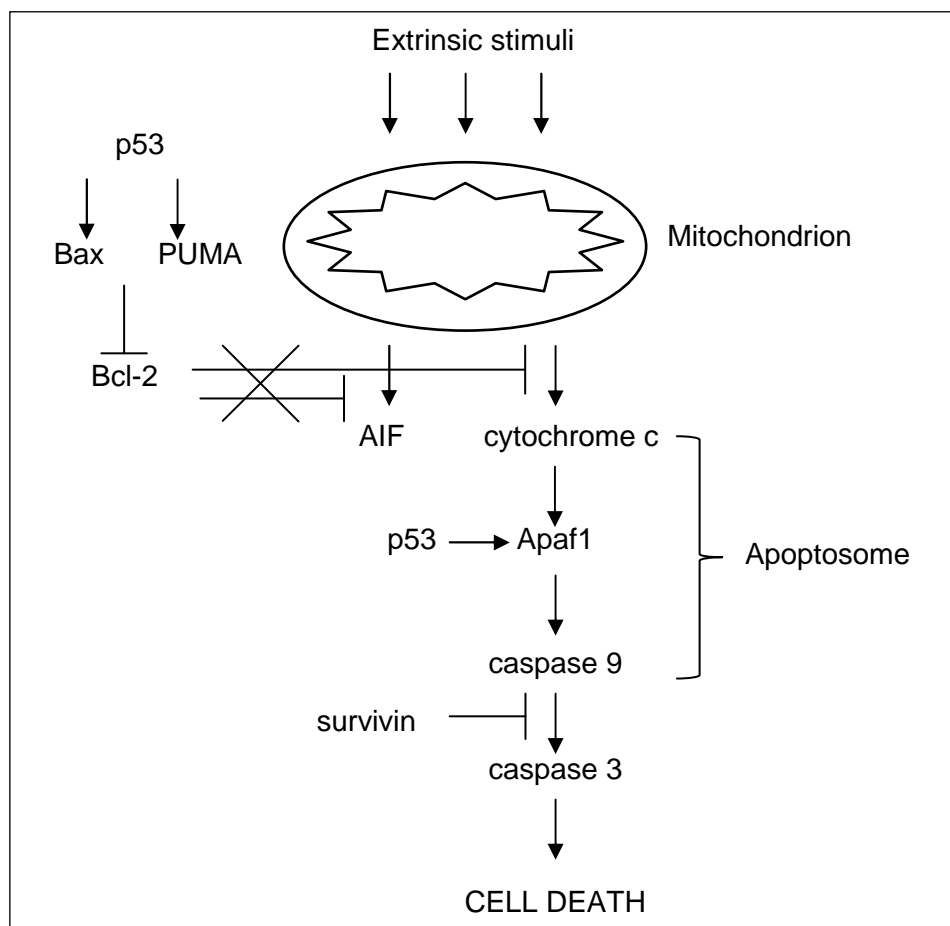
Figure 5. p53-dependent apoptotic pathway. Extrinsic and intrinsic stress factors can lead to the activation of apoptosis. p53 induces the expression of pro-apoptotic proteins (e.g. Apaf1, Bax, PUMA), which promote the release of cytochrome c and AIF from mitochondria. After formation of apoptosome, the caspase cleavage cascade is activated, which leads to the proteolytical degradation of the cellular components and following cell death (adapted from Riedl et al. 2004).

Apoptotic pathway (Fig. 5) can be activated when the cell encounters external (i.e. ligand binding to the cell membrane) or internal (i.e. disruption of mitochondrial functions) stimuli (Helton et al. 2007). Under situation of extreme DNA damage, the cell can initiate p53-dependent apoptosis, which occurs within a few hours after irradiation, without the requirement of cell division. p53 promotes the extrinsic cell death pathway through up-regulation of death receptors (i.e. DR4, DR5). It can also

activate the intrinsic pathway by induction of pro-apoptotic proteins, including Apaf1 (apoptotic protease activating factor 1) or members of the Bcl-2 family (i.e. Bax, PUMA). Through translocation to the mitochondria, p53 initiates apoptosis by provoking the release of several proteins into cytoplasm, for instance cytochrome c or the apoptosis-inducing factor (Mihara et al. 2003, Riedl et al. 2004). When in cytoplasm, cytochrome c binds with Apaf1, ATP and pro-caspase 9 to create a protein complex known as apoptosome (Riedl et al. 2007). Formation of the apoptosome activates the caspase cleavage cascade. Caspase 3 plays a central role in the execution of the apoptotic program through proteolytical degradation of further intracellular proteins (Porter et al. 1999). It is primarily responsible for the cleavage of poly (ADP-ribose) polymerase (PARP), considered as an indicator of late apoptosis (D'Amours et al. 2001). It is possible that large amounts of DNA double strand breaks can also lead to caspase-independent cell death, like necrosis or autophagy (Kroemer et al. 2005).

1.2 Molecularly targeted chemoradiotherapy

A key objective of the radiation therapy is to maximize the radiation dose aiming at tumor cells while minimizing the damage to surrounding organs. Effects of the radiotherapy are limited by the radiosensitivity of targeted tissue that differs from individual to individual. Cellular radiosensitivity is influenced by multiple intrinsic factors, such as the accumulation of genetic mutations in oncogenes and tumor suppressor genes, DNA damage repair proficiency, cell cycle phase and activation of apoptotic programs (Bernier et al. 2004). For example, specific mutations in DNA repair pathways lead to enhanced radiosensitivity as shown for ataxia telangiectasia syndrome, where gene encoding ATM is mutated (Taylor et al. 1975). Additionally, the environmental factors, including oxygen and nutrient supply or elimination of metabolic waste, may influence the response to irradiation (Bernier et al. 2004). Different cancer types respond differently to radiotherapy and are able to acquire mechanisms of resistance during the treatment.

Chemotherapeutics can be used as a supporting treatment together with radiation (so called adjuvant therapy) to improve the overall survival rate and reduce disease-specific symptoms (Seiwert et al. 2007, Bischoff et al. 2009). Multiple proteins

involved in the signal transduction pathways, cell cycle checkpoints or the initiation of cell death have been identified as potential targets for chemoradiotherapy (Ma et al. 2003). Many of these molecules are mutated, abnormally expressed, or have alternative functions in tumor cells, which distinguishes them from non-malignant cells and confirms them as available drug targets. A group of proteins have been identified that regulate the radiation response and are involved in acquiring radioresistance (i.e. ATM, PARP, EGFR, Akt). Targeting radioresistance-associated proteins can lead to the sensitization of tumor cells to IR. For instance, it has been shown that the radiation response of cancer cells might be modulated by targeting of growth factor receptors (i.e. EGFR, VEGFR) due to the improvement of the oxygenation level of tumors and the reduction of their proliferation rate (Bussink et al. 2007). Furthermore, the activation of pro-survival PI3K-Akt pathway has been associated with radioresistance in many cancers including those of the colon, brain, prostate and cervix (Li et al. 2009b). Inhibition of Akt impairs DNA repair after IR and results in the enhancement of the radiation response of several cancer cell lines (Toulany et al. 2008). Mutant activation of the *ras* oncogene and following downstream Raf-MEK-ERK pathway is also involved in acquiring radioresistance by tumor cells (Gupta et al. 2001). Inhibition of individual members of this pathway (i.e. Raf-1 or MEK) leads to radiosensitization of human cancer cell lines (Gupta et al. 2000, Kasid et al. 2003).

These, and many other potential therapeutic single targets, have been discovered in the recent years, but when applied to a clinical setting the effects have been generally weaker than expected and cell type-dependent (Camphausen et al. 2007). Cancer cells are often capable of activating parallel signaling cascades or negative feedback loops to evade the inhibitory effects of the drugs. Therefore, it is of special interest to search for targets that would influence more than one radioresistance-associated protein and to use a so called multi-target approach to radiosensitization (Camphausen et al. 2007). A promising protein that could fulfill this criterion is the heat shock protein 90 (Hsp90).

1.3 Heat shock protein 90 (Hsp90)

Hsp90 belongs to a group of proteins highly conserved in the evolution and whose expression is induced in response to extrinsic or intrinsic stress factors. These proteins function as molecular chaperones, assisting by folding and unfolding of other proteins. Mammalian heat shock proteins (Hsps) are classified in five families according to their molecular weight: Hsp110, Hsp90, Hsp70, Hsp40 and small Hsps with molecular weight 15–30 kDa (Kampinga et al. 2009). Among Hsps are constitutively expressed and stress-induced proteins, which are present in different subcellular compartments. Tumor cells are often characterized by the up-regulation of heat shock proteins. Clinical studies correlate the expression of Hsps with poor prognosis and resistance to therapies (Calderwood et al. 2006).

The rapid induction of Hsps expression in response to stress stimuli is regulated by a series of events known as heat shock response (HSR). HSR is mediated by three heat shock factors, of which Hsf1 is a central player (Powers et al. 2007b). Under normal conditions, Hsf1 is kept in inactive monomeric form through the transient interaction with Hsp90 (Guo et al. 2001). In response to stress, it is activated and dissociates from its complex with Hsp90. Then, Hsf1 undergoes homotrimerization and phosphorylation, and translocates to the nucleus. There, Hsf1 binds to the heat-shock elements that drive the expression of responsive genes, among others of various heat shock proteins (Mahalingam et al. 2009).

The Hsp90 family comprises five members including Hsp90α – major, stress-inducible and Hsp90β – minor, constitutive isoform, which are encoded by two different genes. Additionally, Grp94, which is found in endoplasmic reticulum, and TRAP1 in the mitochondria belong to the Hsp90 family (Csermely et al.1998).

Table 1. Heat shock proteins mentioned in this thesis (adapted from Kampinga et al. 2009).

Family	No. of family members	Protein	Gene name	Human gene ID
Hsp90 (HSPC)	5	Hsp90α	*HSPC1*	3320
		Hsp90β	*HSPC3*	3326
		Grp94	*HSPC4*	7184
		TRAP1	*HSPC5*	10131
Hsp70 (HSPA)	13	Hsp70	*HSPA1A*	3303
		Hsc70	*HSPA8*	3312

Hsp90 is mainly a constitutive homodimer (αα or ββ); however, monomers (α or β), heterodimers (αβ) and oligomers of both isoforms can also exist. There is evidence that Hsp90 isoforms fulfill different functions in cell differentiation and embryonic development in various organisms (Sreedhar et al. 2004).

Hsp90 monomer consists of three functional domains (Fig. 6): i) the N-terminal domain with adenine binding pocket, which is responsible for ATPase activity of Hsp90; ii) the middle domain where co-chaperones (i.e. Hsp70, p23, Aha1) can bind; and iii) the C-terminal domain responsible for the dimerization of the chaperone (Pearl et al. 2006). Further co-chaperones can bind to the C-terminal domain due to the presence of the tetratricopeptide repeat-binding (TRP) motif (Jego et al. 2010).
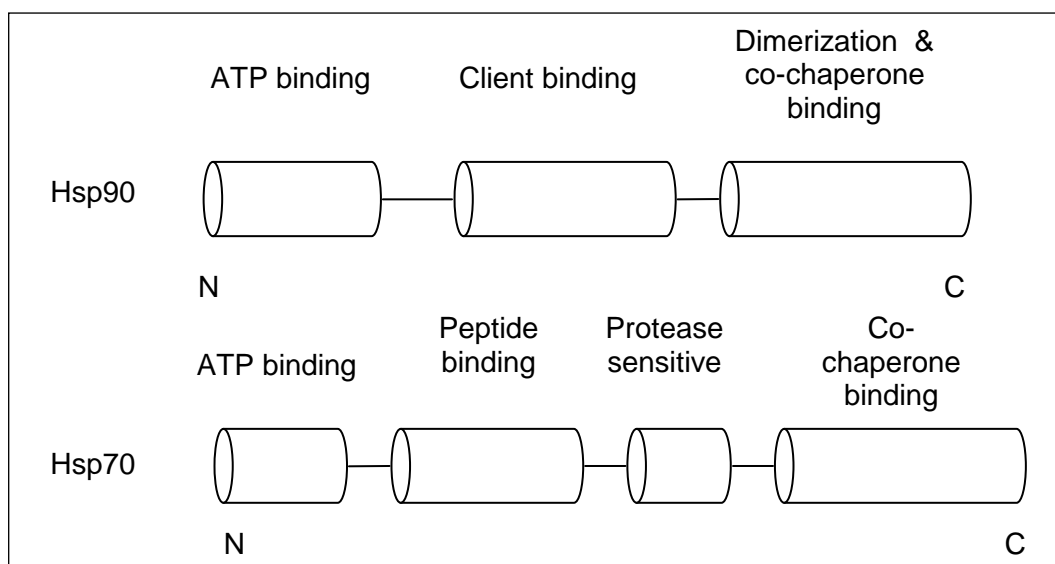
Figure 6. Functional domains of Hsp90 and Hsp70. The Hsp90 monomer consists of the N-terminal domain with ATP binding pocket, the middle domain necessary for client binding and the C-terminal domain responsible for dimerization and co-chaperone binding (adapted from Pearl et al. 2006).
Hsp70 is made up of 4 domains, at the N-terminus the ATPase domain is present, followed by the peptide binding domain and the region with protease sensitive site. The C-terminal domain is the binding site for other Hsps and co-chaperones (adapted from Daugaard et al. 2007).

Heat shock protein 90 is a highly abundant chaperone protein expressed by all eukaryotic cells and often up-regulated in cancer cells (Neckers et al. 2007). Hsp90, together with various co-chaperones, (i.e. Hsp70, Hop, p23) builds a multi-chaperone complex essential for the folding, stabilization and activation of more than 200 proteins, so called Hsp90 clients (Picard et al. 2002, Zhang et al. 2004; for complete list of Hsp90 clients see http://www.picard.ch/Hsp90Int). Different post-translational modifications of Hsp90 (i.e. phosphorylation, acetylation, nitrosylation) regulate the functions of the chaperone complex by modulating the Hsp90 cycle rate and delivering specific substrates (Taipale et al. 2010).

The Hsp90 multi-chaperone complex cycles between two major conformations: the open and the closed state (Fig. 7). The open state allows for the loading of a client protein onto Hsp90, and then the energy from ATP is needed to switch to the closed state conformation, in which N-terminal domains are dimerized and associated with middle domains. When the complex is closed, the conformational maturation and activation of client protein follows. Next, the N-terminal domains dissociate, ADP and client protein are released, whereas Hsp90 returns to the open conformation. If the

client protein cannot be folded, Hsp90 directs them to the ubiquitin-proteasome system for degradation (Li et al. 2011d, Taipale et al. 2010).
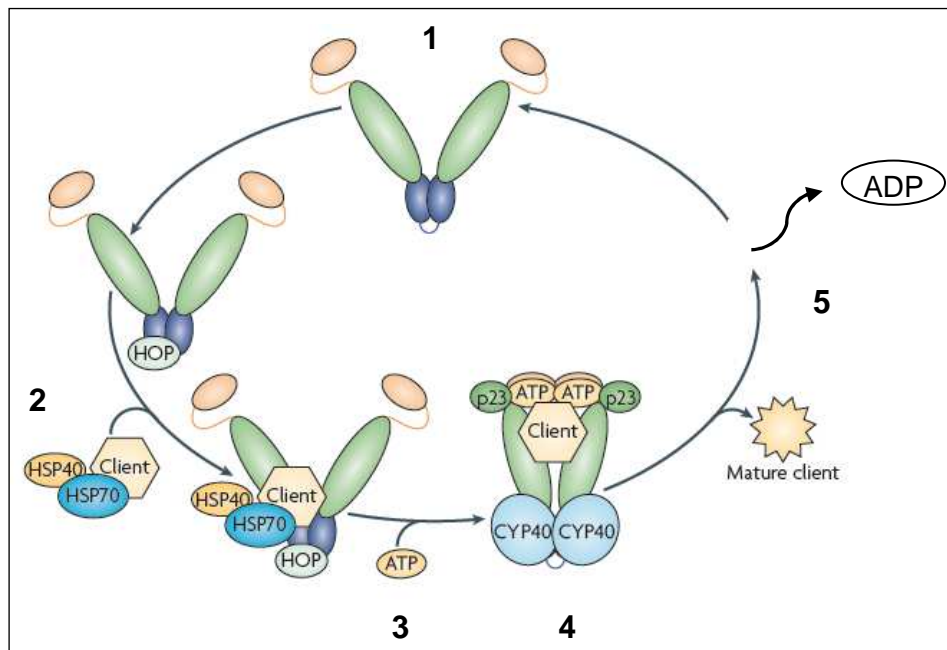
Figure 7. The Hsp90 chaperone cycle. 1) The C-terminal domains (dark blue) are responsible for Hsp90 dimerization. Chaperone is in the open state. 2) Co-chaperones (e.g. Hop, Hsp70 and Hsp40) deliver Hsp90 client, which binds to the middle domain (green) of Hsp90. 3) The energy from ATP is needed for switching to the closed state conformation. ATP binding site is present on the N terminus (orange) of Hsp90 monomer. 4) Further co-chaperones can bind to the chaperone complex (i.e. p23, CYP40). The maturation of the client takes place. 5) Mature client and ADP are released, and Hsp90 returns to the open state (adapted from Taipale et al. 2010).

Apart chaperoning functions, heat shock protein 90 is also involved in the regulation of apoptosis, through the stabilization of several client proteins such as Akt, survivin or death associated protein kinase 1 (Piper et al. 2011). Furthermore, Hsp90 can inhibit the formation of the apoptosome by binding to Apaf1 (Pandey et al. 2000).

Hsp90 clients include members of the steroid receptor family, transcription factors, receptor tyrosine kinases and cell cycle regulators (Zhang et al. 2004). Many of the clients are involved in signal transduction pathways, contributing to the initiation and development of malignancies. Thus, it is suggested that heat shock protein 90 facilitates the so called oncogene addiction of tumor cells and promotes their survival (Luo et al. 2009, Trepel et al. 2010).

It has been reported that, in cancer cells of different origin (i.e. lung carcinoma, melanoma or lymphoma), part of Hsp90 is specifically expressed on the cell surface, where it is responsible for cell motility and invasiveness (Tsutsumi et al. 2007).

1.4 Hsp90 inhibition as a method for sensitizing tumor cells to irradiation

Given the importance of multiple Hsp90 clients in the development and maintaining of carcinogenesis (Fig. 8), this chaperone became an interesting target for cancer treatment.
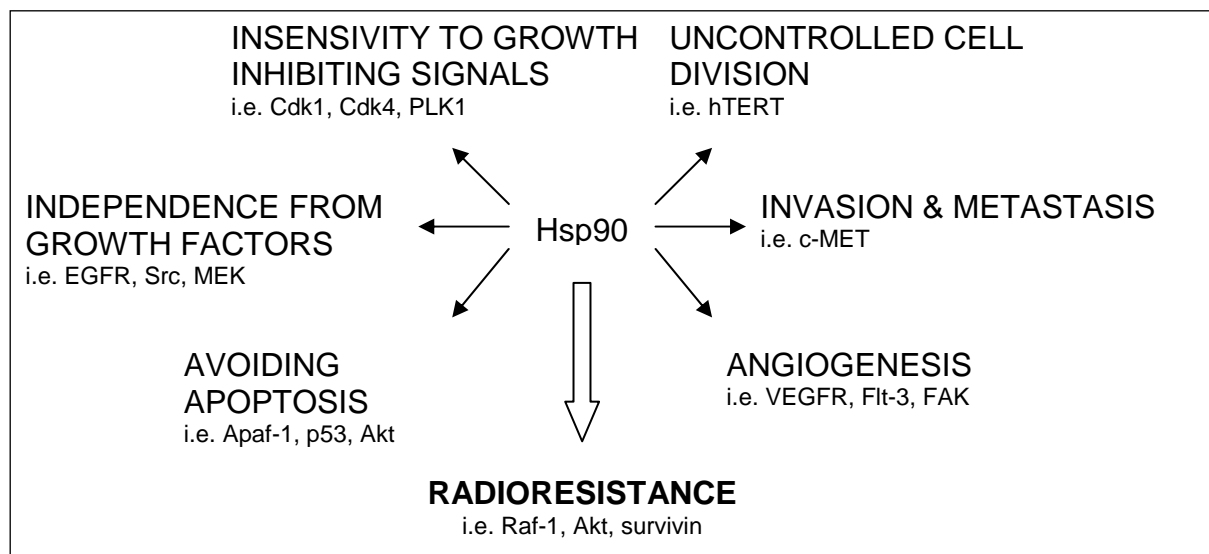
Figure 8. Hsp90 clients (example proteins below every characteristic) contribute to six hallmarks of tumor cells: the uncontrolled growth and cell division; the independence from growth factors, the evasion of apoptosis; the ability to migrate, invade and promote blood vessel growth. Additionally, Hsp90 clients involved in resistance to chemo- and radiotherapy have been identified (adapted from Hanahan et al. 2000, Zhang et al. 2004).
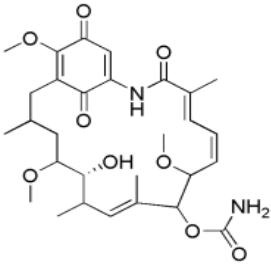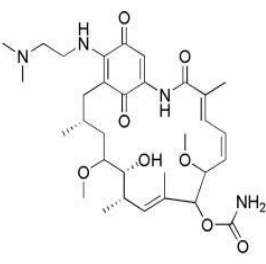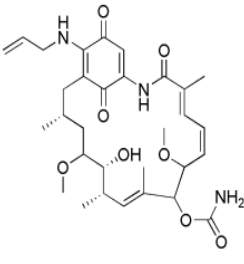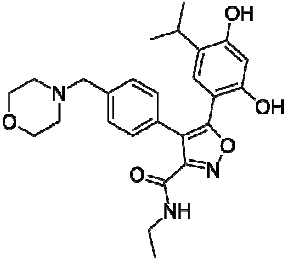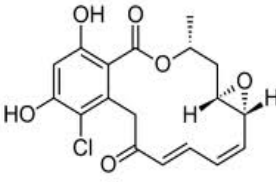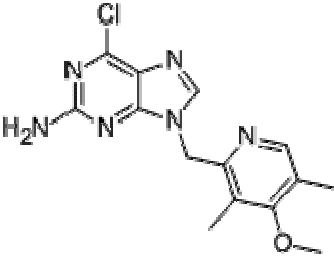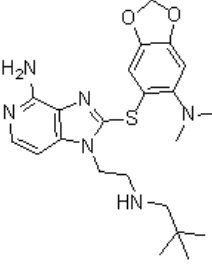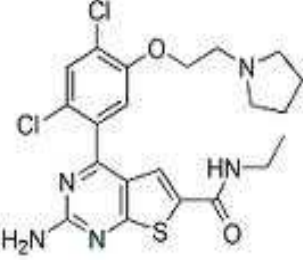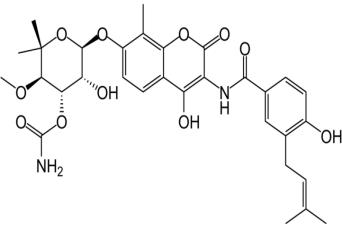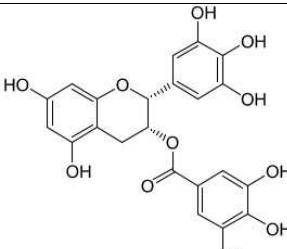
It has been suggested that Hsp90 inhibition would result in the simultaneous disruption or blockade of many oncogenic signal transduction pathways leading to enhanced tumor cell killing. This idea has been intensively investigated since the discovery of the earliest Hsp90 inhibitors geldanamycin and radicicol. Geldanamycin was shown to deplete Hsp90 clients and exhibit anti-tumor effects *in vitro*, but it failed the *in vivo* tests because of the poor solubility and significant hepatotoxicity (Supko et al. 1995). Nevertheless, the studies on geldanamycin and resolving the crystal structure of Hsp90 protein (Stebbins et al. 1997) enabled the development of more efficient and clinically applicable small Hsp90 inhibitors. Drugs targeting Hsp90 can be classified into several groups: i) molecules that inhibit the binding of ATP in the adenine-binding pocket (so called N-terminal inhibitors), ii) C-terminal Hsp90 inhibitors, iii) substances that disrupt the binding of co-chaperones and

iv) modulators of Hsp90 post-translational modifications (Patel et al. 2012). Most research has been concentrated on N-terminal Hsp90 inhibitors (starting from geldanamycin and radicicol), which lock the Hsp90 chaperone complex in the open state, disabling its functions and leading to the degradation of client protein via a ubiquitin-proteasome pathway (Zhang et al. 2004). Among the N-terminal compounds targeting Hsp90 several classes can be distinguished based on their structure, including pyrazole/isoxazole inhibitors (Eccles et al. 2008), benzoquinone ansamycins (Smith et al. 2005) and drugs with purine scaffold (Lundgren et al. 2009; Table 2).

Different Hsp90 clients show different sensitivity to Hsp90 inhibitors. For instance, ErbB2 (also known as Her-2) is one of the most sensitive clients, being degraded within 2 hours after Hsp90 suppression, whereas the down-regulation of Akt only starts 24 hours later (Zhang et al. 2004). It is likely that malignancies dependent on more sensitive Hsp90 clients will better respond to Hsp90 inhibition (Patel et al. 2012). Indeed, to date the best clinical results, as shown by tumor regression, were obtained with 17-DMAG when given in combination with trastuzumab (EGFR inhibitor) to patients with metastatic breast cancer expressing ErbB2 (ErbB2+ breast cancer, Miller et al. 2007). Further potential malignancies that could benefit most from Hsp90 inhibition are small cell lung cancer (SCLC) with activated Akt, melanoma with B-Raf mutations, chronic myelogeonous leukemia (CML) with Bcr-Abl gene fusions or non-small cell lung cancer (NSCLC) with ALK (anaplastic lymphoma kinase) rearrangements (Patel et al. 2012).

Because Hsp90 protects cells from stress factors, it was hypothesized that Hsp90 inhibitors will sensitize tumor cells to the toxic effects of chemotherapeutics and radiotherapy. Many studies *in vitro* and in animal models have confirmed synergistic or additive effects of Hsp90 inhibition in combination with drugs used in chemotherapy, including taxanes, histone deacetylase or proteasome inhibitors (Jhaveri et al. 2012b). At the moment there are 34 open clinical studies testing the clinical activity of the most promising Hsp90 inhibitors alone or in combination with other chemotherapeutics (according to www.clinicaltrials.gov).

Table 2. Chemical structure of chosen Hsp90 inhibitors.

N-terminal Hsp90 inhibitors		
Benzoquinone ansamycins		
Geldanamycin	17-AAG (tanespimycin)	17-DMAG (alvespimycin)
Pyrazole/isoxazole derivatives		
NVP-AUY922	Radicicol	
Purine scaffold		
BIIB021	Debio-0932	
Other		
NVP-BEP800	SNX-5422	
C-terminal Hsp90 inhibitors		
Novobiocin	Epigallocatechin-3-gallate	

Furthermore, many studies have corroborated that drugs targeting Hsp90 are able to increase the radiation response of cancer cells (Enmon et al. 2003, Machida et al. 2003, Russell et al. 2003, Bull et al. 2004, Dote et al. 2005, Noguchi et al. 2006, Shintani et al. 2006, Koll et al. 2008, Schilling et al. 2011). For instance, 17-AAG potentiated both the *in vitro* and *in vivo* radiation response of cervical carcinoma cells (Bisht et al. 2003). The radiosensitization was observed when cells were exposed to IR within 6 to 48 hours after drug treatment. Machida et al. 2003 reported similar findings for combined geldanamycin-IR treatment in lung carcinoma and colon adenocarcinoma cell lines *in vitro*. Most studies with Hsp90 inhibitors have used a schedule whereby drug exposure was followed by irradiation (Bisht et al. 2003, Machida et al. 2003, Bull et al. 2004, Dote et al. 2006, Noguchi et al. 2006, Shintani et al. 2006). Koll et al. 2008 tested several schedules for the combination of 17-DMAG and IR treatment in NSCLC cell lines. Cells were irradiated before, after or simultaneously with 17-DMAG treatment and the sequence of administration was critical for gaining synergistic effects (Koll et al. 2008). In the report from Enmon et al. 2003, human prostate tumor cells in the form of spheroids were incubated for 96 hours with increasing doses of 17-AAG before and after irradiation. The radiation-first schedule was the most effective in delaying spheroid growth (Enmon et al. 2003). It is apparent that the schedule of treatment is crucial in combination studies with Hsp90 inhibitors and IR to obtain the best therapeutic outcome.

The major concern relating to Hsp90 inhibition was the fact that this chaperone is abundantly expressed not only in cancer cells, but also in non-malignant tissues, and therefore Hsp90 targeting could impair their proper functioning. Fortunately, it was shown that Hsp90 inhibitors concentrate in tumor tissue, while being rapidly removed from healthy tissues and blood (Banerji et al. 2005). Other group observed that vascular smooth muscle cells (pericytes) *in vitro* had to be treated with 10-fold higher doses of 17-AAG to achieve similar inhibition of cell proliferation as gastric cancer cells (Lang et al. 2007).

The exact mechanism of Hsp90 inhibitors' selectivity towards malignant cells has not yet been elucidated. It is suggested that cancer cells are more dependent or addicted to Hsp90 chaperoning functions because of stressful environmental conditions and the accumulation of oncoproteins. A report from Kamal et al. 2003 showed that Hsp90 derived from tumor cells has a 100-fold higher binding affinity for 17-AAG than Hsp90 does from normal cells.

Nevertheless, there are some limitations associated with Hsp90 inhibitors that have to be taken into consideration when planning studies with these substances. It has been shown that, in some cases, 17-AAG apart from depleting many Hsp90 clients was able to transiently activate Src kinase in prostate and breast cancer, which led to development of bone metastases (Price et al. 2005).

It is apparent that tumors can exhibit resistance to some Hsp90 inhibitors, both intrinsic and acquired. Geldanamycin derivatives are substrates of the P-glycoprotein (P-gp) efflux pump that contributes to multi-drug resistance and its over-expression is related with resistance to Hsp90 inhibitors (Zhang et al. 2010, Piper et al. 2011). Low activity of NQO1/DT-diaphorase has been linked *in vitro* and *in vivo* to intrinsic resistance to these Hsp90 inhibitors (Kelland et al. 1999). NQO1/DT-diaphorase is an obligate, two-electron reducing, flavin-containing enzyme catalyzing the direct reduction of quinones to hydroquinones. 17-AAG and 17-DMAG are metabolized by this enzyme to their more active hydroquinone forms. A study from Gaspar et al. 2009 described the mechanism of acquired resistance to 17-AAG in four glioblastoma cell lines, which exhibited lower NQO1/DT expression. Apart from being catalyzed by NQO1/DT-diaphorase, the benzoquinone ansamycins can also undergo reduction by other enzymes such as cytochrome P450 reductase (Piper et al. 2011). Resistance to 17-AAG or 17-DMAG of cancer cells can be avoided by using other Hsp90 inhibitors that do not possess quinone moiety, such as NVP-AUY922 or BIIB021.

The activation of the heat shock response is now recognized as one of the most important causes of acquired resistance to all N-terminal Hsp90 inhibitors. The anti-apoptotic properties of Hsp90 itself and of other heat shock proteins (especially heat shock protein 70) counteract the activity of the Hsp90 targeting drugs. One solution is switching to the C-terminal Hsp90 inhibitors that do not induce such strong HSR (Piper et al. 2011). Alternatively it should be possible to overcome the induction of HSR by combining the N-terminal Hsp90 inhibitors with other drugs, i.e. Hsf1 or Hsp70 inhibitors.

1.5 Heat shock protein 70 (Hsp70)

It has been demonstrated that heat shock protein 70 (Hsp70) is a key co-chaperone in the Hsp90 chaperone complex (Hutchison et al. 1994, Taipale et al. 2010). Hsp70 (encoded by the *HSPA1A* gene) belongs to a family of thirteen homologous chaperone proteins (Kampinga et al. 2009; Table 1). Proteins from the Hsp70 family have a similar structure, consisting of i) the conserved ATPase domain, ii) the peptide-binding domain, iii) the middle region with protease sensitive site and iv) the C-terminal region containing the binding site for co-chaperones and other Hsps (Fig. 6). The regulation of Hsp70 activity involves cooperation with co-chaperones such as Hsp40, Bag-1, Hip and Hop (Daugaard et al. 2007).

In response to stress, Hsp70 expression massively increases and the chaperone protects its protein substrates from denaturation or aggregation until the conditions improve. Hsp70 also assists in the folding of newly synthesized proteins, the transport of the proteins and the formation of protein complexes (Evans et al. 2010).

Hsp70 is a protein with strong anti-apoptotic properties; it interferes directly with apoptotic pathway at all major levels and protects cells from cell death (Lanneau et al. 2007, Fig. 9). At the pre-mitochondrial level, Hsp70 binds to c-Jun N-terminal kinase 1 and blocks its functions, disabling the signal initiating apoptosis (Park et al. 2001). At the level of mitochondria, Hsp70 inhibits the translocation of Bax protein, thereby preventing the release of cytochrome c and AIF (Stankiewicz et al. 2005). It has been shown that Hsp70 can bind directly to Apaf1, disabling the building of apoptosome (Beere et al. 2000). Heat shock protein 70 is also able to rescue the cells from later phases of apoptosis, downstream of caspase 3 activation, as well as prevent caspase-independent pathways (Jaattela et al. 1998).
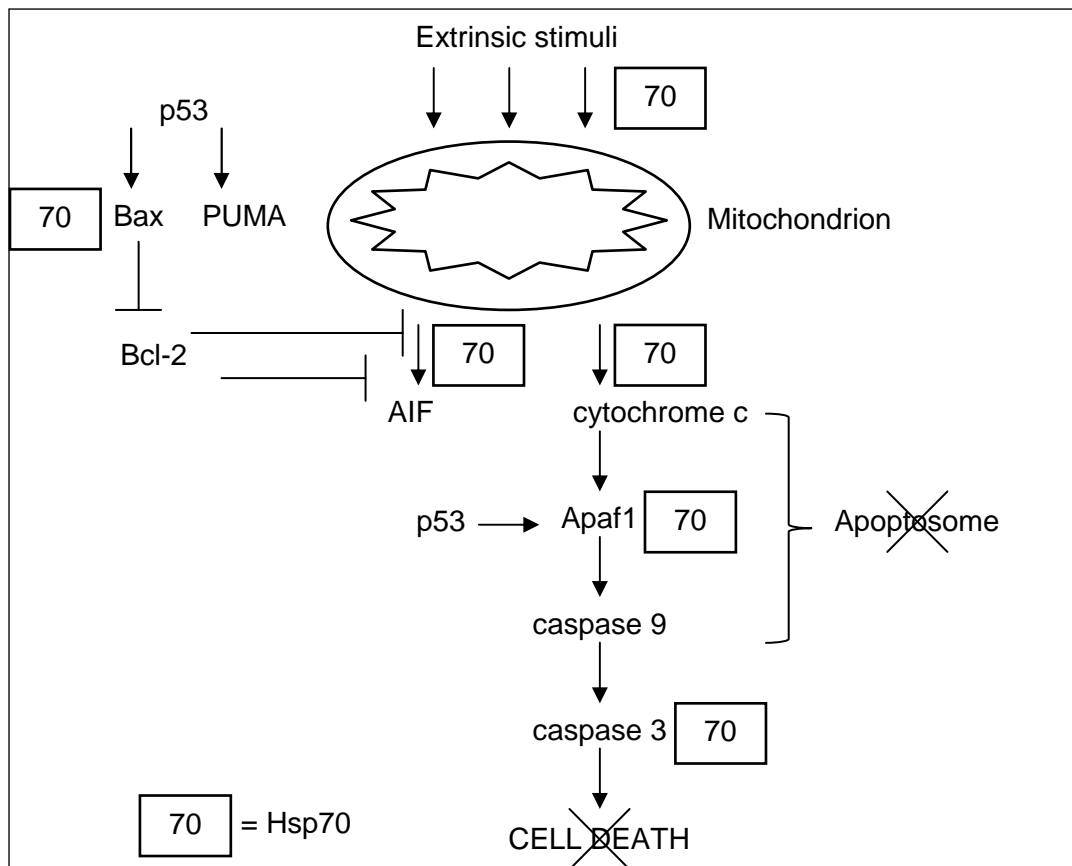
Figure 9. Anti-apoptotic properties of heat shock protein 70. Hsp70 can block the signal initiating apoptosis (i.e. by binding to c-Jun N-terminal kinase 1) at the pre-mitochondrial level. Later, it prevents the release of cytochrome c and AIF from mitochondria. Hsp70 can bind to Apaf1 to inhibit the formation of apoptosome. At later phases, Hsp70 interacts with the caspase cascade, protecting the cell from the proteolytical degradation (adapted from Riedl et al. 2004, Lanneau et al. 2007).

Another important Hsp70 family member is Hsc70 or heat shock cognate 70 protein, which is constitutively expressed (Kampinga et al. 2009). Hsc70 is considered an essential house-keeping protein, indispensable for the cell survival of non-malignant cells. Hsc70 knock-out in mice is lethal (Florin et al. 2004) and RNA interference-based knock-down of the protein results in cell death in various cell types (Rohde et al. 2005). Hsc70 has been reported to be involved in the folding of nascent proteins, protein translocation and chaperone-mediated autophagy (Daugaard et al. 2007).

It was reported that cancer cells from different origin exhibit up-regulated expression of Hsp70 and Hsc70. The expression of heat shock protein 70 in malignant tumors correlates with increased cell proliferation, poor differentiation, lymph node metastases and poor therapeutic outcome (Daugaard et al. 2007). Hsp70 seems to be an essential regulator of tumor cell survival by maintaining the protein homeostasis. Additionally, it was shown that the induction of Hsp70 reduces the

effects of Hsp90 inhibition in the human prostate (Gabai et al. 2005) and leukaemia cell lines (Guo et al. 2005).

1.6 Inhibition of Hsp70 in cancer therapy

The inhibition of Hsp70 proved to be more challenging than Hsp90 targeting, because of the structure of the ATP binding pocket (Massey et al. 2010) and high similarities between members of the Hsp70 family. At the moment there are several small molecule inhibitors that bind to both Hsp70 and Hsc70, including 15-deoxyspergualin, dihydropirymidines (Evans et al. 2010) or VER-155008 (Massey et al. 2010; Table 3). VER-155008 is an adenosine derived compound that binds to ATPase domain of Hsp70 family members and it was shown to induce apoptosis in breast cancer cells and colon cancer cells *in vitro*, but has not been yet tested *in vivo* (Massey et al. 2010).

A recent report from Leu et al. 2009 presented a potentially new drug, a small molecule 2-phenylethynesulfonamide (PES) that specifically interacts with Hsp70, which lead to the aggregation of misfolded proteins and to the destabilization of lysosome membranes. PES selectively killed cells from several types of cancer through caspase-dependent apoptosis (Leu et al. 2009).
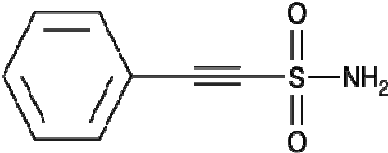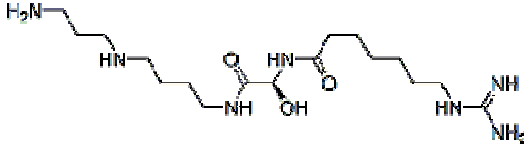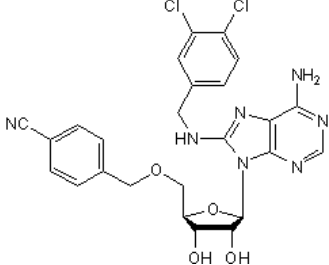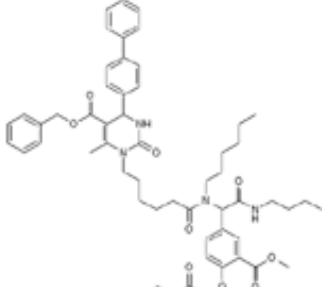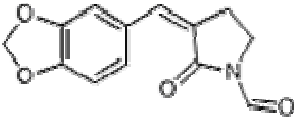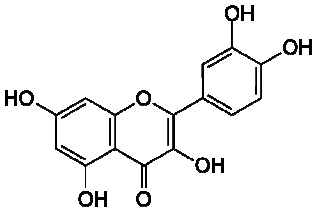
Specific targeting of Hsp70 or Hsc70 can be achieved by RNA interference or antisense oligonucleotides. Peptide aptamers and siRNAs are isoform specific and were shown to induce apoptosis and to increase sensitivity to other chemotherapeutics such as cisplatin (Rerole et al. 2011). Interestingly, it has been demonstrated that simultaneous Hsc70/Hsp70 silencing induced effects mimicking Hsp90 inhibition in cancer cell lines, whereas the same combination of siRNA did not influence the response of non-tumorigenic cells (Powers et al. 2007a).

A different approach for Hsp70 inhibition is targeting its interaction with co-chaperones. For example, MAL3-101 inhibits the ability of Hsp40 co-chaperone to stimulate Hsp70 ATPase activity (Braunstein et al. 2011). Exposure to MAL3-101 inhibited the cell proliferation of multiple myeloma cells *in vitro* and *in vivo*. The cell growth inhibition was associated with cell cycle arrest and initiation of apoptosis (Braunstein et al. 2011).

Another method of indirect Hsp70 inhibition is the use of Hsf1 inhibitors, for instance quercetin or KNK437, which hinder the synthesis of stress-inducible heat shock

proteins including Hsp70, Hsp110, Hsp40 (Yokota et al. 2000). In our group, the inhibitory effects of KNK437 increased the radiation response of lung carcinoma cells (Stingl et al. 2011).

Table 3. Chemical structure of chosen Hsp70 inhibitors.

Hsp70 inhibitors
binding to Hsp70 only

PES

| binding to Hsc70 and Hsp70 |

15-deoxyspergualin

VER-155008

| indirect Hsp70 inhibitors |

MAL3-101
(inhibits interaction between Hsp40 and Hsp70)

KNK437
(inhibits synthesis of stress-inducible Hsps)

quercetin
(HSR inhibitor)

Cancer cells can be distinguished from non-malignant cells because they express Hsp70 on the plasma membrane. This fact was utilized to generate specific monoclonal antibody cmHsp70.1mAb (Stangl et al. 2011). It has been demonstrated that this antibody can induce cytotoxicity in mouse tumor cells *in vitro*. When injected into tumor-bearing mice, cmHsp70.1mAb inhibited tumor growth and enhanced the overall survival rate (Stangl et al. 2011).

The role of Hsp70 inhibition in the radiosensitization of malignant cells has to be elucidated. To our knowledge, there is only one study showing that Hsp70 silencing by siRNA sensitized the endometrial cancer cell line to irradiation (Du et al. 2009).

In the previous chapter, the combination of Hsp90 and Hsp70 inhibitors was mentioned as a possible solution to overcome the induction of heat shock response. Powers et al. 2007a tested the effect of 17-AAG on the proliferation of HCT116 colon and A2780 ovarian carcinoma cell lines transfected with Hsp70 siRNA. In this study Hsp70 knock-down resulted in increased 17-AAG-induced apoptosis (Powers et al. 2007a). Similar results were obtained in myeloma cells which were transfected with specific shRNA targeting Hsp70 and treated with 17-AAG (Davenport et al. 2010), as well as in breast cancer cell lines silenced for Hsp70 and treated with geldanamycin (Havik et al. 2007).

2. Objectives

Heat shock protein 90 is in the focus of research and development efforts due to its interactions with multiple oncogenic pathways (Zhang et al. 2004, Whitesell et al. 2005). It has been demonstrated that Hsp90 inhibitors have anti-tumor activities and proved to be beneficial in cancer treatment (Supko et al. 1995, Smith et al. 2005, Trepel et al. 2010). However, the most commonly used Hsp90 inhibitors, including 17-AAG and 17-DMAG, exhibit some limitations, for instance toxicity, poor solubility or drug-resistance (Solit et al. 2007, Porter et al. 2010). These problems led to synthesis of further Hsp90 inhibitors with improved pharmacokinetic properties. One of them is NVP-AUY922, which was able to reduce tumor growth in a variety of cancer cell lines and human xenograft models (Brough et al. 2008). Exposure to NVP-AUY922 induced the same effects on the protein level, such as Hsp70 over-expression and depletion of Hsp90 clients, as treatment with geldanamycin or its derivatives (Brough et al. 2008, Eccles et al. 2008, Stühmer et al. 2008). Cell fate following NVP-AUY922-treatment differed between cell lines and involved cytostasis or caspase-dependent and –independent cell death (Eccles et al. 2008).

Another promising novel inhibitor is NVP-BEP800, a fully synthetic, orally bioavailable drug that binds to the N-terminal domain of Hsp90 and has exhibited inhibitory effects in a panel of tumor cell lines and xenografts (Brough et al. 2009). NVP-BEP800 showed the greatest selectivity towards Hsp90 versus Grp94 and TRAP1 in comparison with other Hsp90 targeting drugs (Massey et al. 2010). NVP-AUY922 and NVP-BEP800 are the most potent N-terminal Hsp90 inhibitors described thus far (Brough et al. 2008, 2009).

Taking into account the strong anti-tumor activities and optimal pharmacokinetic profile of these two Hsp90 inhibitors, the radiosensitizing potential of NVP-AUY922 and NVP-BEP800 in several cancer cell lines was tested by our group. Tumor cells of different origin pre-treated with either Hsp90 inhibitor for 24 hours were sensitized to the following irradiation (Stingl et al. 2010). In the literature on combination studies with geldanamycin derivatives and irradiation there were some discrepancies regarding the sequence of the treatment (Enmon et al. 2003, Russell et al. 2003, Bull et al. 2004, Dote et al. 2005, Koll et al. 2008). Most studies reported that drug-first treatment increases the radiosensitivity of cancer cell lines (i.e. Bisht et al. 2003,

Machida et al. 2003, Bull et al. 2004). In contrast, others showed that irradiation before Hsp90 inhibition is superior in tumor cell killing (Enmon et al. 2003, Koll et al. 2008). In this work we tested whether a schedule other than drug-first treatment could sensitize cancer cells to irradiation. Lung carcinoma (A549) and glioblastoma (SNB19) cells were treated with NVP-AUY922 or NVP-BEP800 shortly before irradiation and incubated in a drug-containing medium for up to 48 hours post IR (this will be referred as simultaneous drug-IR treatment). We have analyzed the colony-forming ability, radiation-induced DNA damage and repair, cell cycle distribution and expression of Hsp90 and its clients at different time points after drug-IR treatment.

The introduction of novel drugs into clinical studies depends not only on their anti-tumor potential, but also on their impact on non-malignant tissue. It has been demonstrated that NVP-AUY922 and NVP-BEP800 are potent agents for cancer treatment (Brough et al. 2008, 2009), but their effects on non-malignant cells were not evaluated. Therefore, we have investigated the cellular response of two human normal skin fibroblast strains (HFib1 and HFib2) to treatment with NVP-AUY922 or NVP-BEP800 in combination with radiation. As with tumor cell lines (A549 and SNB19) the Hsp90 inhibitor was applied on fibroblasts one hour before IR, and then left in the medium for up to 48 hours post-radiation. Then, at various time points, the colony-forming ability, radiation-induced DNA damage and repair, cell cycle distribution and expression of several marker proteins were examined.

As expected from previous studies with NVP-AUY922 and NVP-BEP800 (Eccles et al. 2008, Stühmer et al. 2009, Stingl et al. 2010), the treatment resulted in the induction of the heat shock response and the up-regulation of heat shock proteins, including Hsp90 and Hsp70. It has been suggested that anti-apoptotic activities of Hsp70 could reduce the therapeutic potential of Hsp90 inhibitors (Gabai et al. 2005, Guo et al. 2005). Therefore, the objective of the third part of this thesis was to prevent the induction of Hsp70 with the help of specific siRNA-mediated knock-down. We have applied siRNAs targeting Hsp70 and its closest relative Hsc70 separately or simultaneously in two cancer cell lines: A549 and SNB19. Pre-silencing was used to reduce the NVP-AUY922-mediated Hsp70 over-expression and to increase the radiosensitizing effect of the drug. The cellular response of transfected, drug-treated and irradiated cells was analyzed by proliferation and colony forming assays. We

examined the expression of heat shock proteins and several marker proteins (Akt, Raf-1, Cdk1, Cdk4, caspase 3). To assess the level of DNA damage and repair kinetics, as well as cell cycle distribution flow cytometrical measurements were performed.

The questions of this thesis can be summarized as follows:

1. How important is drug and irradiation schedule?

    - Can the Hsp90 inhibitors added simultaneously with IR and kept thereafter better radiosensitize tumor cells?

    - Which pathways are involved in the cellular response to the simultaneous drug-IR treatment?

    - If there are any differences between tested cell lines, what are the underlying causes?

2. What are the effects of Hsp90 inhibition in combination with irradiation on non-malignant cells?

    - How do normal human skin fibroblasts respond to NVP-AUY922-IR or NVP-BEP800-IR treatment?

    - What is the response of non-malignant cells to the simultaneous drug-IR treatment in comparison to tumor cells?

3. Is it possible to increase the radiosensitizing potential of NVP-AUY922?

    - Does the knock-down of proteins from Hsp70 family affect the radiation response of tumor cells?

    - Can Hsp70 pre-silencing influence the activity of Hsp90 inhibitor?

3. Materials and methods

3.1 Materials

3.1.1 Antibodies

In Tables 4, 5 and 6 antibodies used in this thesis are listed.

Table 4. Primary antibodies.

Name	Origin	Molecular weight	Supplier
Akt	rabbit polyclonal	60 kDa	Cell Signalling Technology Inc. (Danvers, MA, USA)
pAkt (Ser473)	mouse monoclonal	60 kDa	
Bcl-xL	rabbit polyclonal	30 kDa	
caspase 3	mouse polyclonal	17, 19, 35 kDa	
cleaved caspase 3	rabbit monoclonal	17, 19 kDa	
Cdk1 (=Cdc2)	mouse monoclonal	34 kDa	
Ku80	rabbit polyclonal	86 kDa	
Ku70	rabbit polyclonal	70 kDa	
p24 MAP Kinase	rabbit polyclonal	42 kDa	
PARP	rabbit polyclonal	116, 89 kDa	
cleaved PARP	rabbit monoclonal	89 kDa	
PI3K p110	rabbit polyclonal	110 kDa	
PI3K p85	rabbit polyclonal	85 kDa	
PTEN	rabbit polyclonal	54 kDa	
pRb	rabbit polyclonal	110 kDa	
Cdk4	rabbit polyclonal	33 kDa	Santa Cruz Biotechnology Inc. (Santa Cruz, CA, USA)
Hsc70	rabbit polyclonal	70 kDa	
k-RAS	mouse monoclonal	21 kDa	
MDM2	mouse monoclonal	90 kDa	
p16	mouse polyclonal	16 kDa	
p19^{ARF}	rabbit polyclonal	19 kDa	
Raf-1	rabbit polyclonal	72 kDa	
Hsp90	mouse polyclonal	90 kDa	BD Pharmigen (Heidelberg, Germany)
Hsp70	mouse polyclonal	70 kDa	

Continuation of Table 4 from previous page.

Name	Origin	Molecular weight	Supplier
ß-actin	mouse monoclonal	42 kDa	Sigma-Aldrich (Deisenhofen, Germany)
p21^{Waf1}	mouse monoclonal	21 kDa	Fischer Scientific GmbH (Schwerte, Germany)
p53	mouse polyclonal	53 kDa	Calbiochem (Merck KGA, Darmstadt, Germany)
survivin	rabbit polyclonal	19 kDa	R&D Systems (Minneapolis, USA)

Table 5. Secondary antibodies

Name	Origin	Supplier
anti-mouse	goat polyclonal, HRP-conjugated	DAKO (Hamburg, Germany)
anti-rabbit	goat polyclonal, HRP-conjugated	

Table 6. Antibodies conjugated with fluorescent dye

Name	Origin	Supplier
phospho-H2AX (Ser139), FITC conjugate	mouse	Milipore (Temecula, USA)
phospho-H2AX (Ser139), Alexa Fluor®647 conjugate	mouse	BD Pharmigen (Heidelberg, Germany)

3.1.2 Buffers and reagents

10x PBS
80 g NaCl
2 g KCl
14.4 g Na_2HPO_4
2.4 g KH_2PO_4
set pH at 7.4, fill with H_2O to final volume 1000 ml

Colony survival assay
Fixing solution   methanol : acetic acid (3:1), ice-cold
Crystal violet   0.6% in H_2O

Cell lysates

RIPA buffer	790 mg Tris-base
	900 mg NaCl, set pH at 7.4
	10 ml of 10% NP-40
	2.5 ml of 10% sodium deoxycholate
	1 ml of 100 mM EDTA
	fill with H_2O to final volume of 100 ml
Protease inhibitors	10 µl of 1 mM DTT
(for 1 ml RIPA buffer)	0.5 µl of 1 µg/ml aprotitin
	2 µl of 1 µg/ml leupeptin
	2 µl of 1 µg/ml pepstatin A
Phosphatase inhibitors (for 1 ml RIPA buffer)	2 µl of 500 nM $NaVO_3$
	1 µl of 1 M NaF

Western blot

pre-cast gels	NuPAGE® 4-12% Bis-Tris Gel, NuPAGE® 3-8% Tris acetate Gel	
sample reagents	NuPAGE® 4x LDS Sample buffer, NuPAGE® 10x Sample Reducing Agent, NuPAGE® Antioxidant	Life Technologies GmbH (Darmstadt, Germany)
running buffer	NuPAGE® 20x MOPS SDS Running buffer, NuPAGE® 20x Tris-Acetate SDS Running buffer	
transfer buffer	NuPAGE® Transfer buffer	
protein molecular weight marker	Precision Plus All Blue Protein Ladder	BioRAD (Munich, Germany)

Protein expression analysis

blocking buffer	4% milk powder/BSA, 0.1% Tween in PBS
washing buffer	0.1% Tween in PBS
home made ECL	0.25 g/l luminol sodium salt in 0.1 M Tris-HCl, pH 8.6 (solution A)
	1.1 mg/ml p-coumaric acid in DMSO (solution B)
	Shortly before use mix: 5 ml solution A with 0.5 ml solution B and 5 µl 30% H_2O_2

Flow cytometry

Block 9	0.1 g BSA
	8 ml mouse serum
	1 ml of 10 mg/ml RNase
	1 ml of 1M NaF
	200 µl of 500 nM $NaVO_3$
	0.025 g herring sperm DNA
	100 µl Triton X-100
	2.5 ml of 200 mM EDTA
	2.5 ml of 2% NaN_3
	10 ml 10x PBS
	fill with H_2O to final volume of 100 ml

DNA staining solution   1% saponin in PBS
20 µg/ml PI
50 µg/ml RNase

RT-PCR

agarose	
ethidium bromide	Roth (Karlsruhe, Germany)
6x DNA Loading Dye	
50x TAE	Fischer Scientific GmbH (Schwerte, Germany)
electrophoresis buffer	
Quick load 100 bp DNA Ladder	New England Biolabs (Frankfurt, Germany)

3.1.3 siRNA sequences

Name	Target	Sequence (5'→3')	Source
1	Hsc70	CCG AAC CAC UCC AAG CUA U	Powers et al. 2007a
2	Hsc70	CUG UCC UCA UCA AGC GUA A	
3	Hsp70	GGA CAU CAG CCA GAA CAA G	Wu et al. 2009
4	Hsp70	GCG AGA GGG UGU CAG CCA A	
AllStars Neg. Control	non-silencing	unknown	Qiagen (Hilden, Germany)
Mm/Hs_MAPK1 control siRNA	MAPK1	UGC UGA CUC CAA AGC UCU GTT	

siRNAs 1-4 were purchased by Eurofins MWG Operon (Ebersberg, Germany)

3.1.4 Primers

Target	Forward/reverse	Sequence (5'→3')
Hsc70	forward	GGA GCC AGG CCT ACA CCC CA
Hsc70	reverse	GAC CTT GGG CCT GCC AGC AT
Hsp70	forward	TCA CCA ACG ACA AGG CCG GC
Hsp70	reverse	ACA GCA ATC TTG GAA AGG CCC C
Hsp90α	forward	CAA GAC CAA CCG ATG GAG G
Hsp90α	reverse	ACC AGC CTG CAA AGC TTC C
GAPDH	forward	CAA GGT CAT CCA TGA CAA CTT TG
GAPDH	reverse	GTC CAC CAC CCT GTT GCT GTA G

All oligonucleotides were purchased by Eurofins MWG Operon (Ebersberg, Germany).

3.1.5 Equipment

Name	Supplier
Spectrophotometer SmartSpec™ Plus	BioRAD (Munich, Germany)
trUView™ Cuvette	
High Current Supplier PowerPac™ HC	
C100 Thermocycler	
XCell SureLock™ blot module	Life Technologies GmbH (Darmstadt, Germany)
X-Ray film processor ECOMAX™	Protec Medical Systems (Oberstenfeld, Germany)
Gel documentation system Gel iX Imager	Intas (Göttingen, Germany)
FACSCalibur™	BD Biosciences (Heidelberg, Germany)
FACSCantoII™	

3.1.6. Others

The chemicals were obtained from Roth (Karlsruhe, Germany), Serva (Heidelberg, Germany), BD Pharmigen (Heidelberg, Germany) or Sigma (Deisenhofen, Germany). Plastic and glass materials were purchased from Greiner (Frickenhausen, Germany), Eppendorf (Hamburg, Germany) and Merck (Darmstadt, Germany).

3.2 Methods

3.2.1 Cell lines and cell culture

Tumor cell lines A549 and SNB19 were obtained from the American Type Culture Collection (Manassas, USA). Human skin fibroblast cell lines HFib1 and HFib2 were purchased from Cell Lining GmbH (Berlin, Germany). A summary of characteristics of tumor and normal cell lines is presented in Table 7. Cell culture media and reagents were obtained from PAA Laboratorie GmbH (Pasching, Austria).

Table 7. Short characteristics of used cell lines

Cell line	Cell type	Origin	Characteristics
A549	human lung carcinoma	established from explanted lung tumor from a 58-year-old man	hypotriploid; mutations reported in genes: *CDKN2A*, *KRAS*, *SMARCA4*, *STK11*
SNB19	human astrocytoma	established from the resection of glioblastoma from a 47-year-old man	hypotriploid; mutations reported in genes: *CDKN2A*, *PTEN*, *TP53*
HFib1	human skin fibroblast	established from healthy 41-year-old woman	diploid
HFib2	human skin fibroblast	established from healthy 32-year-old woman	diploid

Mutation status according to Catalogue of Somatic Mutations in Cancer (COSMIC).

Cells were grown at 37°C in a humidified atmosphere of 5% CO_2 in Dulbecco's modified Eagle's medium (DMEM low glucose) supplemented with 10% FCS, 1 mM L-glutamine and antibiotics (100 Units/ml penicillin and 100 µg/ml streptomycin). Cells were routinely split three times a week to keep the cultures in exponential phase.

3.2.2 Drug treatment

Hsp90 inhibitors NVP-AUY922 and NVP-BEP800 were kindly provided by Novartis Institute for Biomedical Research (Basel, Switzerland). Drugs were diluted in DMSO and stored at -20°C. Either Hsp90 inhibitor (200 nM) was added to the complete growth medium one hour before irradiation and left in CGM for up to 48 hours. Control cells were treated in parallel with respective amounts of DMSO as a vehicle control. In the experiment with Hsp70 knock-down, the concentration of Hsp90 inhibitor was reduced to 50 nM.

3.2.3 X-ray irradiation

Irradiation was performed at room temperature using a 6 MV Siemens linear accelerator (Siemens, Concord, USA) at a dose rate of 2 Gy/min. After irradiation, cells were kept in a drug-containing CGM for the indicated time until harvest.

3.2.4 Cell viability assay

Cell viability was determined based on the intracellular ATP level with CellTiter-Glo Luminescent Cell Viability Assay from Promega (Madison, USA) according to the manufacturer's instructions. Cells were treated for 24 and 48 hours with serial dilutions of Hsp90 inhibitors (5 nM - 5 µM) in CGM. The cytotoxicity of each drug was determined in at least three quadruplicate experiments. Control samples contained the respective amount of DMSO. Mean ATP content data (±SE) were normalized against DMSO-treated controls to generate dose response curves and then analyzed with the standard four-parameter logistic model (4PLM):

$$Y = \frac{A_1 - A_2}{1 + (c/\mathrm{IC}_{50})^p} + A_2 \qquad \text{(Eq. 1)},$$

where Y is the cell viability; the abscissa c is drug concentration given in nM; A_1 and A_2 are the upper and lower asymptotes, respectively; IC_{50} is the 50% inhibitory concentration (nM); and p is the Hill slope.

3.2.5 Colony survival assay

Cell survival curves were generated by a standard colony survival assay (Djuzenova et al. 2004). Subconfluent monolayers of control and drug-treated cells were irradiated at room temperature with a single radiation dose within range of 0-10 Gy. Then, the cells were seeded in Petri dishes according to schema (Table 8) and incubated for 10-14 days in normal growth conditions (37°C, 5% CO_2). Four replicates were carried out for each exposure point. After incubation, the cells were fixed and stained with crystal violet. Colonies of at least 50 cells were scored as survivors. Mean survival data (±SE) for each individual cell line were fitted to the linear quadratic (LQ) model:

$$SF = \exp\left(-\alpha X - \beta X^2\right) \qquad \text{(Eq. 2)},$$

where SF is the survival fraction, X is the radiation dose and α and β are the fitted parameters. Calculations and fitting of the curves were done with Origin 8.5 (Micrococal Software Inc, Northampton, USA). For better comparison, the values of plating efficiency (PE), survival fraction at 2 Gy (SF2), radiation dose yielding 10% survival (D_{10}) and growth inhibition factor (IF_{10}) were calculated.

Table 8. Seeding schema for colony survival assay

Dose (Gy)	Amount of seeded cells (pro Petri dish)			
	A549	SNB19	HFib1	HFib2
0	500	1000	500	1000
2	1000	1000	1000	2000
3	1000	2000	1000	2000
5	2000	2000	10000	10000
7	2000	5000	15000	20000
8	5000	5000	20000	20000

3.2.6 Cell lysates

Subconfluent monolayers of non-treated and drug-treated cells were irradiated at room temperature with a single dose (2 or 8 Gy). After that, the samples, together with non-irradiated controls, were cultivated in the drug-containing medium. Thirty minutes, 24 hours and 48 hours post IR, floating cells were collected and the adherent cells were trypsinized according to standard procedures. After washing it with PBS, the pellet was lysed in the RIPA buffer supplemented with protease and phosphatase inhibitors for 30 minutes on ice. After this time the probes were centrifuged (12 min, 12000 rpm, 4°C) and supernatants were collected for storage at -20°C until analysis.

3.2.7 Western blot

Protein concentration in cell lysates was determined by DC Protein Assay Kit from BioRAD (Munich, Germany). Samples equivalent to 5-40 µg of protein were separated using SDS-PAGE and transferred to nitrocellulose membranes according to manufacturer's prescriptions (Life Technologies GmbH, Darmstadt, Germany). For protein detection, the membrane was incubated with the respective primary antibody (Table 4) in the blocking buffer overnight at +4°C. After washing steps, the incubation with the species-specific peroxidase-labeled secondary antibody (Table 5) followed. Home made ECL reaction enabled detection of selected proteins (3.1.2). Levels of protein expression were quantified using the ImageJ (Wane Rasband, NIH, USA) and normalized to the β-actin levels.

3.2.8 Detection of histone γH2AX expression and cell cycle phase distribution by flow cytometry

Non-treated and drug-treated cell cultures were irradiated with a single dose (2 or 8 Gy) at room temperature. Afterwards, cells were incubated in the drug-containing medium under standard conditions and analyzed by flow cytometry 30 minutes, 1 day and 2 days after IR. For analysis, floating cells were collected and the adherent cells were trypsinized. After washing them twice with PBS, the samples were fixed 30 minutes, 24 and 48 hours post IR and stained with anti-γH2AX antibody (Table 6) for DNA double strand breaks (Muslimovic et al. 2008). For the cell cycle analysis the samples were counterstained with propidium iodide (Djuzenova et al. 1994). At least 20,000 cells were assayed for histone γH2AX expression and cell cycle distribution using a flow cytometer FACSCalibur or FACSCantoII (BD Biosciences, Heidelberg). In fibroblast samples, we additionally analyzed the extent of hypodiploid cells and cellular debris (PI in logarithmic scale). HIstograms were analyzed using WinMDI obtained from J. Trotter (Scripps Research Institute, La Jolla, USA) and ModFit LT (Verity Software House, Topsham, USA).

3.2.9 siRNA transfection

Prior to transfection, cells were seeded in 6-well plates (2×10^5 cells/well) or petri dishes (1×10^6 cells/dish) and were incubated overnight under normal growth conditions. HiPerfect Transfection Reagent (Qiagen, Hilden, Germany) was used, as recommended by the manufacturer. Cells were transfected with 100 nM siRNA for transfection with Hsp70 siRNA or Hsc70 siRNA (sequences in 3.1.3).

A549

	Light microscopy	Fluorescent microscopy
24 h		
48 h		

SNB19

	Light microscopy	Fluorescent microscopy
24 h		
48 h		
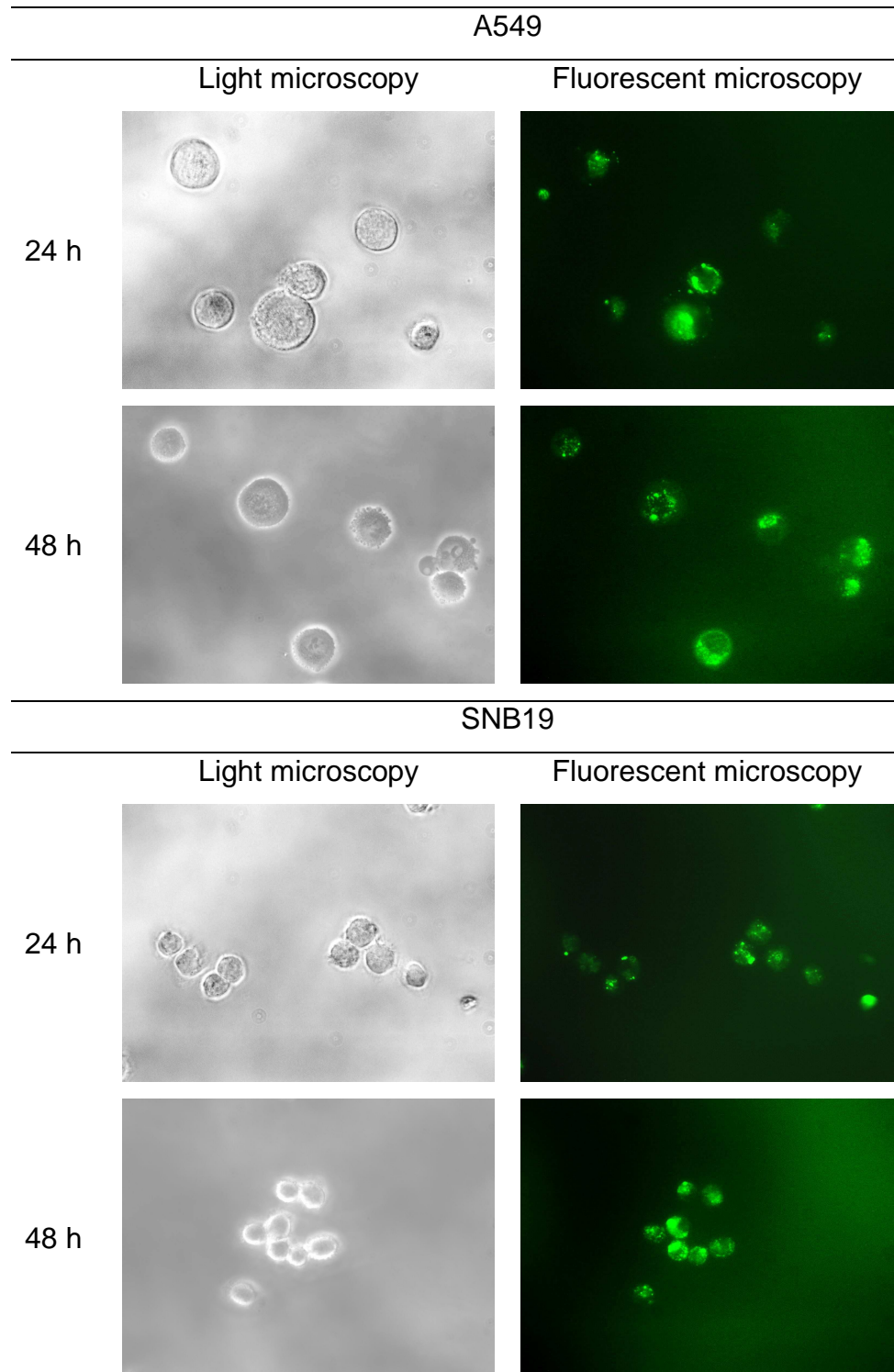
Figure 10 Representative photographs from light (on the left) and fluorescent (on the right) microscopy of tumor cell lines A549 and SNB19 transfected with non-silencing control siRNA coupled with Alexa488. Twenty four and forty eight hours after transfection, cells were trypsinized and analyzed under epifluorescence microscope.

For simultaneous Hsc70/Hsp70 the cells were transfected with 50 nM of each target specific siRNA. 25 nM non-silencing siRNA (Qiagen, Hilden, Germany) served as negative control (referred to henceforth as control siRNA). As a positive control we

used siRNA targeting MAP kinase (Qiagen, Hilden, Germany). To control the transfection efficiency we used negative control siRNA coupled with Alexa488 (Qiagen, Hilden, Germany) and examined the cells (Fig. 10) under Leica DMLB epifluorescence microscope coupled with CCD camera (Olympus Europa GmbH, Hamburg, Germany). As seen in Figure 10, nearly 100% of A549 and SNB19 cells were successful transfected with non-silencing siRNA.

3.2.10 RT-PCR

Cells pre-silenced with specific siRNA and non-transfected controls were trypsinized 24 or 48 hours after transfection. Cell pellets were used for total RNA isolation by SV Total RNA Isolation Kit (Promega, Madison, USA) according to the manufacturer's protocol. This system incorporates the DNase digestion step and yields up to 50 µg RNA that was stored at $-70^{o}C$. Isolated RNA was used to generate cDNA with First Strand cDNA Synthesis Kit (Fischer Scientific GmbH, Schwerte, Germany) using random hexamer primers and M-MuLV Reverse Transcriptase (see Table 9). cDNA coding the housekeeping gene GAPDH was amplified as control. Using specific primers and GoTaq® PCR Core System (Promega, Madison, USA) Hsp70, Hsc70 and Hsp90α genes were amplified (Table 9). The amount of $MgCl_2$ and the number of reaction cycles was optimized for each PCR product. PCR products were analyzed by agarose gel electrophoresis. Levels of mRNA were quantified using ImageJ (Wane Rasband, NIH, USA) and normalized to GAPDH levels.

Table 9. PCR reaction conditions

cDNA synthesis - mastermix		PCR conditions
5x reaction buffer	4 µl	5 min, 25°C
RiboLock^{TM} RNase inhibitor	1 µl	60 min, 37°C
10 mM dNTP mix	2 µl	5 min, 70°C
M-MuLV Reverse transcriptase	2 µl	
total RNA	0.1-5 µg	
random hexamer primer	1 µl	
H$_2$O	to 20 µl	
GoTaq® PCR - mastermix		PCR conditions
25 mM MgCl$_2$	2-8 µl	2 min, 95°C (1 cycle)
5x Green GoTaq® Flexi Buffer	10 µl	30 s, 95°C
10 mM PCR Nucleotide Mix	1 µl	15 s, 58°C (25-35 cycles)
forward primer	5-50 pmol	30 s, 72°C
reverse primer	5-50 pmol	5 min, 72°C (1 cycle)
5 U/µl GoTaq® DNA polymerase	0.25 µl	
cDNA	0.5-1 µg	
H$_2$O	to 50 µl	

3.2.11 Cell growth after transfection

Cells were seeded in 12-well plates (1x10^{5} cells/well) and transfected with non-silencing siRNA, Hsp70 siRNA, Hsc70 siRNA, or both siRNAs simultaneously. Samples that were non-transfected or incubated with only HiPerfect Transfection Reagent (Qiagen, Hilden, Germany) served as controls. Control and transfected cells were trypsinized 24, 48, 72 and 96 hours after transfection. Cell numbers were determined by counting in haemocytometer every day up to 96 hours after transfection.

3.2.12 BrdU incorporation assay

Twenty four hours after irradiation control, transfected and drug-treated cell samples were incubated with 5-bromo-2'-deoxyuridine (BrdU) for one hour and stored at -80°C until staining. Thawed cells were stained according to BrdU Flow Kit Staining Protocol (BD Pharmigen, Heidelberg, Germany) with FITC-conjugated anti-BrdU antibody and analyzed for the DNA synthesis frequency using FACSCalibur flow cytometer (BD Biosciences, Heidelberg, Germany). Together with BrdU-FITC staining, we stained the DNA with 7-AAD dye to enable the analysis of cell cycle progression. Output data presented as dot blots were analyzed using WinMDI

obtained from J. Trotter (Scripps Research Institute, La Jolla, USA) and ModFit LT (Verity Software House, Topsham, USA).

3.2.13 Statistics
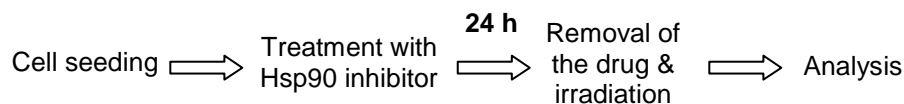
Data are presented as means (±SD or ±SE). Mean values were compared by the Student's *t*-test. The threshold of statistical significance was set at $p < 0.05$. Statistics and fitting of experimental curves were performed with Origin 8.5 (Micrococal Software Inc., Northampton, USA).

4. Results

4.1 Effects of NVP-AUY922 and NVP-BEP800 on radiation response of lung carcinoma A549 and glioblastoma SNB19 cell lines

Previous studies with various Hsp90 inhibitors (e.g. geldanamycin, 17-DMAG) showed that Hsp90 inhibition can sensitize cancer cells to irradiation (Russell et al. 2003, Koll et al. 2004, Bull et al. 2008). Recent findings in our group demonstrated that the Hsp90 inhibitors NVP-AUY922 and NVP-BEP800 added 24 hours before irradiation can radiosensitize tumor cell lines under normoxic (Stingl et al. 2010) as well as under hypoxic conditions (Djuzenova et al. 2012).

A) drug-first treatment (Stingl et al. 2010)

24 h

Cell seeding ⟹ Treatment with Hsp90 inhibitor ⟹ Removal of the drug & irradiation ⟹ Analysis

B) simultaneous drug-IR treatment (Niewidok et al. 2012)

1 h

Cell seeding ⟹ Treatment with Hsp90 inhibitor ⟹ Irradiation ⟹ Incubation in drug-containing medium & analysis
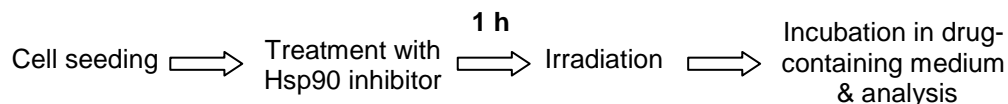
Figure 11. Comparison of treatment schedules used in the combination studies with Hsp90 inhibitors NVP-AUY922 and NVP-BEP800 and irradiation, (A) drug-first treatment and (B) simultaneous drug-IR treatment.

In the first experimental part of the thesis we investigated the importance of the sequence of Hsp90 inhibition and irradiation on the radiosensitivity of A549 and SNB19 tumor cell lines. In contrast to the drug-first treatment used in report from Sting et al. 2010 (Fig. 11A), here we added the Hsp90 inhibitors shortly before IR and kept up to 48 hours thereafter (Fig. 11B).

4.1.1 Cytotoxicity of Hsp90 inhibitors to tumor cells

First, we determined the cytotoxic potential of NVP-AUY922 and NVP-BEP800. To this end, cell lines A549 and SNB19 were treated with either Hsp90 inhibitor over a concentration range from 10 nM to 5 μM and incubated in the drug-containing medium for 24 and 48 hours. Then, the cell viability was assessed with ATP-based assay as described in the section 3.2.4. Cellular ATP levels were normalized against DMSO-treated controls, plotted versus drug concentration and fitted to the 4PLM model (Fig. 12).

A) A549
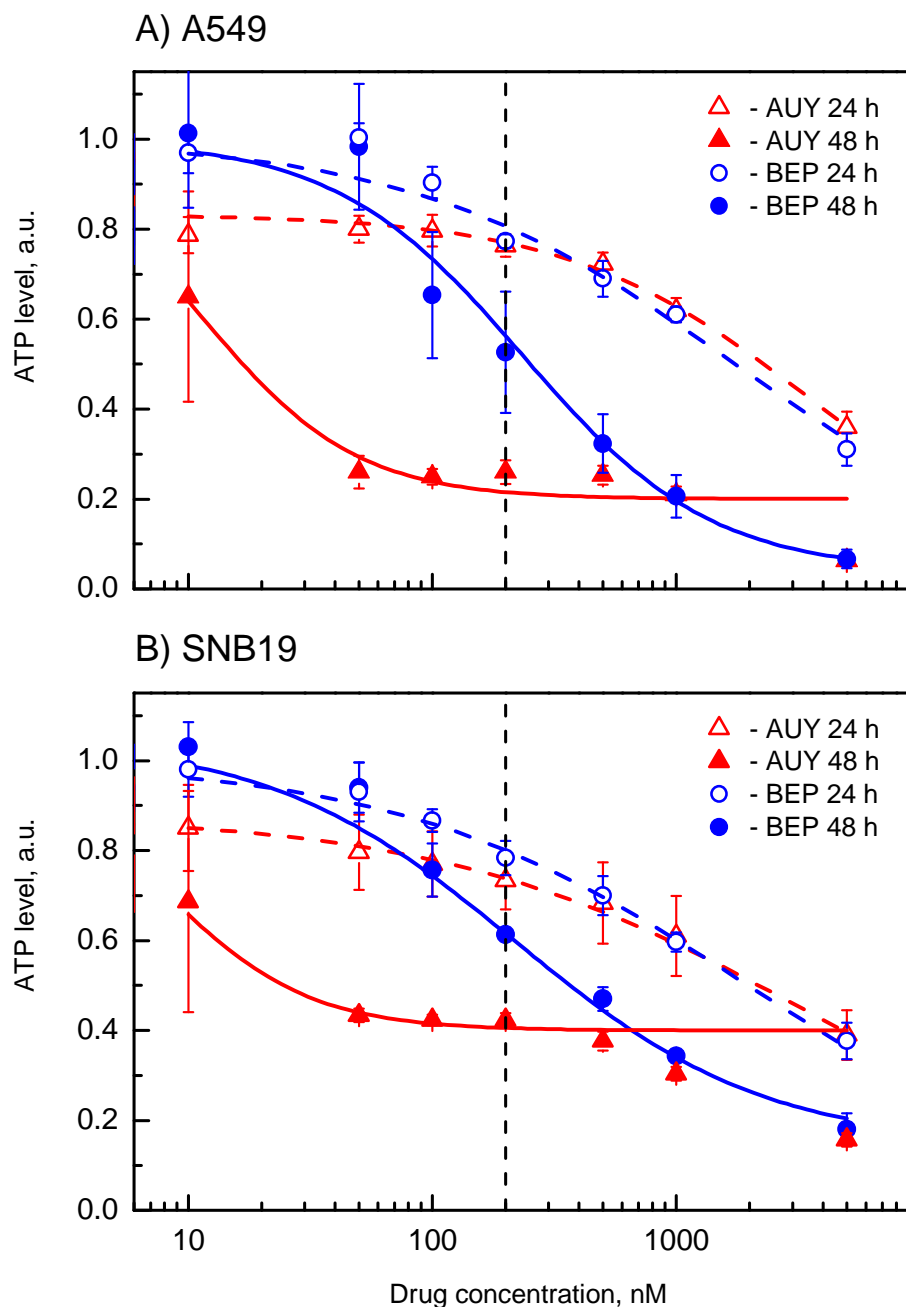
B) SNB19

Figure 12. Changes of intracellular ATP levels in A549 (A) and SNB19 (B) cell lines. Samples were treated with serial dilutions of NVP-AUY922 (red triangles) and NVP-BEP800 (blue circles) for 24 or 48 hours (open and filled symbols respectively). Data from at least three experiments were averaged and normalized against DMSO-treated controls. ATP levels (±SE) are given as a percentage to the corresponding controls. The vertical, dashed line indicates the concentration of 200 nM, which was used for further experiments (modified from Niewidok et al. 2012 with kind permission from Neoplasia Press).

As evident from Figure 12, ATP content depends on the drug concentration and on the duration of the drug treatment. The cell viability decreased with increasing concentration of each Hsp90 inhibitor 24 hours post treatment. Forty-eight hour

incubation shifted the dose-response curve of A549 and SNB19 cell lines toward lower drug concentrations (Fig. 12). Intermediate concentrations of NVP-AUY922 were more toxic to A549 (the ATP level ≈ 0.2 a.u.) than to SNB19 cells (ATP ≈ 0.45 a.u.). For further experiments, the working concentration of 200 nM of NVP-AUY922 or NVP-BEP800 was chosen. In both tested cell lines, 24-hour long incubation with such concentration of either Hsp90 inhibitor reduced the cell ATP content to ~0.8 a.u. The exposure for 48 hours to 200 nM NVP-AUY922 further decreased the ATP content in A549 to ~0.3 a.u. and on SNB19 to ~0.4 a.u. The cell viability after 48-hour incubation with 200 nM NVP-BEP800 dropped to ~0.5 a.u. in lung carcinoma and to ~0.6 a.u. in glioblastoma samples (Fig. 12).

4.1.2 Colony survival of irradiated A549 and SNB19 cells after treatment with NVP-AUY922 and NVP-BEP800

Control and drug-treated lung carcinoma A549 and glioblastoma SNB19 cell lines were irradiated with a single dose up to 10 Gy and kept in culture for 30 minutes, 24 hours or 48 hours until plated for colony-forming assay (3.2.5). Normalized cell survival responses were plotted versus the radiation dose as shown in Figure 13. Experiments were repeated at least three times and the following parameters were calculated: plating efficiency of non-irradiated samples, surviving fraction at 2 Gy (SF2), radiation dose resulting in 10% survival (D_{10}) and growth inhibition factor IF_{10} (Table 10).
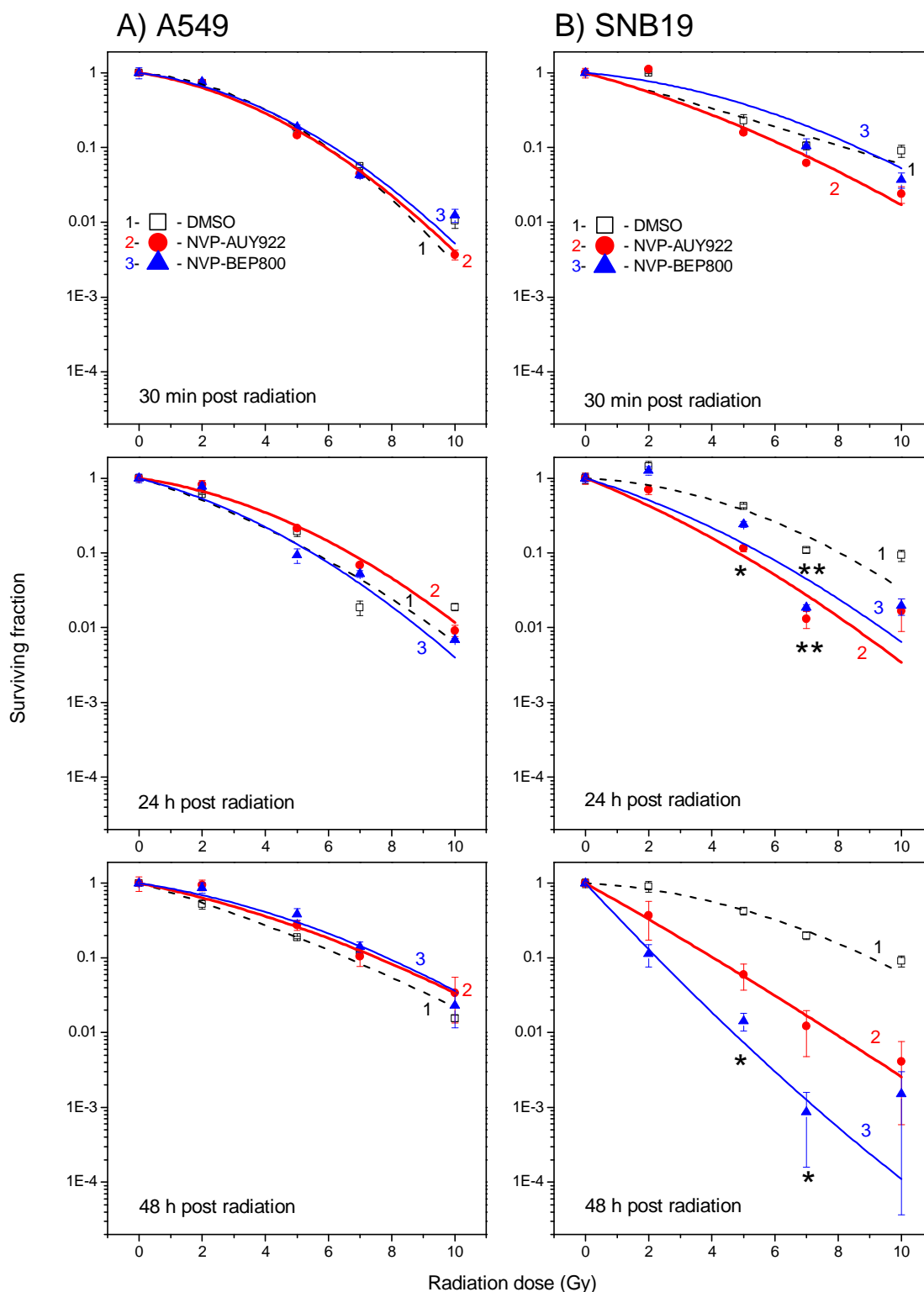
Figure 13. Representative clonogenic survival curves of A549 (A) and SNB19 (B) cell lines. Cells were treated with DMSO (black squares), NVP-AUY922 (red circles) or NVP-BEP800 (blue triangles), irradiated one hour later with single dose and plated for colony-forming assay at indicated time point. After staining and scoring the colonies, the cell survival curves were generated. The experiment was repeated at least three times. Significant differences between controls and cells treated with Hsp90 inhibitor are indicated *$p < 0.05$, **$p < 0.01$ (reproduced from Niewidok et al. 2012 with kind permission from Neoplasia Press).

Table 10. Plating efficiencies and radiosensitivity parameters[a] of drug-treated and irradiated cancer cell lines A549 and SNB19 (reproduced from Niewidok et al. 2012 with kind permission from Neoplasia Press).

	PE	SF2 [b]	D_{10} [c] (Gy)	IF_{10} [d]
A549				
30 minutes post radiation				
DMSO	0.4±0.1	0.59±0.1	6.1	1.0
NVP-AUY922	0.4±0.1	0.55±0.1	5.6	1.1
NVP-BEP800	0.4±0.1	0.60±0.1	5.9	1.1
24 hours post radiation				
DMSO	0.5±0.2	0.61±0.1	6.2	1.0
NVP-AUY922	0.2±0.1	0.65±0.2	6.4	1.0
NVP-BEP800	0.3±0.2	0.54±0.2	5.6	1.1
48 hours post radiation				
DMSO	0.4±0.07	0.60±0.2	6.9	1.0
NVP-AUY922	0.06±0.02	0.73±0.2	7.6	0.9
NVP-BEP800	0.1±0.06	0.72±0.2	7.1	1.1
SNB19				
30 minutes post radiation				
DMSO	0.1±0.03	0.56±0.2	5.7	1.0
NVP-AUY922	0.1±0.03	0.50±0.2	5.0	1.1
NVP-BEP800	0.08±0.0	0.71±0.2	6.7	0.9
24 hours post radiation				
DMSO	0.09±0.01	0.76±0.2	7.6	1.0
NVP-AUY922	0.03±0.01	0.45±0.3	4.5	1.9
NVP-BEP800	0.06±0.01	0.58±0.2	4.9	1.5
48 hours post radiation				
DMSO	0.1±0.09	0.72±0.2	8.0	1.0
NVP-AUY922	0.03±0.02	0.30±0.1	3.9	2.0
NVP-BEP800	0.06±0.05	0.23±0.2	3.0	3.2

[a] Mean (±SD) from at least three independent experiments
[b] SF2 is the surviving fraction at 2 Gy
[c] D_{10} is the radiation dose resulting in 10% cell survival
[d] IF_{10} was calculated as $(D_{10\ control})/(D_{10\ inhibitor})$

The changes of plating efficiency of non-irradiated cells indicate the possible cytotoxic and/or anti-proliferative effects of Hsp90 inhibitors. Table 10 shows that the PE values of both cell lines decreased with increasing incubation time in the drug-containing medium. Forty-eight-hour treatment with NVP-AUY922 reduced the PE of A549 cells from 0.4 to 0.06, whereas incubation with NVP-BEP800 changed it from 0.4 to 0.1. In the case of SNB19, the plating efficiency diminished from 0.1 to 0.03 for NVP-AUY922 and to 0.06 for NVP-BEP800 (48 hours after drug treatment).

Treatment with NVP-AUY922 or NVP-BEP800 did not influence the radiation response of A549 cells throughout the whole range of incubation times (0.5-48 hours). The dose-response curves of treated cells overlap with the control curves; accordingly, there were no changes in the SF2 and D_{10} values (compare Table 10; SF2≈ 0.65±0.2 and D_{10}≈ 6.6±1.0). In contrast, Hsp90 inhibition in SNB19 cells sensitized them significantly to ionizing radiation (Fig. 13B). The longer the incubation with either NVP-AUY922 or NVP-BEP800, the more sensitive glioblastoma cells were to IR. In concordance, the SF2 values decreased from 0.7 in the DMSO control to 0.3 for NVP-AUY922 and to 0.23 for NVP-BEP800 48 hours post drug-IR treatment (Table 10).

4.1.3 Influence of Hsp90 inhibition and IR on the expression of Hsp90 clients and apoptotic marker proteins in tumor cells

Sub-confluent A549 and SNB19 cell cultures were treated with 200 nM NVP-AUY922 or NVP-BEP800 one hour before irradiation. Cell lysates were prepared according to protocol (3.2.6) and the samples were probed for the expression of various proteins. Firstly, we tested examined the expression of Hsp90, Hsp70, Akt, Raf-1 and survivin at different time points after drug-only, IR-only or combined drug-IR treatment. Representative results are shown in Figures 14 and 15; protein expression was quantified by the protein/actin ratios given in arbitrary units.

Figure 14. Expression of Hsp90, Hsp70, Akt, Raf-1 and survivin in A549 cells. Samples were treated with DMSO, NVP-AUY922 or NVP-BEP800 and irradiated (with 2 or 8 Gy). Each protein band was normalized to β-actin and the ratios are given in numbers (reproduced from Niewidok et al. 2012 with kind permission from Neoplasia Press).
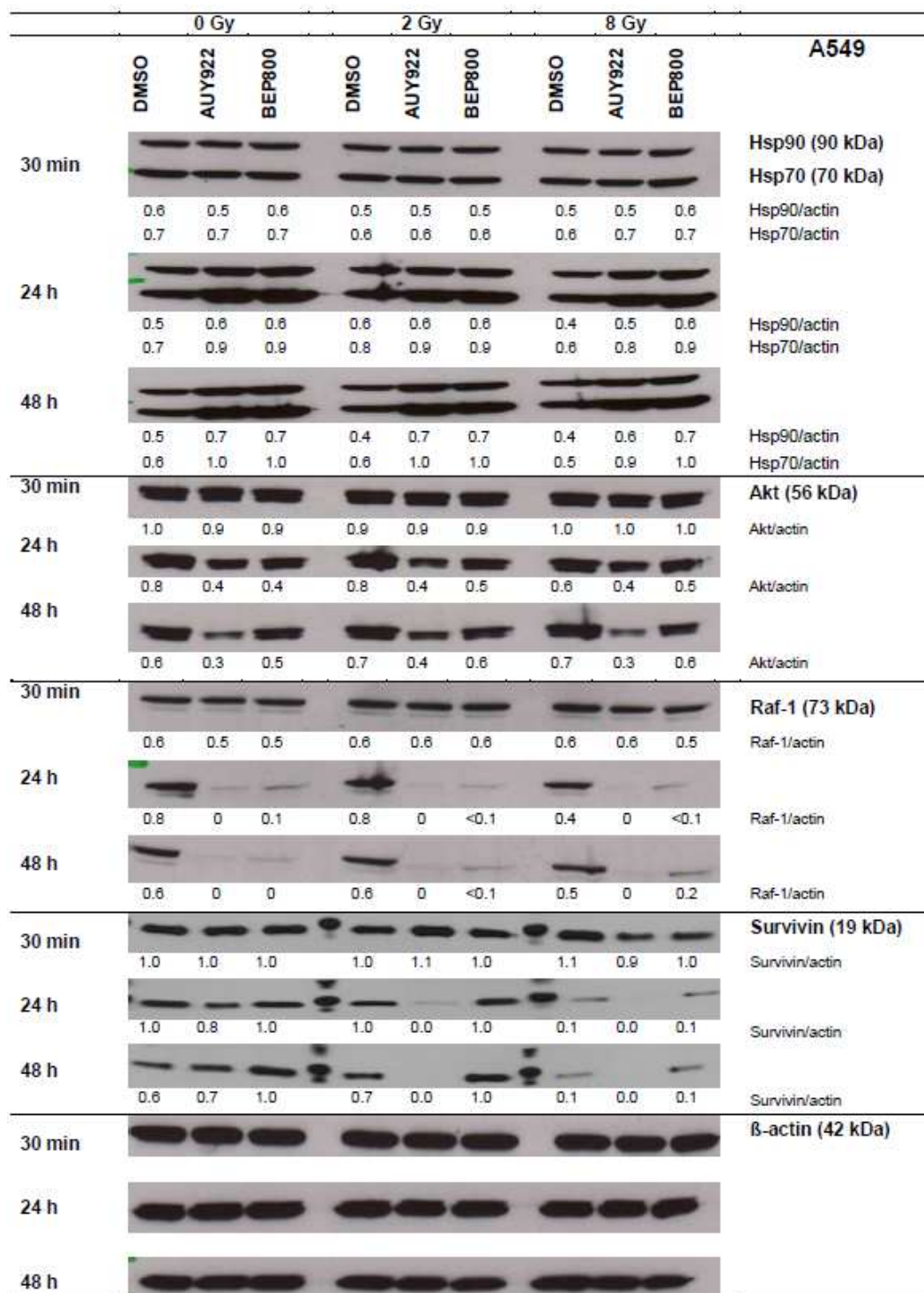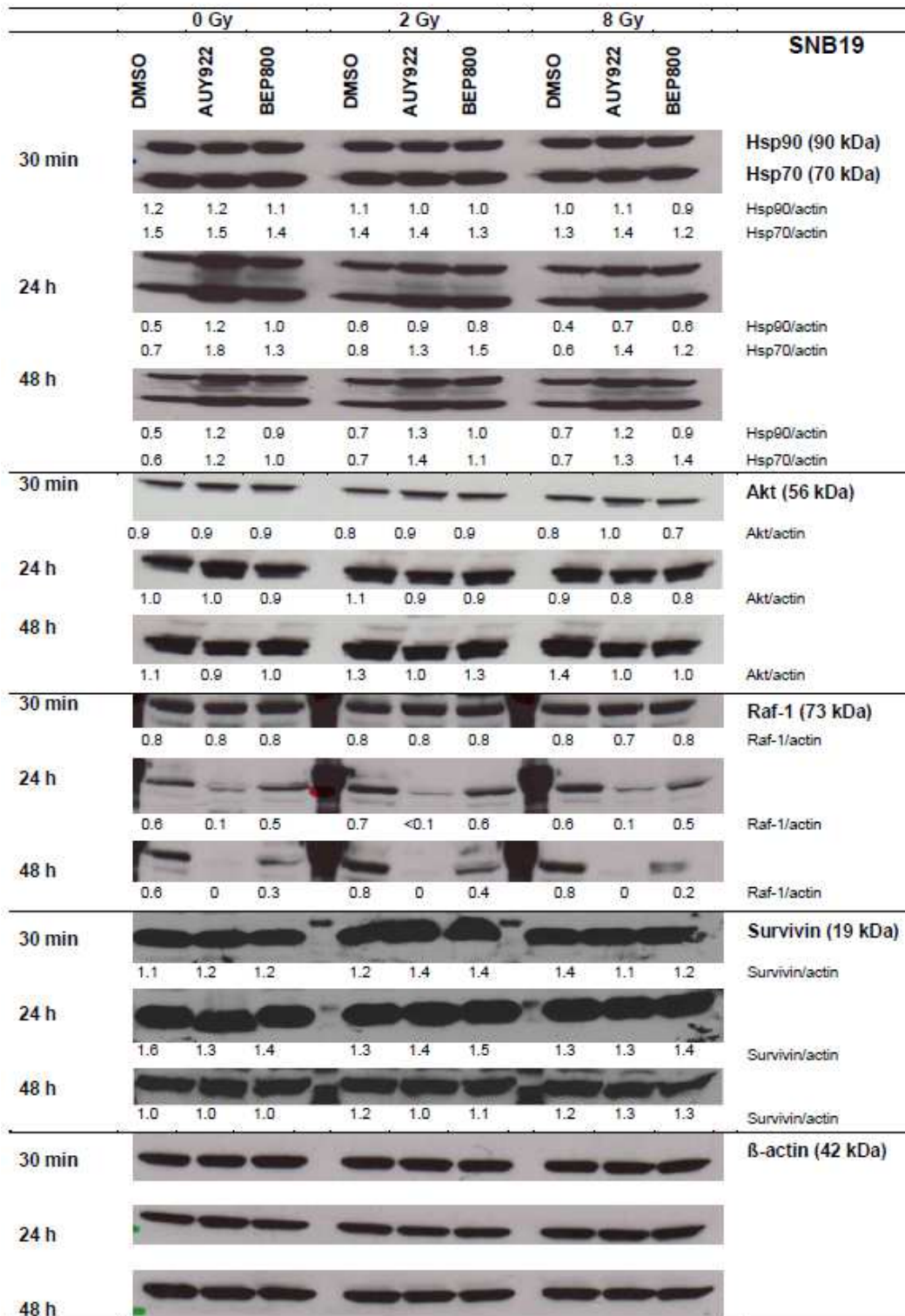
Figure 15. Expression of Hsp90, Hsp70, Akt, Raf-1 and survivin in SNB19 cells. Samples were treated with DMSO, NVP-AUY922 or NVP-BEP800 and irradiated (with 2 or 8 Gy). Each protein band was normalized to β-actin and the ratios are given in numbers (reproduced from Niewidok et al. 2012 with kind permission from Neoplasia Press).

NVP-AUY922 or NVP-BEP800 alone did not change the expression of analyzed proteins 30 minutes after treatment compared with DMSO-treated control cells (Figs. 14, 15). Twenty four and forty eight hours after drug-only treatment we observed an increase in the expression of heat shock proteins Hsp90 and Hsp70 in lung carcinoma cells (Fig. 14, Hsp90: 0.5 -> 0.7 a.u., Hsp70: 0.6 -> 1.0 a.u., 48 hours post NVP-AUY922 treatment). Exposure for 48 hours to either Hsp90 inhibitor induced the down-regulation of Akt (from 0.8 to 0.4 a.u.) and the depletion of Raf-1 (from 0.8 to ~0 a.u.) in A549 samples. Moreover, the treatment with NVP-AUY922 reduced the expression of survivin (from 1.6 to 1.2 a.u.).

Irradiation with 2 Gy of DMSO-treated cells resulted in no changes in the expression of Hsp90, Hsp70, Akt and Raf-1. At the same time we observed a decrease in the amount of survivin (from 1.0 to 0.7 a.u.). When the radiation dose increased to 8 Gy, there were no changes in the levels of Hsp90, Hsp70, Akt and survivin, whereas Raf-1 was down-regulated by ~50% (from 0.8 to 0.4 a.u.). The combination of irradiation with Hsp90 inhibition in A549 cells triggered no additional changes in the expression of studied marker proteins (Hsp90, Hsp70, Akt, and Raf-1), with the exception of survivin, whose expression decreased 48 hours after NVP-AUY922-IR treatment (Fig. 14).

Alterations in the expression of chosen proteins in SNB19 (Fig. 15) resembled the changes observed in lung carcinoma cells. The induction of heat shock proteins was greater than in A549 (48 hours post NVP-AUY922-IR treatment), for Hsp90 from 0.7 to 1.2 a.u., and Hsp70 from 0.7 to 1.3 a.u. In contrast, we observed weaker reduction of Akt in SNB19 (1.4 to 1.0 a.u.) than in A549 cells. Another difference between the cell lines was the expression of survivin, whose expression remained constant in glioblastoma samples independent from the applied treatment. Furthermore, the administration of NVP-AUY922 for 48 hours caused Raf-1 to vanish, whereas NVP-BEP800 only partially depleted this protein (from 0.6 to 0.3 a.u.) in SNB19 cells (Fig. 15).

Figure 16. Expression of k-RAS, PTEN and two subunits of PI3K in A549 cells. Samples were treated with DMSO, NVP-AUY922 or NVP-BEP800 and irradiated (with 2 or 8 Gy). Each protein band was normalized to β-actin and the ratios are given in numbers (modified from Niewidok et al. 2012 with kind permission from Neoplasia Press).

Contrasting results from the colony-forming assay prompted us to look closer at the differences between A549 and SNB19 cell lines. After database research for mutations we identified p53, k-RAS and PTEN (Table 7, chapter 3.2.1) as potential key regulators of the cellular response. Therefore, we tested A549 and SNB19 samples for the expression of these oncoproteins and some of their downstream targets after combined drug-IR treatment (Figs. 16-21).
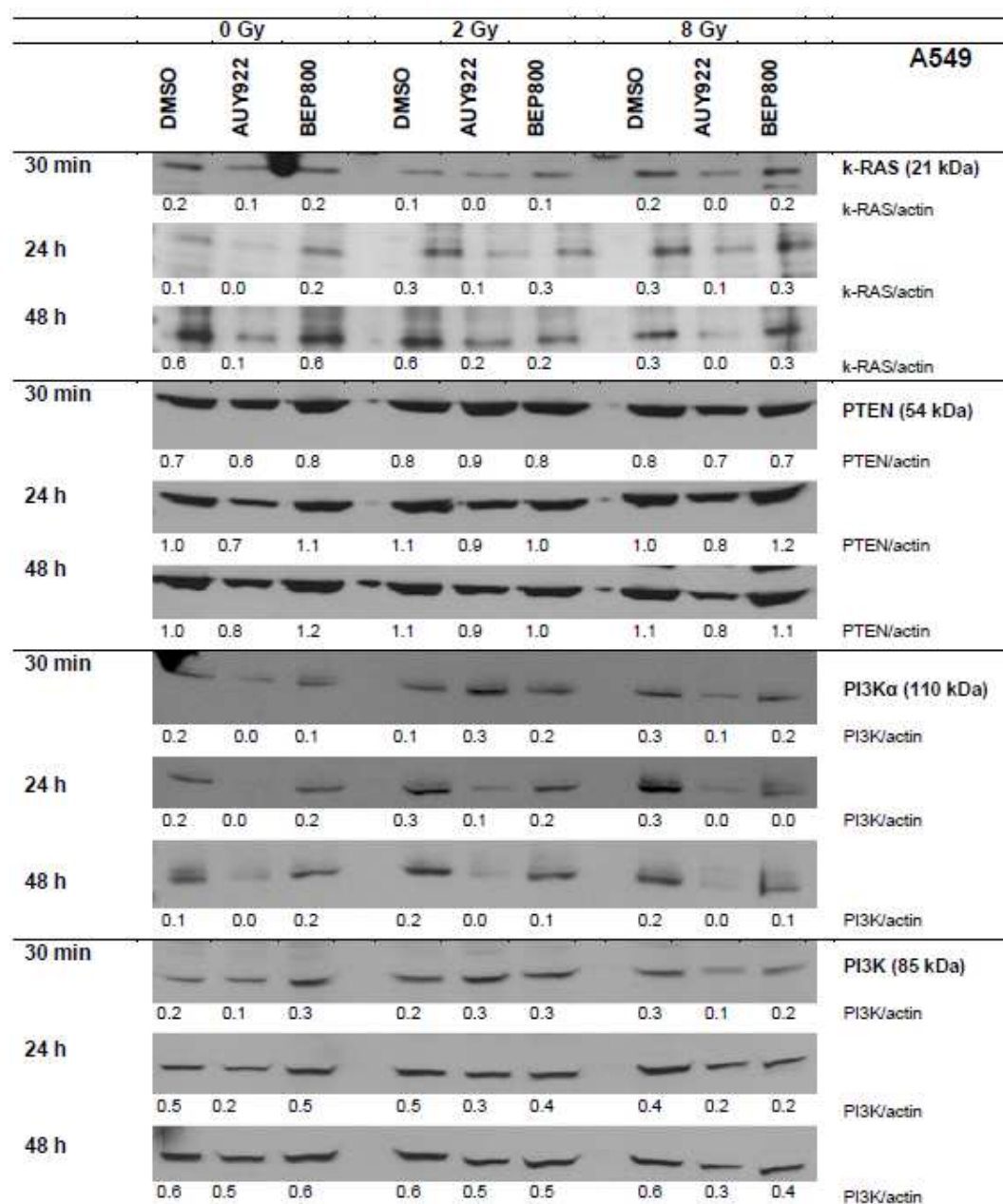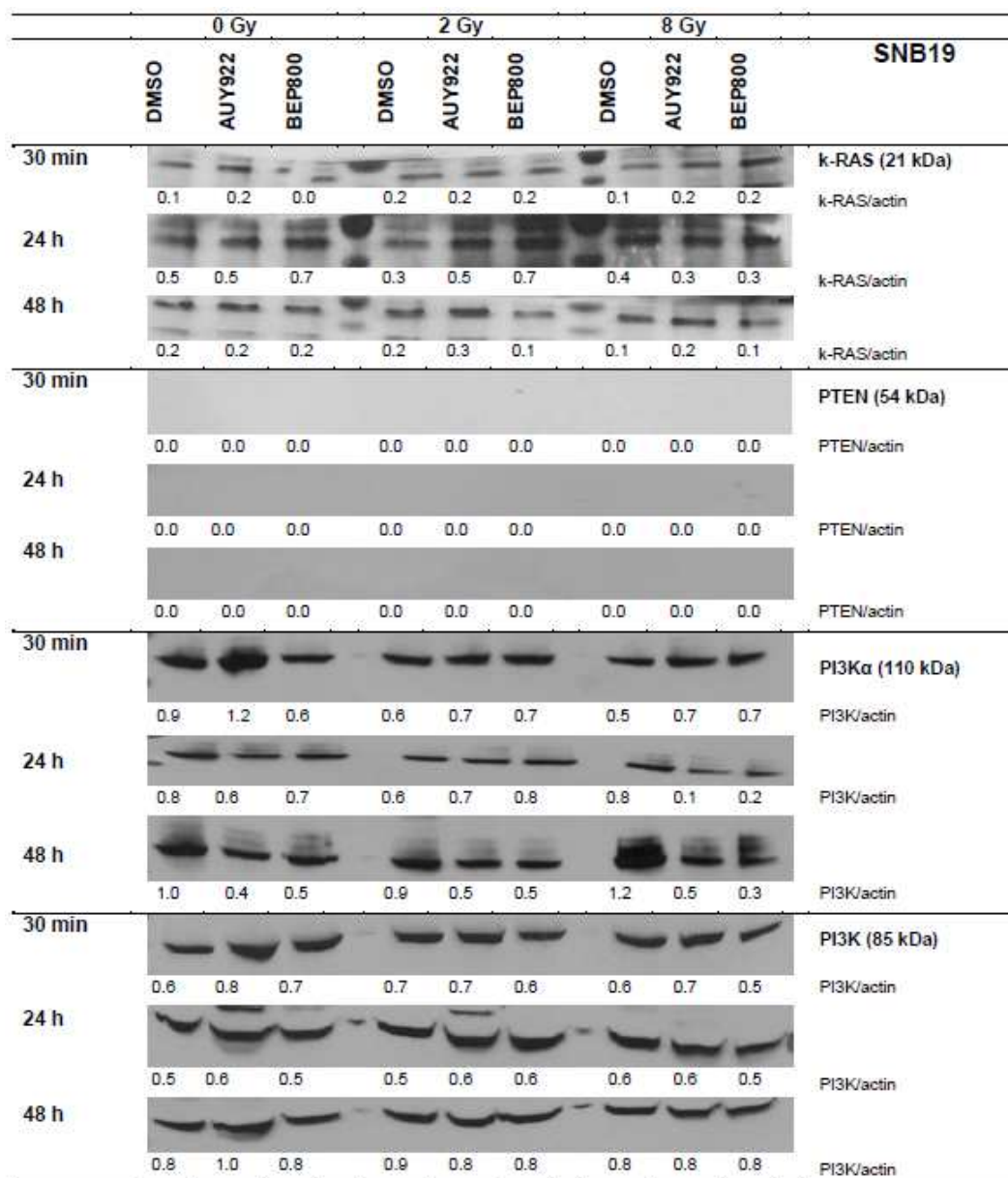
Figure 17. Expression of k-RAS, PTEN and two subunits of PI3K in SNB19 cells. Samples were treated with DMSO, NVP-AUY922 or NVP-BEP800 and irradiated (with 2 or 8 Gy). Each protein band was normalized to β-actin and the ratios are given in numbers (modified from Niewidok et al. 2012 with kind permission from Neoplasia Press).

Forty-eight-hour exposure of A549 cells to NVP-AUY922 (with or without IR) down-regulated k-RAS (0.6 -> 0.1 a.u.), whereas NVP-BEP800 had to be combined with IR to decrease the level of this protein (Fig. 16). At the same time, the expression level of k-RAS in glioblastoma samples remained unchanged, independent from the applied drug-IR treatment (Fig. 17).
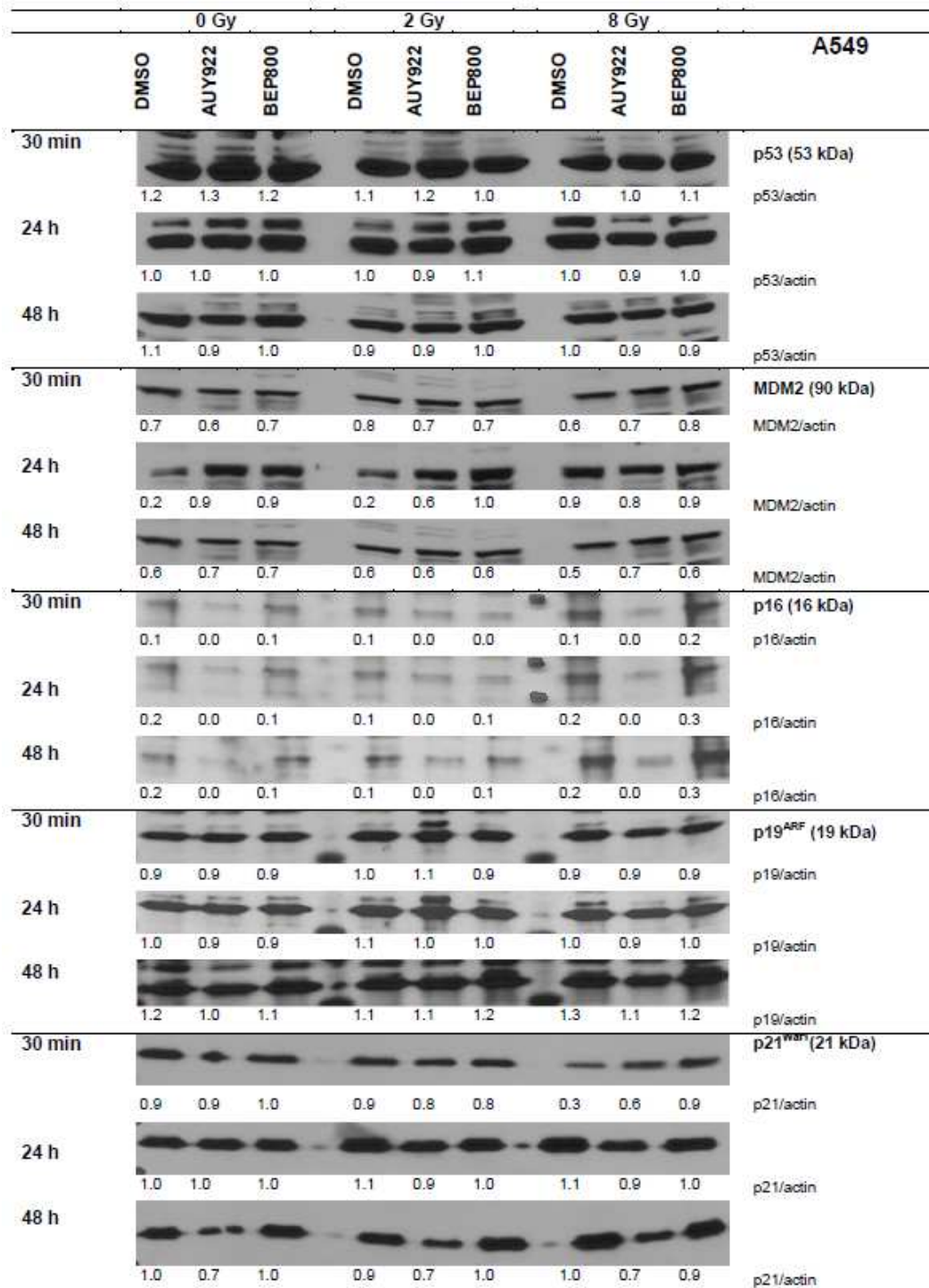
Figure 18. Expression of p53, MDM2, p16, p19[ARF] and p21[Waf1] in A549 cells. Samples were treated with DMSO, NVP-AUY922 or NVP-BEP800 and irradiated (with 2 or 8 Gy). Each protein band was normalized to β-actin and the ratios are given in numbers (modified from Niewidok et al. 2012 with kind permission from Neoplasia Press).
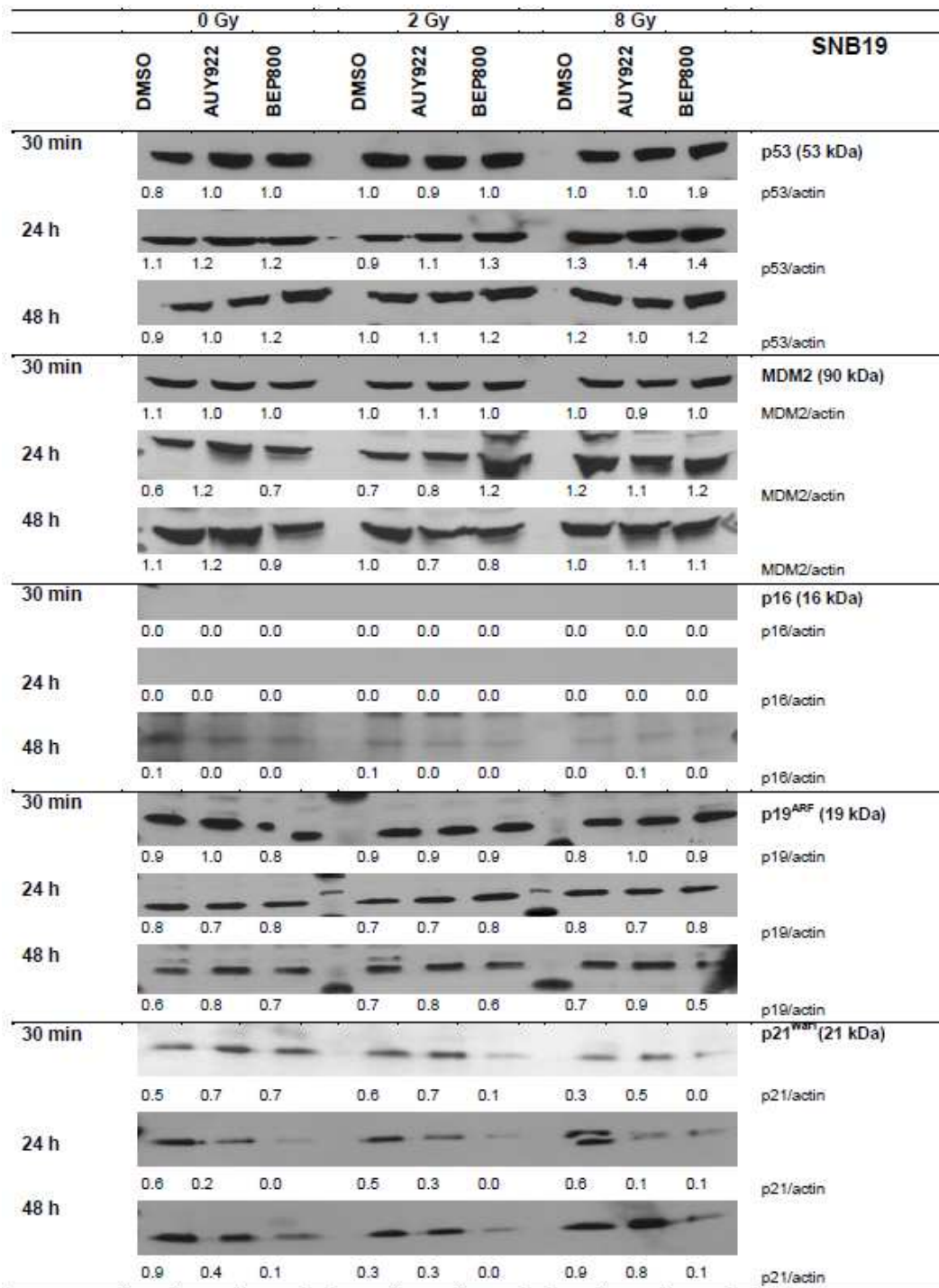
Figure 19. Expression of p53, MDM2, p16, p19^ARF and p21^Waf1 in SNB19 cells. Samples were treated with DMSO, NVP-AUY922 or NVP-BEP800 and irradiated (with 2 or 8 Gy). Each protein band was normalized to β-actin and the ratios are given in numbers (modified from Niewidok et al. 2012 with kind permission from Neoplasia Press).

The incubation of A549 samples with NVP-AUY922 (independent from IR) for 48 hours induced the down-regulation of cell cycle inhibitors p16 (0.2 -> 0.0 a.u.) and p21^{Waf1} (1.0 -> 0.7 a.u.), but not of p19^{ARF} (Fig. 18). In SNB19 the expression of p16 was under the detection level. At the same time, NVP-AUY922 slightly up-regulated the levels of p19 (0.6 -> 0.8 a.u.), whereas the amount of p21^{Waf1} decreased (0.9 -> 0.4 a.u.; Fig. 19).
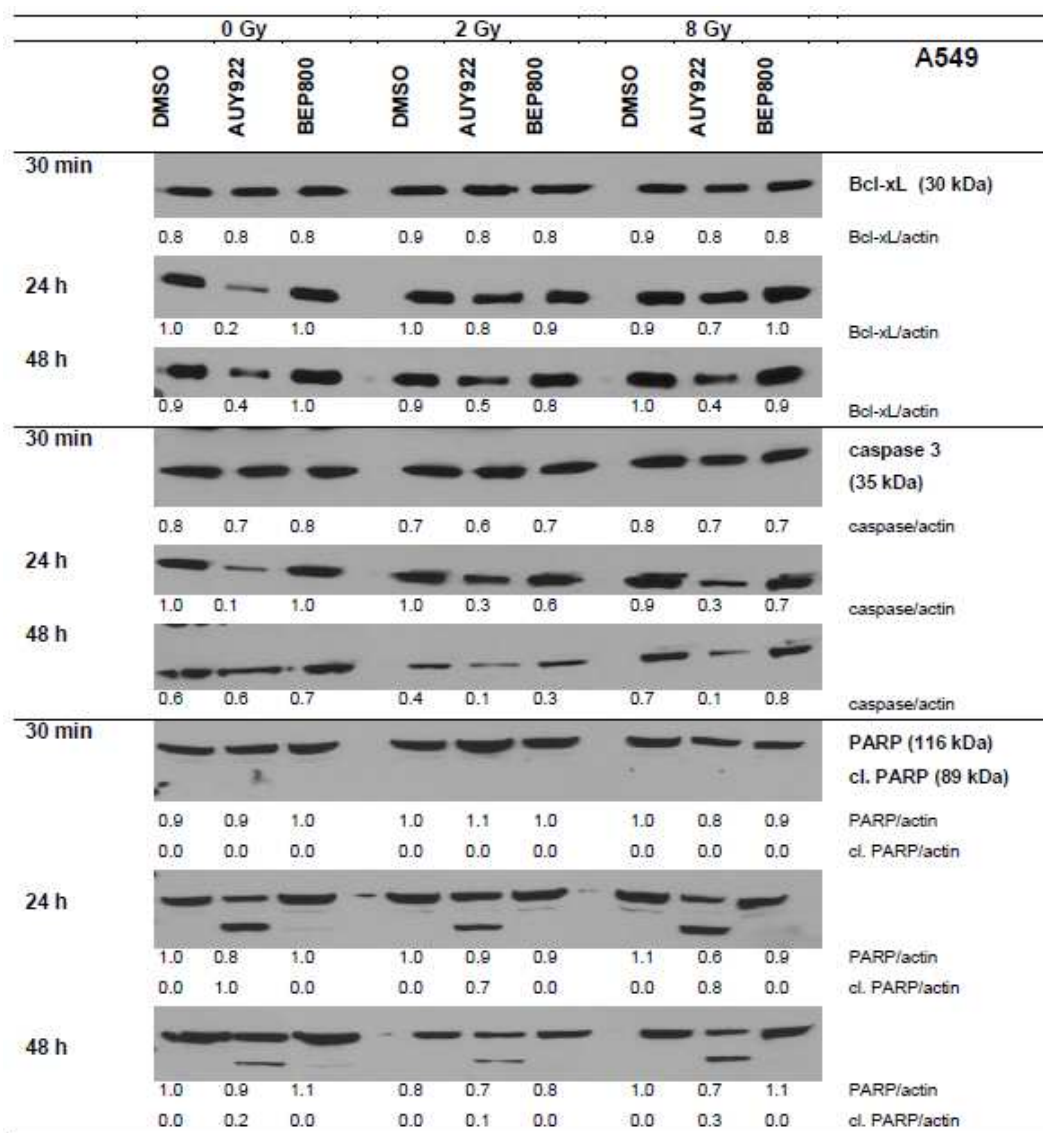
Figure 20. Expression of Bcl-xL, caspase 3 and PARP in A549 cells. Samples were treated with DMSO, NVP-AUY922 or NVP-BEP800 and irradiated (with 2 or 8 Gy). Each protein band was normalized to β-actin and the ratios are given in numbers (modified from Niewidok et al. 2012 with kind permission from Neoplasia Press).
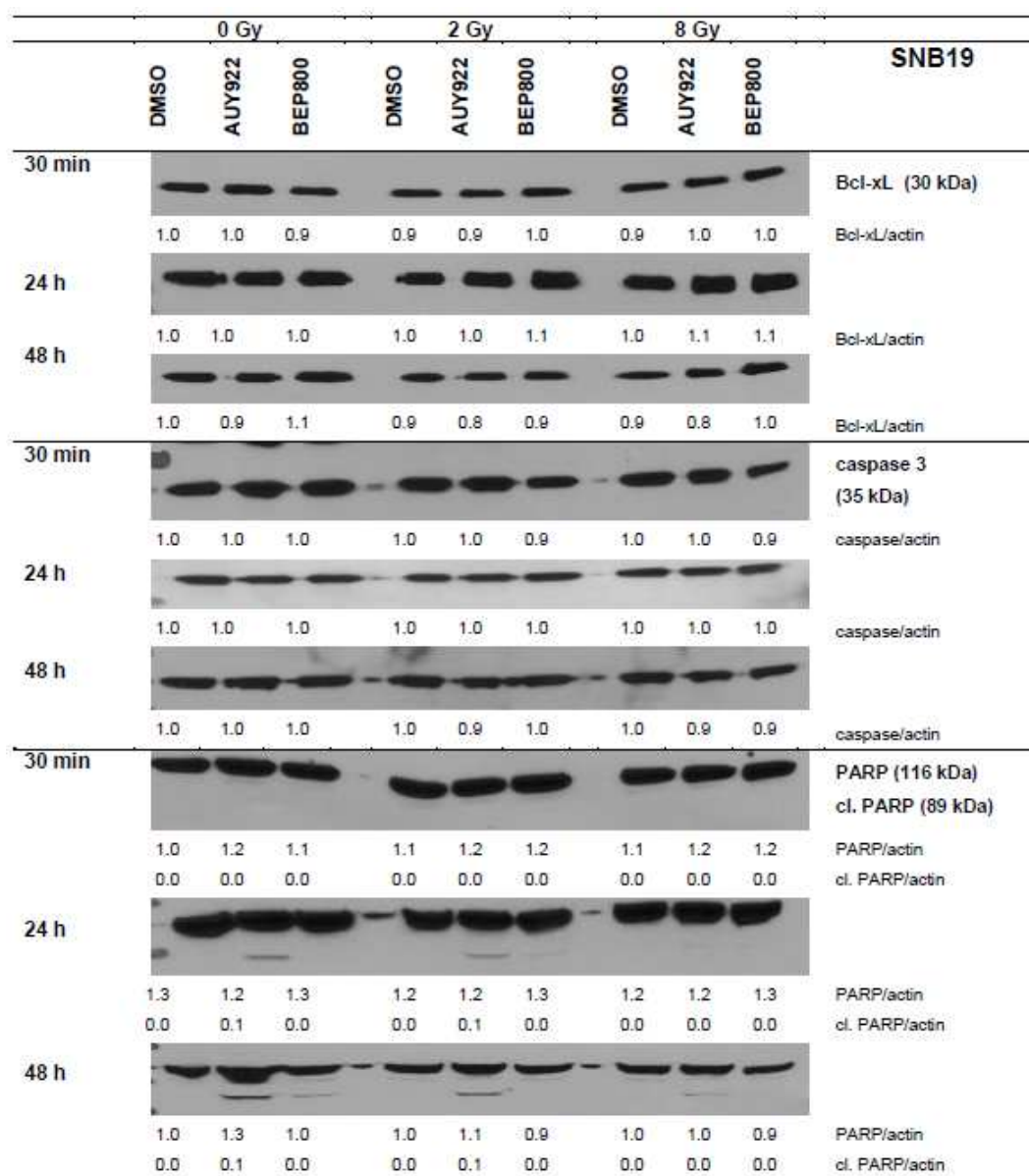
Figure 21. Expression of Bcl-xL, caspase 3 and PARP in SNB19 cells. Samples were treated with DMSO, NVP-AUY922 or NVP-BEP800 and irradiated (with 2 or 8 Gy). Each protein band was normalized to β-actin and the ratios are given in numbers (modified from Niewidok et al. 2012 with kind permission from Neoplasia Press).

Forty-eight-hour incubation with NVP-AUY922 down-regulated the expression of anti-apoptotic protein Bcl-xL in A549 cells (0.9 -> 0.4 a.u.; Fig. 20), whereas in SNB19 its level did not change (Fig. 21). Furthermore, in lung carcinoma we observed signs of apoptosis, in the form of decreased amount of caspase 3 (0.7 -> 0.1 a.u.) and PARP cleavage (48 hours post NVP-AUY922-IR, Fig. 20). At the same time, in glioblastoma cells caspase 3 and PARP levels remained at the level of control samples (Fig. 21).

4.1.4 Effects of Hsp90 inhibition and irradiation on the induction and repair of DNA damage in A549 and SNB19 cells

One of the reasons for the radiosensitization could be the higher amount of DNA damage or the impairment of DNA damage repair pathways. As a marker for DNA damage we measured the expression of phosphorylated H2AX (γH2AX), which is one of the earliest events after DNA double strand break. A549 and SNB19 cell samples were drug-treated and irradiated (as described in section 3.2.8). Thirty minutes, 24 hours and 48 hours after IR the cells were fixed in ice-cold ethanol and stained with anti-γH2AX antibody. Representative histograms are shown in Figure 22.

A) A549

B) SNB19

Histone γH2AX content, a.u.
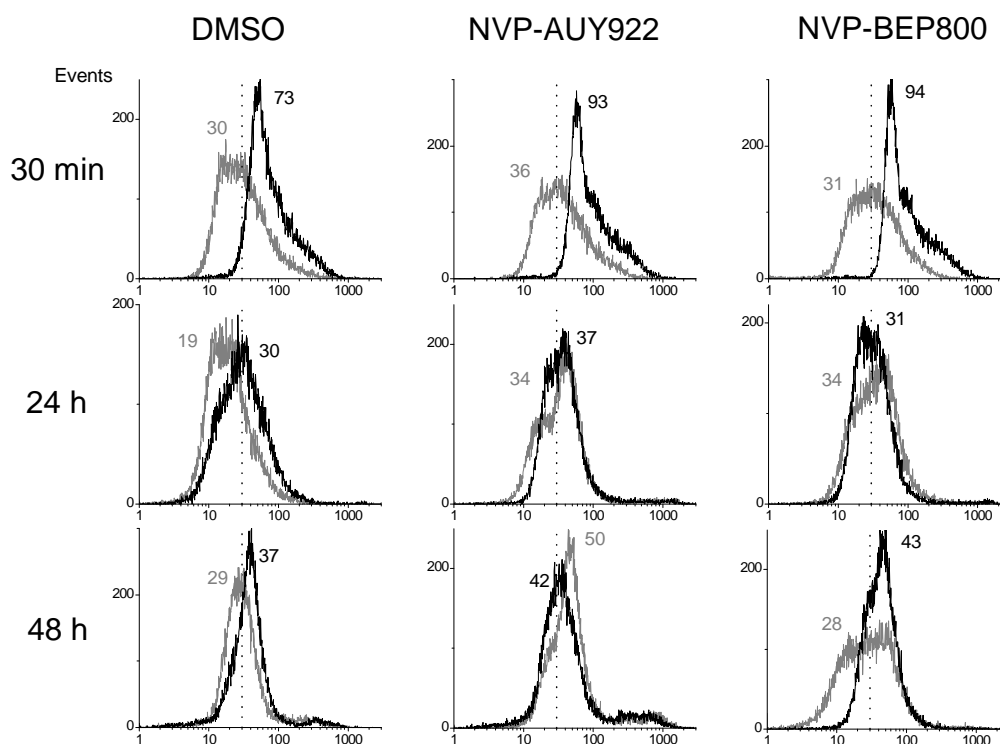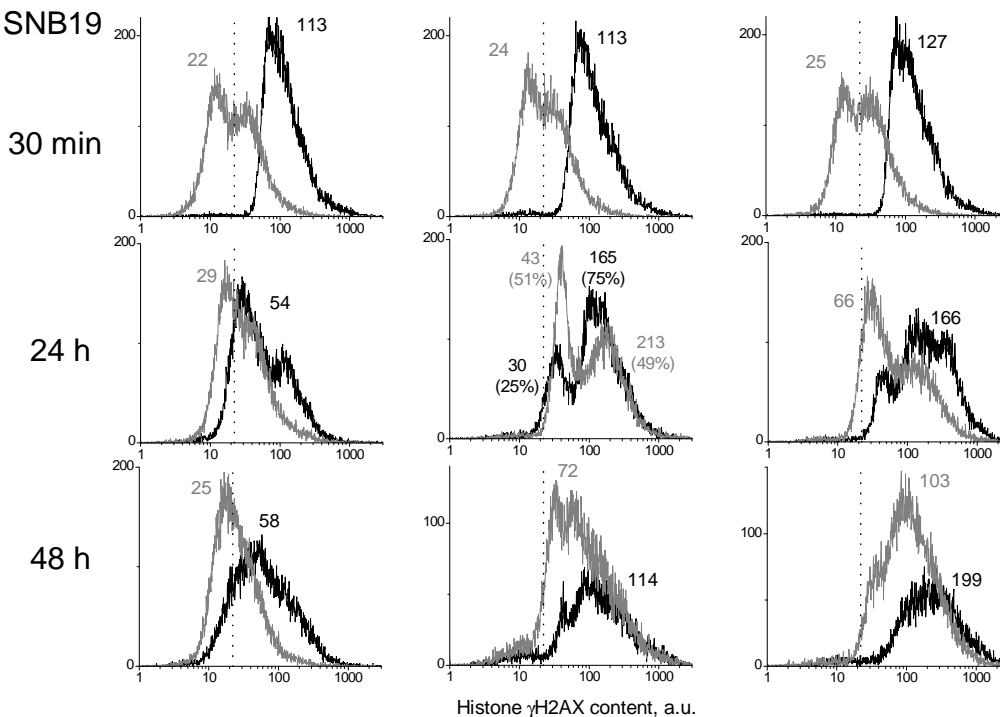
Figure 22. Histograms showing distribution of γH2AX, as a marker of DNA double strand breaks, in A549 (A) and SNB19 (B) cells. DMSO-treated controls and samples treated with NVP-AUY922 or NVP-BEP800 were irradiated with single dose (8 Gy, black histograms) and incubated in the drug-containing medium for indicated time. Gray histograms represent corresponding non-irradiated samples. Numbers denote the mean γH2AX expression for the respective cell sample. The vertical, dashed line marks the γH2AX value of DMSO-treated, non-irradiated control (reproduced from Niewidok et al. 2012 with kind permission from Neoplasia Press).

As shown in Figure 22, the background expression level of γH2AX was similar in control samples of A549 and SNB19 (Fig. 22A, B). Thirty minutes after irradiation with 8 Gy, the amount of γH2AX increased from 30 to 73 a.u. in A549 cells (Fig. 22A) and in SNB19 from 22 to 113 a.u. (Fig. 22B). After one day, the IR-induced DNA damage in lung carcinoma A549 cells was restored to background level (from 73 to 30 a.u.). In contrast, SNB19 only partially repaired the damage (from 113 to 54 a.u.). Prolonging the time of incubation to 48 hours post IR did not further affect the γH2AX expression in both cell lines.

Thirty-minute incubation with either Hsp90 inhibitor alone induced no or few changes in the level of DNA damage in both examined cell lines (Fig. 22A, B; first row, gray histograms). The extension of incubation time to 24 and 48 hours also did not influence the γH2AX expression in A549 cells. As opposed to A549, longer exposure of glioblastoma cells to NVP-AUY922 increased the amount of the γH2AX three-fold (to 72 a.u.) and to NVP-BEP800 even four-fold (to 103 a.u.) when compared with DMSO-treated controls (Fig. 22B).

The combination of each Hsp90 inhibitor and irradiation induced the accumulation of γH2AX from 31-36 a.u. for drug-treated, non-irradiated A549 cells to 93-94 a.u. for the combined drug-IR treatment (Fig. 22A, first row, black histograms). One and two days later the expression of γH2AX was restored to background level, suggesting that DNA damage repair pathways functioned efficiently. In glioblastoma samples, the combined drug-IR treatment (Fig. 22B, first row) increased the γH2AX amount four to five times (113-127 a.u.) compared with drug-treated cells (24-25 a.u.). Interestingly, SNB19 cells seemed to be unable to repair the DNA damage; 24 and 48 hours after drug-IR treatment the γH2AX levels remained elevated (for NVP-AUY922) or even further increased with time (for NVP-BEP800).

In addition to γH2AX measurements, we tested the expression of the proteins playing important role in DNA DSB repair (Fig. 23 and 24).
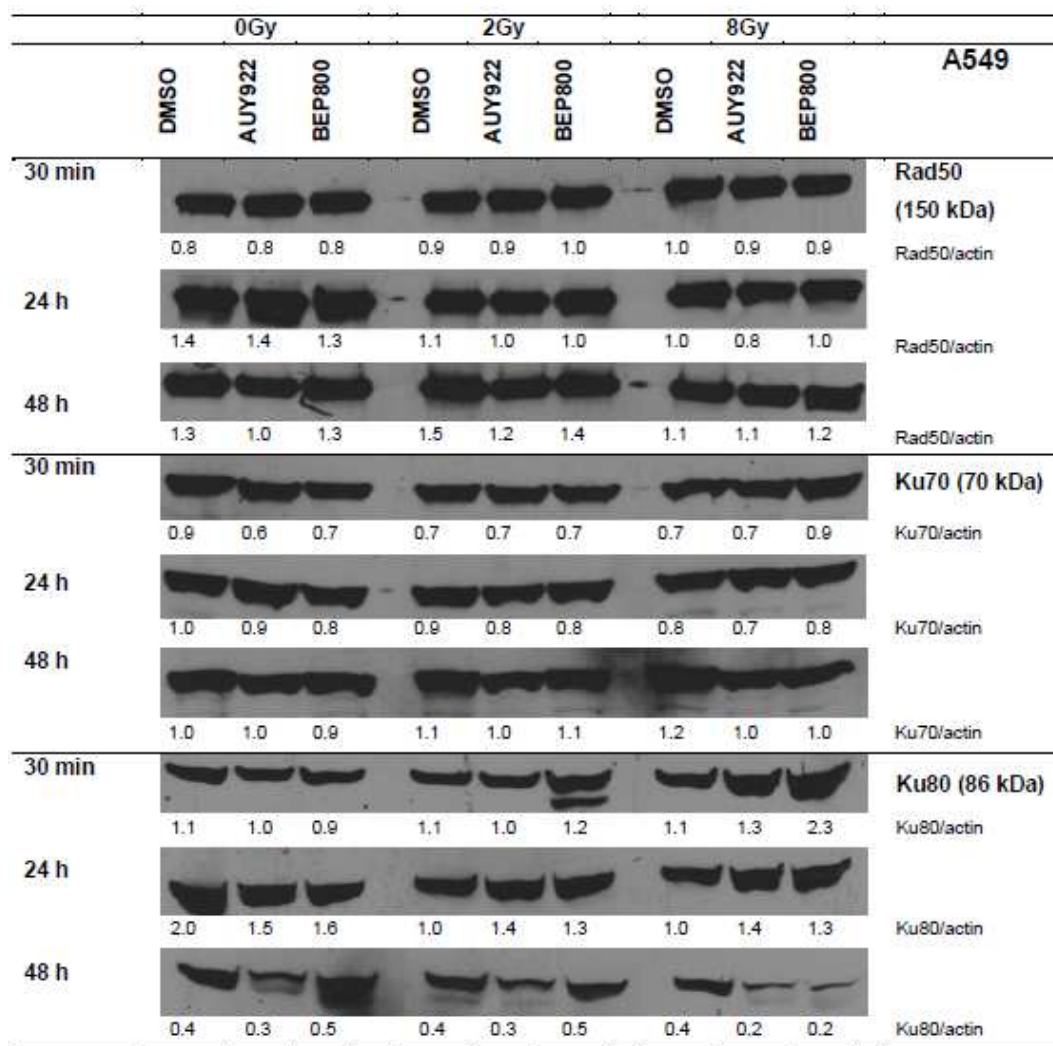
Figure 23. Expression of Rad50, Ku70 and Ku80 in A549 cells. Samples were treated with DMSO, NVP-AUY922 or NVP-BEP800 and irradiated (with 2 or 8 Gy). Each protein band was normalized to β-actin and the ratios are given in numbers (reproduced from Niewidok et al. 2012 with kind permission from Neoplasia Press).
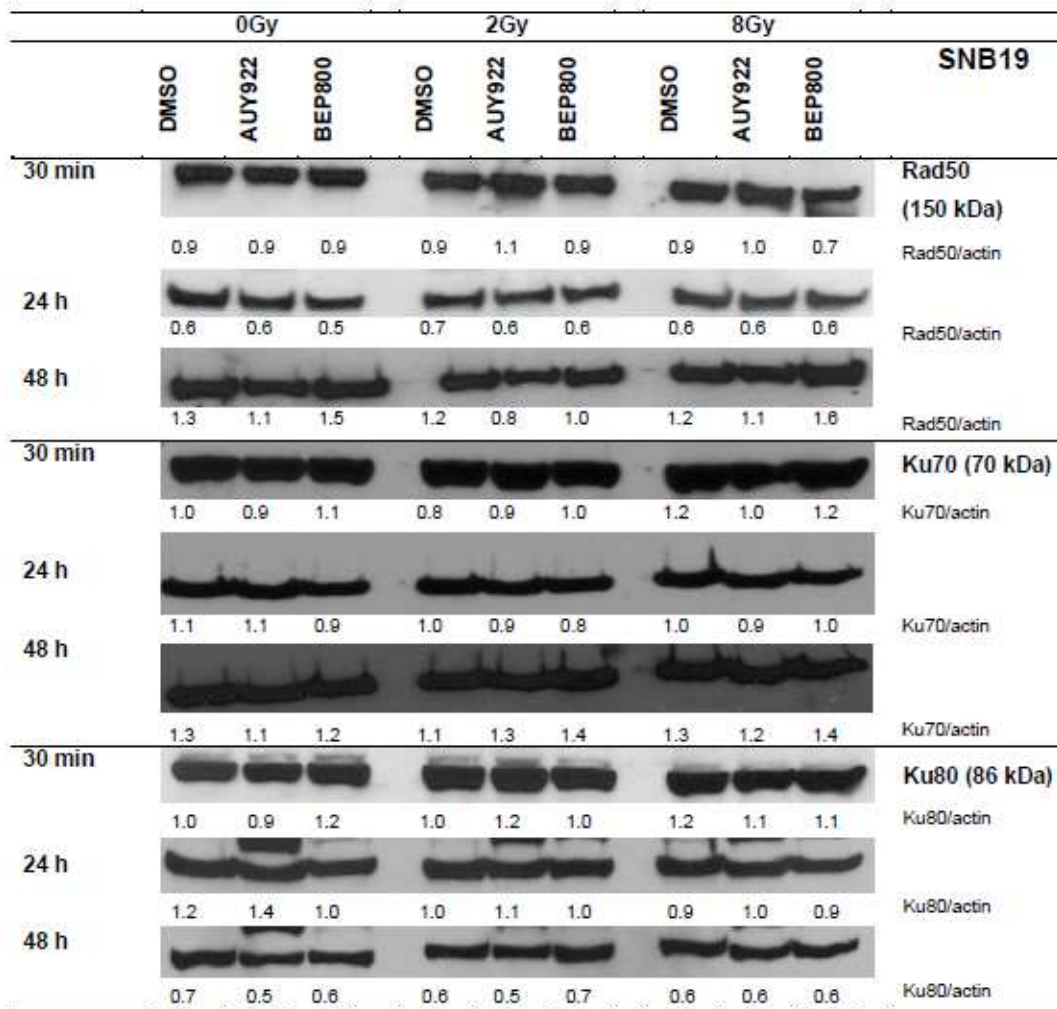
Figure 24. Expression of Rad50, Ku70 and Ku80 in SNB19 cells. Samples were treated with DMSO, NVP-AUY922 or NVP-BEP800 and irradiated (with 2 or 8 Gy). Each protein band was normalized to β-actin and the ratios are given in numbers (reproduced from Niewidok et al. 2012 with kind permission from Neoplasia Press).

The combination of Hsp90 inhibition and irradiation did not influence the expression of Rad50 (protein forming MRN complex) in tested cell lines (Fig. 23, 24). Thirty minutes after drug-IR treatment in A549 cells we detected an increase of Ku80 (1.1 -> 2.3 a.u. NVP-BEP800-IR), protein playing an important role in non-homologous end joining (Fig. 23). After 2 days the levels of Ku80 dropped to a level below control samples. There were no significant changes in the expression of Ku70 and Ku80 in glioblastoma cells throughout the time of experiments (Fig. 24).

4.1.5 Changes in the cell cycle progression after Hsp90 inhibition and irradiation in tumor cell lines A549 and SNB19

Simultaneously, with the measurements of γH2AX expression, we analyzed the cell cycle phase distribution in A549 and SNB19 samples (according to protocol in 3.2.8). Representative histograms are shown in Figures 25 and 26 and a statistical summary can be found in Tables 11 and 12.

Thirty minutes after irradiation only, we observed no changes in the cell cycle distribution in either examined cell line (Fig. 25A, 26A). The radiation-induced changes appeared 24 and 48 hours after IR, and in these samples we observed the S phase depletion together with an increase in G2/M peak (Figs. 25, 26B, C).

The administration of each Hsp90 inhibitor alone to A549 and SNB19 samples resulted in changes in the cell cycle distribution similar to these seen after irradiation alone. Short exposure (30 minutes) to the drug triggered no or little changes (Figs. 25A, 26A, first row), but 24 and 48 hours incubation shifted the cells from S phase to G2/M phase (Figs. 25, 26B, C).
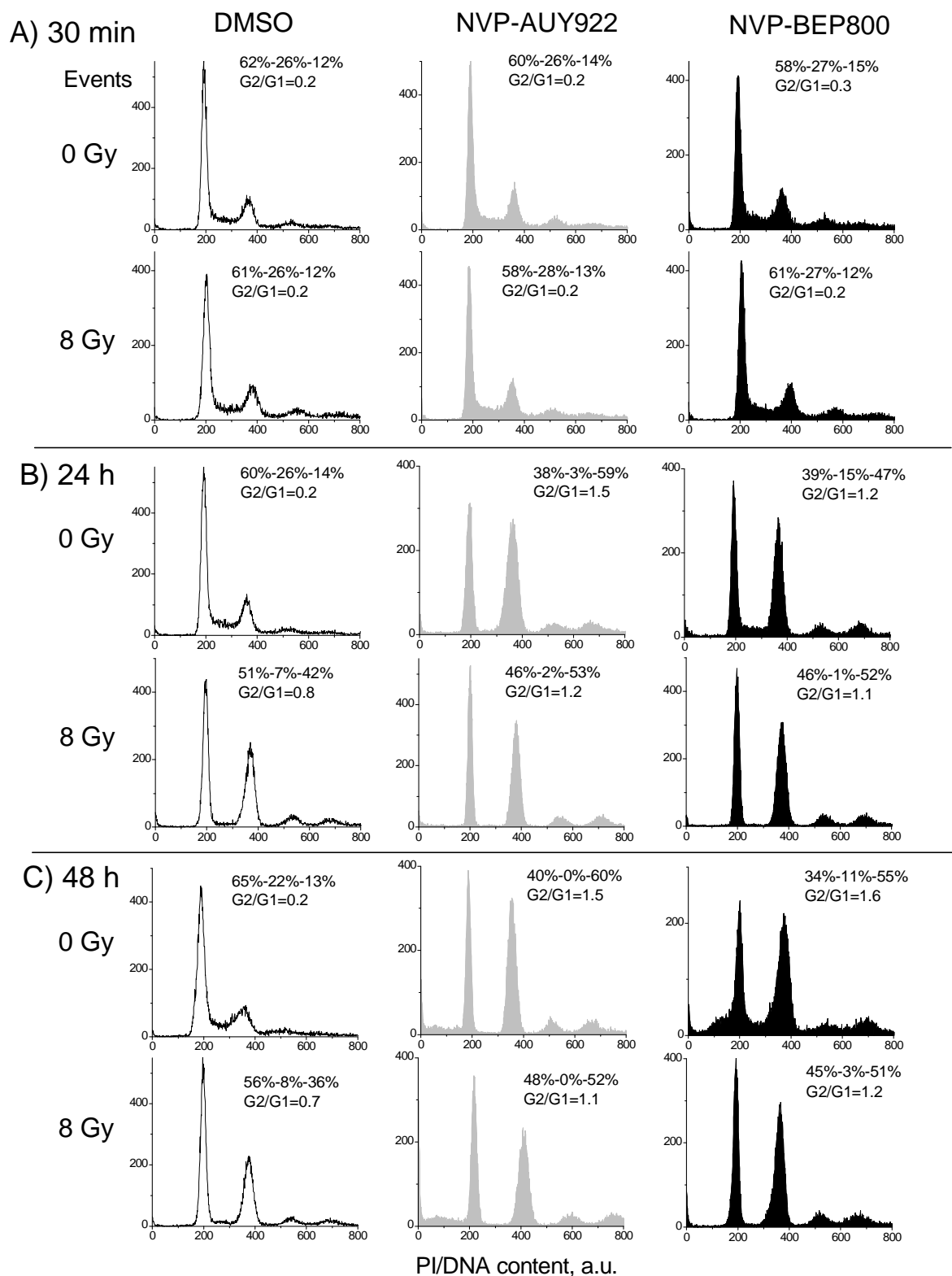
Figure 25. Cell cycle distribution of A549 cells treated with DMSO (unfilled histograms), NVP-AUY922 (gray histograms) or NVP-BEP800 (black histograms) and irradiated (8 Gy). Samples were fixed for staining 30 minutes (A), 24 hours (B) and 48 hours (C) post irradiation. The percentage of cells in each phase (G1%-S%-G2%) and G2/G1 ratio are shown (reproduced from Niewidok et al. 2012 with kind permission from Neoplasia Press).
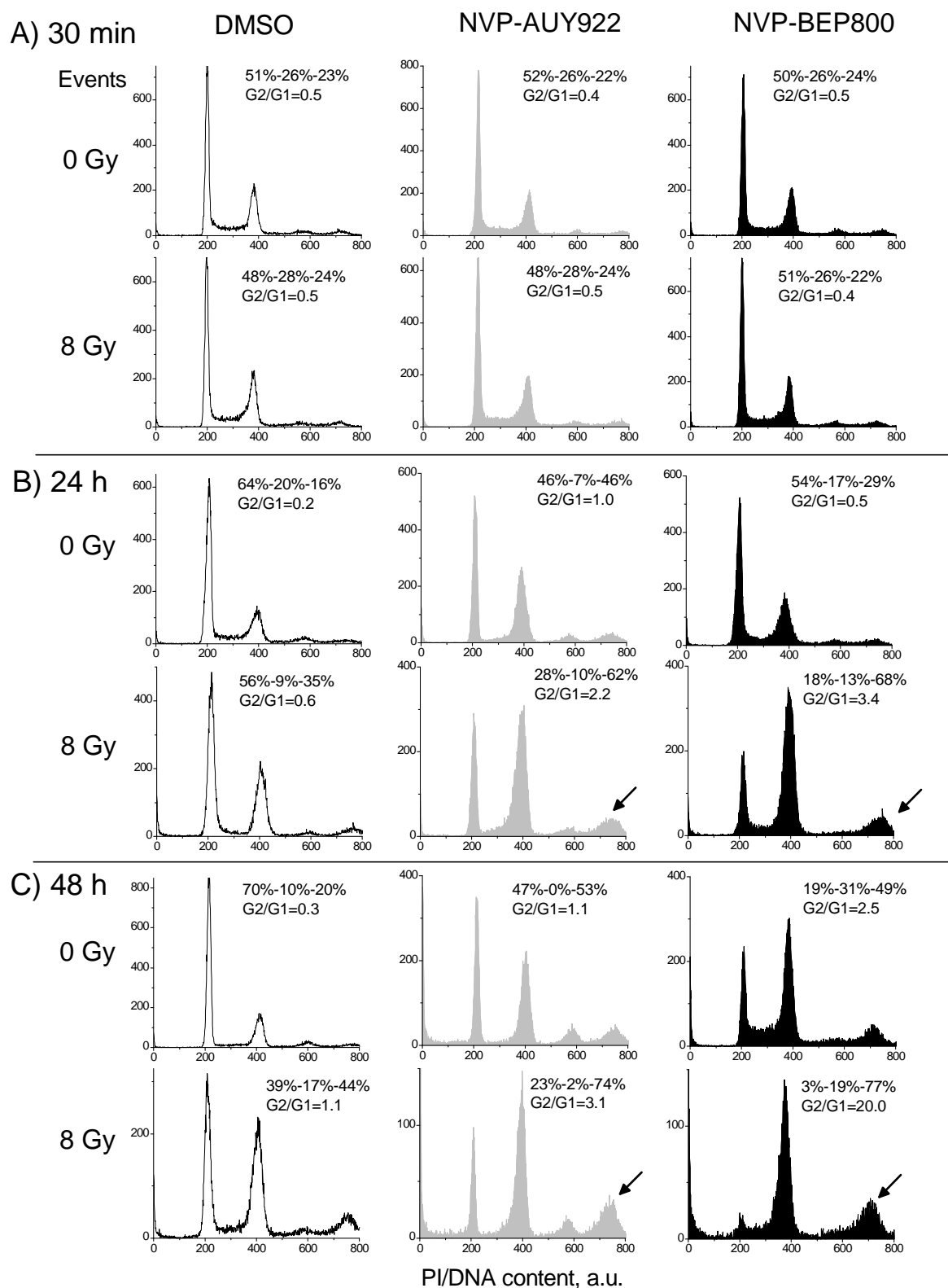
Figure 26. Cell cycle distribution of SNB19 cells treated with DMSO (unfilled histograms), NVP-AUY922 (gray histograms) or NVP-BEP800 (black histograms) and irradiated (8 Gy). Samples were fixed for staining 30 minutes (A), 24 hours (B) and 48 hours (C) post irradiation. The percentage of cells in each phase (G1%-S%-G2%) and G2/G1 ratio are shown. Arrows indicate polyploid cells (reproduced from Niewidok et al. 2012 with kind permission from Neoplasia Press).

Table 11. Cell cycle distribution in A549 cells detected 30 minutes (A), 24 hours (B) and 48 hours (C) after simultaneous drug-IR treatment. Data are presented as means (±SD) from at least three independent experiments (reproduced from Niewidok et al. 2012 with kind permission from Neoplasia Press).

Dose	Treatment	G0/G1, %	S, %	G2/M, %	G2/G1
A) 30 minutes post radiation					
0 Gy	DMSO	58±6	26±3	16±4	0.3
	NVP-AUY922	56±5	27±2	18±3	0.3
	NVP-BEP800	59±5	24±2	18±3	0.3
8 Gy	DMSO	56±6	26±3	18±4	0.3
	NVP-AUY922	58±6	26±3	16±3	0.3
	NVP-BEP800	60±5	25±3	16±2	0.3
B) 24 hours post radiation					
0 Gy	DMSO	58±1	32±2	10±1	0.2
	NVP-AUY922	42±8	7±3	52±11	1.2
	NVP-BEP800	48±7	21±6	31±12	0.6
8 Gy	DMSO	61±5	12±3	27±6	0.4
	NVP-AUY922	48±2	2±0	50±2	1.0
	NVP-BEP800	54±7	5±2	41±9	0.8
C) 48 hours post radiation					
0 Gy	DMSO	77±4	13±3	10±1	0.1
	NVP-AUY922	44±7	6±4	51±12	1.1
	NVP-BEP800	52±14	11±1	38±14	0.7
8 Gy	DMSO	70±5	5±1	25±5	0.4
	NVP-AUY922	48±2	2±2	50±3	1.0
	NVP-BEP800	50±9	5±1	44±9	1.1

Table 12. Cell cycle distribution in SNB19 cells detected 30 minutes (A), 24 hours (B) and 48 hours (C) after simultaneous drug-IR treatment. Data are presented as means (±SD) from at least three independent experiments (reproduced from Niewidok et al. 2012 with kind permission from Neoplasia Press).

Dose	Treatment	G0/G1, %	S, %	G2/M, %	G2/G1
A) 30 minutes post radiation					
0 Gy	DMSO	41±4	30±4	29±2	0.7
	NVP-AUY922	42±3	31±2	27±2	0.7
	NVP-BEP800	42±4	29±3	29±2	0.7
8 Gy	DMSO	39±4	30±3	30±2	0.8
	NVP-AUY922	40±5	31±4	28±3	0.7
	NVP-BEP800	43±3	30±4	26±2	0.6
B) 24 hours post radiation					
0 Gy	DMSO	55±4	24±2	21±2	0.4
	NVP-AUY922	34±3	11±1	54±2	1.4
	NVP-BEP800	48±2	15±1	36±2	0.7
8 Gy	DMSO	47±5	7±1	46±6	0.9
	NVP-AUY922	19±5	13±2	68±5	3.5
	NVP-BEP800	15±3	14±3	71±4	4.9
C) 48 hours post radiation					
0 Gy	DMSO	72±3	10±1	18±2	0.3
	NVP-AUY922	44±4	2±2	54±2	1.3
	NVP-BEP800	20±3	32±3	48±1	2.4
8 Gy	DMSO	38±5	16±0	45±5	1.3
	NVP-AUY922	20±5	5±1	74±5	4.6
	NVP-BEP800	5±1	20±1	74±2	14.2

The combination of NVP-AUY922 or NVP-BEP800 with irradiation did not affect the cell cycle distribution of A549 samples when compared with drug or IR alone. Interestingly, SNB19 responded with a significant increase in G2/M peak and a higher amount of cells with hyperdiploid DNA content after combined drug-IR treatment (Fig. 26B, C). The very high G2/M-to-G1 ratio (Table 12, G2/G1=14.2) of

NVP-BEP800-treated and irradiated SNB19 cells suggested an additive effect of combined treatment (Fig. 26B, C).

4.1.6 Influence of Hsp90 inhibition and IR on the expression of cell cycle-related proteins in tumor cell lines A549 and SNB19

Among Hsp90 clients are proteins regulating the progression of the cell cycle, therefore we analyzed the expression of several marker proteins including Cdk1, Cdk4 and pRb (Figs. 27, 28).
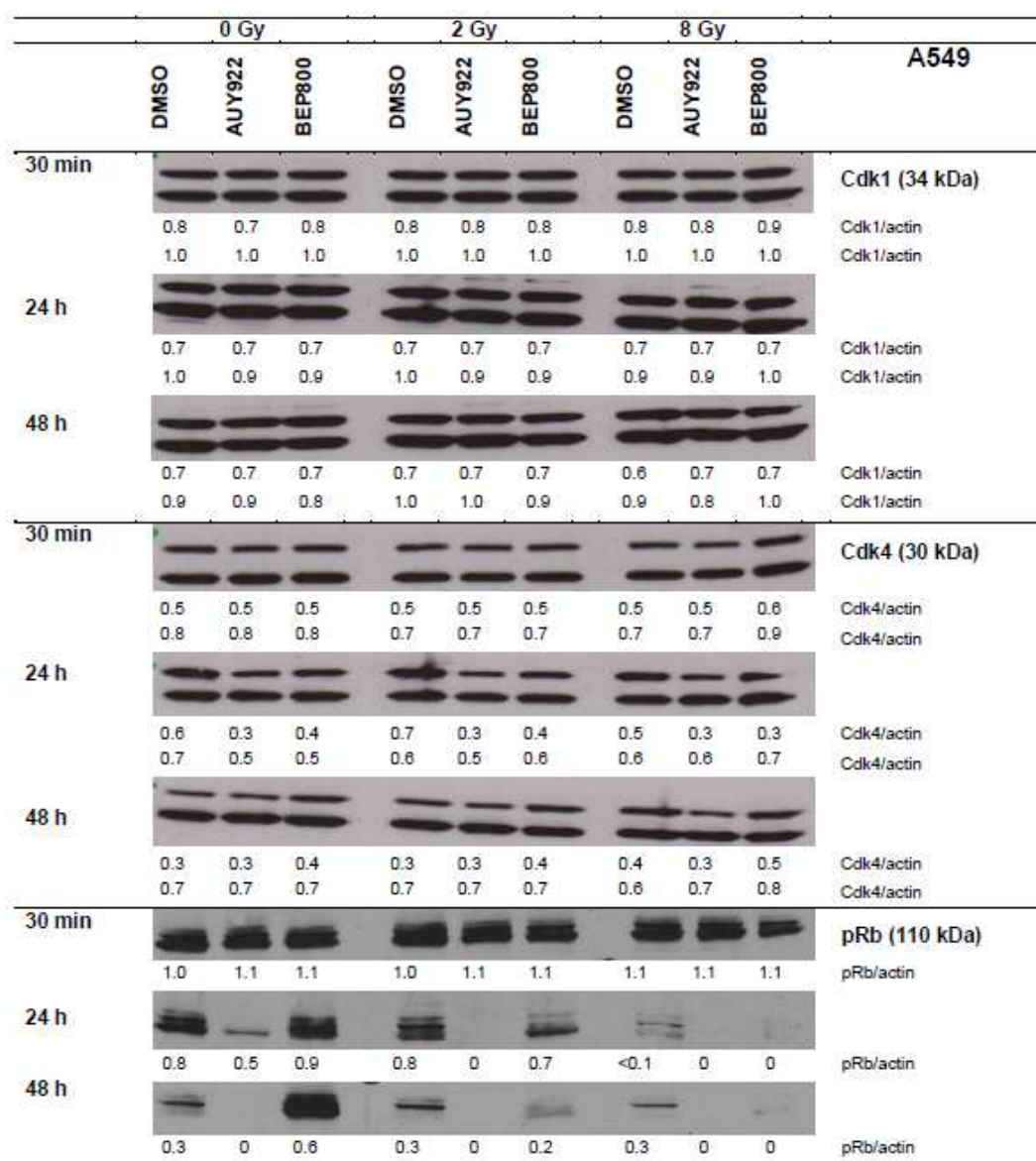
Figure 27. Expression of Cdk1, Cdk4 and pRb in A549 cells. Samples were treated with DMSO, NVP-AUY922 or NVP-BEP800 and irradiated (with 2 or 8 Gy). Each protein band was normalized to β-actin and the ratios are given in numbers (reproduced from Niewidok et al. 2012 with kind permission from Neoplasia Press).

- 67 -
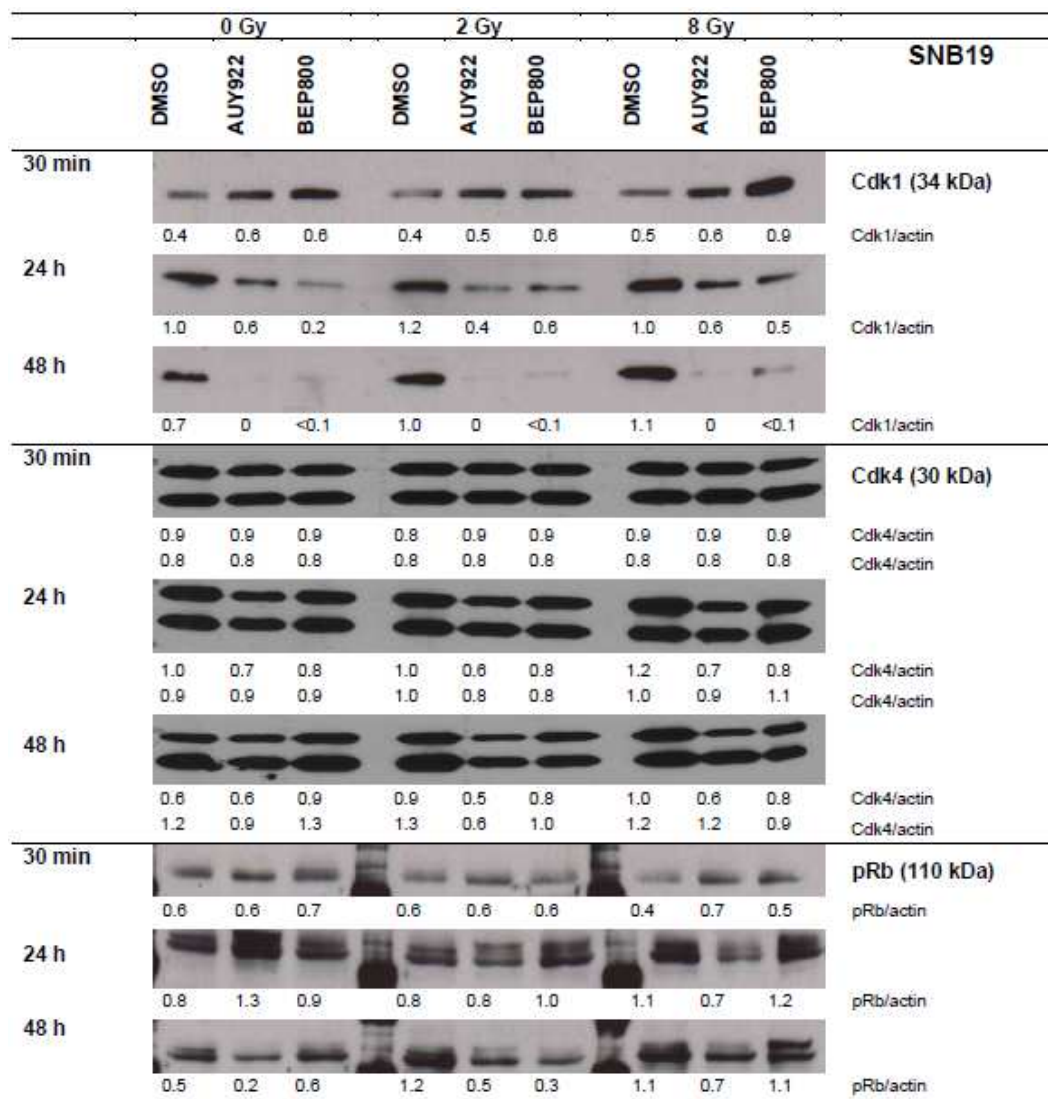
Figure 28. Expression of Cdk1, Cdk4 and pRb in SNB19 cells. Samples were treated with DMSO, NVP-AUY922 or NVP-BEP800 and irradiated (with 2 or 8 Gy). Each protein band was normalized to β-actin and the ratios are given in numbers (reproduced from Niewidok et al. 2012 with kind permission from Neoplasia Press).

Irradiation alone triggered a significant decrease in the level of pRb 24 hours after IR (0.8 -> 0.1 a.u.), but did not influence the expression of cyclin-dependent kinases in lung carcinoma cells (Fig. 27). Twenty-four-hour treatment of A549 with NVP-AUY922 or NVP-BEP800 alone induced the down-regulation of Cdk4 (0.6 -> 0.3 a.u.) and pRb (0.8 -> 0.5 a.u.), but not Cdk1. In SNB19, pRb (0.5 -> 0.2 a.u.) and Cdk4 (1.0 -> 0.7 a.u.) were also down-regulated (Fig. 28), but to a lesser extent than in A549 cells. In contrast, the Hsp90 inhibitors caused the depletion of Cdk1 (0.7 -> 0 a.u.) in SNB19 cells. The combined drug-IR treatment induced no additional changes in the expression of chosen cell cycle-related proteins in comparison to drug treatment alone (Figs. 27, 28).

To summarize, data presented in chapter 4.1 showed that simultaneous Hsp90 inhibition and ionizing radiation may induce radiosensitization or cytotoxicity, depending on the cell type. These results confirmed the importance of time schedule when the Hsp90 inhibition is combined with radiation therapy. A short 30-minute exposure to each Hsp90 inhibitor did not affect the radiosensitivity of the examined A549 and SNB19 cells. Longer incubation enhanced the radiation response of glioblastoma SNB19 cells, which correlated with an increased amount of DNA damage, impairment of DNA damage repair and massive cell cycle alterations. For lung carcinoma A549 cells the combined drug-IR treatment was highly cytotoxic. Furthermore, we observed the depletion of Hsp90 clients Akt and Raf-1 in both cell lines examined, and, additionally, survivin in A549. We analyzed the expression of potential oncoproteins, including p53, k-RAS and PTEN, regulating the response of the two lines tested.

We have shown that NVP-AUY922 and NVP-BEP800 are potent agents that, in combination with radiation, enhanced the killing of cancer cells *in vitro* (Stingl et al. 2010, Djuzenova et al. 2012, Niewidok et al. 2012). These results prompted us to further investigate the effects of NVP-AUY922 and NVP-BEP800 on non-malignant cells, which will be described in chapter 4.2. In the last chapter (4.3) we have evaluated whether Hsp70 pre-silencing could increase the radiosensitizing potential of Hsp90 inhibitor NVP-AUY922.

4.2 Effects of NVP-AUY922 and NVP-BEP800 on the radiation response of normal skin fibroblast strains HFib1 and HFib2

In chapter 4.1 we have shown that Hsp90 inhibition in cancer cells leads to the impairment of multiple signaling pathways and, in combination with irradiation induces tumor cell killing. Success of Hsp90 inhibition as a multi-target therapy depends on the selectivity of the drug towards tumor cells over non-malignant cells. Until now, the activity of NVP-AUY922 and NVP-BEP800 has not been tested in non-malignant tissues. In the second experimental chapter we added either NVP-AUY922 or NVP-BEP800 shortly before irradiation to the normal human skin fibroblast strains HFib1 and HFib2. Exposure to the drug lasted up to 48 hours after radiation, and the cellular response of HFib1 and HFib2 to drug only, IR only or combined drug-IR treatment was analyzed. The schedule of the experiments was identical with that previously described for tumor cell lines A549 and SNB19 (Fig. 11B).

4.2.1 Cytotoxicity of Hsp90 inhibitors to fibroblast cell lines

Firstly, we tested the cytotoxic potential of NVP-AUY922 and NVP-BEP800 on non-irradiated HFib1 and HFib2 fibroblast strains. Cells were treated with either Hsp90 inhibitor over a concentration range from 5 nM to 1 µM for 24 and 48 hours. The cell viability was determined based on cellular ATP levels (as described in section 3.2.4), which were normalized against DMSO-treated cells and are shown in Figure 29.
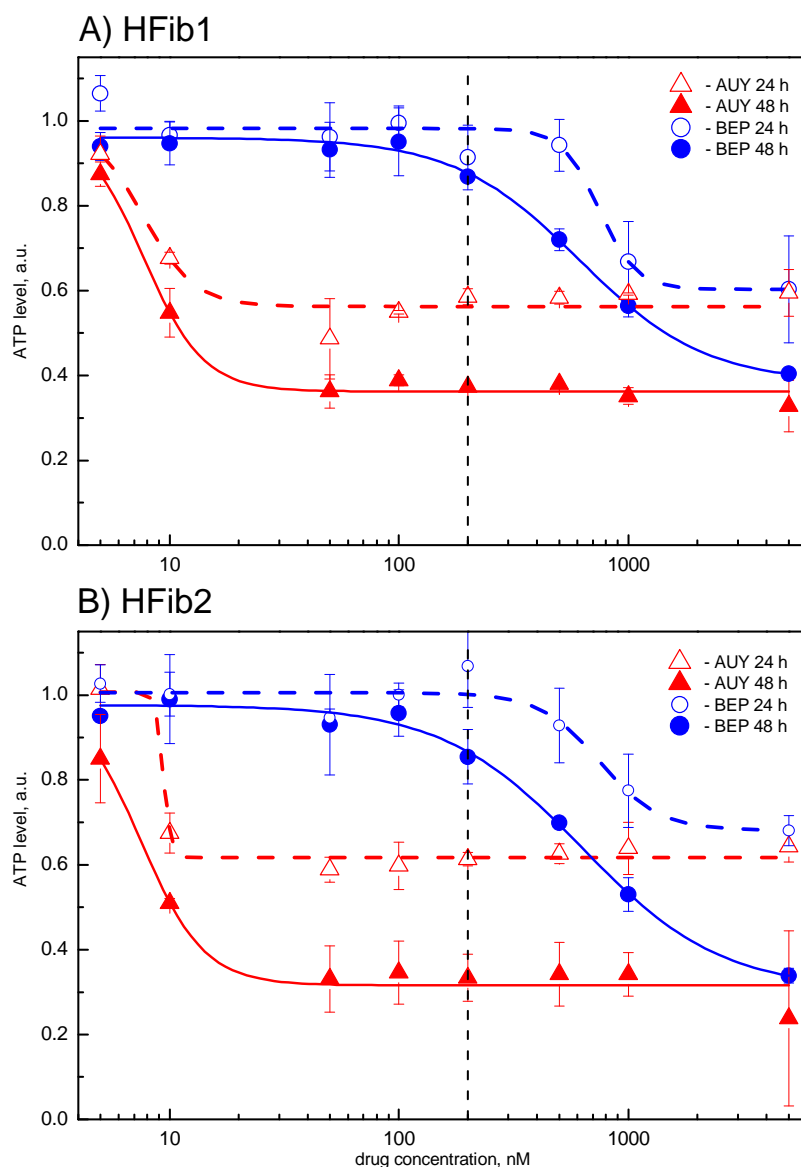
Figure 29. Changes of intracellular ATP levels in HFib1 (A) and HFib2 (B) cell lines. Samples were treated with serial dilutions of NVP-AUY922 (red triangles) and NVP-BEP800 (blue circles) for 24 or 48 hours (open and filled symbols respectively). Data from at least three experiments were averaged and normalized against DMSO-treated controls. ATP levels (±SE) are given as a percentage to the corresponding controls. The vertical, dashed line indicates the concentration of 200 nM, which was used for further experiments.

NVP-AUY922 was more cytotoxic to both examined fibroblast strains than NVP-BEP800 (Fig. 29). Twenty-four-hour incubation with NVP-AUY922 at small concentrations (5-50 nM) decreased the cell viability to ~0.6 a.u. in HFib1 and HFib2 cells (Fig. 29). Further increase of NVP-AUY922 concentration (100-5000 nM) did not affect the ATP content in either strain examined. Twenty-four-hour exposure to NVP-BEP800 (concentration range 5-200 nM) did not influence the cell viability of HFib1

and HFib2 cells. Increasing the concentration to 500 nM NVP-BEP800 resulted in the diminishing of ATP levels in HFib1 and HFib2 strains, reaching ~0.6 a.u. for the highest used concentration (5000 nM).

Further incubation (48 hours) with NVP-AUY922 reduced the ATP levels in fibroblast strains, reaching ~0.3-0.4 a.u. already at 50 nM concentration and remaining at this level with the increasing concentration (Fig. 29). In the case of NVP-BEP800, small concentrations (5-100 nM) of Hsp90 inhibitor caused only moderate reduction of ATP content, to ~0.9 a.u. The further increase of NVP-BEP800 concentration led to the decrease of viability of HFib1 to ~0.4 a.u. and of HFib2 to ~0.3 a.u. (Fig. 29; 48-hour incubation, 5000 nM).

For further experiments, the working concentration of 200 nM of each Hsp90 inhibitor was chosen (Fig. 29). Incubation with 200 nM NVP-AUY922 led to the decrease of HFib1 and HFib2 cell viability to ~0.6 a.u. (24 hours) and ~0.3-0.4 a.u. (48 hours). Twenty-four-hour exposure to 200 nM NVP-BEP did not influence the ATP levels of examined fibroblast strains. Longer incubation with 200 nM NVP-BEP800 resulted in decrease of HFib1 and HFib2 cell viability to ~0.9 a.u.

4.2.2 Colony survival of irradiated normal human fibroblast strains HFib1 and HFib2 after treatment with NVP-AUY922 and NVP-BEP800

To determine the radiation response of HFib1 and HFib2 cell strains, the samples were treated with either NVP-AUY922 or NVP-BEP800 (200 nM), irradiated one hour later and seeded out for colony-forming assay 30 minutes, 24 and 48 hours post IR. Figure 30 shows the representative normalized survival response of HFib1 cells compared with glioblastoma cell line SNB19, tested in the chapter 4.1. The colony survival assay of HFib1 and HFib2 cell lines was repeated at least three times and the following parameters were calculated with the linear quadratic (LQ) model: PE, SF2, D_{10} and IF_{10} (Table 13).
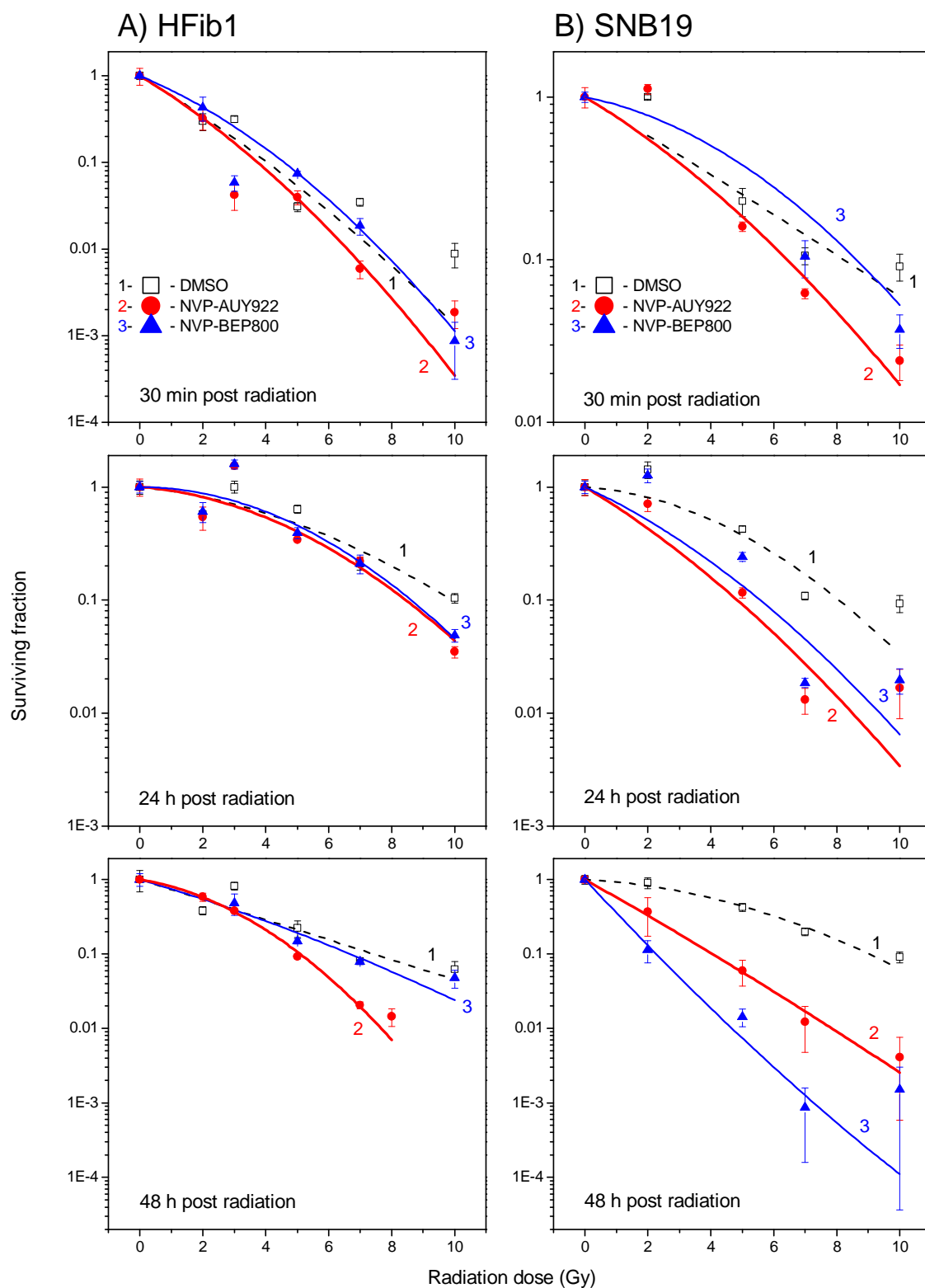
Figure 30. Representative clonogenic survival of HFib1 (A) and SNB19 (B) cell lines. Cells were treated with DMSO (squares), NVP-AUY922 (red circles) or NVP-BEP800 (blue triangles), irradiated one hour later with single dose and plated for colony-forming assay at indicated time point. After staining and scoring the colonies, cell survival curves were generated. Detailed data for SNB19 cells are presented in section 4.1.2. The experiment was repeated at least three times.

Table 13. Plating efficiencies and radiosensitivity parameters[a] of drug-treated and irradiated fibroblast strains HFib1 and HFib2.

	PE	SF2 [b]	D_{10} [c] (Gy)	IF_{10} [d]
HFib1				
30 minutes post radiation				
DMSO	0.06±0.05	0.29±0.1	3.6	1.0
NVP-AUY922	0.06±0.04	0.29±0.1	3.6	1.0
NVP-BEP800	0.04±0.03	0.45±0.02	4.6	0.8
24 hours post radiation				
DMSO	0.03±0.01	0.68±0.2	7.3	1.0
NVP-AUY922	0.02±0.01	0.62±0.1	6.4	1.1
NVP-BEP800	0.03±0.01	0.62±0.2	6.4	1.1
48 hours post radiation				
DMSO	0.02±0.02	0.61±0.3	6.0	1.0
NVP-AUY922	0.02±0.01	0.52±0.2	5.1	1.4
NVP-BEP800	0.02±0.01	0.51±0.1	6.6	0.8
HFib2				
30 minutes post radiation				
DMSO	0.05±0.01	0.43±0.3	4.2	1.0
NVP-AUY922	0.04±0.01	0.37±0.3	3.7	1.1
NVP-BEP800	0.06±0.02	0.60±0.2	4.9	0.9
24 hours post radiation				
DMSO	0.02±0.01	0.76±0.1	7.1	1.0
NVP-AUY922	0.03±0.02	0.42±0.1	5.1	1.3
NVP-BEP800	0.02±0.01	0.65±0.2	6.8	1.0
48 hours post radiation				
DMSO	0.04±0.02	0.58±0.1	6.5	1.0
NVP-AUY922	0.03±0.02	0.69±0.1	5.5	1.3
NVP-BEP800	0.03±0.01	0.61±0.2	7.4	1.0

[a] Mean (±SD) from at least three independent experiments
[b] SF2 is the surviving fraction at 2 Gy
[c] D_{10} is the radiation dose resulting in 10% cell survival
[d] IF_{10} was calculated as $(D_{10\ control})/(D_{10\ inhibitor})$

As seen in Figure 30, the radiation response of drug-treated fibroblasts differed strongly from the response of malignant SNB19 cells. Glioblastoma cells were sensitized to irradiation 24 and 48 hours after NVP-AUY922 as well as after NVP-BEP800 treatment (Fig. 30B). Forty-eight-hour exposure to NVP-BEP800 induced stronger radiosensitization in SNB19 cells than exposure to NVP-AUY922 (for details see section 4.1.2).

In contrast to previously described tumor cell lines (4.1.2, Table 10), the plating efficiency of non-irradiated and drug-treated fibroblast strains did not change (Table 13). After 48-hour incubation, the PE of HFib1 cells sustained at ~0.02, independently from the applied Hsp90 inhibitor. In the case of HFib2 cell line, 48 hours treatment with NVP-AUY922 and NVP-BEP800 resulted in the decrease of PE from ~0.04 to ~0.03 (Table 13). Plating efficiency of glioblastoma cells diminished 2- to 3-fold 48 hours after treatment with either Hsp90 inhibitor (Table 10).

Thirty-minute and twenty-four-hour exposure to either Hsp90 inhibitor did not affect the dose-response curves of the examined fibroblast strains (Fig. 30A). Accordingly, the calculated values of SF2 or D_{10} were similar to the corresponding DMSO-treated controls. Forty eight hours after NVP-AUY922-IR treatment, HFib1 (Fig. 30A) and HFib2 cells were moderately sensitized to irradiation. The D_{10} value decreased from ~6.0 to ~5.1 for HFib1 cells and from ~6.5 to ~5.5 for HFib2 respectively (Table 13). On the contrary, 48 hours incubation of fibroblasts after NVP-BEP800-IR treatment induced some resistance to IR as indicated by the increased D_{10} values from ~6.0 to ~6.6 and from ~6.5 to ~7.4 in HFib1 and HFib2 respectively (Table 13).

The findings presented in Figure 30 and Table 13 showed that the novel Hsp90 inhibitors NVP-AUY922 and NVP-BEP800 more strongly radiosensitized malignant cells compared with normal tissue. Next, we explored the possible mechanism(s) for this drug selectivity.

4.2.3 Influence of Hsp90 inhibition and IR on the expression of Hsp90 clients and apoptotic marker proteins in fibroblasts

The expression of Hsp90, Hsp70, and several marker proteins involved in the regulation of proliferative and apoptotic pathways (Akt, pAkt, Raf-1, survivin, PARP, caspase 3 and Bcl-xL) in drug-treated and irradiated HFib1 and HFib2 cells was

analyzed. Protein expression was quantified by the protein/actin ratios given in arbitrary units and the representative results are shown in Figures 31-34.
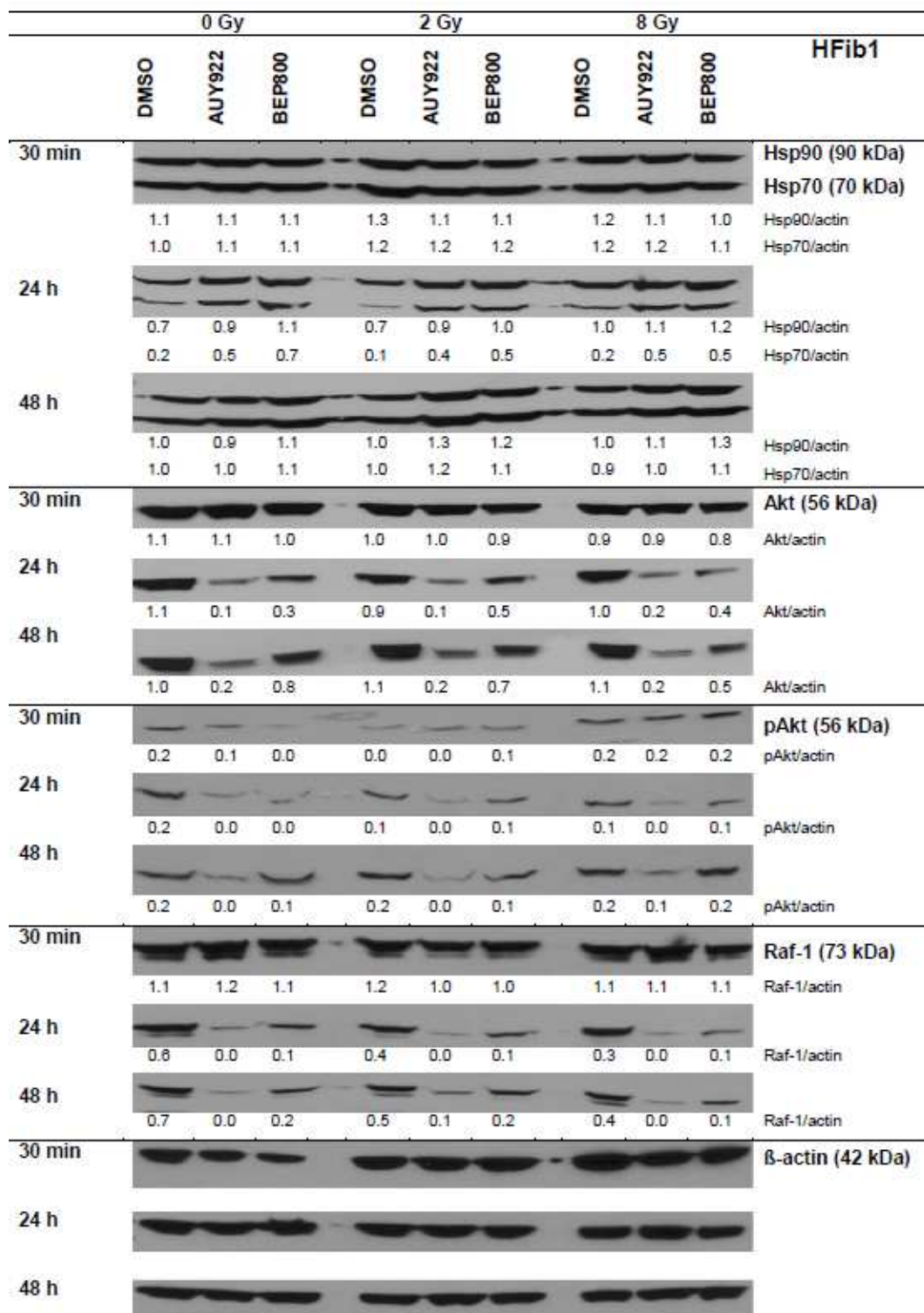
Figure 31. Expression of Hsp90, Hsp70, Akt, pAkt and Raf-1 in HFib1 cells. Samples were treated with DMSO, NVP-AUY922 or NVP-BEP800 and irradiated (with 2 or 8 Gy). Each protein band was normalized to β-actin and the ratios are given in numbers.
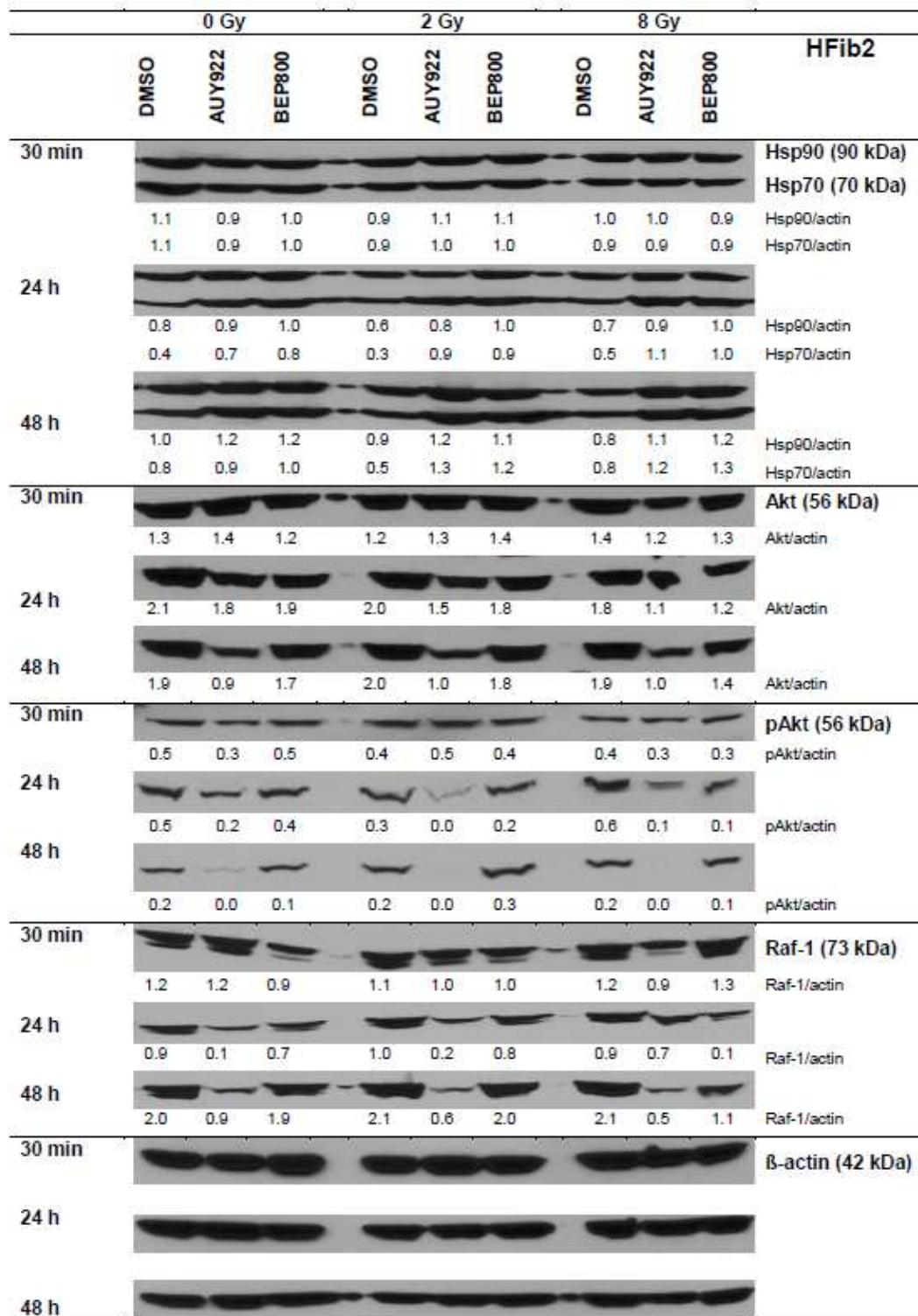
Figure 32. Expression of Hsp90, Hsp70, Akt, pAkt and Raf-1 in HFib2 cells. Samples were treated with DMSO, NVP-AUY922 or NVP-BEP800 and irradiated (with 2 or 8 Gy). Each protein band was normalized to β-actin and the ratios are given in numbers.

A thirty-minute exposure to either NVP-AUY922 or NVP-BEP800 alone did not affect the expression of chosen proteins in examined fibroblast strains (Figs. 31-34).

Further incubation (24 and 48 hours) up-regulated the expression of heat shock proteins in HFib1 cells, i.e. 24 hours after NVP-AUY922 treatment from 0.7 to 0.9 a.u. for Hsp90 and from 0.2 to 0.5 a.u. for Hsp70 respectively (Fig. 31).
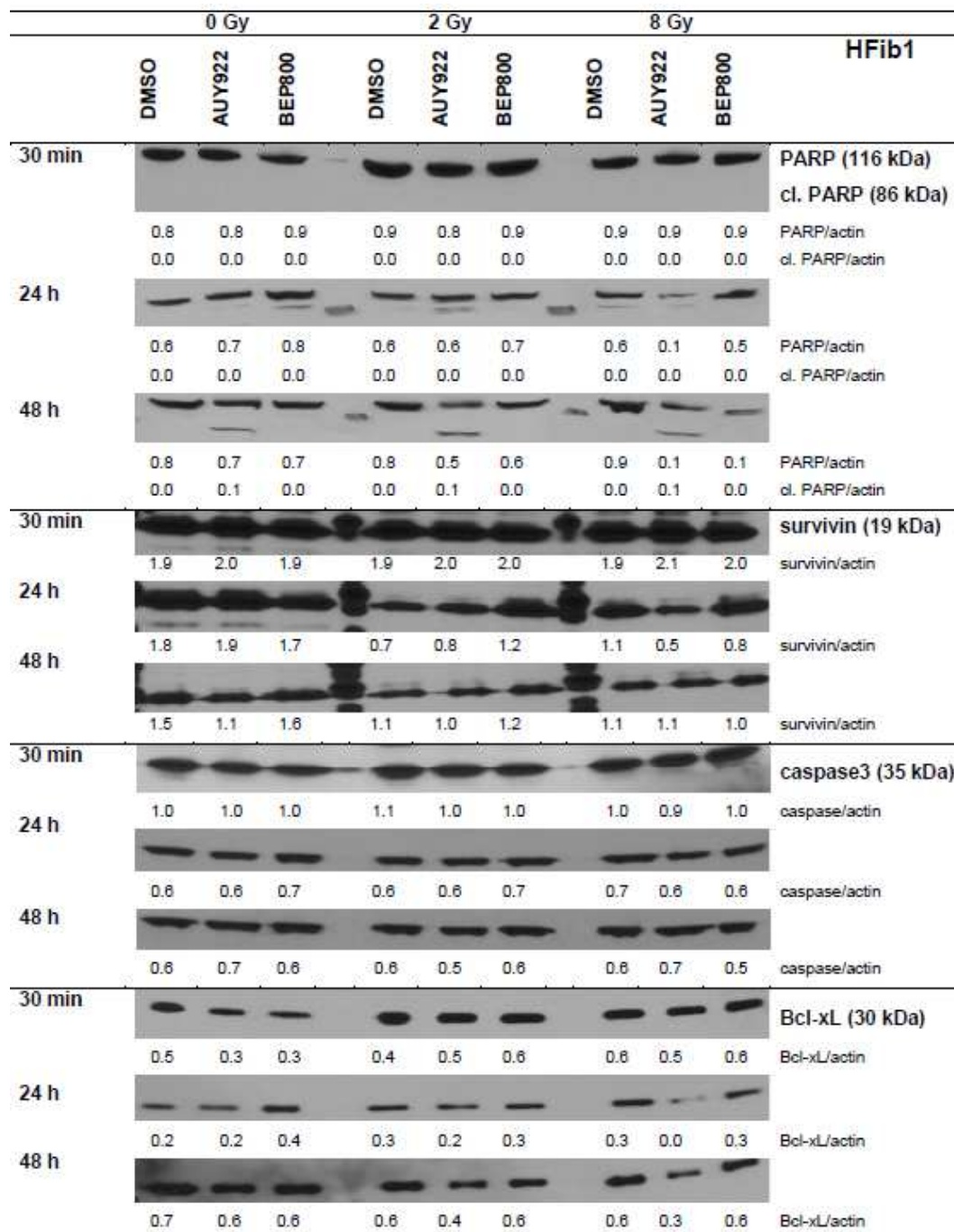
Figure 33. Expression of PARP, cleaved PARP, survivin, caspase 3 and Bcl-xL in HFib1 cells. Samples were treated with DMSO, NVP-AUY922 or NVP-BEP800 and irradiated (with 2 or 8 Gy). Each protein band was normalized to β-actin and the ratios are given in numbers.
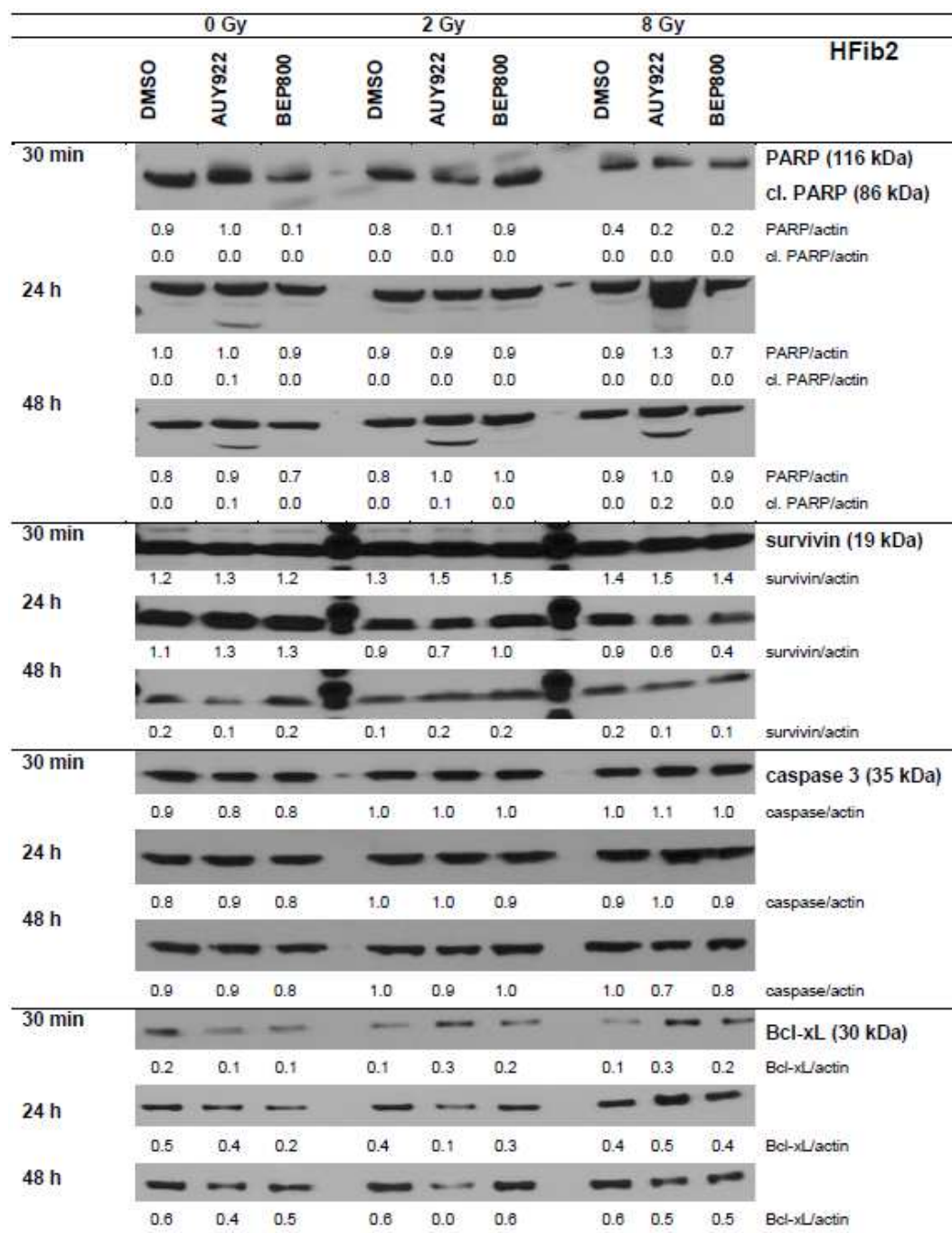
Figure 34. Expression of PARP, cleaved PARP, survivin, caspase 3 and Bcl-xL in HFib2 cells. Samples were treated with DMSO, NVP-AUY922 or NVP-BEP800 and irradiated (with 2 or 8 Gy). Each protein band was normalized to β-actin and the ratios are given in numbers.

The over-expression of heat shock proteins was also observed in HFib2 cells (i.e. Fig. 32, 24 hours post NVP-AUY922 treatment, Hsp90: from 0.8 to 0.9 a.u., Hsp70: from 0.4 to 0.7 a.u.). After twenty-four-hour incubation with NVP-AUY922 we detected the down-regulation of Akt (HFib1: 1.1 -> 0.1 a.u., HFib2: 2.1 -> 1.8 a.u.), pAkt (HFib1: 0.2 -> 0.0 a.u., HFib2: 0.5 -> 0.2 a.u.) and Raf-1 (HFib1: 0.6 -> 0.0 a.u.,

HFib2: 0.9 -> 0.1 a.u.) in both fibroblast strains (Figs. 31, 32). Depletion of these Hsp90 clients (Akt, pAkt and Raf-1) was sustained 48 hours post NVP-AUY922 treatment. Another Hsp90 client, survivin, was down-regulated 48 hours after NVP-AUY922 treatment in both examined fibroblast strains (Figs. 31, 32; HFib1: 1.5 -> 1.1 a.u., HFib2: 0.2 -> 0.1 a.u.). In addition, 48-hour incubation with NVP-AUY922 induced the cleavage of PARP in HFib1 and HFib2 cells (Figs. 33, 34) which may be a sign of ongoing apoptosis.

The exposure of HFib1 and HFib2 to NVP-BEP800 for 24 and 48 hours led to the down-regulation of several marker proteins (Figs. 31, 32). For example, after 24 hours incubation, the Akt level decreased from 1.1 to 0.3 a.u. in HFib1 and from 2.1 to 1.9 a.u. in HFib2 samples. Twenty-four-hour treatment with NVP-BEP800 resulted in complete depletion of pAkt in HFib1 cells (Fig. 31), whereas it had no impact on this protein in HFib2 samples (Fig. 32). At the same time point, Raf-1 was down-regulated in both fibroblast strains (HFib1: 0.6 -> 0.1 a.u., HFib2: 0.9 -> 0.7 a.u.). The expression of survivin remained unchanged independently from the duration of NVP-BEP800 treatment (Figs. 33, 34).

As evident from Figures 31-34, thirty-minute incubation after irradiation alone (2 or 8 Gy) did not induce alterations in the expression of examined marker proteins in HFib1 cells. In contrast, in HFib2 samples the expression of PARP (0.9 -> 0.5 a.u.) and Bcl-xL (0.2 -> 0.1 a.u.) decreased (Fig. 34, 30 minutes post IR). Prolonging the incubation to 24 hours after irradiation in both fibroblast strains decreased the expression of survivin (Figs. 33, 34; 24 hours post IR). Additionally, in irradiated HFib1 cells we detected increase in the expression of Bcl-xL (Fig. 33, 24 hours post IR, 0.2 -> 0.4 a.u.).

The combination of Hsp90 inhibition with ionizing radiation (2 or 8 Gy) induced no additional changes in the protein expression in comparison to these observed after Hsp90 inhibition alone (Figs. 31-34). The only exception was the down-regulation of the pro-survival protein Bcl-xL 24 and 48 hours post NVP-AUY922-IR treatment in both examined fibroblast strains (Figs. 32, 33), indicating the activation of pathway leading to cell death. However, the expression of caspase 3 remained unchanged, independent from applied drug and IR treatment (Figs. 32, 33).

4.2.4. Effects of Hsp90 inhibitors and irradiation on the induction and repair of DNA damage in HFib1 and HFib2 cells

As the next step, we evaluated the induction and repair kinetics of DNA double strand breaks measured by the expression of histone γH2AX in human skin fibroblasts HFib1 and HFib2 after a combination of Hsp90 inhibition and IR. Cell samples were fixed at different time points (0.5, 24, 48 hours after IR) and stained with anti-γH2AX antibody as described in section 3.2.9. Representative histograms are shown in Figure 35.

The background γH2AX expression was at a similar level in examined fibroblast strains, 60 a.u. and 64 a.u. in HFib1 and HFib2 respectively (Fig. 35). Application of NVP-AUY922 or NVP-BEP800 alone on HFib1 and HFib2 cells for 30 minutes induced no changes in γH2AX expression (Fig. 35, gray histograms). In HFib2 samples incubated with NVP-AUY922 for 24 hours we observed an increase of γH2AX expression from 49 to 68 a.u. Forty eight hours exposure of fibroblasts to NVP-AUY922 led to the accumulation of DNA DSBs (HFib1 from 50 to 75 a.u., HFib2 from 66 to 163 a.u.). In addition, we observed an increase of events with low γH2AX expression (~5-6 a.u.) in both fibroblasts strains examined (Fig. 35, 48 hours after NVP-AUY922 treatment). Presumably this was cell debris with defragmented DNA, coming from cells going through apoptosis.

Irradiation alone (8 Gy) resulted in an increase of γH2AX expression in HFib1 from 60 to 105 a.u., in HFib2 from 64 to 126 a.u. compared to non-irradiated controls (Fig. 35, 30 minutes, black histograms). Measurements at 24 and 48 hours after IR alone showed that the amount of irradiation-induced DNA DSBs returned to background level, indicating that the DNA damage repair took place.
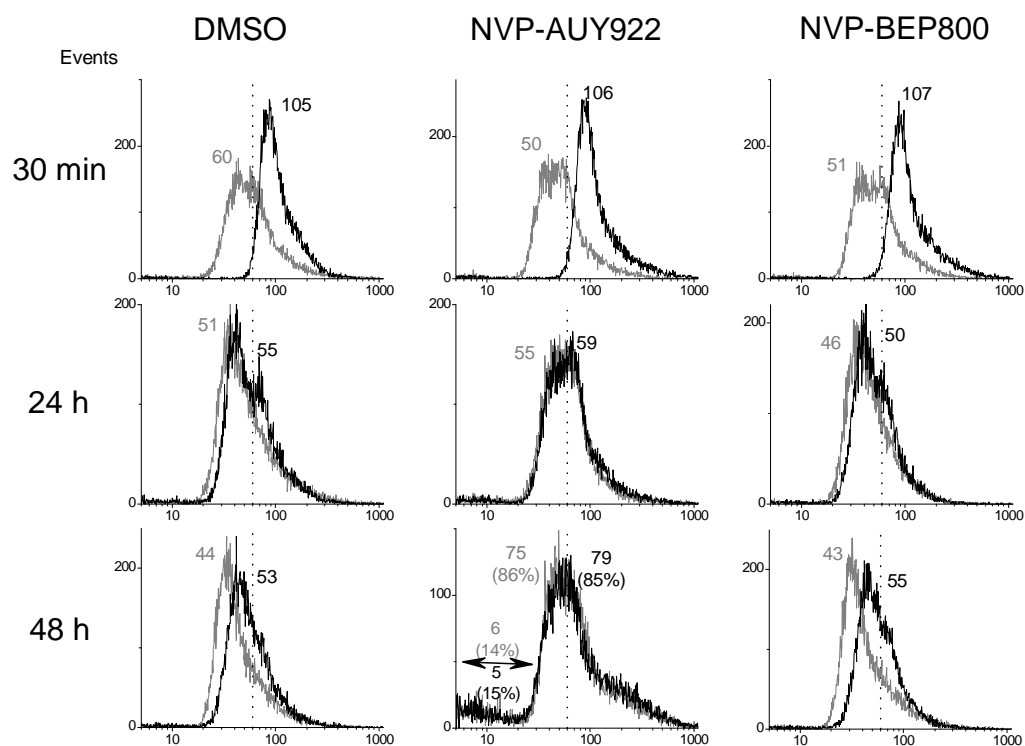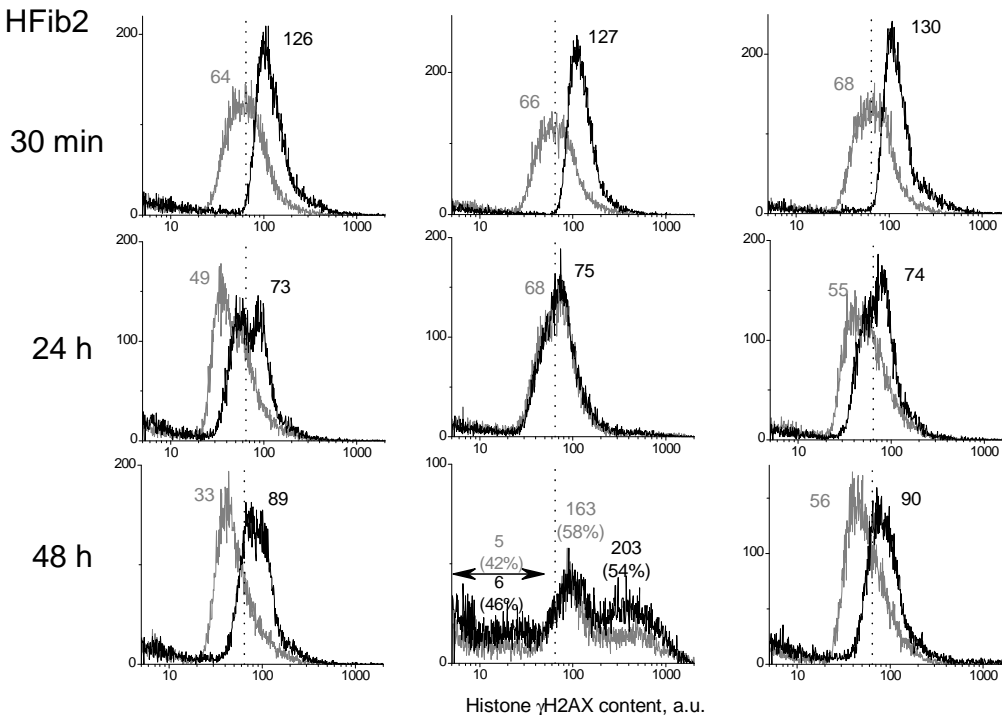
Figure 35. Histograms showing distribution of γH2AX, as a marker of DNA double strand breaks, in HFib1 (A) and HFib2 (B) cells. DMSO-treated controls and samples treated with NVP-AUY922 or NVP-BEP800 were irradiated with single dose (8 Gy, black histograms) and incubated in drug-containing medium for indicated time. Gray histograms represent corresponding non-irradiated samples. Numbers denote the mean γH2AX expression for the respective cell sample. The vertical, dashed line marks the γH2AX value of DMSO-treated, non-irradiated control.

Thirty minutes after combined drug-IR treatment (either with NVP-AUY922 or NVP-BEP800) we observed no additional DNA damage when compared with irradiated controls (Fig. 35). Twenty four hours later in both HFib1 and HFib2 cell lines the amount of DNA DSBs induced by drug-IR treatment decreased (HFib1: 106 -> 59 a.u., HFib2: 127 -> 75 a.u. for NVP-AUY922-IR; HFib1: 107 -> 50 a.u., HFib2: 130 -> 74 a.u. for NVP-BEP800-IR). Prolonging the incubation after NVP-BEP800-IR treatment to 48 hours did not further affect the amount of DNA damage in either examined fibroblast strain (Fig. 35). In contrast, 48-hour incubation of NVP-AUY922-treated and irradiated HFib1 cells led to an increase of γH2AX expression, in the same way as after drug treatment alone (to 79 a.u.). In HFib2 samples the combination of NVP-AUY922 and IR resulted in the accumulation of DNA DSBs to ~203 a.u. as compared with ~163 a.u. for non-irradiated controls (Fig. 35B, 48 hours after NVP-AUY922-IR).

4.2.5 Changes in the cell cycle progression of fibroblast strains HFib1 and HFib2 after Hsp90 inhibition and irradiation

Cell probes analyzed for γH2AX expression were counterstained with propidium iodide to examine the cell cycle progression (according to protocol in section 3.2.9). The representative cell cycle distributions of drug-treated and irradiated HFib1 and HFib2 cells 30 minutes, 24 and 48 hours after treatment are shown in Figures 36 and 37. The statistical summary is presented in Tables 14 and 15.
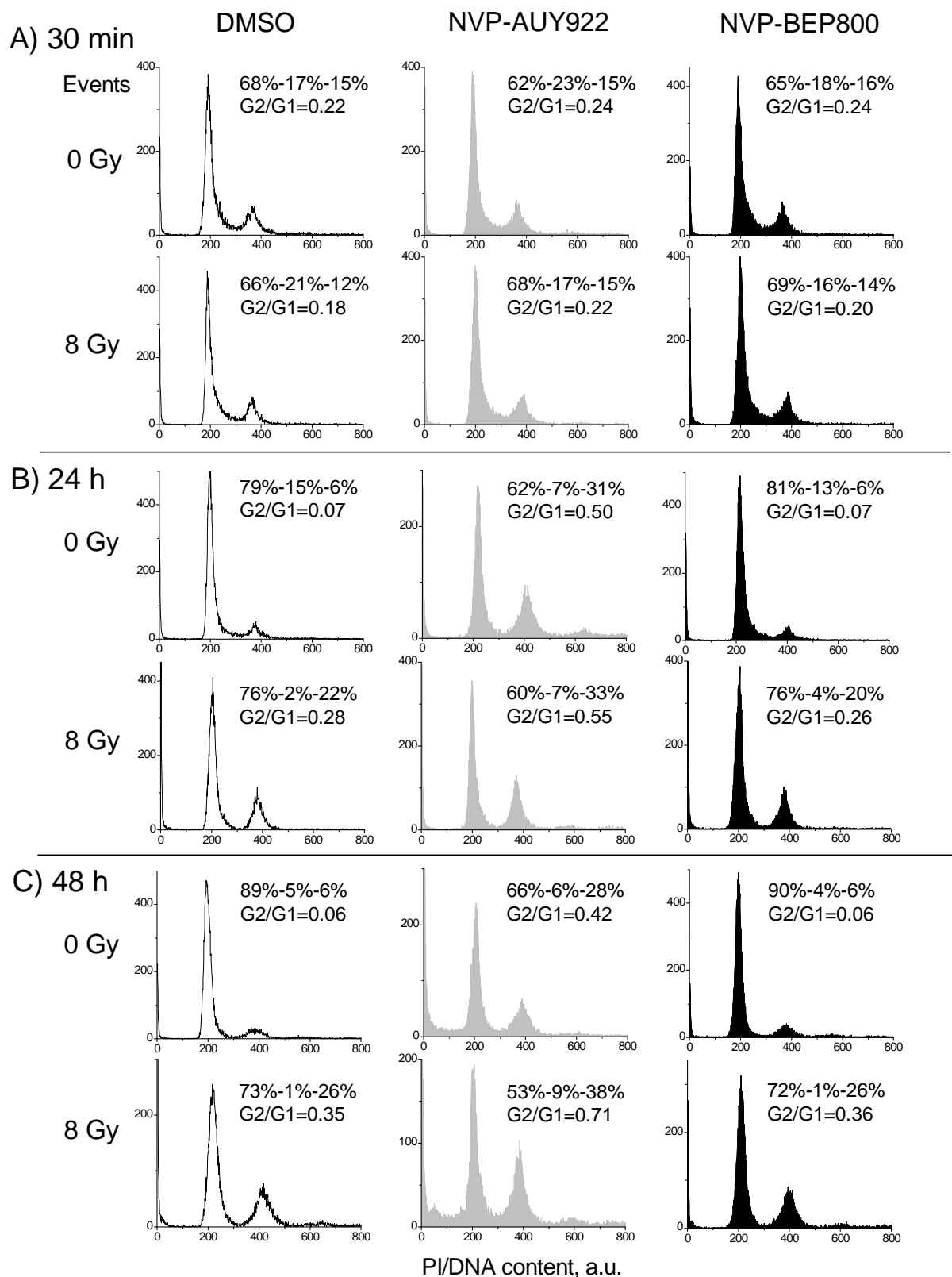
Figure 36. Cell cycle distribution of HFib1 cells treated with DMSO (unfilled histograms), NVP-AUY922 (gray histograms) or NVP-BEP800 (black histograms) and irradiated (8 Gy). Samples were fixed for staining 30 minutes (A), 24 hours (B) and 48 hours (C) post irradiation. The percentage of cells in each phase (G1%-S%-G2%) and G2/G1 ratio are shown.
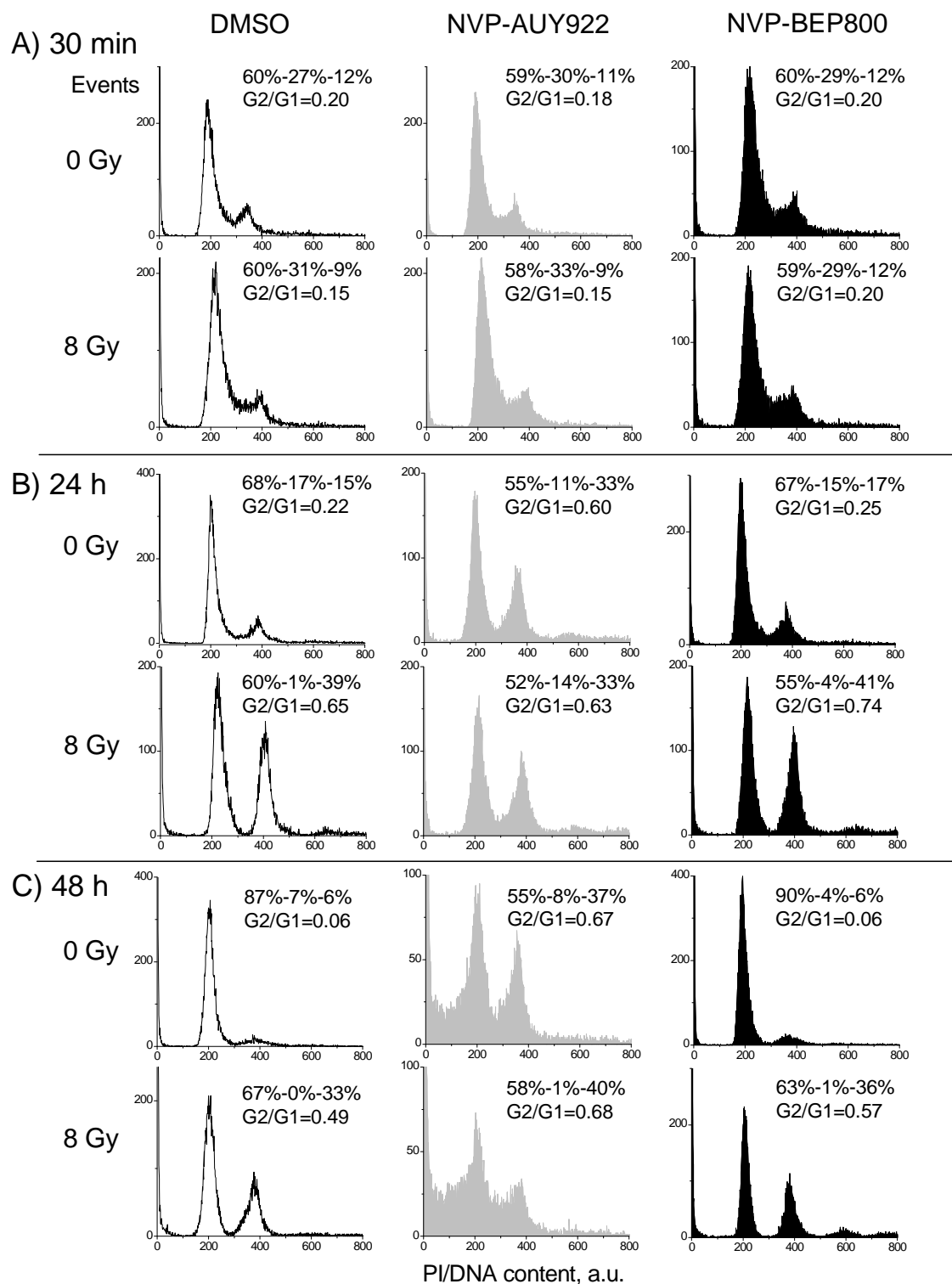
Figure 37. Cell cycle distribution of HFib2 cells treated with DMSO (unfilled histograms), NVP-AUY922 (gray histograms) or NVP-BEP800 (black histograms) and irradiated (8 Gy). Samples were fixed for staining 30 minutes (A), 24 hours (B) and 48 hours (C) post irradiation. The percentage of cells in each phase (G1%-S%-G2%) and G2/G1 ratio are shown.

Table 14. Cell cycle distribution in HFib1 cells detected 30 minutes (A), 24 hours (B) and 48 hours (C) after simultaneous drug-IR treatment. Data are presented as means (±SE) from at least three independent experiments.

Dose	Treatment	G0/G1, %	S, %	G2/M, %	G2/G1
A) 30 minutes post radiation					
0 Gy	DMSO	60±6	21±5	17±1	0.3
	NVP-AUY922	59±5	24±4	18±1	0.3
	NVP-BEP800	59±5	21±4	18±1	0.3
8 Gy	DMSO	60±5	22±4	16±2	0.3
	NVP-AUY922	61±7	21±5	17±1	0.3
	NVP-BEP800	61±8	22±7	16±1	0.3
B) 24 hours post radiation					
0 Gy	DMSO	76±2	13±2	10±2	0.1
	NVP-AUY922	61±5	4±1	34±4	0.6
	NVP-BEP800	80±1	7±3	11±2	0.1
8 Gy	DMSO	67±6	2±1	30±4	0.5
	NVP-AUY922	58±5	6±2	36±3	0.6
	NVP-BEP800	69±4	1±1	29±5	0.4
C) 48 hours post radiation					
0 Gy	DMSO	87±2	4±1	8±2	0.1
	NVP-AUY922	62±6	6±1	31±7	0.5
	NVP-BEP800	86±2	4±1	8±2	0.1
8 Gy	DMSO	71±2	1±1	28±1	0.4
	NVP-AUY922	57±5	5±1	37±5	0.7
	NVP-BEP800	67±2	3±2	28±3	0.4

Table 15. Cell cycle distribution in HFib2 cells detected 30 minutes (A), 24 hours (B) and 48 hours (C) after simultaneous drug-IR treatment. Data are presented as means (±SE) from at least three independent experiments.

Dose	Treatment	G0/G1, %	S, %	G2/M, %	G2/G1
A) 30 minutes post radiation					
0 Gy	DMSO	66±3	19±3	14±2	0.2
	NVP-AUY922	65±4	21±4	12±2	0.2
	NVP-BEP800	66±4	21±4	13±3	0.2
8 Gy	DMSO	66±3	21±3	12±2	0.2
	NVP-AUY922	65±3	22±4	11±1	0.2
	NVP-BEP800	64±3	21±3	13±3	0.2
B) 24 hours post radiation					
0 Gy	DMSO	73±2	12±2	14±1	0.2
	NVP-AUY922	65±4	4±2	29±2	0.5
	NVP-BEP800	72±2	10±1	16±1	0.2
8 Gy	DMSO	65±2	1±1	33±2	0.5
	NVP-AUY922	61±3	5±3	32±1	0.5
	NVP-BEP800	62±3	2±1	34±2	0.5
C) 48 hours post radiation					
0 Gy	DMSO	85±2	7±1	7±1	0.1
	NVP-AUY922	61±2	2±2	36±1	0.6
	NVP-BEP800	86±1	4±1	8±1	0.1
8 Gy	DMSO	69±1	0±1	30±1	0.4
	NVP-AUY922	60±3	0±1	38±3	0.7
	NVP-BEP800	67±1	1±0	31±1	0.5

Thirty minutes after irradiation alone or drug treatment alone we did not observe any changes in the cell cycle distribution in HFib1 (Fig. 36A) or in HFib2 cells (Fig. 37A). Longer incubation (24 and 48 hours) of not-irradiated, DMSO-treated fibroblasts led to cell cycle arrest at the G1/S checkpoint (Figs. 36, 37B, C). Incubation of HFib1 and HFib2 after irradiation alone for 24 and 48 hours resulted in the depletion of cells in the S phase and an increased G2/M peak (Figs. 36, 37B, C). Similarly, twenty-four-hour exposure to NVP-AUY922 shifted more HFib1 and HFib2 cells into the G2/M

phase and reduced the amount of cells in the S phase (Figs. 36B, 37B). In addition, further incubation with NVP-AUY922 (48 hours) resulted in an increase of the sub-G1 phase in both tested fibroblast strains (Figs. 36, 37). The treatment of fibroblast strains with NVP-BEP800 for 24 or 48 hours did not affect the cell cycle distribution when compared with control samples (Figs. 36, 37).

Simultaneous NVP-BEP800-IR treatment led to the depletion of the S phase and to the increase of G2/M peak in fibroblasts (24 and 48 hours post drug-IR) as was the case with DMSO-treated, irradiated samples (Figs. 36, 37B, C). Combined NVP-AUY922-IR treatment in HFib1 and HFib2 cells induced stronger G2/M arrest than in samples treated with NVP-AUY922 alone (Figs. 36, 37; 24 and 48 hours).

We further analyzed the sub-G1 phase and cellular debris as an indicator of late-stage apoptosis measured 48 hours post drug-IR treatment. Representative histograms are depicted in Figure 38.
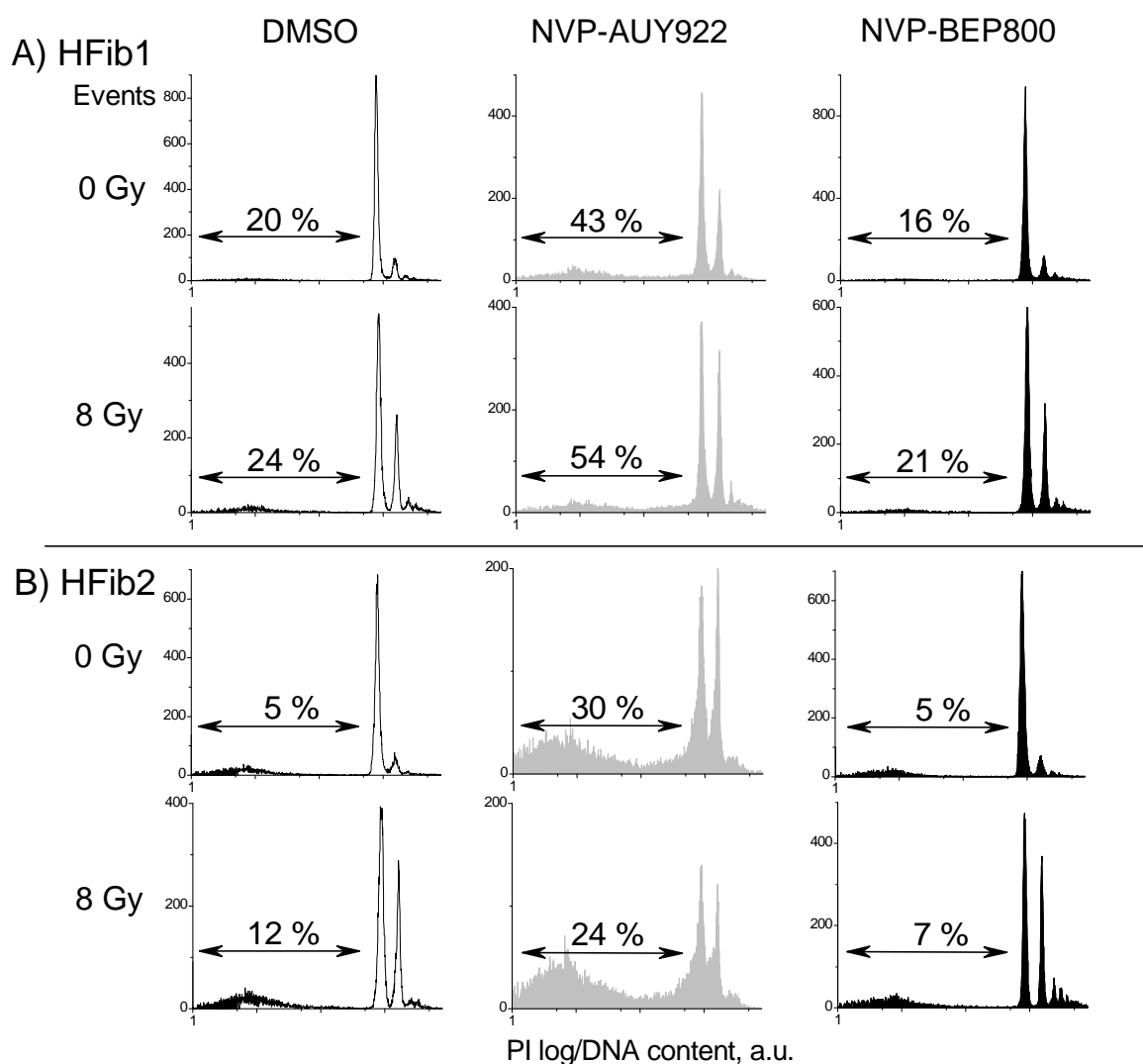
Figure 38. Percentage of cells with hypodiploid DNA content and cellular debris in drug-treated and irradiated HFib1 (A) and HFib2 (B) cells. Samples were incubated for 48 hours after DMSO (unfilled histograms), NVP-AUY922 (gray histograms) or NVP-BEP800 (black histograms) treatment and IR. Both floating and adherent cells were collected, fixed and stained with PI. Depicted are the percentages of events for hypodiploid nuclei and debris, computed by WinMDI (Scripps Research Institute, La Jolla, USA). The experiment was repeated three times for each cell line.

The combination of NVP-AUY922 and irradiation increased the amount of hypodiploid cells in HFib1 to 54%, compared to 24% detected in irradiated controls (Fig. 38A). In NVP-AUY922-treated, irradiated HFib2 cells the extent of the sub-G1 phase (24%) was similar to that observed after NVP-AUY922 treatment only (30%, Fig. 38B). In contrast to NVP-AUY922, incubation with NVP-BEP800 did not increase the sub-G1 phase of HFib1 or HFib2 cells as was the case with DMSO-treated controls (Fig. 38).

4.2.6. Influence of Hsp90 inhibition and IR on the expression of cell cycle-related proteins in fibroblast strains HFib1 and HFib2

Next, we performed an analysis of expression of cell cycle-related proteins, including cyclin-dependent kinases Cdk1, Cdk4 and pRb protein (Figs. 38, 39).
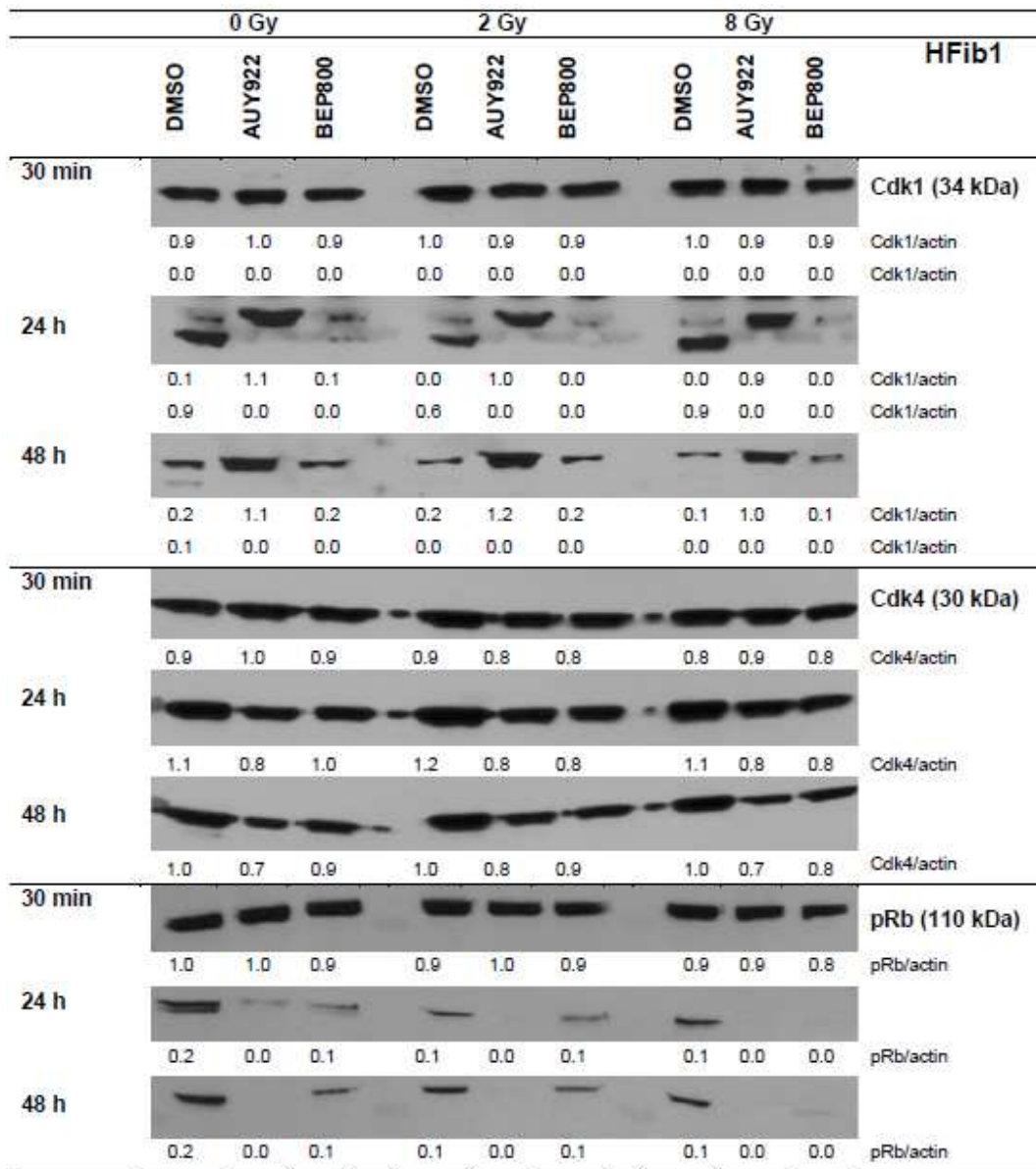
Figure 39. Expression of Cdk1, Cdk4 and pRb in HFib1 cells. Samples were treated with DMSO, NVP-AUY922 or NVP-BEP800 and irradiated (with 2 or 8 Gy). Each protein band was normalized to β-actin and the ratios are given in numbers.

Thirty-minute incubation after irradiation alone (2 or 8 Gy) or treatment with either Hsp90 inhibitor did not influence the expression of the chosen cell cycle-related proteins (Figs. 39, 40). However, the expression of pRb in HFib1 (1.0 -> 0.2 -> 0.2

a.u.) and HFib2 (0.7 -> 0.2 -> 0.2 a.u.) control samples decreased with increased incubation time.
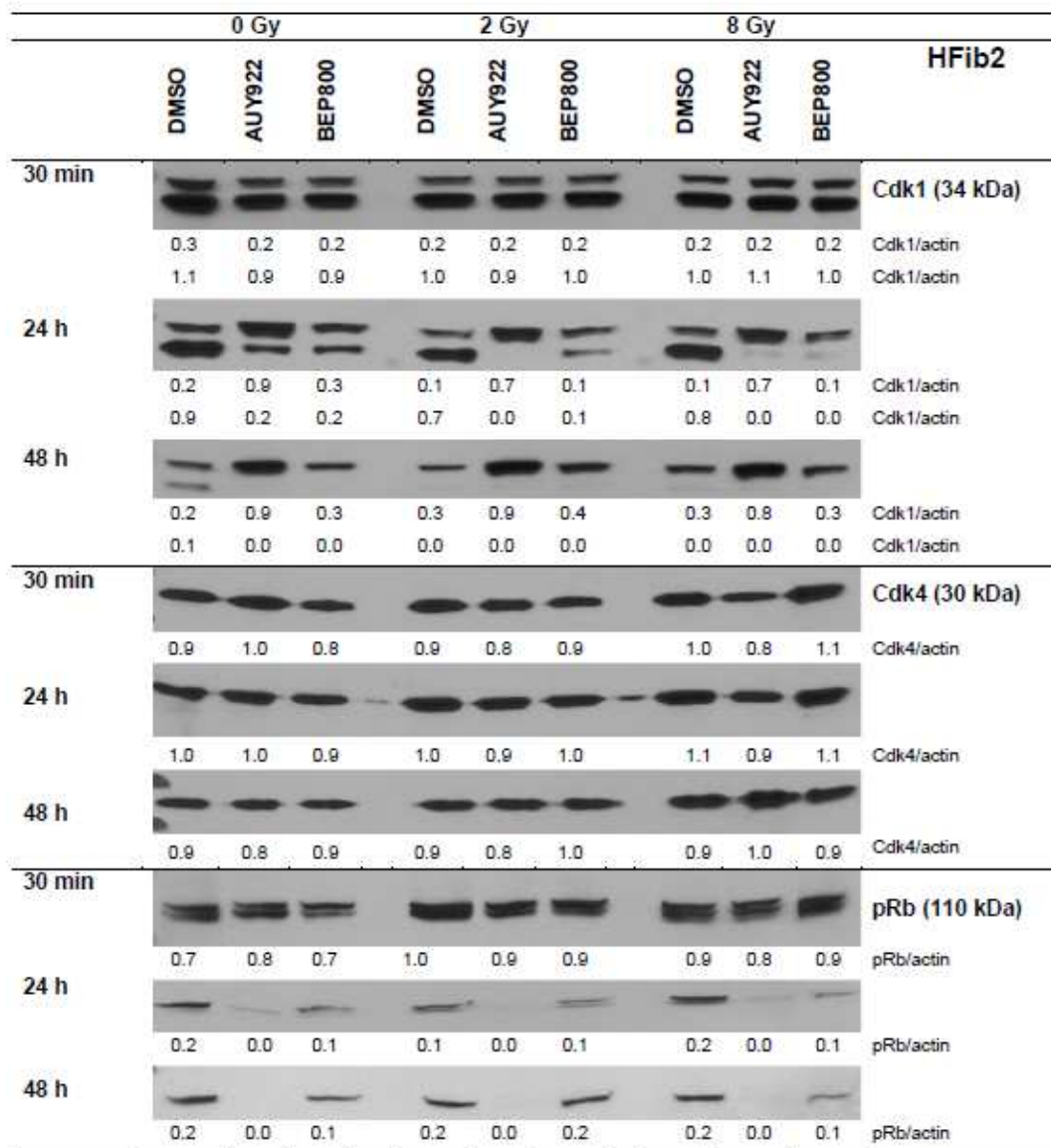
Figure 40. Expression of Cdk1, Cdk4 and pRb in HFib2 cells. Samples were treated with DMSO, NVP-AUY922 or NVP-BEP800 and irradiated (with 2 or 8 Gy). Each protein band was normalized to β-actin and the ratios are given in numbers.

Twenty four and forty eight hours after treatment with NVP-AUY922, the up-regulation of Cdk1 was observed in both fibroblast strains examined (i.e. Figs. 39, 40; 48 hours post drug treatment, HFib1: 0.2 -> 1.1 a.u., HFib2: 0.2 -> 0.9 a.u.). In fibroblasts treated with NVP-BEP800, the expression of Cdk1 was similar to that in DMSO-treated samples. Incubation with NVP-AUY922 for 24 and 48 hours led to the depletion of pRb in HFib1 and HFib2 cells. Treatment with NVP-BEP800 resulted in the decrease in the level of pRb in both strains to ~50% (Figs. 39, 40). In NVP-

AUY922-treated HFib1 cells Cdk4 was down-regulated from 1.1 to 0.8 a.u. In HFib2 cells, the expression of this cyclin-dependent kinase remained unchanged 24 hours after NVP-AUY922 treatment. In contrast to NVP-AUY922, the incubation with NVP-BEP800 for 24 and 48 hours did not affect the expression of Cdk4 (Figs. 39, 40).

The combination of NVP-AUY922 and irradiation did not induce any additional changes in the expression of examined proteins controlling cell cycle progression. In irradiated, NVP-BEP800-treated fibroblasts, Cdk1 was depleted 24 hours after treatment (Figs. 39, 40). Additionally, simultaneous NVP-BEP800-IR treatment led to the depletion of pRb in HFib1 cells (Fig. 39, 24 and 48 hours post treatment, 0.1 -> 0.0 a.u.).

To summarize, we analyzed the influence of NVP-AUY922 and NVP-BEP800 in combination with irradiation on normal human skin fibroblasts. The response of HFib1 and HFib2 fibroblasts to Hsp90 inhibition and irradiation was different from that previously described for tumor cell lines A549 and SNB19. The plating efficiency of HFib1 and HFib2 strains was not affected by the treatment with either Hsp90 inhibitor. We have shown that only 48 hours after NVP-AUY922-treatment, HFib1 and HFib2 cells were moderately sensitized to irradiation. Forty-eight-hour incubation of HFib1 and HFib2 strains with NVP-AUY922 led to the accumulation of DNA damage and an increased sub-G1 phase, suggesting that this Hsp90 inhibitor can induce apoptosis in fibroblasts. At the same time, the treatment with NVP-BEP800 did not increase the radiosensitivity of the examined fibroblast strains. In concordance, we observed no additional DNA damage in NVP-BEP800-treated fibroblasts in comparison to control samples. Incubation of HFib1 and HFib2 cells with either NVP-AUY922 or NVP-BEP800 (with/without IR) caused the up-regulation of Hsp90 and Hsp70, but to a lesser extent than in tumor cell lines. However, the depletion of several Hsp90 clients (including Raf-1, Akt and pAkt) after Hsp90 inhibition alone or in combination with irradiation was similar to that observed in tumor cells.

4.3 Influence of Hsp70 silencing combined with NVP-AUY922 on the radiation response of cancer cell lines A549 and SNB19

As shown previously treatment with Hsp90 inhibitors, including NVP-AUY922 and NVP-BEP800, induces the up-regulation of heat shock proteins 90 and 70 through heat shock response (Stingl et al. 2010, Niewidok et al. 2012, Patel et al. 2012). The drug-induced over-expression of Hsp70 is considered as a major drawback of Hsp90 inhibition. Therefore, the objective of this part of the thesis was to inhibit Hsp70 up-regulation induced by NVP-AUY922 in cancer cell lines. Taking into account the lack of potent, pharmacological Hsp70 inhibitors (Goloudina et al. 2012), we decided to use siRNA technique as the most specific way to inhibit the chaperone. Two proteins from the Hsp70 family, constitutively expressed Hsc70 and stress-inducible Hsp70, were chosen as targets. Firstly, we tested the effects of siRNA-mediated inhibition on the proliferation of tumor cell lines A549 and SNB19.

Cell seeding ⟹ Transfection **24 h** ⟹ Treatment with NVP-AUY922 **24 h** ⟹ Irradiation ⟹ Analysis
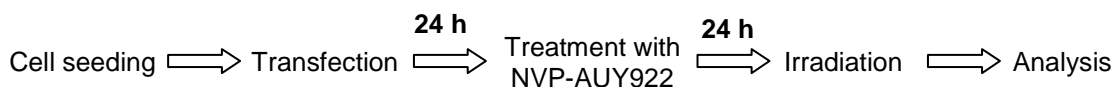
Figure 41. The sequence of experiments. Before analysis tumor cell lines A549 and SNB19 were transfected with Hsp70 siRNA, then treated with 50 nM NVP-AUY922 and irradiated.

Then, Hsp70 pre-silencing was combined with NVP-AUY922 treatment and irradiation (Fig. 41) and the cellular response to the applied treatment was analyzed.

4.3.1 Analysis of heat shock proteins' expression at mRNA and protein level in A549 and SNB19 tumor cell lines after Hsc70 and Hsp70 knock-down

In order to optimize the conditions of transfection, two different siRNA sequences for Hsp70 and Hsc70 have been tested (siRNA sequences in section 3.1.3). To control the efficiency of transfection, A549 and SNB19 cells were transfected with non-silencing siRNA coupled with the fluorescence molecule Alexa488 (Section 3.2.10, Fig. 10). siRNA targeting MAP kinase was used as the positive control. Then, the concentration of Hsp70- and Hsc70-siRNAs needed for effective transfection was determined (Fig. 42).

As seen in Figure 42, Hsp70- and Hsc70-specific siRNAs caused the suppression of target proteins up to 72 hours after transfection, independently from used siRNA concentration (100 nM and 200 nM). In lung carcinoma A549 cells, transfection with Hsp70 siRNA reduced the level of target protein from 1.1 to ~0.6 a.u. (Fig. 42A). Hsc70 siRNA caused the decrease from 1.2 to ~0.5-0.7 a.u. of the target (Fig. 42A). In SNB19 cell samples, transfection with Hsp70 siRNA and Hsc70 siRNA suppressed the expression of the target proteins from 0.6 to 0.3 a.u. and from 0.2 to 0.1 a.u. respectively (Fig. 42B). In both cell lines, silencing of Hsc70 resulted in the up-regulation of Hsp70 (A549: 1.1 -> 1.3 a.u., SNB19: 0.6 -> 1.0 a.u.).

A)
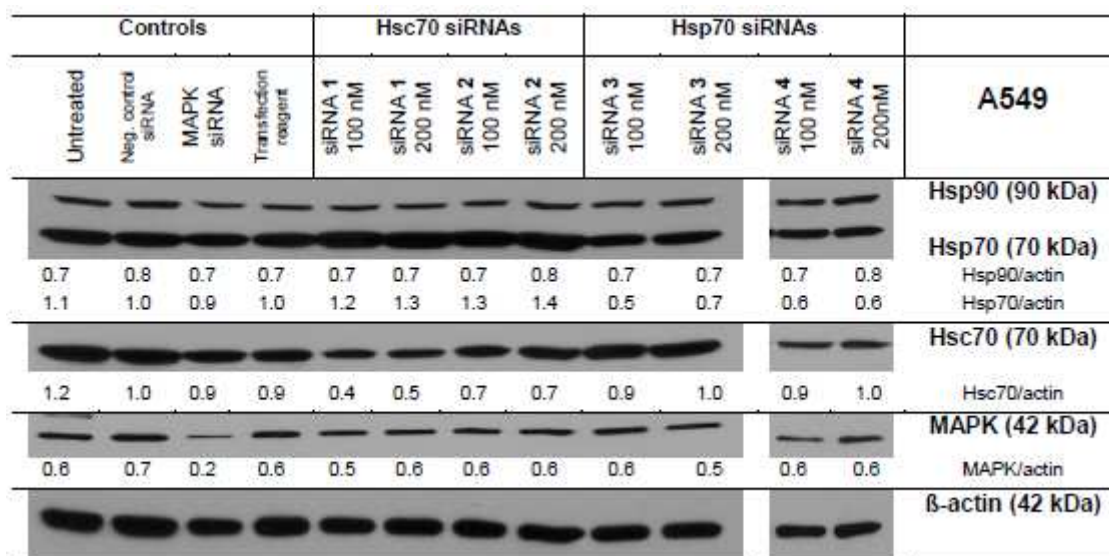
B)
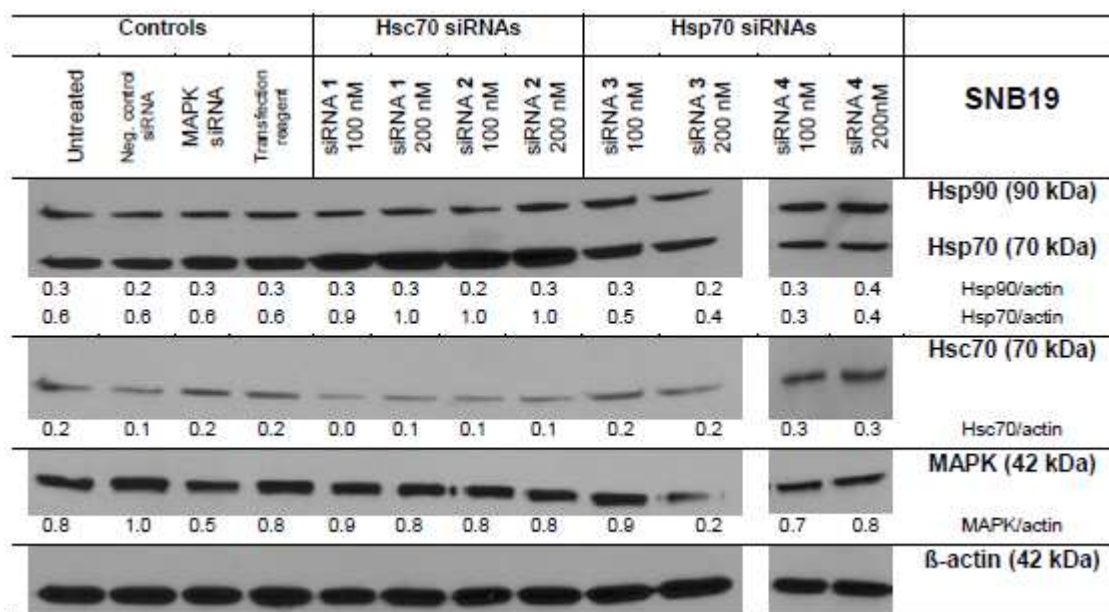
Figure 42. Expression of Hsp90, Hsp70, Hsc70 and MAPK in A549 (A) and SNB19 (B) cell lines. Samples were transfected with negative control siRNA, MAPK siRNA or siRNAs targeting Hsc70 and Hsp70. Seventy two hours after transfection the cell lysates were prepared and analyzed. Each protein band was normalized to β-actin and the ratios are given in numbers.

Both siRNA sequences caused similar silencing of the target proteins, so we chose one siRNA pro target for further experiments (section 3.1.3, siRNAs 2 and 3). In the following experiments we used siRNAs at 100 nM for single transfection and 50 nM for combined Hsc70/Hsp70 knock-down.

Then, we examined the changes in mRNA expression by reverse transcriptase-PCR after siRNA-mediated Hsp70 and Hsc70 inhibition in tumor cell lines A549 and SNB19, as shown in Figure 43.
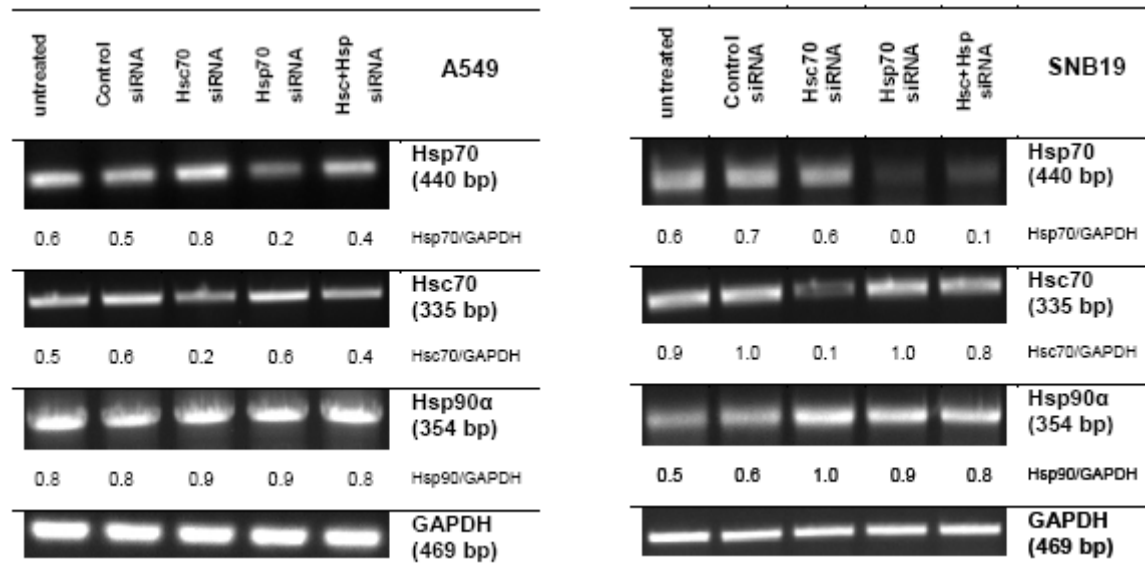
Figure 43. mRNA levels of Hsp70, Hsc70 and Hsp90α in A549 (on the left) and SNB19 (on the right) tumor cell lines. Cells were treated with control, non-silencing siRNA or siRNA targeting Hsp70 and/or Hsc70 and analyzed by RT-PCR 24 hours after transfection. Each band was normalized to GAPDH expression and the ratios are given in numbers.

Hsp70-siRNA reduced the mRNA level 3-fold in lung carcinoma cells (Fig. 43, on the left, 0.6 -> 0.2 a.u.) and completely depleted the transcript in glioblastoma cells (Fig. 43, on the right, 0.6 -> 0.0 a.u.). The reduction of Hsc70 was stronger in SNB19 (0.9 -> 0.1 a.u.) than in A549 samples (0.5 -> 0.2 a.u.). Simultaneous knock-down of both proteins decreased the mRNA levels to a lesser extent than single siRNAs did (Fig. 43, A549: Hsp70 0.6 -> 0.4 a.u., Hsc70 0.5 -> 0.4 a.u.; SNB19: Hsp70 0.6 -> 0.1 a.u., Hsc70 0.9 -> 0.8 a.u.). In addition, in SNB19 samples transfected with Hsp70 siRNA, Hsc70 siRNA or combined siRNAs, Hsp90α mRNA levels increased (0.5 -> ~0.9 a.u.). Hsp90α is a stress-inducible isoform of Hsp90 (Sreedhar et al. 2004) and its increase suggests that transfection could induce stress response in SNB19 cells. In contrast, we observed no changes in the Hsp90α mRNA level in A549 cells (Fig. 43, on the left).

4.3.2 Influence of Hsc70/Hsp70 silencing on the proliferation of A549 and SNB19 cells

The effects of single and combined Hsc70/Hsp70 silencing on the growth of lung carcinoma and glioblastoma cells were determined as described in section 3.2.12. Cell numbers of transfected and non-transfected cells counted up to 4 days post transfection were averaged through 4 independent experiments and are shown in Figure 44.
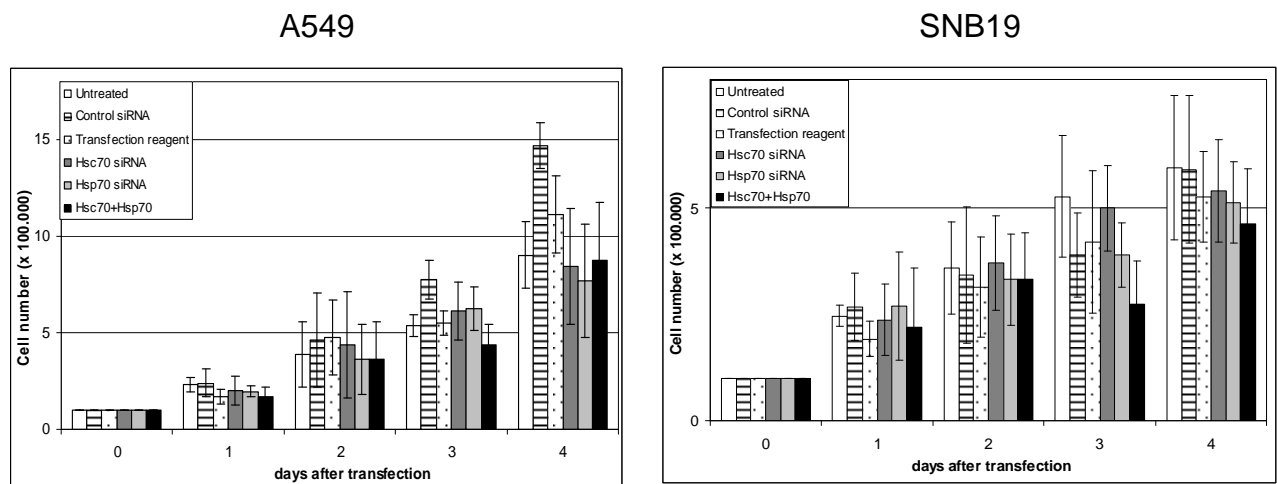
Figure 44. Proliferation of A549 (on the left) and SNB19 (on the right) cells after transfection with negative control siRNA or siRNA targeting Hsc70/Hsp70. Cells were seeded (day 0), 24 hours later transfected and during the following 4 days the cell numbers were scored. Data are shown as means ± SD from 4 independent experiments. According to Student's t-test there were no significant differences between untreated and transfected cells.

As seen in Figure 44, control A549 cells proliferated faster than SNB19 cells (white columns). Transfection reagent alone (dotted columns) or non-silencing negative control (dashed columns) did not affect the proliferation of both examined cell lines (Fig. 44). A549 cells treated with Hsp70 siRNA divided slower than control samples at day 4 after transfection (Fig. 44, light gray columns). Double Hsc70/Hsp70 knock-down resulted in reduced proliferation of A549 cells 72 hours post transfection (Fig. 44, black columns). In the case of SNB19 cells, Hsp70 siRNA reduced their ability to proliferate 72 and 96 hours post transfection (Fig. 44, light gray columns). Simultaneous Hsc70/Hsp70 silencing decreased the proliferation rate of SNB19 dells to the greatest extent at days 3 and 4 after transfection (Fig. 44, on the right, black columns). However, according to Student's t-test the differences between non-transfected and transfected cell samples were not significant.

Taking into account the anti-apoptotic activities of stress-inducible Hsp70 (see details in chapter 1.5) during following experiments we combined Hsp70 pre-silencing with Hsp90 inhibition and irradiation.

4.3.3 Analysis of heat shock proteins' expression at mRNA and protein level in A549 and SNB19 cells after combination of Hsp70 knock-down, NVP-AUY922 addition and IR

The changes at mRNA level after Hsp70 silencing in combination with NVP-AUY922 treatment were examined by reverse transcriptase PCR, as shown in Figure 45.
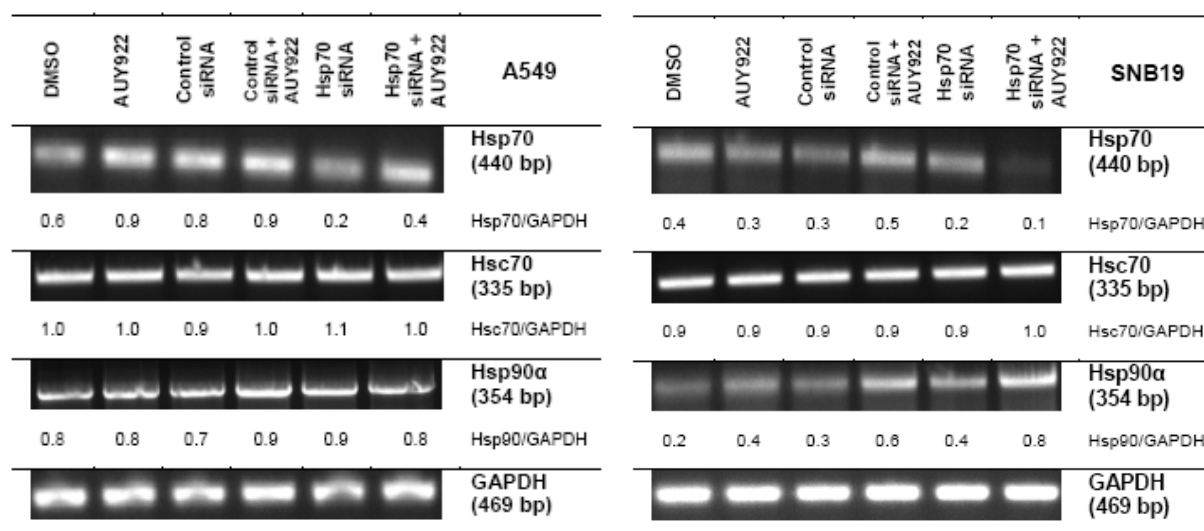
Figure 45. mRNA levels of Hsp70, Hsc70 and Hsp90α in A549 (on the left) and SNB19 (on the right) tumor cell lines. Cells were transfected with either control or Hsp70 siRNA and 24 hours after silencing treated with NVP-AUY922. Forty eight hours after transfection the samples were analyzed by RT-PCR. Each band was normalized to GAPDH expression and the ratios are given in numbers.

A549 and SNB19 cell samples were probed for Hsp70, Hsc70, Hsp90α and GAPDH expression. The treatment with NVP-AUY922 alone increased the level of Hsp70 mRNA in A549 from 0.6 to 0.9 a.u. (Fig. 45, on the left). Twenty four hours after Hsp70 siRNA transfection, the mRNA level of the target protein was reduced from 0.6 to 0.2 a.u. When pre-silenced A549 cells were treated with Hsp90 inhibitor, the amount of Hsp70 mRNA decreased from 0.6 to 0.4 a.u. At the same time the levels of Hsc70 and Hsp90α (stress-inducible Hsp90 isoform) remained unaffected by the applied treatments (Fig. 45, on the left).

Exposure of SNB19 cells to NVP-AUY922 led to the up-regulation of Hsp90α at mRNA level (0.2 -> 0.4 a.u.), whereas it did not influence the expression of Hsp70 (~0.4 - 0.3 a.u., Fig. 45, on the right). Transfection with Hsp70 siRNA induced the suppression of target mRNA (0.4 -> 0.2 a.u.). The combination of Hsp70 pre-silencing and NVP-AUY922 in SNB19 cells decreased Hsp70 mRNA level from 0.4 to 0.1 a.u. At the same time the level of Hsp90α mRNA increased (0.2 -> 0.4 a.u.). Hsc70 mRNA levels stayed constant independent from the applied treatment (Fig. 45, on the right).

Next, the effects of combined Hsp70-siRNA-NVP-AUY922 treatment and IR on the protein expression of Hsp90, Hsp70 and Hsc70 in A549 and SNB19 cells were investigated (Figs. 46 and 47).
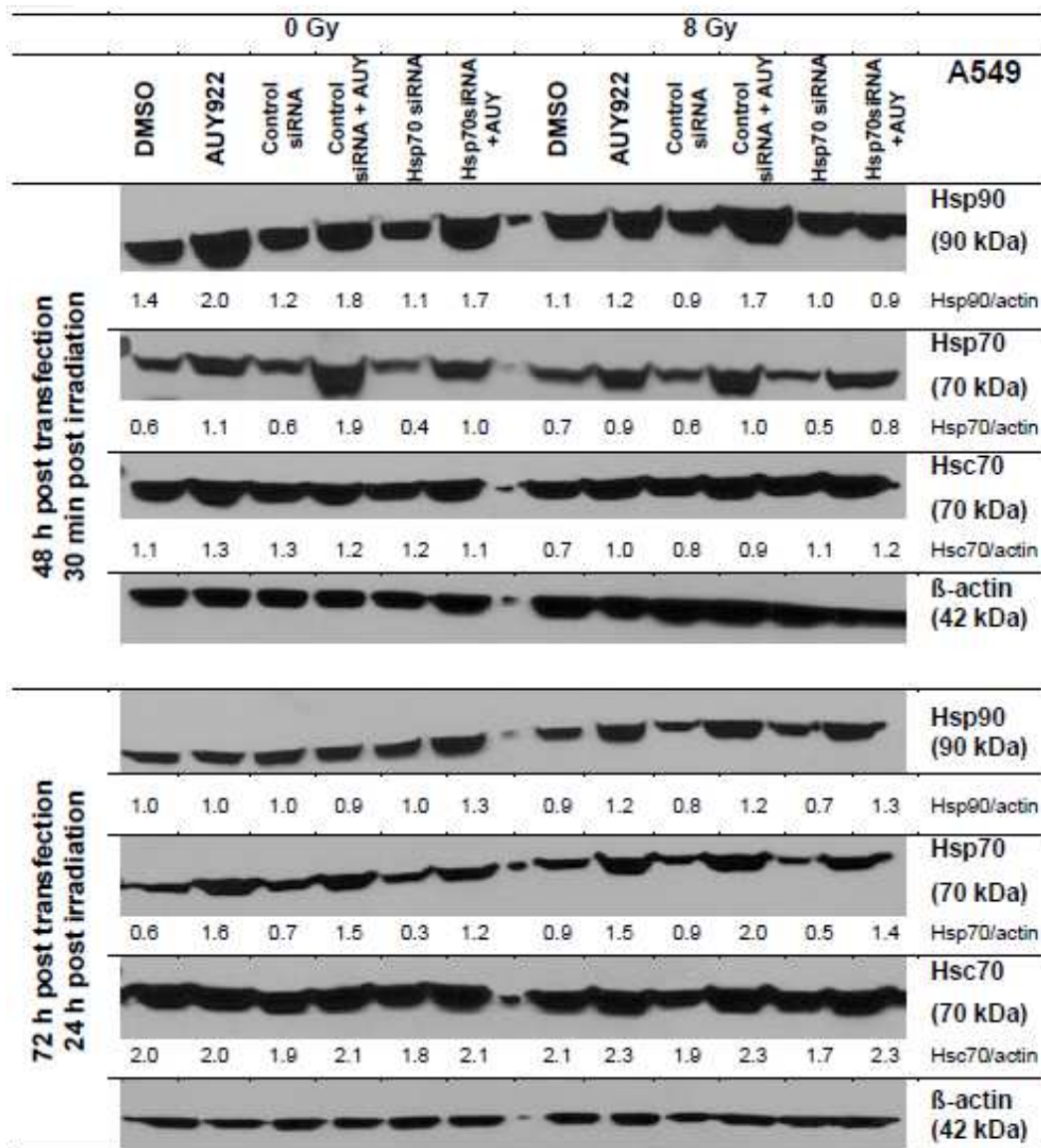
Figure 46. Expression of Hsp90, Hsp70 and Hsc70 in A549 cells. Samples were transfected, on the next day treated with NVP-AUY922 and irradiated 24 hours later (8 Gy). The analysis was performed 30 minutes and 24 hours after IR. Each protein band was normalized to β-actin and the ratios are given in numbers.

Treatment with Hsp70 siRNA alone reduced the target protein level from 0.6 for controls to 0.4 a.u. in A549 (Fig. 46), and from 0.9 to 0.7 a.u. in SNB19 (Fig. 47) cells (48 hours post transfection). At the same time no changes were observed in the expression levels of Hsp90 and Hsc70 in both cancer cell lines. NVP-AUY922 alone caused strong up-regulation of analyzed heat shock proteins in A549 and SNB19 cells (Figs. 46, 47, i.e. SNB19: Hsp90 0.7 -> 1.3 a.u., Hsp70 0.9 -> 2.0 a.u., Hsc70 1.0 -> 2.0 a.u.). In A549 cells pre-silenced for Hsp70 and treated with NVP-AUY922 we observed the up-regulation of Hsp70 from 0.6 to 1.0 a.u. (Fig. 46, 48 hours post transfection).
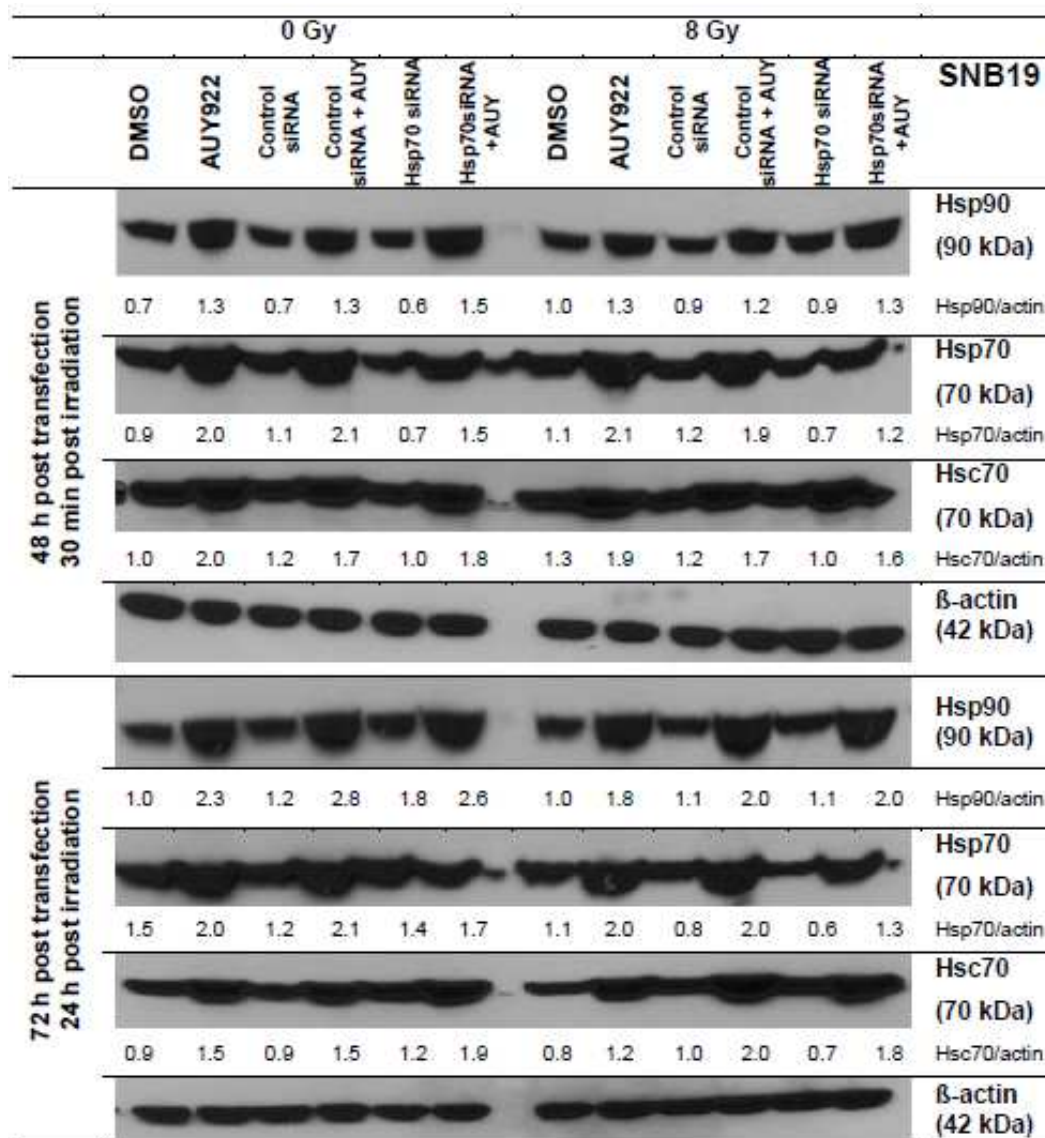
Figure 47. Expression of Hsp90, Hsp70 and Hsc70 in SNB19 cells. Samples were transfected, on the next day treated with NVP-AUY922 and irradiated 24 hours later (with 8 Gy). The analysis was performed 30 minutes and 24 hours after IR. Each protein band was normalized to β-actin and the ratios are given in numbers.

When the Hsp90 inhibitor NVP-AUY922 was added to SNB19 cells transfected with Hsp70 siRNA (Fig. 47), the expression of Hsp70 increased (0.9 -> 1.5 a.u.), but the induction was weaker than after NVP-AUY922 treatment alone (0.9 -> 2.0 a.u.). However, it did not influence the up-regulation of other chaperones i.e. Hsp90 and Hsc70 in either examined tumor cell line (Figs. 46, 47). Irradiation (8 Gy) of Hsp70-presilenced, NVP-AUY922-treated tumor cells did not further affect the expression of tested heat shock proteins (Figs. 46, 47).

Thus, we have shown that Hsp70 knock-down successfully suppressed the NVP-AUY922-induced over-expression of heat shock protein 70 at the mRNA and protein level.

4.3.4 Colony survival of irradiated A549 and SNB19 cells after Hsp70 pre-silencing and treatment with NVP-AUY922

Next, colony-forming assay was performed to analyze whether Hsp70 pre-silencing could increase the radiosensitizing effect of NVP-AUY922 in A549 and SNB19 cells. Representative cell survival curves of transfected, NVP-AUY922-treated samples plotted against the radiation dose are shown in Figure 48. The statistical analysis was performed from at least 3 independent experiments and summarized in Table 16.
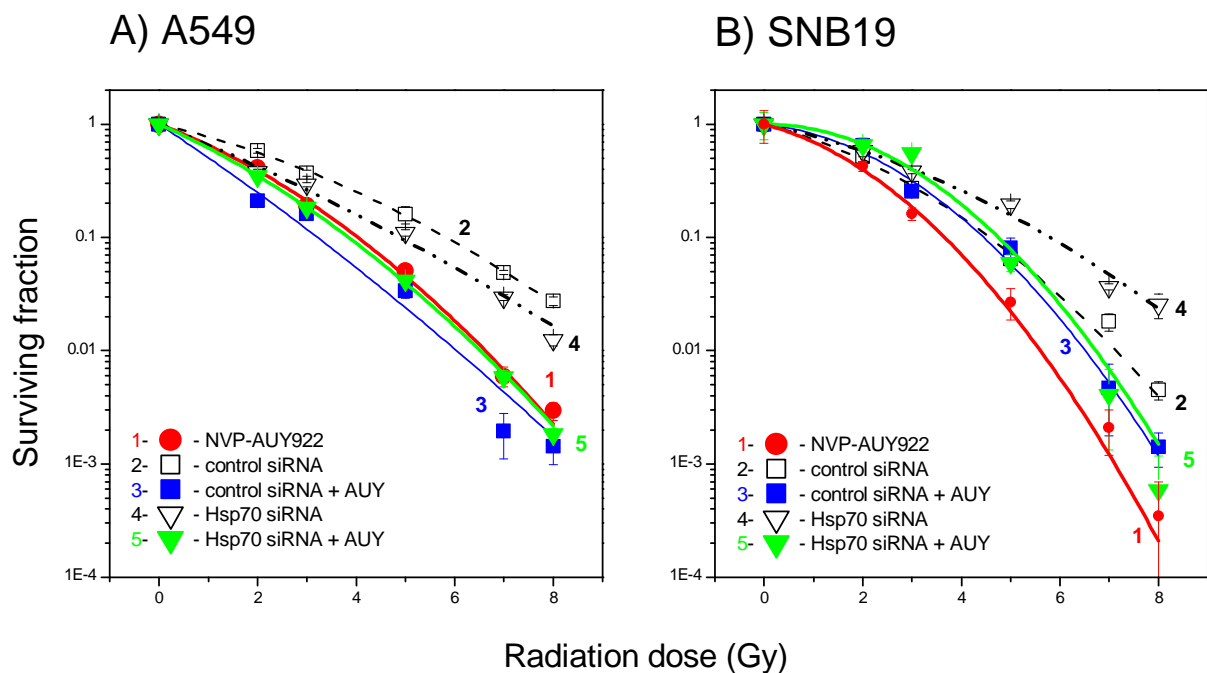
Figure 48. Representative clonogenic survival curves of A549 (A) and SNB19 (B) cell lines. Cells transfected with control siRNA (unfilled squares) or with Hsp70 siRNA (unfilled triangles), treated with NVP-AUY922 (colored symbols) were irradiated and seeded for colony-forming assay. After staining and scoring the colonies, cell survival curves were generated.

Table 16. Plating efficiencies and radiosensitivity parameters[a] of transfected, NVP-AUY922-treated and irradiated A549 and SNB19 tumor cell lines.

	PE	SF2 [b]	D_{10} [c] (Gy)	IF_{10} [d]
A549				
DMSO	0.35±0.1	0.59±0.1	5.9	1.0
NVP-AUY922	0.26±0.1	0.54±0.2	4.9	1.2
control siRNA	0.38±0.1	0.57±0.1	5.8	1.0
control siRNA +AUY	0.23±0.1	0.33±0.1	3.6	1.6
Hsp70 siRNA	0.38±0.2	0.54±0.1	5.4	1.1
Hsp70 siRNA +AUY	0.32±0.1	0.43±0.1	4.4	1.3
SNB19				
DMSO	0.12±0.1	0.65±0.2	5.8	1.0
NVP-AUY922	0.07±0.05	0.51±0.2	4.2	1.4
control siRNA	0.14±0.1	0.59±0.1	5.0	1.1
control siRNA +AUY	0.07±0.05	0.56±0.1	4.5	1.3
Hsp70 siRNA	0.15±0.1	0.67±0.2	6.0	1.0
Hsp70 siRNA +AUY	0.07±0.02	0.75±0.1	5.8	1.0

[a] Mean (±SD) from at least three independent experiments
[b] SF2 is the surviving fraction at 2 Gy
[c] D_{10} is the radiation dose resulting in 10% cell survival
[d] IF_{10} was calculated as $(D_{10\ control})/(D_{10\ inhibitor})$

Transfection with Hsp70 siRNA alone did not affect the plating efficiency of either examined cancer cell line (Table 16). Treatment with NVP-AUY922 (alone or in combination with siRNA) reduced PE from ~0.12 to ~0.07 in glioblastoma cells. In lung carcinoma samples, NVP-AUY922 alone decreased PE from ~0.35 to ~0.26, but when it was combined with Hsp70 siRNA the decrease was minimal (Table 16, PE≈ 0.32).

As evident from Figure 48, treatment with 50 nM NVP-AUY922 alone sensitized both examined tumor cell lines to radiation. In SNB19 samples, SF2 was reduced from ~0.65 to ~0.51 and D_{10} from 5.7 to 4.2, whereas in A549, D_{10} decreased from 5.9 to 4.9, but SF2 did not change markedly (from ~0.59 to ~0.54, Table 16). Hsp70 silencing alone did not affect the radiosensitivity of SNB19 or A549 cells, as

evidenced by the unchanged SF2 and D_{10} in comparison to control samples (Table 16). The survival curve of A549 cells pre-silenced with Hsp70 siRNA and treated with NVP-AUY922 overlapped with that of cells treated with the drug only (Fig. 48A). In comparison to Hsp70 silencing alone, the combination treatment of Hsp70 siRNA and NVP-AUY922 sensitized SNB19 cells to radiation. However, the observed radiosensitization was weaker than after NVP-AUY992 treatment alone (Fig. 48B).

4.3.5 Changes in the expression of several marker proteins after combined Hsp70 knock-down, NVP-AUY922 addition and irradiation

Next, the protein expression analysis was performed in tumor cell lines A549 and SNB19 after combined Hsp70 siRNA-NVP-AUY922 treatment and irradiation. Figures 49-52 show representative expression levels of marker proteins involved in cell proliferation (Akt, Raf-1), cell cycle (Cdk1, Cdk4, pRb) and apoptosis (caspase 3, survivin, PARP).

Figure 49. Expression of Akt, Raf-1, survivin, Cdk1, Cdk4, pRb, PARP and caspase 3 in A549 cells 30 minutes post radiation (48 hours post transfection). Samples were transfected with Hsp70 siRNA, treated with NVP-AUY922 and irradiated with 8 Gy. Each band was normalized to ß-actin and the ratios are given in numbers.

As shown in Figure 49, Hsp90 clients Akt (0.9 -> 0.6 a.u.) and Raf-1 (1.0 -> 0.8 a.u.) were down-regulated in non-irradiated, NVP-AUY922-treated A549 cells. Furthermore, we detected a reduction in the levels of Cdk1 (1.1 -> 0.6 a.u.) and Cdk4 (1.2 -> 0.9 a.u.) in these A549 samples, indicating possible cell cycle disturbances. Treatment with NVP-AUY922 did not affect the expression of survivin in A549 cells (Fig. 49).
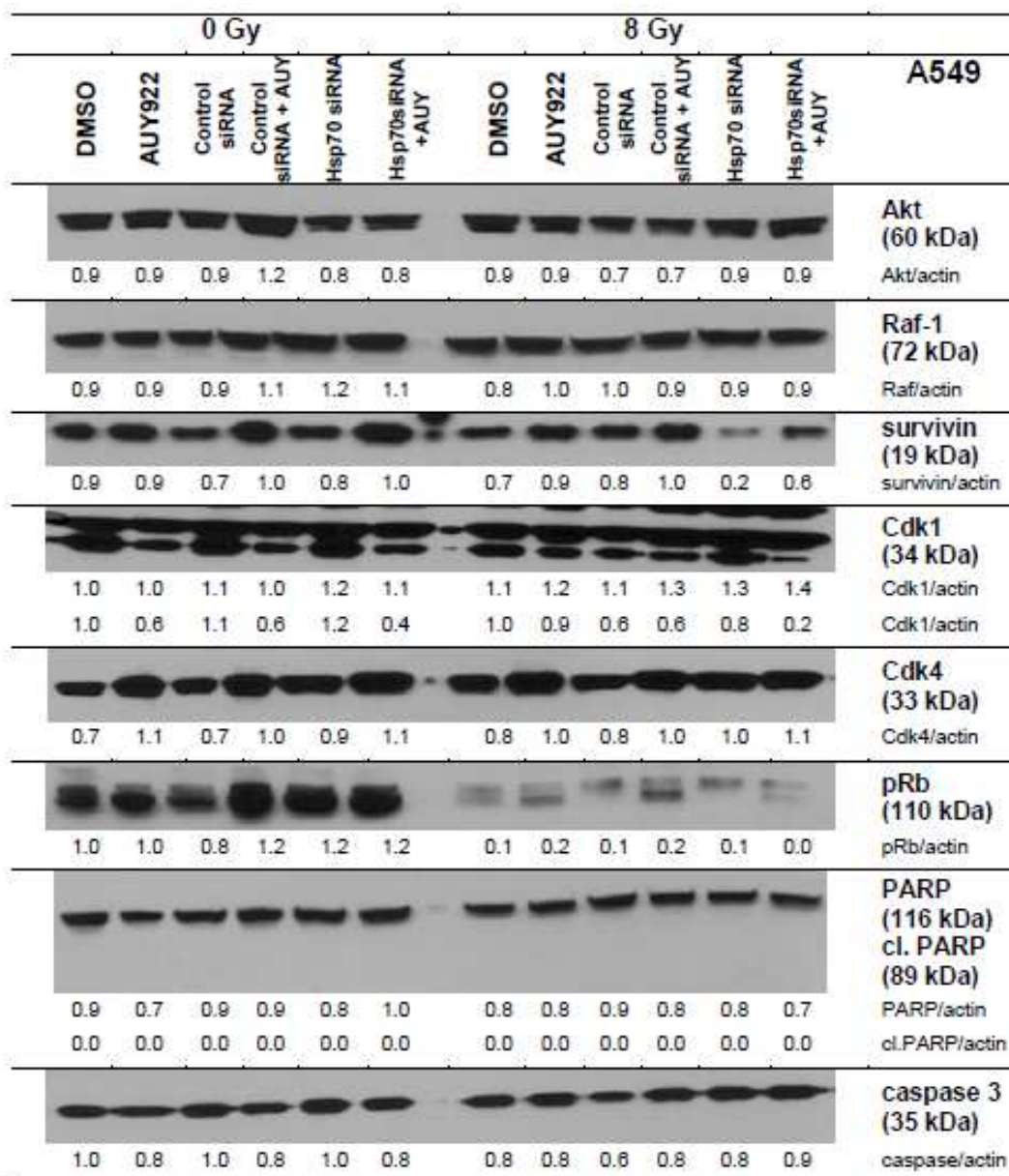
Figure 50. Expression of Akt, Raf-1, survivin, Cdk1, Cdk4, pRb, PARP and caspase 3 in A549 cells 24 hours post radiation (72 hours post transfection). Samples were transfected with Hsp70 siRNA, treated with NVP-AUY922 and irradiated with 8 Gy. Each band was normalized to ß-actin and the ratios are given in numbers.

In glioblastoma cells, Akt was depleted (1.2 -> 1.0 a.u.) and Raf-1 nearly completely vanished (from 0.8 to 0.1 a.u.) after NVP-AUY922 treatment (Fig. 51). Cyclin-dependent kinases Cdk1 (1.0 -> 0.3 a.u.) and Cdk4 (0.6 -> 0.3 a.u.) were down-regulated, as was the case with lung carcinoma cells. Treatment with NVP-AUY922 alone did not influence the expression of survivin, caspase 3 or PARP in glioblastoma cells (Fig. 51).
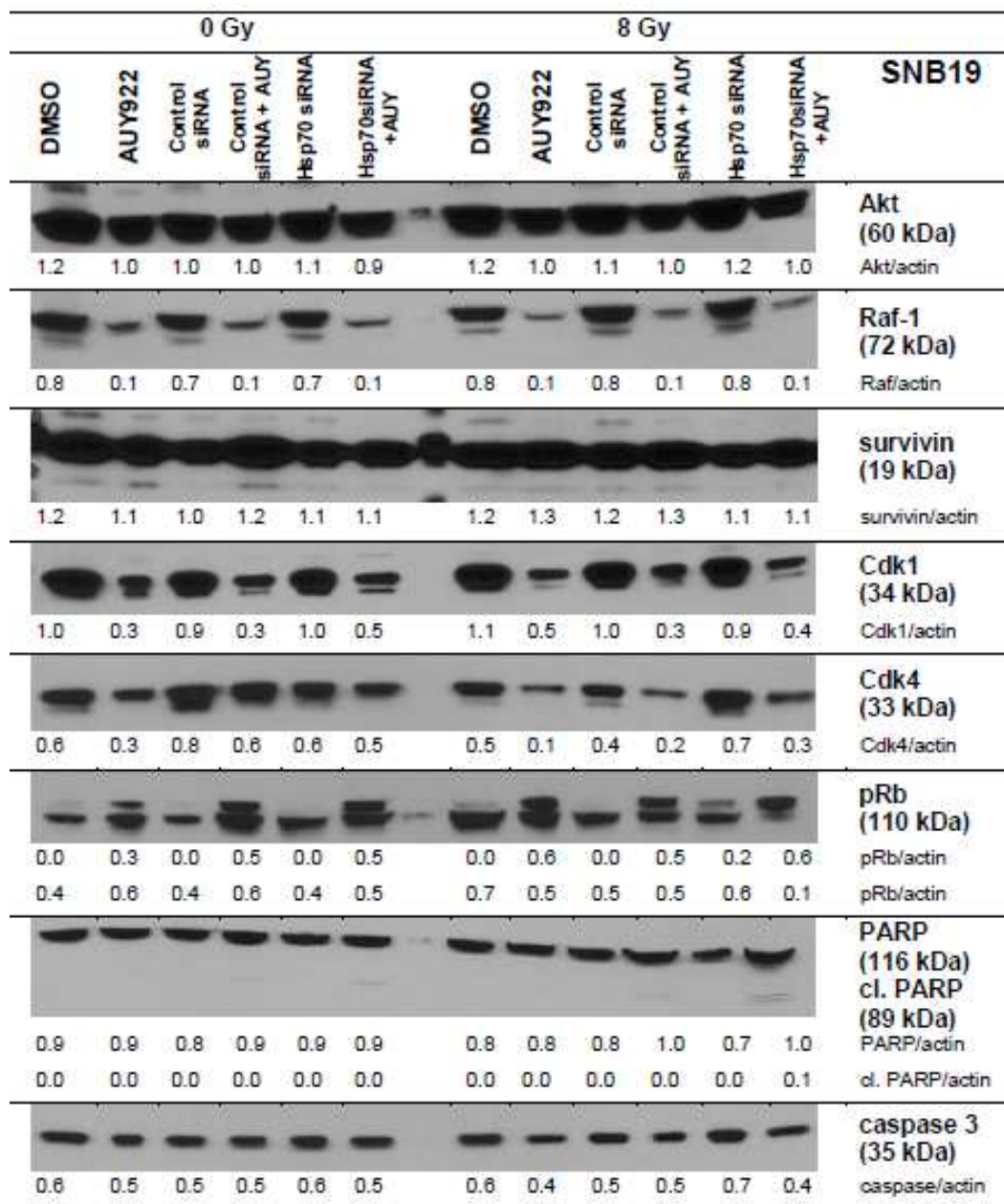
Figure 51. Expression of Akt, Raf-1, survivin, Cdk1, Cdk4, pRb, PARP and caspase 3 in SNB19 cells 30 minutes post radiation (48 hours post transfection). Samples were transfected with Hsp70 siRNA, treated with NVP-AUY922 and irradiated with 8 Gy. Each band was normalized to ß-actin and the ratios are given in numbers.

The silencing of Hsp70 alone did not induce any significant changes in the expression of examined proteins in comparison to control samples (Figs. 49-51). The combination of Hsp70 pre-silencing with NVP-AUY922 caused mostly the same protein level alterations as NVP-AUY922 alone in both examined tumor cell lines (Figs. 49-51). One exception was survivin, which was down-regulated from 1.0 to 0.4 a.u. in A549 cells after combined Hsp70 siRNA-NVP-AUY922 treatment (Fig. 49, 48 hours post transfection).

In pre-silenced and NVP-AUY922-treated SNB19 cells we detected the cleaved form of PARP (Fig. 51, 72 hours after transfection).
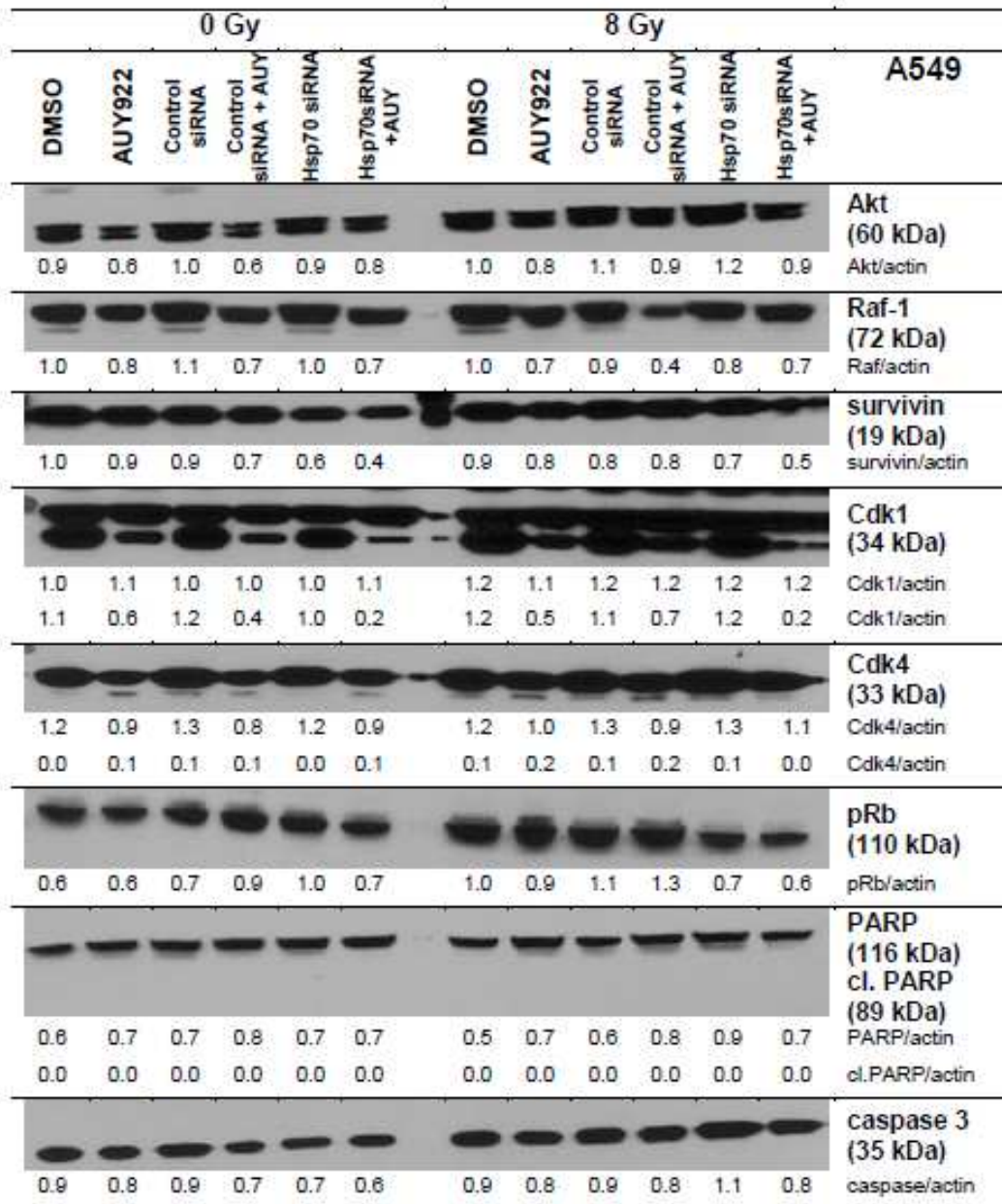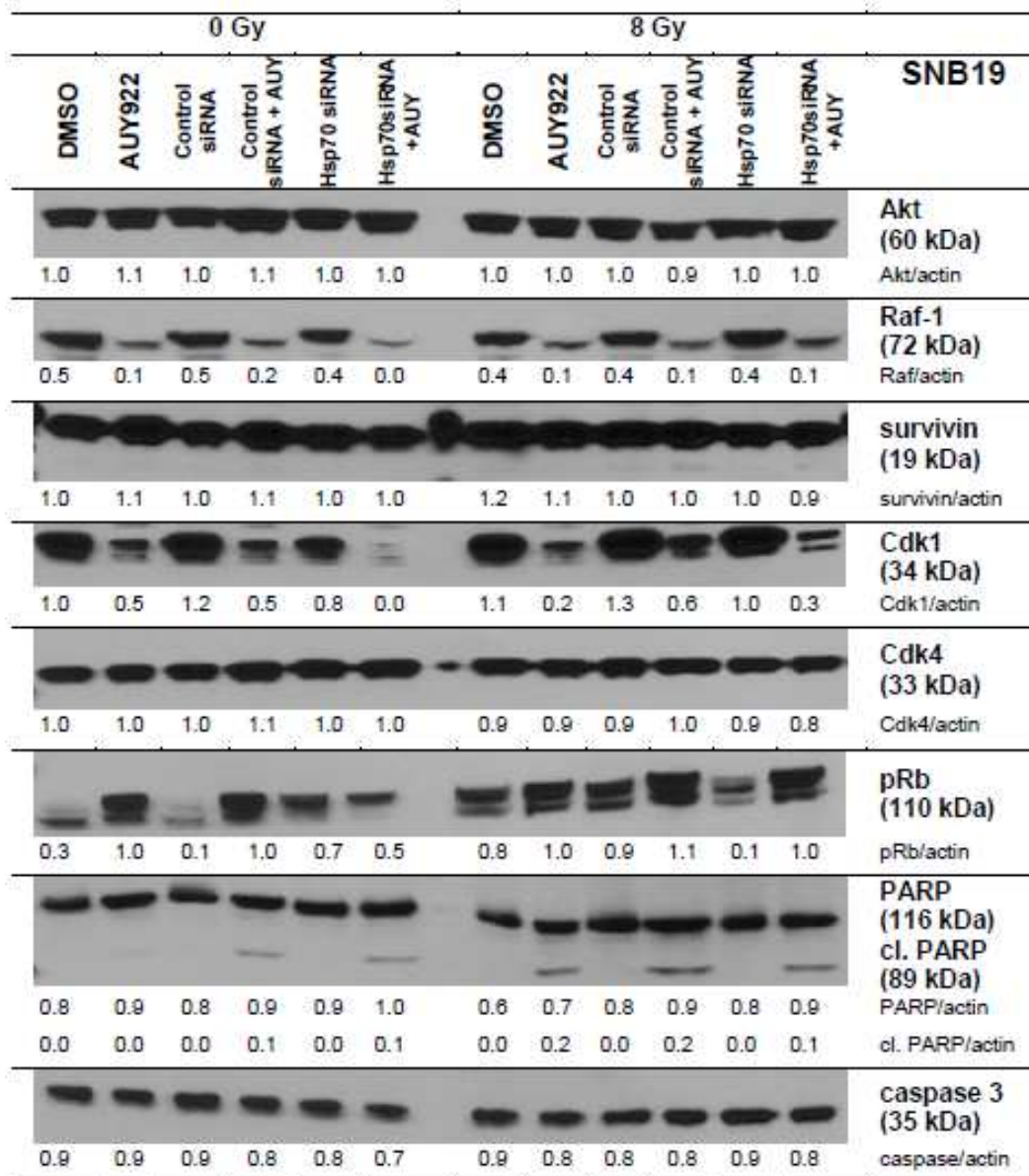

Figure 52. Expression of Akt, Raf-1, survivin, Cdk1, Cdk4, pRb, PARP and caspase 3 in SNB19 cells 24 hours post radiation (72 hours post transfection). Samples were transfected with Hsp70 siRNA, treated with NVP-AUY922 and irradiated with 8 Gy. Each band was normalized to ß-actin and the ratios are given in numbers.

SNB19 cells treated with NVP-AUY922 and IR, either with or without siRNA transfection, expressed cleaved PARP (Fig. 52, 24 hours post IR). The expression of other tested proteins in pre-silenced, NVP-AUY922-treated and irradiated A549 and SNB19 cells was similar to that observed in samples after NVP-AUY922-IR treatment (Figs. 49-52).

4.3.6 DNA damage repair and cell cycle progression after combined Hsp70 silencing, NVP-AUY922 addition and irradiation

Finally, we determined the effects of Hsp70 pre-silencing in combination with Hsp90 inhibition and irradiation on DNA damage and cell cycle distribution by flow cytometry. Pre-silenced for Hsp70, NVP-AUY922-treated and irradiated A549 and SNB19 cells were fixed 30 minutes and 24 hours after IR and stained for γH2AX as a marker of DNA double strand breaks. Representative histograms are shown in Figure 53.

A) A549
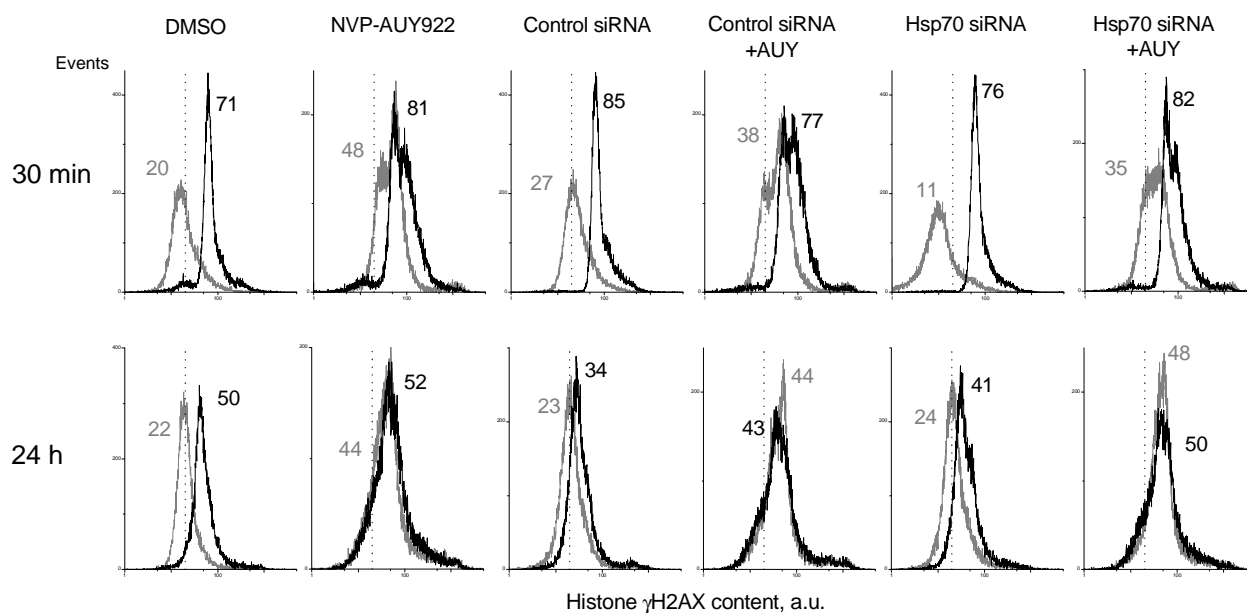
B) SNB19
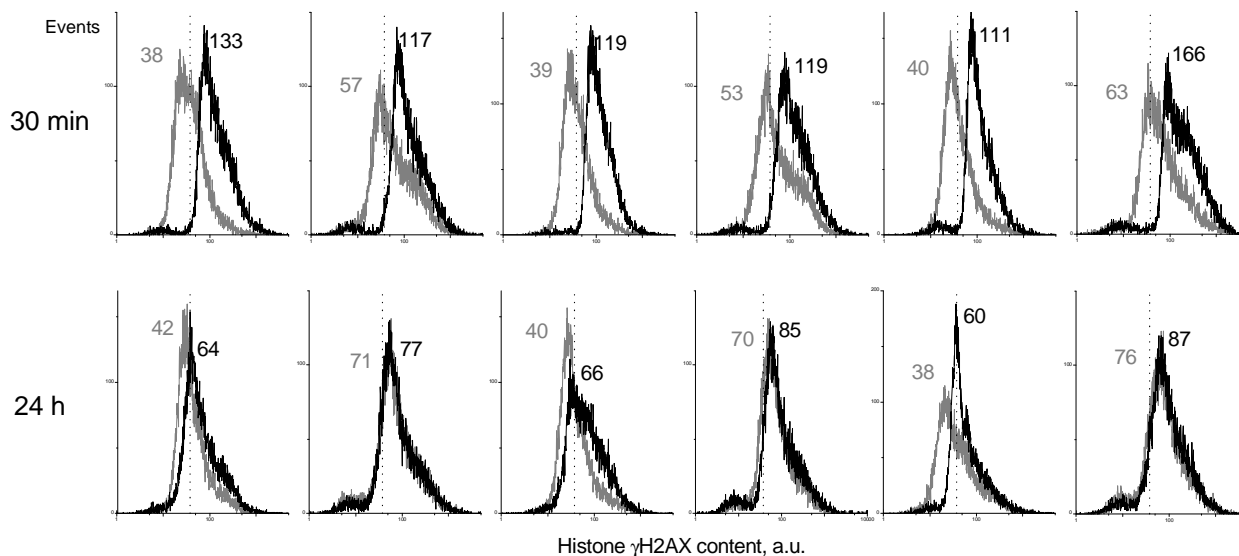
Figure 53. Histograms showing distribution of γH2AX, as a marker of DNA double strand breaks, in A549 (A) and SNB19 (B) cells. Transfected with Hsp70 siRNA, NVP-AUY922-treated samples were irradiated with single dose (8 Gy, black histograms) and analyzed 30 minutes and 24 hours post IR. Gray histograms represent non-irradiated samples. Numbers denote the mean γH2AX expression for the respective cell sample. The vertical, dashed line marks the γH2AX value of DMSO-treated, non-irradiated control.

As observed in Figure 53, the background levels of γH2AX expression was 20 a.u. and 38 a.u. for A549 and SNB19 control samples respectively (30 minutes, gray histograms). Hsp70 silencing alone did not influence the amount of DNA damage in A549 or SNB19 (Fig. 53, A549 ~11 a.u., SNB19 ~40 a.u.). Treatment with 50 nM

NVP-AUY922 increased the levels of γH2AX about 2-fold in both tested cell lines (A549 from 20 to 48 a.u., SNB19 from 38 to 57 a.u.). The combination of Hsp70-presilencing and NVP-AUY922 treatment in SNB19 samples did not further affect the γH2AX expression (~63 a.u.; Fig. 53B). In pre-silenced, NVP-AUY922-treated A549 cells we measured DNA damage at ~35 a.u., which was higher than in controls, but lower than after NVP-AUY922 treatment alone (Fig. 53A).

Irradiation alone induced the γH2AX expression in A549 from 20 to 71 a.u. and in SNB19 from 38 to 133 a.u. cells (Fig. 53, 30 minutes, black histograms). Pre-silenced, NVP-AUY922-treated and irradiated SNB19 cells exhibited the highest amount of DNA damage of ~166 a.u. (Fig. 53B, 30 minutes, black histograms). In A549, the combination treatment Hsp70 siRNA-NVP-AUY922 and irradiation induced similar levels of γH2AX expression (~81 a.u.) as after NVP-AUY922-IR treatment (Fig. 53A, 30 minutes, black histograms).

The treatment-induced DNA damage in A549 cell samples was restored to the level of controls within 24 hours (Fig. 53A, black histograms). In SNB19 we also observed DNA damage repair at 24 hours after irradiation, however it was slower in NVP-AUY922-treated samples (with/without siRNA) (Fig. 53B, black histograms).

In addition to γH2AX measurements, the cell cycle analysis of the silenced, NVP-AUY922-treated and irradiated A549 and SNB19 was performed (Fig. 54). The statistical analysis from 3 independent experiments was summarized in Tables 17 and 18.

A) A549

PI/DNA content, a.u.

B) SNB19

PI/DNA content, a.u.
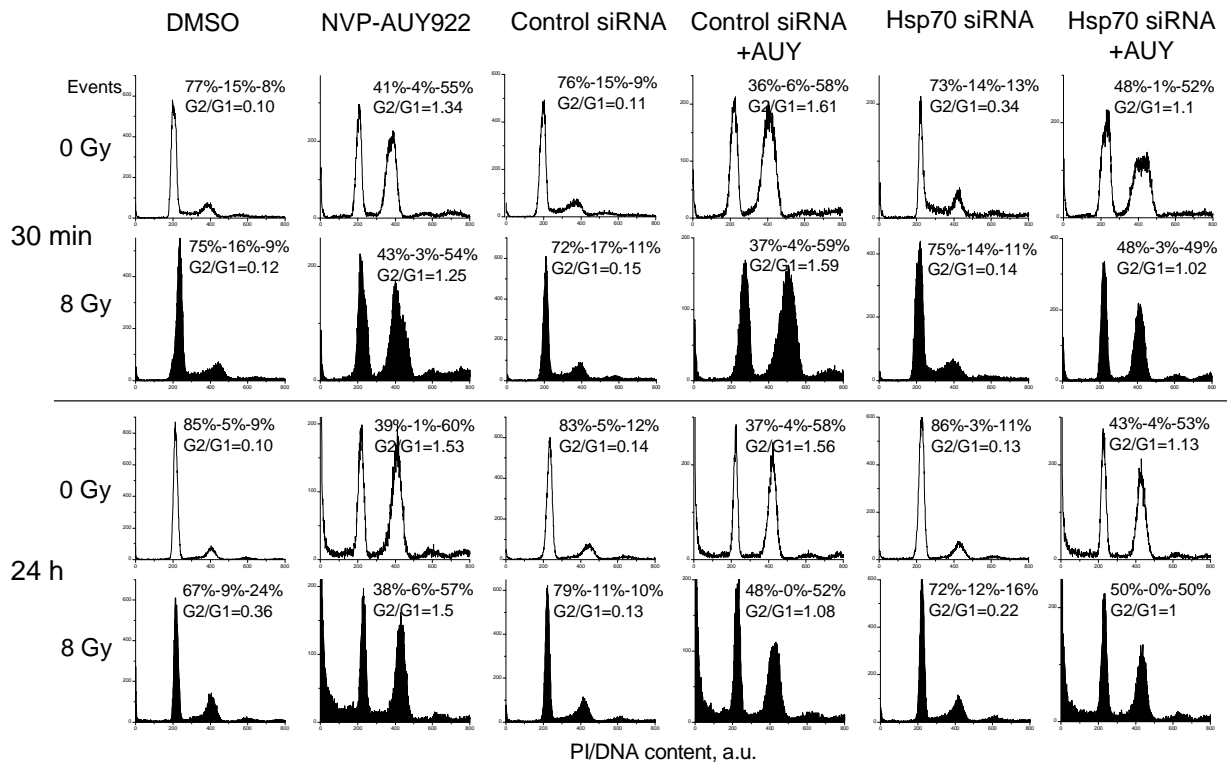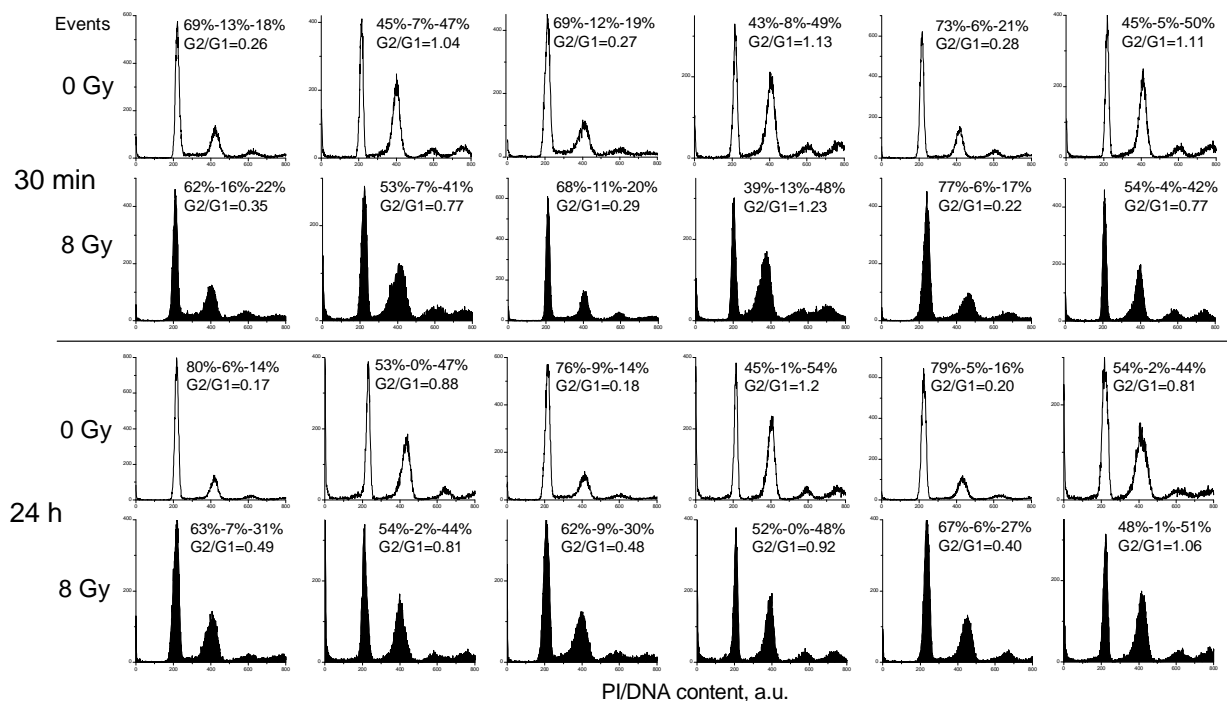
Figure 54. Cell cycle distribution of A549 (A) and SNB19 (B) tumor cell lines. Pre-silenced for Hsp70, NVP-AUY922-treated and irradiated (8 Gy) samples were fixed 30 minutes and 24 hours post irradiation. The percentage of cells in each phase (G1%-S%-G2%) and G2/G1 ratio are shown.

Table 17. Cell cycle distribution in A549 cells detected 30 minutes (A) and 24 hours (B) after irradiation. Samples were transfected, NVP-AUY922-treated and irradiated. Data are presented as means (±SD) from at least three independent experiments.

Dose	Treatment	G0/G1, %	S, %	G2/M, %	G2/G1
A) 30 minutes post radiation (48 hours post transfection)					
0 Gy	DMSO	67±4	24±3	8±1	0.1
	NVP-AUY922	55±7	15±7	28±14	0.6
	control siRNA	68±4	23±3	8±1	0.1
	control siRNA +AUY	52±9	16±5	31±14	0.8
	Hsp70 siRNA	68±4	20±6	11±3	0.2
	Hsp70 siRNA +AUY	62±6	11±5	26±10	0.5
8 Gy	DMSO	66±3	20±6	12±4	0.2
	NVP-AUY922	63±8	13±5	24±12	0.5
	control siRNA	67±4	19±7	13±3	0.2
	control siRNA +AUY	57±7	11±6	31±12	0.6
	Hsp70 siRNA	67±3	18±6	14±5	0.2
	Hsp70 siRNA +AUY	64±5	12±2	22±10	0.4
B) 24 hours post radiation (72 hours post transfection)					
0 Gy	DMSO	80±7	11±6	8±1	0.1
	NVP-AUY922	64±10	12±4	23±12	0.5
	control siRNA	78±7	12±7	9±1	0.1
	control siRNA +AUY	62±10	13±3	24±13	0.5
	Hsp70 siRNA	78±7	12±6	9±1	0.1
	Hsp70 siRNA +AUY	57±8	14±4	27±11	0.5
8 Gy	DMSO	53±5	4±1	42±6	0.8
	NVP-AUY922	50±7	5±2	44±6	1.0
	control siRNA	59±8	7±1	33±9	0.6
	control siRNA +AUY	53±3	4±1	41±4	0.8
	Hsp70 siRNA	56±7	5±2	38±9	0.8
	Hsp70 siRNA +AUY	52±4	2±1	45±4	0.9

Table 18. Cell cycle distribution in SNB19 cells detected 30 minutes (A) and 24 hours (B) after irradiation. Samples were transfected, NVP-AUY922-treated and irradiated. Data are presented as means (±SD) from at least three independent experiments.

Dose	Treatment	G0/G1, %	S, %	G2/M, %	G2/G1
A) 30 minutes post radiation (48 hours post transfection)					
0 Gy	DMSO	64±2	16±2	18±1	0.3
	NVP-AUY922	53±4	9±2	38±3	0.7
	control siRNA	65±2	17±1	17±1	0.3
	control siRNA +AUY	49±5	7±2	42±6	0.8
	Hsp70 siRNA	75±1	8±1	16±2	0.2
	Hsp70 siRNA +AUY	51±6	8±1	40±6	0.8
8 Gy	DMSO	66±1	12±1	20±1	0.3
	NVP-AUY922	52±5	8±1	39±4	0.7
	control siRNA	63±3	18±4	17±1	0.3
	control siRNA +AUY	47±4	11±2	40±3	0.8
	Hsp70 siRNA	74±1	8±1	17±0	0.2
	Hsp70 siRNA +AUY	51±4	6±1	42±3	0.8
B) 24 hours post radiation (72 hours post transfection)					
0 Gy	DMSO	79±3	6±1	13±2	0.2
	NVP-AUY922	34±11	19±9	45±5	1.3
	control siRNA	75±2	7±1	17±1	0.2
	control siRNA +AUY	31±9	21±11	46±7	1.5
	Hsp70 siRNA	76±3	8±1	15±2	0.2
	Hsp70 siRNA +AUY	42±6	15±5	42±3	1.0
8 Gy	DMSO	62±4	7±0	30±3	0.5
	NVP-AUY922	30±14	19±10	49±8	1.6
	control siRNA	57±4	10±2	31±2	0.5
	control siRNA +AUY	29±13	24±12	45±5	1.5
	Hsp70 siRNA	70±2	5±1	24±1	0.3
	Hsp70 siRNA +AUY	31±8	17±6	51±3	1.6

As seen in Figure 54, no changes in the cell cycle distribution were revealed after Hsp70 silencing alone in the examined cancer cell lines. Exposure of A549 and SNB19 samples to NVP-AUY922, alone or in combination with Hsp70 siRNA, induced the S phase depletion and the increase of G2/M peak (Fig. 54).

In NVP-AUY922-treated and irradiated A549 cells the fraction of sub-G1 phase increased (Fig. 54A, 24 hours post IR). Apart from that, irradiation (8 Gy) of pre-silenced and/or NVP-AUY922-treated cells did not further affect the cell cycle distribution.

To gain deeper insight into the proliferation of pre-silenced, NVP-AUY922-treated and irradiated A549 and SNB19 cells, BrdU incorporation assay was performed and representative dot plots are shown in Figure 55.
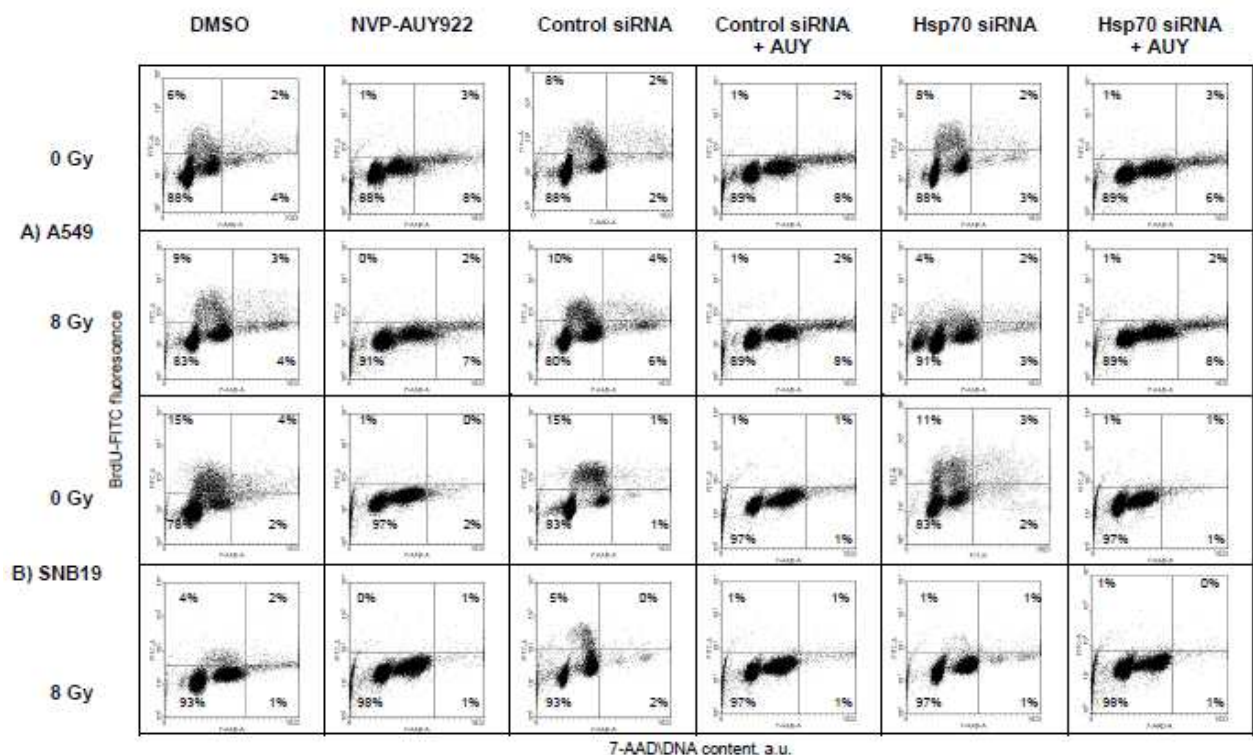
Figure 55. BrdU incorporation assay of A549 (A) and SNB19 (B) cells. Transfected, NVP-AUY922-treated and irradiated samples were incubated with BrdU for one hour. Staining with anti-BrdU antibody presents the incorporation of BrdU and thus the replication abilities of the cells. 7-AAD was used for cell cycle analysis. The percentage of the events in each quadrant is shown.

As evident from Figure 55, NVP-AUY922 treatment alone depleted the amount of events in the S phase of both tested cell lines (A549: 6% -> 1%, SNB19: 15% -> 1%; left upper quadrant). Hsp70 silencing alone did not affect the replication abilities of A549 or SNB19 when compared with controls. The combination of Hsp70 knock-down and NVP-AUY922 reduced the S phase of tested cells to the same extent as NVP-AUY922 treatment alone (Fig. 55). Irradiation (8 Gy) did not affect the replication phase of lung carcinoma cells (Fig. 55A). In contrast, in irradiated

glioblastoma samples the S phase was reduced from 15% to 4% (Fig. 55B). Exposure to NVP-AUY922 and/or Hsp70 siRNA in combination with IR completely depleted the S phase in A549 and SNB19 cells (Fig. 55).

To summarize, Hsp70 and Hsc70 were successfully silenced in examined tumor cell lines A549 and SNB19. The down-regulation of the proteins was confirmed at the mRNA and protein level up to 72 hours after transfection. A reduced cell proliferation was observed after single and combined Hsc70/Hsp70 silencing. Hsp70 pre-silencing suppressed NVP-AUY922-induced Hsp70 over-expression in A549 and SNB19 cell lines. The combination of Hsp70 pre-silencing and NVP-AUY922 treatment did not increase the radiosensitivity of tumor cell lines when compared with drug treatment only. The combined Hsp70-siRNA-NVP-AUY922 treatment induced similar effects at the protein expression level, DNA damage or cell cycle distribution as did the NVP-AUY922 treatment alone.

5. Discussion

Nearly 50% of patients with solid tumors receive radiotherapy at some stage of their treatment (Bernier et al. 2004). Radiation therapy is usually combined with various chemotherapeutics that can sensitize tumor cells to irradiation (Seiwert et al. 2007, Bischoff et al. 2009). Heat shock protein 90 seems to be a promising target for cancer treatment, as it plays central role in the folding and activation of more than 200 clients, among them proteins associated with radiation response (Picard et al. 2002, Zhang et al. 2004, Dote et al. 2005). Inhibition of Hsp90 can provide an approach for the simultaneous targeting of multiple proteins contributing to carcinogenesis (Camphausen et al. 2007). One possibility for impairing Hsp90 functions is to block the binding of ATP to the N-terminal domain of the chaperone (Zhang et al. 2004, Patel et al. 2012). Small molecule Hsp90 inhibitors NVP-AUY922 and NVP-BEP800 belong to drugs targeting the N-terminal domain (Brough et al. 2008, 2009) and were tested in the course of this work in combination with irradiation on human tumor and normal cell lines of different origin.

5.1 Effects of NVP-AUY922 and NVP-BEP800 on the radiation response of lung carcinoma A549 and glioblastoma SNB19 cell lines

Recent works in our group showed that treatment with novel Hsp90 inhibitors NVP-AUY922 and NVP-BEP800 induced radiosensitization of cancer cell lines under normoxic (Stingl et al. 2010) and hypoxic (Djuzenova et al. 2012) conditions. Stingl et al. 2010 incubated tumor cells with either Hsp90 inhibitor for 24 hours before irradiation and removed the drug from the medium before IR (drug-first treatment). The cellular response to the combination of drug-first treatment was p53-independent and involved the degradation of several Hsp90 clients, impaired DNA repair, cell cycle arrest and increased apoptosis (Stingl et al. 2010).

Most studies with Hsp90 inhibitors applied drug-first treatment to combination studies with irradiation (i.e. Bisht et al. 2003, Machida et al. 2003, Bull et al. 2004, Dote et al. 2006, Noguchi et al. 2006, Shintani et al. 2006). However, contradictory report can

be found showing that Hsp90 inhibitors administered after IR were superior in prostate cancer cell killing than the drug-first treatment (Enmon et al. 2003). These discrepancies prompted us to analyze whether the sequence of Hsp90 inhibition and irradiation could influence the radiosensitizing potential of NVP-AUY922 and NVP-BEP800.

Surprisingly, the simultaneous drug-IR treatment induced different effects in A549 and SNB19 tumor cells when compared with the drug-first treatment used in the report from Stingl et al. 2010. When the simultaneous drug-IR treatment was applied to lung carcinoma cells, we observed strong cytotoxicity of the drugs, accompanied by the G1/S arrest and the induction of apoptosis. On the contrary, the drug-first treatment resulted in radiosensitization of A549 cells (Stingl et al. 2010). Glioblastoma SNB19 cells were sensitized to irradiation after the simultaneous drug-IR treatment, as well as after the drug-first regimen (Stingl et al. 2010). However, judging by the SF2 and D_{10} values (48 hours post drug-IR), NVP-AUY922 and NVP-BEP800 induced stronger radiosensitization after the simultaneous drug-IR treatment used here (Niewidok et al. 2012).

To elucidate the different responses of A549 and SNB19 cell lines to the simultaneous drug-IR treatment, we analyzed the extent of DNA damage and its restitution, the expression of marker proteins and the cell cycle distribution. In A549 lung carcinoma cells more DNA damage was induced by the simultaneous drug-IR treatment than by IR alone (30 minutes after treatment) and it was repaired within 24 hours. In SNB19 glioblastoma cells 24 and 48 hours after Hsp90 inhibition and IR we observed an increased amount of DNA DSBs compared with control irradiated samples. At the protein level we observed both pro-survival (i.e. over-expression of Hsp90 and Hsp70) as well as pro-apoptotic effects (i.e. depletion of Akt or survivin) after Hsp90 inhibition with and without IR. Furthermore, we found marked changes in the expression of the cell cycle-related proteins (Cdk1, Cdk4 and pRb) 24 and 48 hours after treatment with NVP-AUY922 and NVP-BEP800. Hsp90 inhibitors down-regulated Cdk1 level in glioblastoma cells, whereas in lung carcinoma its level remained stable. The vanishing of Cdk1, protein regulating the progression into mitosis, would explain the massive G2/M arrest which was seen in SNB19 cells. In both tested cell lines the expression of Cdk4 and pRb decreased, but to a greater extent in A549 cells. The down-regulation of Cdk4 and pRb together with the fact that

lung carcinoma cells express wild type p53 corresponds with the observed G1/S arrest 24 and 48 hours after drug-IR treatment.

As shown by the example of ErbB2 and Bcr-Abl, genetic alterations in cancer cells can be associated with the response to targeted therapeutics (Sos et al. 2009). Thus, based on the known mutations in A549 and SNB19 (3.2.1) we analyzed the expression of several oncoproteins, including p53, PTEN and k-RAS, to further examine the signaling pathways involved in the cellular response to the simultaneous drug-IR treatment (Fig. 56).
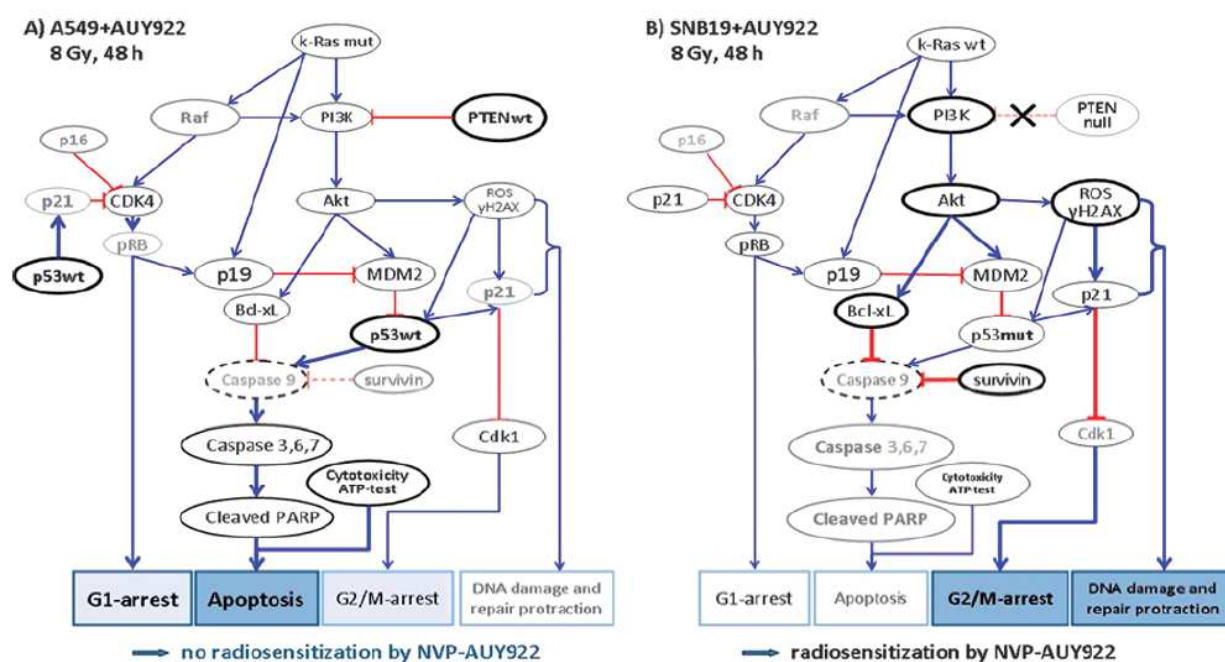
Figure 56. Signalling pathways playing a role in the cellular response of A549 (A) and SNB19 (B) cells to Hsp90 inhibitor NVP-AUY922 and irradiation. In A549 cells (A) PTEN together with Hsp90 inhibition suppressed the PI3K-Akt pathway, which resulted in the reduction of Bcl-xL. The treatment activated caspase-dependent apoptosis through p53-dependent mechanisms. The drug-induced decrease of Cdk4 led to the G1/S arrest in lung carcinoma cells. In SNB19 cells (B) the pro-survival PI3K-Akt pathway was activated. Combined NVP-AUY922-IR treatment induced DNA DSBs which could not be restored during the time of the experiment. The extent of DNA damage led to the over-expression of p21^{Waf1} that could block the cell cycle progression before entering mitosis.
The schema was proposed using the data presented in Figures 12-28 and Tables 10-12. Note the size of the letters/symbols and the thickness of the lines; gray means strong reduction or depletion of proteins. For the detailed description see text (reproduced from Niewidok et al. 2012 with kind permission from Neoplasia Press).

In more than 50% of human cancers, mutations occur in *TP53* gene. Hsp90 interacts with mutant p53 and protects it from the degradation by blocking the ligase activity of

MDM2 (Li et al. 2011c). It has been demonstrated that p53-mutant squamous carcinoma cells were less sensitive to 17-AAG treatment (Shintani et al. 2006). In contrast, we observed that SNB19 cells (p53mut) were more sensitive to the simultaneous drug-IR treatment than A549 (p53wt). It seems that p53 status can not be used for explaining or predicting the response of tumor cells to Hsp90 inhibition.

Another difference between A549 and SNB19 cell lines is PTEN status. PTEN is a phosphatase whose activity restricts growth and survival signals mediated by the PI3K-Akt pathway and the loss of functional PTEN can lead to constitutive activation of this pathway (Ramaswany et al. 1999). Akt is a key regulator of cell survival and proliferation; it protects the cells from apoptosis by hindering the release of cytochrome c from mitochondria. Activated Akt stimulates the pro-survival protein Bcl-xL through Bcl-2-associated death promoter (Bad) and thereby inhibits apoptosis (Kennedy et al. 1999). Furthermore, Akt can inhibit caspase 3 and caspase 9 activation, possibly by direct phosphorylation of caspase 9 (Zhou et al. 2000, Mayo et al. 2001). Akt can also interact with MDM2 to keep p53 in its inactive form (Haupt et al. 1997, Kubbutat et al. 1997). We observed elevated levels of PI3K and Akt in SNB19 samples, which indicate that the PI3K-Akt pathway was activated and could contribute to the cancer cell survival. In agreement, we observed no alterations in the expression of apoptotic markers caspase 3 and PARP. In A549 cells, wild type PTEN negatively regulates the PI3K-Akt pathway which, together with the down-regulation of Akt, survivin and Bcl-xL by simultaneous drug-IR treatment, resulted in the initiation of apoptosis, as confirmed by caspase 3 activation and PARP cleavage.

k-RAS status was identified as next difference between A549 and SNB19 tumor cell lines. Cells expressing mutant k-RAS express higher levels of p19^{ARF} mRNA, a protein that connects the k-RAS status with p53 expression (Brooks et al. 2001). p19^{ARF} interacts with MDM2 or with p53 directly to destabilize its functions (Palmero et al.1998). k-RAS mutant cells are therefore more prone to DNA damage-induced apoptosis and reduced G2/M arrest. Indeed, lung carcinoma cells (k-RAS mut) exhibited an increased apoptosis rate and G1/S arrest after prolonged incubation with Hsp90 inhibitors and IR. Cells with k-RAS in wild-type form tend to G2/M arrest in response to DNA damage, which is consistent with the response of SNB19 cells. The strong G2/M arrest in SNB19 cells was most likely controlled by p21^{Waf1}. The expression of p21^{Waf1} is regulated by p53, which can be activated by IR-induced

reactive oxygen species (ROS, Vitiello et al. 2009). We did not detect ROS directly, but we measured the expression of γH2AX expression as a marker of DNA DSBs, which are known to correlate with ROS (Kang et al. 2009). Simultaneous drug-IR treatment induced more DNA damage, which persisted longer in SNB19 than in A549 cells.

Figure 57. Summary of radiosensitization and cytotoxicity-related effects of the combined drug-IR (8 Gy) treatment on the protein expression, DNA damage, and cell cycle arrest induced in A549 (red) and SNB19 (blue bars) cell lines detected 48 hours after NVP-AUY922-IR treatment. Relative changes are given in percentage with respect to the corresponding DMSO controls. Data for A549 and SNB19 were taken from Figures 12-28 and Tables 10-12. Radiosensitization was calculated from IF_{10} values (Table 10; reproduced from Niewidok et al. 2010 with kind permission from Neoplasia Press).

48 hours post NVP-BEP800-IR

Figure 58. Summary of radiosensitization and cytotoxicity-related effects of the combined drug-IR (8 Gy) treatment on the protein expression, DNA damage, and cell cycle arrest induced in A549 (red) and SNB19 (blue bars) cell lines detected 48 hours after NVP-BEP800-IR treatment. Cleaved PARP was not detected in cells treated with NVP-BEP800. For further details see legend to Figure 57.

In summary, our data suggest that the cellular response to NVP-AUY922-IR or NVP-BEP800-IR treatment depended on the tumor cell line used and its genetic status (Fig. 56). The combination of Hsp90 inhibition and irradiation may cause radiosensitization or cytotoxicity and cell death in tumor cell lines. The sequence of the treatment involving Hsp90 inhibitors and IR has to be individually adjusted to achieve the best therapeutic outcome.

We observed some differences in the response of tumor cells to NVP-AUY922 in comparison with NVP-BEP800 (Figs. 57, 58), which most likely depended on the pharmacodynamic and pharmacokinetic features of both drugs (Brough et al. 2008, 2009). NVP-BEP800 was less cytotoxic than NVP-AUY922 towards examined tumor cell lines. Incubation of glioblastoma cells with NVP-BEP800 led to stronger radiosensitization that correlated with more DNA damage and increased G2/M arrest than in cells incubated with NVP-AUY922. In contrast to NVP-AUY922, we did not

detect any changes in the expression of k-RAS, PI3K or Bcl-xL 48 hours post NVP-BEP800-IR. Treatment with NVP-BEP800 did not induce the cleavage of PARP. Despite the differences in the action of both drugs, they still proved to be effective Hsp90 inhibitors and promising therapeutics.

5.2 Effects of NVP-AUY922 and NVP-BEP800 on the radiation response of normal fibroblast strains HFib1 and HFib2

The introduction of the potential drug into the clinic depends not only on its effects on cancer cells, but also on its influence on surrounding non-malignant tissue(s). Until now, nothing was known about the activity of NVP-AUY922 or NVP-BEP800 in combination with IR on the non-malignant cells. Thus, in this thesis we investigated the effects of these Hsp90 inhibitors in combination with IR in two normal human skin fibroblast strains HFib1 and HFib2. Fibroblasts were treated in the same way as tumor A549 and SNB19 cell lines (chapter 4.1). Interestingly, forty-eight-hour incubation with either Hsp90 inhibitor did not affect the plating efficiency of HFib1, or decreased it slightly in HFib2 (48 hours after NVP-AUY922, from 0.04 to 0.03). In sharp contrast to fibroblasts, plating efficiency was reduced 3- to 6-fold in lung carcinoma and glioblastoma respectively (48 hours after NVP-AUY922).

Thirty-minute and twenty-four-hour exposure to NVP-AUY922 or NVP-BEP800 did not influence the radiation response of both examined fibroblast strains. Only incubation with NVP-AUY922 for 48 hours post IR could moderately sensitize both fibroblast strains to radiation, as confirmed by the decreased SF2 and D_{10} values (i.e. HFib:1 SF2 ~0.61 -> ~0.52, D_{10} 6.0 -> 5.1). For comparison, in glioblastoma cells, which responded very strongly to NVP-AUY922-IR treatment, SF2 decreased about 2-fold from ~0.72 to ~0.3 and D_{10} from 8 to 3.9 (48 hours post drug-IR). The incubation of glioblastoma cells with NVP-BEP800 for 48 hours after IR resulted in the further decrease of SF2 (to 0.23) and D_{10} (to 3) values and stronger radiosensitization (Table 10). On the contrary, exposure to NVP-BEP800 for 48 hours did not increase the radiosensitivity of HFib1 and HFib2 cells.

It is apparent that NVP-AUY922 and NVP-BEP800 preferentially sensitize tumor cell lines to radiation. To elucidate the mechanisms underlying the selectivity of Hsp90

inhibitors, we analyzed the expression of several marker proteins, DNA repair kinetics and cell cycle distribution.

48 hours post NVP-AUY922-IR

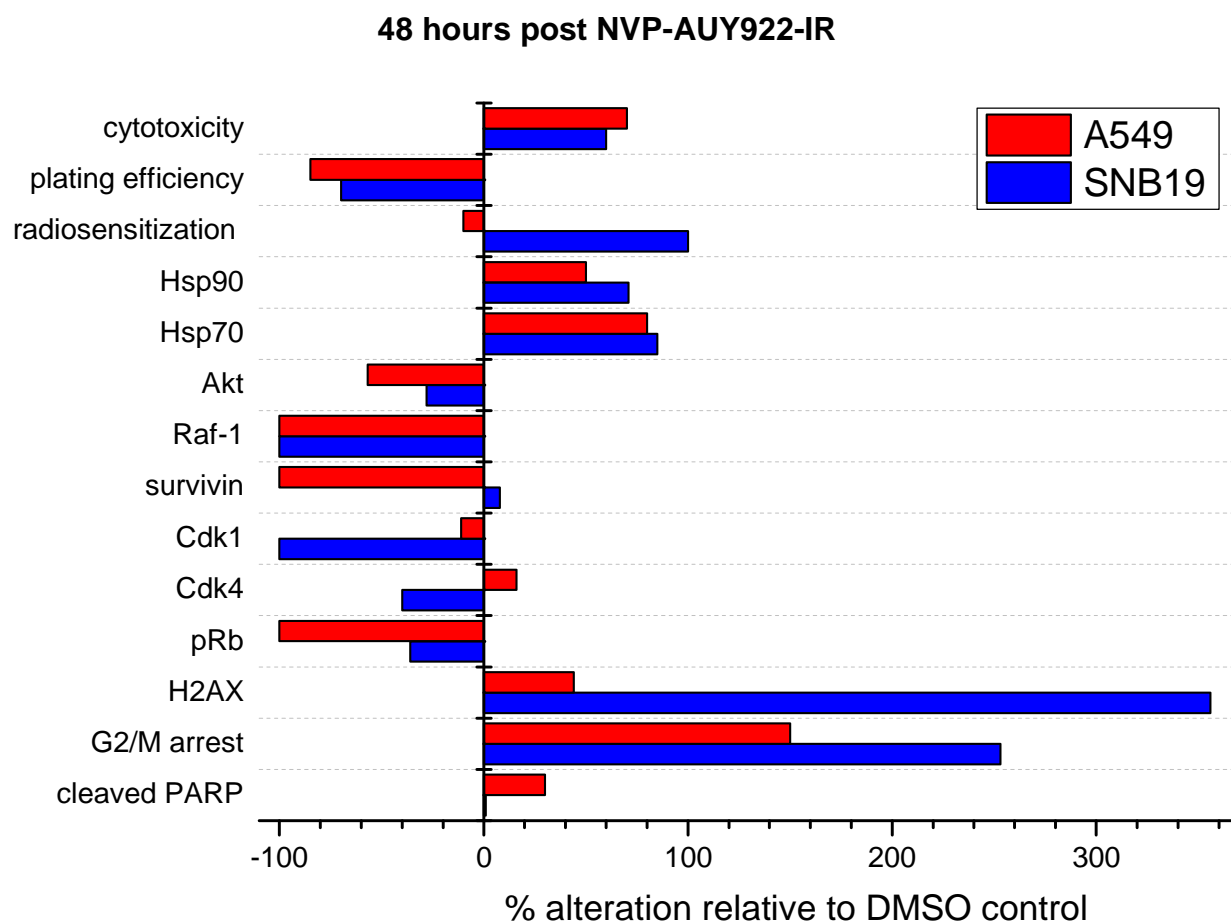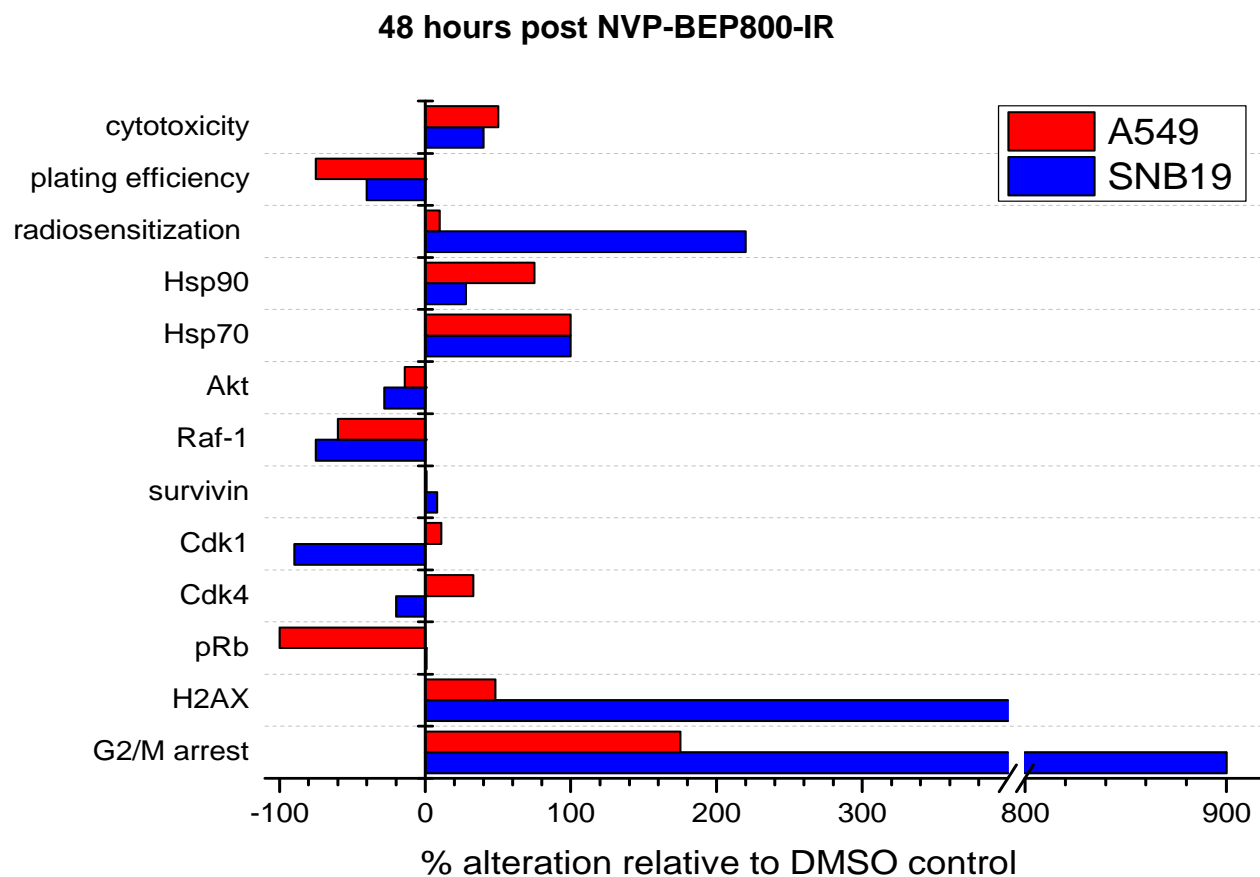
% alteration relative to DMSO control
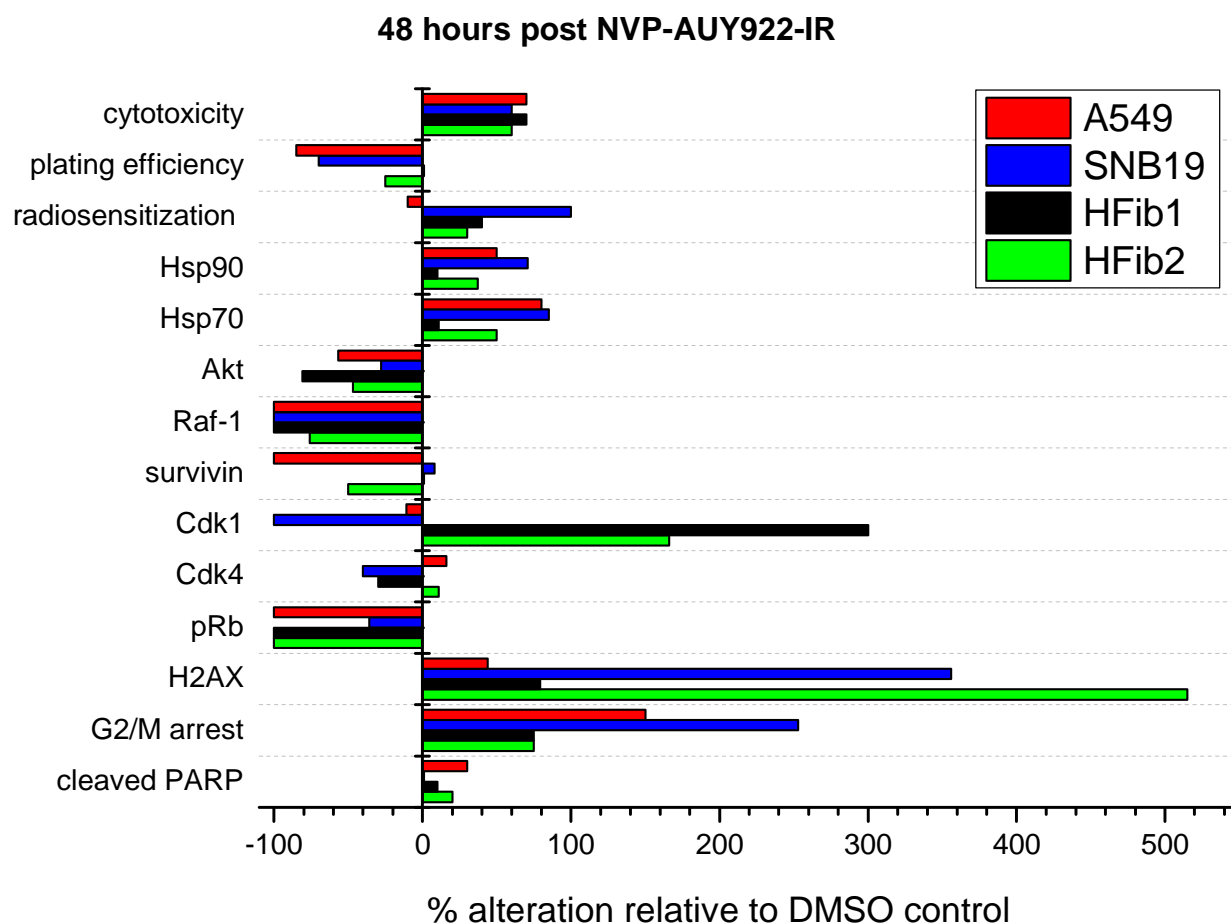
Figure 59. Summary of radiosensitization and cytotoxicity-related effects of the combined drug-IR (8 Gy) treatment on the protein expression, DNA damage, and cell cycle arrest induced in A549 (red), SNB19 (blue), HFib1 (black) and HFib2 (green bars) cell lines, detected 48 hours after NVP-AUY922-IR treatment. Data for fibroblast strains HFib1 and HFib2 were taken from Figures 29-40 and Tables 13-15. For further details see legend to Figure 57.
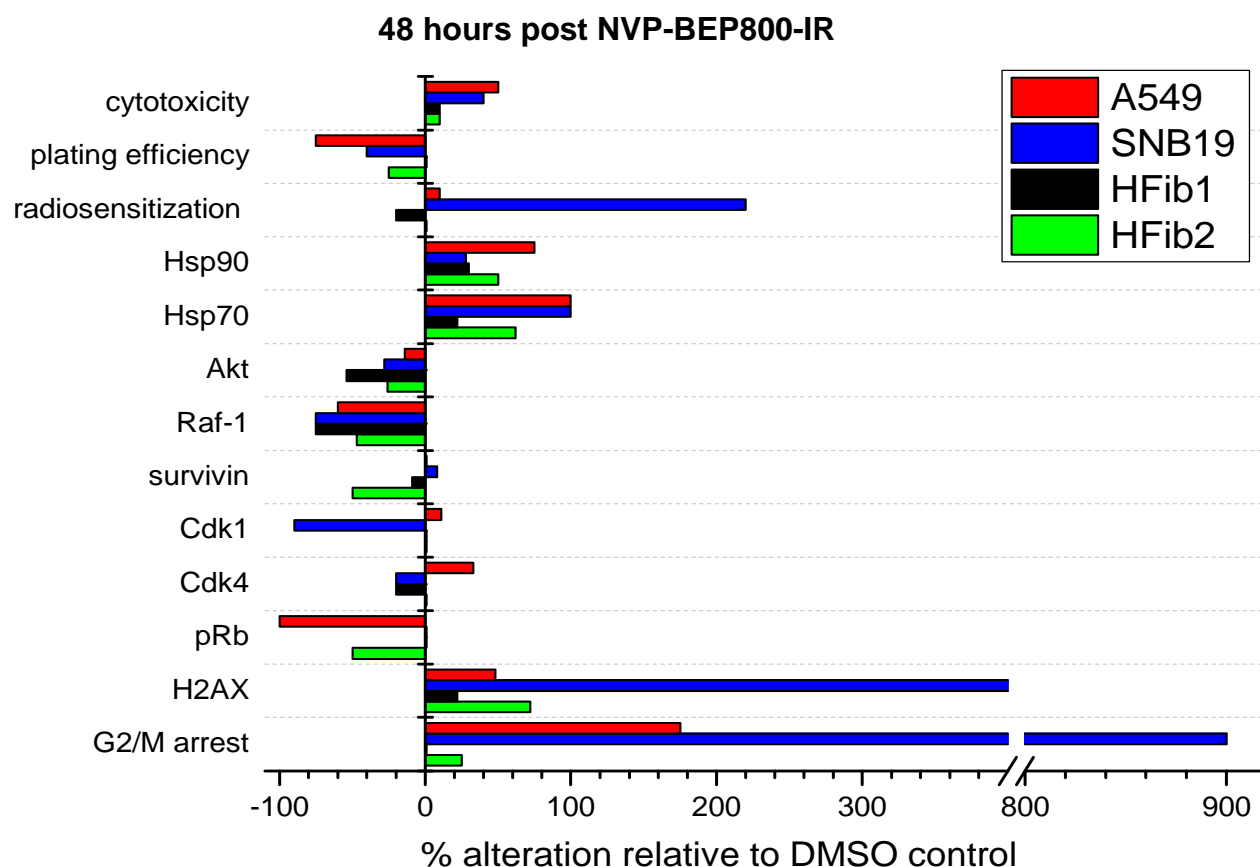
Figure 60. Summary of radiosensitization and cytotoxicity-related effects of the combined drug-IR (8 Gy) treatment on the protein expression, DNA damage, and cell cycle arrest induced in A549 (red), SNB19 (blue), HFib1 (black) and HFib2 (green bars) cell lines, detected 48 hours after NVP-BEP800-IR treatment. Data for fibroblast strains HFib1 and HFib2 were taken from Figures 29-40 and Tables 13-15. For further details see legend to Figure 57.

Our findings showed that the treatment of HFib1 or HFib2 cells with either NVP-AUY922 or NVP-BEP800 up-regulated the expression of Hsp90 and Hsp70, but to a lesser extent than in cancer cell lines (24 and 48 hours post drug-IR treatment). In fibroblasts, as well as in tumor cells, Hsp90 clients (including Akt, pAkt, Raf-1 and survivin) were partially depleted. In addition, we observed cleavage of PARP in fibroblasts after NVP-AUY922 treatment, similarly as in lung carcinoma cells, but different from glioblastoma samples. In contrast to A549 and SNB19 tumor cell lines, where NVP-AUY922-IR treatment caused the depletion of Cdk1, in fibroblasts we observed an up-regulation of this kinase. Cyclin-dependent kinase 1 not only regulates G2/M transition, but may also be required for the induction of particular cell death pathways (Castedo et al. 2002). Forty-eight-hour incubation of HFib1 or HFib2 cells after NVP-BEP800-IR treatment did not influence the expression of Cdk1.

The accumulation of DNA damage and the increased amount of events with low γH2AX expression in fibroblasts was observed 24 and 48 hours after NVP-AUY922-IR treatment. On the contrary to NVP-AUY922, exposure to NVP-BEP800-IR for 48 hours did not induce any additional DNA damage as compared with corresponding control samples. This differed from results previously described for cancer cells, where both Hsp90 inhibitors induced massive DNA damage in glioblastoma cells after the simultaneous drug-IR treatment that could not be restored throughout the duration of the experiments.

The cell cycle analysis revealed further differences in the response of tumor and non-malignant cells to combination of Hsp90 inhibition and IR. HFib1 and HFib2 cells treated with NVP-BEP800 (with/without IR) tended to moderate G1/S arrest, similarly as lung carcinoma cells. On the other hand, simultaneous NVP-AUY922-IR treatment shifted more HFib1 and HFib2 cells into the G2/M phase and depleted the S phase (24 hours post drug-IR). However, the G2/M arrest in fibroblasts was weaker than that observed in glioblastoma cell samples. In contrast to glioblastoma cells, treatment of both fibroblast strains with NVP-AUY922 for 48 hours (with or without IR) resulted in the increase of the sub-G1 phase. This together with cleavage of PARP indicates that 48-hour incubation with NVP-AUY922 could lead to the initiation of apoptosis in fibroblast strains.

In summary, the cellular response of non-malignant fibroblasts to the combination of Hsp90 inhibition and irradiation differed from that observed in cancer cell lines (Figs. 59, 60). The reasons underlying the selectivity of Hsp90 inhibitors, and especially NVP-AUY922 and NVP-BEP800, towards malignant cells remain elusive. Heat shock protein 90 is responsible for sustaining protein homeostasis in every human cell by the protein folding, intracellular transport and protein degradation of multiple regulators of cell growth and survival (Whitesell et al. 2005). It is apparent that non-malignant cells are not as susceptible to Hsp90 inhibition as cancer cells. Work from Kamal et al. 2003 showed that Hsp90 isolated from normal cells has a 100-fold lower binding affinity to 17-AAG than Hsp90 from cancer cells. However, this was contradicted by a report that showed equal time-dependent binding of geldanamycin to Hsp90 from different cell types (Gooljarsingh et al. 2006). Hsp90 inhibitors including 17-AAG or 17-DMAG are known to concentrate in tumors, but not in normal cells (Banerji et al. 2005). It is suggested that heat shock protein 90 in non-malignant

cells does not form super-complexes with co-chaperones and has lower ATPase activity than in cancer cells (Kamal et al. 2004). More recent analysis proposed the presence of two distinctive forms of Hsp90 (Moulick et al. 2011). One form should function in non-malignant cells, whereas the other form would specifically chaperone aberrant mutant proteins required for tumor cell survival.

Another probable explanation involves so called non-oncogene addiction hypothesis (Solimini et al. 2007). The development of malignancy includes an accumulation of mutations, which results in the expression of proteins that acquire new functions necessary for the survival of cancer cells or that cannot be correctly folded and aggregate. Apart from changed signalling pathways, tumor cells have to cope with extreme growth conditions like hypoxia or nutrient deprivation (Höckel et al. 2001, Luo et al. 2009). These intrinsic and extrinsic stress factors lead to the increasing dependency of cancer cells on the up-regulation of stress response pathways, and above all on the buffering potential of Hsp90 (Travers et al. 2012). When Hsp90 is inhibited, the protein homeostasis gets deregulated and cancer cells tend to be more vulnerable to therapy and drug-induced cell death (Hartl et al. 2011). Non-malignant cells do not experience such stress and therefore are less susceptible to Hsp90 inhibition than tumor cells (Luo et al. 2009).

5.3 Influence of Hsp70 pre-silencing combined with NVP-AUY922-treatment on the radiation response of cancer cell lines A549 and SNB19

A major problem of Hsp90 inhibitors is the drug-induced initiation of heat shock response, leading to the over-expression of heat shock proteins, including Hsp90 and Hsp70. In chapter 4.1 we have shown that exposure to NVP-AUY922 and NVP-BEP800 increased the expression of Hsp90 and Hsp70 in A549 and SNB19 tumor cell lines (Figs. 14, 15). Heat shock protein 70 is characterized by strong anti-apoptotic activities (see details in chapter 1.2.2), which promote cancer cell survival and can diminish the effects of Hsp90 inhibitors. Thus, one of the objectives of this thesis was to explore whether the suppression of Hsp70 up-regulation could influence the radiosensitizing effect of Hsp90 inhibitor NVP-AUY922. Since at the moment there are no specific, pharmacological inhibitors available, we used specific

siRNA to down-regulate stress-inducible Hsp70 and constitutively expressed Hsc70. Hsp70 or Hsc70 siRNA significantly decreased the expression of target proteins at mRNA and protein level in A549 and SNB19 cell samples up to 72 hours after transfection. Apart from the target suppression, Hsc70 knock-down induced the expression of Hsp70. Similar results were presented by Powers et al. 2007a, where the authors proposed that either Hsp70 or Hsc70 can form a complex with Hsp90. When Hsp70 was silenced, Hsc70 could take over its place and functions in the Hsp90 chaperone complex (Powers et al. 2007a).

Contrary data can be found in the literature on the influence of Hsp70 silencing on cell proliferation. Stable Hsp70 knock-down by shRNA reduced the cell growth and induced apoptosis in xenograft mouse models (Cai et al. 2011). Another report showed that the depletion of Hsp70 by adenovirus expressing antisense Hsp70 leads to the increased cell death in various cancer cell lines (i.e. glioblastoma; colon, breast and liver carcinoma, Nylandsted et al. 2006). On the contrary, Hsp70 silencing had no influence on the growth and survival of tumor cells of different origin *in vitro* (i.e. colon, ovarian, prostate and breast carcinoma; Gabai et al. 2005, Powers et al. 2007a). In our hands, the cell growth was slightly reduced when cancer cells were treated with Hsp70 siRNA, Hsc70 siRNA or both siRNAs simultaneously. These discrepancies between the results may come from different design of the experiments and basal expression of heat shock protein 70 in tested cell lines.

Next, we combined Hsp70 pre-silencing with NVP-AUY922 treatment and irradiation. The combination of Hsp70 silencing and Hsp90 inhibition has already been tested by other groups, although without irradiation (Guo et al. 2005, Powers et al. 2007a, Davenport et al. 2010). Hsp70 knock-down prior to treatment with 17-AAG increased the apoptotic effects of the Hsp90 inhibition in colon, ovarian carcinoma (Powers et al. 2007a) and multiple myeloma cells (Davenport et al. 2010). Similarly, the combination of Hsp70 silencing with 17-DMAG led to enhanced apoptosis in leukaemia cells (Guo et al. 2005). As expected from our previous works (Stingl et al. 2010, Niewidok et al, 2012), treatment with NVP-AUY922 alone induced strong over-expression of Hsp90, Hsp70 and Hsc70 in control A549 and SNB19 cells. The silencing of Hsp70 before NVP-AUY922-treatment suppressed the drug-induced Hsp70 up-regulation. At the same time, the combination of Hsp70 knock-down with NVP-AUY922 treatment induced heat shock response as indicated by the over-

expression of Hsp90 and Hsc70. Similar effects at the protein expression level were observed when pre-silenced, NVP-AUY922-treated cells were irradiated.

The influence of Hsp70 inhibition on radiosensitization remains to be elucidated. We have found only one study showing that Hsp70 silencing could sensitize endometrial cancer cells to irradiation (Du et al. 2009). In the present study we observed slight radiosensitization in lung carcinoma A549 cells and no changes in the radiation response of glioblastoma SNB19 cells after Hsp70 knock-down alone. To our knowledge this is the first study that combined Hsp70 silencing with Hsp90 inhibition and irradiation. In lung carcinoma cells, Hsp70 knock-down together with NVP-AUY922 did not induce more radiosensitization than NVP-AUY922 alone. The strongest increase of the radiation response of SNB19 cells was observed after Hsp90 inhibition alone. On the other hand, the combination of Hsp70 siRNA and Hsp90 inhibitor moderately sensitized glioblastoma cells to radiation. Hsp70 silencing alone or with IR did not influence the expression of examined marker proteins, DNA damage response or the cell cycle progression of A549 and SNB19 tumor cell lines. When pre-silenced cells were treated with NVP-AUY922, the observed alterations (i.e. depletion of Hsp90 clients) were similar to those after drug treatment alone.

To summarize, using specific siRNAs we have successfully down-regulated Hsp70 and Hsc70 in A549 and SNB19 tumor cell lines. The knock-down of target proteins lasted for at least 72 hours and slightly reduced the proliferation potential of examined cells. Pre-silencing of Hsp70 suppressed the NVP-AUY922-induced up-regulation of Hsp70 in examined A549 and SNB19 cells. However, the siRNA technique induced only transient target inhibition that was not sufficient for long-lasting experiments like colony survival assay.

6. Summary

Despite the recent improvements in oncology, cancer is still the leading cause of death in economically developed countries (Jemal et al. 2011). Heat shock protein 90 can be a promising target in cancer treatment as it is responsible for sustaining protein homeostasis in every human cell by folding and activating of more than 200 client proteins (Picard et al. 2002, Trepel et al. 2010). Hsp90 inhibition leads to degradation of Hsp90 client proteins by ubiquitin-proteasome pathway and thereby to impairment of multiple signaling pathways contributing to carcinogenesis (Zhang et al. 2004, Neckers et al. 2007). Apart from strong anti-tumor activities *in vitro* (Smith et al. 2005, Lundgren et al. 2009, Zhang et al. 2010) and *in vivo* (Supko et al. 1995, Lang et al. 2007, Solit et al. 2007), Hsp90 inhibitors can sensitize tumor cells to radiation (Bisht et al. 2003, Dote et al. 2005, Koll et al. 2008, Stingl et al.2010, Schilling et al. 2011). In the majority of the studies, the Hsp90 inhibitor was administered before IR (i.e. Bisht et al. 2003, Machida et al. 2003, Dote et al. 2006). However, other report claimed that the opposite schedule (Hsp90 inhibition after IR) was better for prostate cancer cell killing (Enmon et al. 2003).

Recently, our group showed the radiosensitizing potential of two novel Hsp90 inhibitors: NVP-AUY922 and NVP-BEP800 (Stingl et al. 2010). The drugs were administered to cancer cell lines of different origin 24 hours before irradiation (drug-first treatment). In the present work, we explored the effects of a schedule other than drug-first treatment on A549 and SNB19 tumor cell lines. Cell samples were treated with either NVP-AUY922 or NVP-BEP800 one hour before IR and kept in the drug-containing medium for up to 48 hours (simultaneous drug-IR treatment). After the drug-first treatment all tumor cell lines were sensitized to irradiation, regardless of their origin (Stingl et al. 2010). The same cell lines exposed to the simultaneous drug-IR treatment exhibited different cellular responses. SNB19 cells were sensitized to radiation and based on SF2 and D_{10} values, the radiosensitization was stronger than after drug-first treatment. The increase of radiation response correlated with massive DNA lesions that could not be restored during the time of experiment. The extent of DNA damage led to the over-expression of cell cycle inhibitor p21[Waf1] that could stop the cell cycle progression at G2/M checkpoint. Detected elevated PI3K and Akt levels, together with PTEN null mutation, indicated that the PI3K-Akt

pathway was activated and promoted SNB19 cell survival. Lung carcinoma A549 cells exhibited cytotoxicity to simultaneous NVP-AUY922-IR or NVP-BEP800-IR treatment. In contrast to SNB19 cells, lung carcinoma A549 cells express functional PTEN that negatively regulates the pro-survival PI3K-Akt pathway. This, together with the drug-induced down-regulation of several pro-survival proteins Akt, survivin and Bcl-xL, led to the initiation of apoptosis in lung carcinoma cell line. The presence of mutation in k-RAS and the decrease of Cdk4 expression by Hsp90 inhibitors could explain the G1/S arrest observed in lung carcinoma cells.

Overall, our findings showed that depending on the tumor cell line, the combination of Hsp90 inhibition and irradiation may result in radiosensitization or apoptosis of cancer cell lines. It is advised to adjust the sequence of treatment, involving Hsp90 inhibition and irradiation, on the basis of the genetic background of tumor cells.

Before entering the clinic, novel therapeutics should be tested on non-malignant tissue to exclude their possible toxic activities. The effects of NVP-AUY922 and NVP-BEP800 on non-malignant cells have not been studied yet. Thus, we applied the simultaneous drug-IR treatment on human skin fibroblast strains (HFib1 and HFib2). The plating efficiency (PE) of non-malignant HFib1 and HFib2 cells was not affected by incubation with either Hsp90 inhibitor. This contrasted with the findings in tumor cell lines, where PE was strongly reduced 48 hours after NVP-AUY922 treatment. Normal fibroblasts were weakly sensitized to IR when the incubation with NVP-AUY922 lasted 48 hours. Shorter incubation periods (30 minutes and 24 hours post NVP-AUY922-IR) did not affect the radiation response of HFib1 and HFib2 cells. Exposure to NVP-BEP800 did not sensitize human skin fibroblasts to IR; on the contrary it even seemed to induce some resistance to radiation (48 hours post drug-IR). For comparison, 48-hour incubation post NVP-BEP800-IR or NVP-AUY922-IR treatment resulted in the strong radiosensitization of glioblastoma SNB19 cells.

Furthermore, we examined the possible mechanism(s) underlying the selective action of NVP-AUY922 and NVP-BEP800. In contrast to cancer cells, we observed only a moderate up-regulation of Hsp90 and Hsp70 in both fibroblast strains after incubation with either Hsp90 inhibitor. At the same time, the depletion of Hsp90 clients (including Akt, pAkt and Raf-1) after drug treatment was similar to that observed in A549 and SNB19 cell samples.

Forty-eight hours after NVP-AUY922-IR treatment we observed an accumulation of DNA damage and moderate G2/M arrest in HFib1 and HFib2 cell samples. In addition, increased sub-G1 phase and cleavage of PARP indicated that the combined NVP-AUY922-IR treatment could lead to the apoptosis of non-malignant fibroblasts. In contrast to NVP-AUY922, incubation with NVP-BEP800 (with or without IR) did not affect DNA damage mechanisms or cell cycle phase distribution when compared with control fibroblasts.

In conclusion, this work showed that Hsp90 inhibitors NVP-AUY922 and NVP-BEP800 preferentially sensitize tumor cells to radiation, whereas the effect on normal fibroblasts was much weaker. The exact mechanisms underlying the Hsp90 inhibitors' selectivity towards malignant cells remain to be elucidated.

It was shown previously that the administration of Hsp90 inhibitors, including NVP-AUY922 and NVP-BEP800, induces heat shock response (Stingl et al. 2010, Niewidok et al. 2012, Patel et al. 2012). Heat shock response triggers the up-regulation of Hsp70, which, due to its strong anti-apoptotic properties, might be responsible for reducing the effects of Hsp90 inhibition. In order to prevent this, we down-regulated Hsp70 and its constitutively expressed homologue Hsc70 in A549 and SNB19 cancer cell lines using the siRNA-based approach. The silencing of target proteins lasted up to 72 hours and resulted in a reduction of cell proliferation. Next, we examined whether Hsp70 pre-silencing could improve the radiosensitizing potential of NVP-AUY922. Indeed, the transfection with Hsp70 siRNA suppressed the NVP-AUY922-induced over-expression of the target protein. However, on the long-term scale, it did not influence the radiosensitivity of A549 and SNB19 cells.

To summarize, the use of siRNA proved that Hsp70 inhibition could be used to support Hsp90 inhibition on the short-term scale. Therefore, for future works, more potent and stable methods of Hsp70 inhibition are needed, i.e. Hsp70 shRNA stable transfection or specific pharmacological inhibitors.

This thesis presented the effects induced by two novel Hsp90 inhibitors NVP-AUY922 and NVP-BEP800, in combination with irradiation in tumor cell lines as well as in normal skin fibroblasts. Hsp70 pre-silencing was tested as a method for improving radiosensitizing potential of NVP-AUY922. Recently, these *in vitro* results

were corroborated in the *in vivo* study in our group, in which the combination of NVP-AUY922 and IR increased the survival rate of tumor bearing mice (Kuger et al. 2012). In addition, it has been shown that NVP-AUY922 and NVP-BEP800 could decrease the migration and invasion of cancer cells at normoxic and hypoxic conditions (Hartmann et al. 2013). All these results support the use of NVP-AUY922 and NVP-BEP800 in combination with irradiation in future clinical trials. However, further experiments on the extended group of cell lines should be carried out to identify the key regulators of the cell type-specific response to Hsp90 inhibition and IR. The role of Hsp70 in the radiation response of tumor cells and in combination with Hsp90 inhibitors should be further studied.

7. Zusammenfassung

Trotz aller wissenschaftlicher Fortschritte, die in den letzten Jahren in der Onkologie erfolgten, ist Krebs eine der Haupttodesursachen in den wirtschaftlich entwickelten Ländern. Das Hitzeschockprotein 90 (Hsp90) stellt ein vielversprechendes neues Target für die Krebstherapie dar, weil es einen großen Anteil des Proteingleichgewichts in jeder humanen Zelle durch Faltung und Aktivierung seiner Klientenproteine kontrolliert (Picard et al. 2002, Trepel et al. 2010). Die Hsp90 Inhibition verursacht den Abbau von Hsp90 Klientenproteinen durch den Ubiquitin-Proteasom-Signalweg, und dadurch werden gleichzeitig viele Signaltransduktionswege behindert, die zur Krebsentstehung beitragen können (Zhang et al. 2004, Neckers et al. 2007). Es wurde gezeigt, dass Hsp90 Inhibitoren starke anti-proliferative Eigenschaften *in vitro* (Smith et al. 2005, Lundgren et al. 2009, Zhang et al. 2010) und *in vivo* aufweisen (Supko et al. 1995, Lang et al. 2007, Solit et al. 2007). Außerdem führte die Hsp90 Inhibition zur Radiosensibilisierung unterschiedlicher Tumorzelllinien (Bisht et al. 2003, Dote et al. 2005, Koll et al. 2008, Stingl et al.2010, Schilling et al. 2011). In der Mehrheit der Arbeiten wurde der Hsp90 Inhibitor vor der Bestrahlung hinzugegeben (z. B. Bisht et al. 2003, Machida et al. 2003, Stingl et al. 2010). In anderen Arbeiten ist jedoch beschrieben, dass das umgekehrte Behandlungsschema (Hsp90 Inhibition nach der Bestrahlung) stärkere Radiosensibilisierung verursacht (Enmon et al. 2003, Koll et al. 2008).

Vor Kurzem wurde in unserer Arbeitsgruppe gezeigt, dass die neuartigen Hsp90 Inhibitoren NVP-AUY922 und NVP-BEP800 zur Erhöhung der Strahlenempfindlichkeit der Tumorzelllinien führen (Stingl et al. 2010). Die Krebszellen wurden 24 Stunden vor der Bestrahlung behandelt und bestrahlt ('drug-first' Behandlungsschema). In dieser Doktorarbeit wurden die Effekte eines anderen Behandlungsschemas auf die A549 und SNB19 Tumorzelllinien untersucht. Die Zellen wurden entweder mit NVP-AUY922 oder NVP-BEP800 eine Stunde vor der Bestrahlung behandelt und bis zu 48 Stunden nach der Bestrahlung weiterhin mit Hsp90 Inhibitor kultiviert (simultane drug-IR Behandlungsschema). Das 'drug-first' Behandlungsschema führte zur Radiosensibilisierung von Tumorzellen, unabhängig von ihrem Ursprung (Stingl et al. 2010). Die gleichen Tumorzelllinien zeigten bei simultanem Behandlungsschema unterschiedliche zelluläre Antworten.

Die Hsp90 Inhibition in Kombination mit der Bestrahlung erhöhte die Strahlenempfindlichkeit von SNB19-Zellen und, basierend auf den SF2 und D_{10}-Werten, war die Radiosensibilisierung nach simultaner Behandlung stärker als nach dem ‚drug-first' Behandlungsschema. Die Verstärkung der Strahlenantwort in SNB19-Zellen korrelierte mit den DNA Schäden, die während der Zeit des Experimentes nicht repariert werden konnten. Der Umfang von den DNA Doppelstrangbrüchen führte in dieser Glioblastomazelllinie zu einer Überexpression des Zellzyklusinhibitors p21^{Waf1}, was den G2/M Arrest verursachen konnte. Es wurden erhöhte Expressionslevels von PI3K und Akt detektiert, die zusammen mit einer null Mutation in PTEN auf einen aktivierten PI3K-Akt Signalweg hindeuteten, der das Überleben der SNB19-Zellen förderte. Die simultane drug-IR Behandlung rief Zytotoxizität bei A549-Zellen hervor. Im Gegensatz zu SNB19-Zellen exprimieren A549 Lungenkarzinomzellen PTEN Wildtyp, das den PI3K-Akt Signalweg negativ regulieren kann. Dies, zusammen mit der Reduzierung der Expression der ‚pro-survival' Proteine Akt, Survivin und Bcl-xL, die durch die Behandlung induziert wurde, leitete die Apoptose ein. Eine Verminderung der Cdk4 Kinase nach simultaner drug-IR Behandlung und eine vorliegende Mutation in k-RAS führten zu einem G1/S Arrest in den Lungenkarzinomzellen.

Zusammenfassend zeigen die hier gewonnenen Ergebnisse, dass abhängig von der Tumorzelllinie, die Kombination der Hsp90 Inhibition mit Bestrahlung zur Radiosensibilisierung oder zur Apoptose führen kann. Die Reihenfolge der Behandlung mit Hsp90 Inhibitoren und Bestrahlung sollte individuell der Tumorart und den vorliegenden Mutationen angepasst werden.

Bevor Medikamente in der Klinik angewendet werden können, müssen sie auf nicht-malignem Gewebe getestet werden, um eine mögliche toxische Wirkung auszuschließen. Der Einfluss von NVP-AUY922 und NVP-BEP800 wurde noch nicht auf nicht-malignen Zellen getestet. Deshalb wurden in der vorliegenden Arbeit die zwei humane Hautfibroblastenlinien HFib1 und HFib2 nach dem simultanen Behandlungsschema mit Hsp90 Inhibitoren und Bestrahlung behandelt. Die Plattiereffizienz (PE) der nicht-malignen HFib1 und HFib2 Zellen wurde von der Behandlung mit Hsp90 Inhibitoren nicht beeinflusst. Dies stand im Gegensatz zu den Ergebnissen in Tumorzelllinien, bei denen eine starke Reduktion der Plattiereffizienz

beobachtet wurde (48 Stunden nach Behandlung mit NVP-AUY922). Eine schwache Radiosensibilisierung der normalen Fibroblasten wurde nur nach 48 Stunden Inkubation mit NVP-AUY922 erreicht. Kürzere Inkubationszeiten (30 Minuten und 24 Stunden nach NVP-AUY922-IR) hatten keinen Einfluss auf die Strahlenantwort der Zelllinien HFib1 und HFib2. Die Behandlung mit NVP-BEP800 sensibilisierte die Fibroblasten nicht für die Bestrahlung, im Gegenteil, die Substanz induzierte eine geringe Radioresistenz (48 Stunden nach NVP-BEP800-IR). Im Vergleich dazu, zeigten die SNB19 Glioblastoma Zellen die stärkste Radiosensibilisierung 48 Stunden nach NVP-BEP800-IR Behandlung.

Weiterhin wurde nach möglichen Mechanismen, die die selektive Wirkung des NVP-AUY922 und NVP-BEP800 erklären können, untersucht. Im Gegensatz zu Krebszelllinien, wurde nur eine moderate Hochregulierung der Hitzeschockproteine in beiden Fibroblastenlinien beobachtet. Gleichzeitig war die Depletion von Hsp90 Klientenproteinen (Akt, pAkt und Raf-1) nach Behandlung ähnlich wie die, die in A549- und SNB19-Zellen induziert war. Achtundvierzig Stunden nach NVP-AUY922-IR Behandlung wurde eine Akkumulation von DNA Schäden und ein moderater G2/M Arrest in Fibroblasten gesehen. Zusätzlich, deutete eine erhöhter Zahl von Zellen, die sich in der Sub-G1-Phase befunden, und die Spaltung von PARP darauf hin, dass die simultane NVP-AUY922-IR Behandlung den Zelltod in Fibroblasten einleiten konnte. Im Gegensatz zu NVP-AUY922, induzierte die Inkubation mit NVP-BEP800 für 48 Stunden (mit und ohne Bestrahlung) keine zusätzlichen DNA Schäden oder Zellzyklusstörungen verglichen mit den Kontrollen.

Diese Arbeit zeigte, dass NVP-AUY922 und NVP-BEP800 Tumorzelllinien für die Bestrahlung sensibilisieren, wohingegen der Einfluss von Hsp90 Inhibitoren auf normale Fibroblasten geringer war. Der exakte Mechanismus der Selektivität der Hsp90 Inhibitoren auf Krebszellen ist aber noch unbekannt und erfordert weitere Experimente.

Die Behandlung mit N-terminalen Hsp90 Inhibitoren, zum Beispiel mit NVP-AUY922 oder mit NVP-BEP800, induziert die Hitzeschockantwort und unter anderem die Hochregulierung von Hsp70 (Stingl et al. 2010, Niewidok et al. 2012, Patel et al. 2012). Hsp70 ist bekannt für seine starken anti-apoptotischen Eigenschaften, die das therapeutische Potenzial der Hsp90 Inhibitoren reduzieren können. Um das zu

verhindern, wurde eine siRNA-basierte Strategie zur Unterdrückung von Hsp70-Überexpression nach Hsp90 Inhibition getestet. Es wurde eine Verminderung der Expression von induzierbarem Hsp70 und konstitutiv exprimiertem Hsc70 in Krebszelllinien A549 und SNB19 erreicht. Die Unterdrückung von Target-Proteinen dauerte bis zu 72 Stunden und führte zu einer verlangsamten Zellproliferation. Die Behandlung mit siRNA reduzierte die von NVP-AUY922 induzierte Hsp70-Überexpression, aber beeinflusste nicht die Strahlenempfindlichkeit der Tumorzelllinien A549 und SNB19. Die Transfektion mit siRNA hat bewiesen, dass die Hsp70 Inhibition als eine Unterstützung der Hsp90 Inhibition dienen kann. Dies ist jedoch eine kurzzeitige Methode der Hemmung und alternative Methoden, wie zum Beispiel stabile Hsp70 shRNA Transfektion oder pharmakologische Inhibition, zur Hemmung der Hsp70 Aktivitäten nötig sind.

Die in dieser Arbeit gewonnen Erkenntnisse erläutern die Effekte, die von zwei neuartigen Hsp90 Inhibitoren NVP-AUY922 und NVP-BEP800 in Kombination mit Bestrahlung induziert werden, sowohl in Tumorzelllinien als auch in normalen Hautfibroblasten. Hsp70-Silencing wurde als Methode zur Erhöhung des radiosensibilisierenden Potenzials des Inhibitor NVP-AUY922 getestet. Diese *in vitro* Ergebnisse wurden durch eine Studie im Tiermodell bestätigt (Kuger et al. 2012). In dieser Studie erhöhte die Kombination der Hsp90 Inhibition mit Bestrahlung die Überlebensrate der Mäuse. Zusätzlich hat Hartmann et al. 2013 bewiesen, dass die Behandlung mit NVP-AUY922 und NVP-BEP800 die Motilität und Invasion der Tumorzellen unter Normoxie und Hypoxie reduziert. Alle diese Resultate zusammen sprechen für eine Anwendung von NVP-AUY922 und NVP-BEP800 in klinischen Studien, die alleine oder in Kombination mit Bestrahlung erfolgen könnte. Weitere Arbeiten an größeren Gruppen von Zelllinien sind zur Identifizierung von Proteinen nötig, die die zellspezifische Antwort zur Hsp90 Inhibition regulieren. Hier gewonnene Ergebnisse machen weitere Experimente erforderlich, um die exakte Rolle der Hsp70 Proteine für die Strahlenantwort zu verstehen.

8. References

Adams PD. 2001. Regulation of the retinoblastoma tumor suppressor protein by cyclin/cdks. *Biochim. Biophys. Acta* 1471: M123-M133.

Banerji U. et al. 2005. Pharmacokinetic - pharmacodynamic relationships for the heat shock protein 90 molecular chaperone inhibitor 17-allylamno-17-demethoxygeldanamycin in human ovarian cancer xenograft models. *Clin. Cancer Res.* 11: 7023-7032.

Beere HM. et al. 2000. Heat-shock protein 70 inhibits apoptosis by preventing recruitment of procaspase-9 to the Apaf-1 apoptosome. *Nat. Cell Biol.* 2: 469-475.

Bernier J. et al. 2004. Radiation oncology: a century of achievements. *Nat. Rev. Cancer* 4: 737-747.

Bischoff P. et al. 2009. Radiosensitizing agents for the radiotherapy of cancer: advances in traditional and hypoxia targeted radiosensitizers. *Expert Opin. Ther. Pat.* 19: 643-662.

Bisht KS. et al. 2003. Geldanamycin and 17-allylamino-17-demethoxygeldanamycin potentiate the *in vitro* and in vivo radiation response of cervical tumor cells via the heat shock protein 90-mediated intracellular signaling and cytotoxicity. *Cancer Res.* 63: 8984-8995.

Braunstein MJ. et al. 2001. Anti-myeloma effects of heat shock protein 70 molecular chaperone inhibitor MAL3-101. *J. Oncol.* 2011: 232037, doi:10.1155/2011/232037.

Brooks DG. et al. Mutant k-RAS enhances apoptosis in embryonic stem cells in combination with DNA damage and is associated with increased levels of p19[ARF]. *Oncogene* 20: 2144-2152.

Brough PA. et al. 2008. 4,5-diarylisoxazole Hsp90 chaperone inhibitors: potential therapeutic agents for the treatment of cancer. *J. Med. Chem.* 51: 196-218.

Brough PA. et al. 2009. Combining hit identification strategies: fragment based and in silico approaches to orally active 2-aminothieno[2,3-d]pyrimidine inhibitors of the Hsp90 molecular chaperone. *J. Med. Chem.* 52: 4794-4809.

Bull EA. et al. 2004. Enhanced tumor cell radiosensitivity and abrogation of G2 and S phase arrest by the Hsp90 inhibitor 17-dimethylaminoethylamino-17-demethoxygeldanamycin. *Clin. Cancer Res.* 10: 8077-8084.

Burdak-Rothkamm S. et al. 2009. New molecular targets in radiotherapy: DNA damage signaling and repair in targeted and non-targeted cells. *Eur. J. Pharmacol.* 625: 151-155.

Bussink J. et al. 2007. Microenvironmental transformations by VEGF- and EGF-receptor inhibition and potential implications for responsiveness to radiotherapy. *Radiother. Oncol.* 82: 10-17.

Cai H. et al. 2011. shRNA-mediated gene silencing of heat shock protein 70 inhibits human colon cancer cell growth *in vitro* and *in vivo*. *Mol. Cell Biochem.* DOI 10.1007/s11010-011-0990-3.

Camphausen K. et al. 2007. Inhibition of Hsp90: a multitarget approach to radiosensitization. *Clin. Cancer Res.* 13: 4326-4330.

Campisi J. et al. 2007. Cellular senescence: when bad things happen to good cells. *Nat. Rev. Mol. Cell Biol.* 8: 729-740.

Calderwood SK. et al. 2006. Heat shock proteins in cancer: chaperones of tumorigenesis. *Trends Biochem. Sci.* 31: 164-172.

Castedo M. et al. 2002. Cyclin-dependent kinase-1: linking apoptosis to cell cycle and mitotic catastrophe. *Cell Death Differ.* 9: 1287-1293.

Csermely P. et al. 1998. The 90-kDa molecular chaperone family: structure, function, and clinical applications. A comprehensive review. *Pharmacol. Ther.* 79: 129-168.

D'Amours D. et al. 2001. Gain-of-function of poly (ADP-ribose) polymerase-1 upon cleavage by apoptotic proteases: implications for apoptosis. *J. Cell Sci.* 114: 3771-3778.

Daugaard M. et al. 2007. The heat shock protein 70 family: highly homologous proteins with overlapping and distinct functions. *FEBS Lett.* 581: 3702-3710.

Davenport EL. et al. 2010. Targeting heat shock protein 72 enhances Hsp90 inhibitor-induced apoptosis in myeloma. *Leukemia* 24: 1804-1807.

Djuzenova CS. et al. 1994. Effect of electric field pulses on the viability and on the membrane-bound immunoglobulins of LPS-activated murine B-lymphocytes: correlation with the cell cycle. *Cytometry* 15, 35–45.

Djuzenova CS. et al. 2004. Normal expression of DNA repair proteins, hMre11, Rad50 and Rad51, but protracted formation of Rad50 containing foci in X-irradiated skin fibroblasts from radiosensitive cancer patients. *Br. J. Cancer* 90: 2356-2363.

Djuzenova CS. et al. 2012. Hsp90 inhibitor NVP-AUY922 enhances radiation sensitivity of tumor cell lines under hypoxia. *Cancer Biol. Ther.* 13: 425-434.

Dote H. et al. 2005. ErbB3 expression predicts tumor cell radiosensitization induced by Hsp90 inhibition. *Cancer Res.* 65: 6967-6975.

Dote H. et al. 2006. Inhibition of Hsp90 compromises the DNA damage response to radiation. *Cancer Res.* 66: 9211-9220.

Du X. et al. 2009. Silencing of heat shock protein 70 expression enhances radiotherapy efficacy and inhibits cell invasion in endometrial cancer cell lines. *Croat. Med. J.* 50: 143-150.

Eastman A. 2004. Cell cycle checkpoints and their impact on anticancer therapeutic strategies. *J. Cell Biol.* 91: 223-231.

Eccles SA. et al. 2008. NVP-AUY922: a novel heat shock protein 90 inhibitor active against xenograft tumor growth, angiogenesis and metastasis. *Cancer Res.* 68: 2850-2860.

Enmon R. et al. 2003. Combination treatment with 17-N-allylamino-17-demethoxygeldanamycin and acute irradiation produces supra-additive growth suppression in human prostate carcinoma spheroids. *Cancer Res.* 63: 8393-8399.

Eriksson D. et al. 2010. Radiation-induced cell death mechanisms. *Tumour Biol.* 31: 363-372.

Evans CG. et al. 2010. Heat shock protein 70 (Hsp70) as an emerging drug target. *J. Med. Chem.* 53: 4585-4602.

Florin L. et al. 2004. Nuclear translocation of papillomavirus minor capsid protein L2 requires Hsc70. *J. Virol.* 78: 5546-5553.

Gabai VL. et al. 2005. Increased expression of the major heat shock protein Hsp72 in human prostate carcinoma cells is dispensable for their viability but confers resistance to a variety of anticancer agents. *Oncogene* 24: 3328-3338.

Gaspar N. et al. 2009. Acquired resistance to 17-allylamino-17-demethoxygeldanamycin (17-AAG, tanespimycin) in glioblastoma cells. *Cancer Res.* 69: 1966-1975.

Goloudina AR. et al. 2012. Inhibition of Hsp70: a challenging anti-cancer strategy. *Cancer Lett.* 325: 117-124.

Gooljarsingh LT. et al. 2006. A biochemical rationale for the anticancer effects of Hsp90 inhibitors: slow, tight binding inhibition by geldanamycin and its analogues. *Proc. Natl. Acad. Sci. USA* 103: 7625-7630.

Guo F. et al. 2005. Abrogation of heat shock protein 70 induction as a strategy to increase anti-leukemia activity of heat shock protein 90 inhibitor 17-allylamino-demethoxy-geldanamycin. *Cancer Res.* 65: 10536-10544.

Guo Y. et al. 2001. Evidence for a mechanism of repression of heat shock factor 1 transcriptional activity by multichaperone complex. *J. Biol. Chem.* 276: 45791-45799.

Gupta AK. et al. 2000. RAS-mediated radiation resistance is not linked to MAP kinase activation in two bladder carcinoma cell lines. *Radiat. Res.* 154: 64-72.

Gupta AK. et al. 2001. The Ras radiation resistance pathway. *Cancer Res.* 61: 4278-4282.

Haberland J. et al. 2013. German short-term cancer mortality predictions up until 2015. http://www.krebsdaten.de/Krebs/DE/Home/homepage_node.html

Hanahan D. et al. 2000. The hallmarks of cancer. *Cell* 100: 57-70.

Hanahan D. et al. 2011. Hallmarks of cancer: the next generation. *Cell* 144: 646-674.

Hartmann S. et al. 2013. Hsp90 inhibition by NVP-AUY922 and NVP-BEP800 decreases migration and invasion of irradiated normoxic and hypoxic tumor cell lines. *Cancer Lett.* 331: 200-210.

Hartl FU. et al. 2011. Molecular chaperones in protein folding and proteostasis. *Nature* 475: 324-332.

Haupt Y. et al. 1997. Mdm2 promotes the rapid degradation of p53. *Nature* 387: 296-299.

Havik B. et al. 2007. Additive viability-loss following hsp70/hsc70 double interference and hsp90 inhibition in two breast cancer cell lines. *Oncol. Rep.* 17: 1501-1510.

Helton ES. et al. 2007. p53 modulation of the DNA damage response. *J. Cell Biol.* 100: 883-896.

Höckel M. et al. 2001. Tumor hypoxia: definition and current clinical, biologic and molecular aspects. *J. Natl. Cancer Inst.* 93: 266-276.

Hutchison KA. et al. 1994. Proof that hsp70 is required for assembly of the glucocorticoid receptor into a heterocomplex with hsp90. *J. Biol. Chem.* 269: 5043-5049.

Iliakis G. et al. 2003. DNA damage checkpoint control in cells exposed to ionizing radiation. *Oncogene* 22: 5834-5847.

Jaattela M. et al. 1998. Hsp70 exerts its anti-apoptotic function downstream of caspase-3-like proteases. *EMBO J.* 17: 6124-6134.

Jeggo PA. et al. 2011. The role of homologous recombination in radiation-induced double-strand break repair. *Radiother. Oncol.* 1: 7-12.

Jego G. et al. 2010. Targeting heat shock proteins in cancer. *Cancer Lett.* 2: 275-285.

Jemal A. et al. 2011. Global cancer statistics. *CA Cancer J. Clin.* 61: 69-90.

Jhaveri K. et al. 2012a. Advances in the clinical development of heat shock protein 90 (Hsp90) inhibitors. *Biochim. Biophys. Acta* 1823: 742-755.

Jhaveri K. et al. 2012b. Hsp90 inhibitors for cancer therapy and overcoming drug resistance. *Adv. Pharmacol.* 65: 471-517.

Jin P. et al. 1998. Nuclear localization of cyclin B1 controls mitotic entry after DNA damage. *J. Cell Biol.* 141: 875-885.

Kabakov AE. et al. 2008. Radiosensitization of human vascular endothelial cells through Hsp90 inhibition with 17-N-allilamino-17-demethoxygeldanamycin. *Int. J. Radiat. Oncol. Biol. Phys.* 71; 858-865.

Kamal A. et al. 2003. A high affinity conformation of Hsp90 confers tumor selectivity on Hsp90 inhibitors. *Nature* 425: 407-410.

Kamal A. et al. 2004. Hsp90 inhibitors as selective anticancer drugs. *Discov. Med.* 4: 277-280.

Kampinga HH. et al. 2009. Guidelines for the nomenclature of the human heat shock proteins. *Cell Stress Chaperones* 14: 105-111.

Kang MA. et al. 2009. DNA damage induces reactive oxygen species generation through the H2AX-Nox1/Rac1 pathway. *Cell Death Dis.* 3: e249.

Kasid U. et al. 2003. RAF antisense oligonucleotide as a tumor radiosensitizer. *Oncogene* 22: 5876-5884.

Kastan MB. et al. 2004. Cell-cycle checkpoints and cancer. *Nature* 432: 316-323.

Kelland LR. et al. 1999. DT-diaphorase expression and tumor cell sensitivity to 17-allylamino-17-demthoxygeldanamycin, an inhibitor of heat shock protein 90. *J. Natl. Cancer Inst.* 91: 1940-1949.

Kennedy SG. et al. 1999. Akt/protein kinase B inhibits cell death by preventing the release of cytochrome c from mitochondria. *Mol. Cell Biol.* 19: 5800-5810.

Khwaja A. et al. 1997. Matrix adhesion and Ras transformation activate a phosphoinositide 3-OH kinase and protein kinase B/Akt cellular survival pathway. *EMBO J.* 16: 2783-2793.

Koll TT. et al. 2008. Hsp90 inhibitor, DMAG, synergizes with radiation of lung cancer cells by interfering with base excision and ATM-mediated DNA repair. *Mol. Cancer Ther.* 7: 1985-1992.

Kroemer G. et al. 2005. Caspase-independent cell death. *Nat. Med.* 11: 725-730.

Kubbutat MH. et al. 1997. Regulation of p53 stability by MDM2. *Nature* 387: 299-303.

Kuger S. et al. 2012. Novel Hsp90 inhibitor NVP-AUY922 sensitizes human tumor xenografts to radiation. Poster presentation at 18th DEGRO, Wiesbaden, 2012.

Lang SA. et al. 2007. Inhibition of heat shock protein 90 impairs epidermal growth factor-mediated signaling in gastric cancer cells and reduces tumor growth and vascularization *in vivo. Mol. Cancer Ther.* 6: 1123-1132.

Lanneau D. et al. 2007. Apoptosis versus cell differentiation. Role of heat shock proteins Hsp90, Hsp70 and Hsp27. *Prion* 1: 53-60.

Leu JI. et al. 2009. A small molecule inhibitor of inducible heat shock protein 70. *Mol. Cell* 36: 15-27.

Li X. et al. 2008a. Homologous recombination in DNA repair and DNA damage tolerance. *Cell Res.* 18: 99-113.

Li HF. et al. 2009b. Radiation-induced Akt activation modulates radioresistance in human glioblastoma cells. *Radiat. Oncol.* 4: 43.

Li D. et al. 2011c. Functional inactivation of endogenous MDM2 and CHIP by Hsp90 causes aberrant stabilization of mutant p53 in human cancer cells. *Mol. Cancer Res.* 9: 577-588.

Li J. et al. 2011d. The Hsp90 chaperone machinery: conformational dynamics and regulation by co-chaperones. *Biochim. Biophys. Acta* 1823: 624-635.

Lundgren K. et al. 2009. BIIB021, an orally available, fully synthetic small molecule inhibitor of the heat shock protein Hsp90. *Mol. Cancer Ther.* 8: 921-929.

Luo J. et al. 2009. Principles of cancer therapy: oncogene and non-oncogene addiction. *Cell* 136: 823-837.

Ma et al. 2003. Combined-modality treatment of solid tumors using radiotherapy and molecular targeted agents. *J. Clin. Oncol.* 14: 2760-2776.

Machida H. et al. 2003. Geldanamycin, an inhibitor of Hsp90, sensitizes human tumor cells to radiation. *Int. J. Radiat. Biol.* 79: 973-980.

Machida H. et al. 2005. Heat shock protein 90 inhibitor 17-allylamino-17-demethoxygeldanamycin potentiates the radiation response of tumor cells grown as monolayer and spheroid by inducing apoptosis. *Cancer Sci.* 96: 911-917.

Mahalingam D. et al. 2009. Targeting Hsp90 for cancer therapy. *Br. J. Cancer* 100: 1523-1529.

Maser RS. et al. 1997. hMre11 and hRad50 nuclear foci are induced during the normal cellular response to DNA double-strand breaks. *Mol. Cell. Biol.* 17: 6087-6096.

Massey AJ. et al. 2010. A novel, small molecule inhibitor of Hsc70-/Hsp70 potentiates Hsp90 inhibitor induced apoptosis in HCT116 colon carcinoma cells. *Cancer Chemother. Pharmacol.* 66: 535-545.

Massey AJ. et al. 2010. Preclinical antitumor activity of the orally available heat shock protein 90 inhibitor NVP-BEP800. *Mol. Cancer Ther.* 9: 906-919.

Mayo LD. et al. 2001. A phosphatidylinositol 3-kinase/Akt pathway promotes translocation of Mdm2 from the cytoplasm to the nucleus. *Proc. Natl. Acad. Sci. USA* 98: 11598-11603.

Mihara M. et al. 2003. p53 has a direct apoptogenic role at mitochondria. *Mol. Cell* 11: 577-590.

Miller K. et al. 2007. Phase I trial of alvespimycin (KOS-1022; 17-DMAG) and trastuzumab (T). *J. Clin. Oncol.* 25: 1115.

Moulick K. et al. 2011. Affinity-based proteomics reveal cancer-specific networks coordinated by Hsp90. *Nat. Chem. Biol.* 7: 818-826.

Muslimovic A. et al. 2008. An optimized method for measurement of gamma-H2AX on blood mononuclear and cultured cells. *Nat. Protoc.* 3: 1187-1193.

Neckers L. 2007. Heat shock protein 90: the cancer chaperone. *J. Biosci.* 32: 517-530.

Niewidok N. et al. 2012. Hsp90 inhibitors NVP-AUY922 and NVP-BEP800 may exert a significant radiosensitization on tumor cells along with a cell type-specific cytotoxicity. *Transl. Oncol.* 5:356-369.

Noguchi M. et al. 2006. Inhibition of homologous recombination repair in irradiated tumor cells pretreated with Hsp90 inhibitor 17-allylamino-17-demethoxygeldanamycin. *Biochem. Biophys. Res. Commun.* 351: 658-663.

Nylandsted J. et al. 2006. Heat shock protein 70 is required for the survival of cancer cells. *Ann. N. Y. Acad. Sci.* 122-125.

Palmero I. et al. 1998. p19[ARF] links the tumor suppressor p53 to Ras. *Nature* 395: 125-126.

Pandey P. et al. 2000. Negative regulation of cytochrome c-mediated oligomerization of Apaf1 and activation of procaspase-9 by heat shock protein 90. *EMBO J.* 19: 4310-4322.

Pardo B. et al. 2009. DNA double-strand break repair: how to fix a broken relationship. *Cell. Mol. Life Sci.* 66: 1039-1056.

Park HS. et al. 2001. Hsp72 functions as a natural inhibitory protein of c-Jun N-terminal kinase. *EMBO J.* 20: 446-456.

Patel HJ. et al. 2012. Advances in the discovery and development of heat-shock protein 90 inhibitors for cancer treatment. *Expert Opin. Drug Discov.* 5: 559-587.

Pearl LH. et al. 2006. Structure and mechanism of the Hsp90 molecular chaperone machinery. *Annu. Rev. Biochem.* 75: 271-294.

Picard D. et al. 2002. Heat-shock protein 90, a chaperone for folding and regulation. *Cell. Mol. Life Sci.* 59: 1640-1648.

Pines J. et al. 1991. Human cyclins A and B1 are differentially located in the cell and undergo cell cycle-dependent nuclear transport. *J. Cell Biol.* 115: 1-17.

Piper PW. et al. 2011. Mechanisms of resistance to Hsp90 inhibitor drugs: a complex mosaic emerges. *Pharmaceuticals* 4: 1400-1422.

Polager S et al. 2009. p53 and E2F: partners in life and death. *Nat. Rev. Cancer* 9: 738-748.

Porter AG. et al. 1999. Emerging roles of caspase-3 in apoptosis. *Cell Death Differ.* 6: 99-104.

Porter JR. et al. 2010. Discovery and development of Hsp90 inhibitors: a promising pathway for cancer therapy. *Curr. Opin. Chem. Biol.* 14: 412-420.

Portugal J. et al. 2010. Mechanisms of drug-induced mitotic catastrophe in cancer cells. *Curr. Pharm. Des.* 16: 69-78.

Powers MV. et al. 2007a. Dual targeting of Hsc70 and Hsp72 inhibits Hsp90 function and induces tumor-specific apoptosis. *Cancer Cell* 14: 250-262.

Powers MV. et al. 2007b. Inhibitors of the heat shock response: biology and pharmacology. *FEBS Lett.* 581: 3758-3769.

Price JT. et al. 2005. The heat shock protein inhibitor, 17-allylamino-17-demethoxygeldanamycin, enhances osteoclast formation and potentiates bone metastasis of a human breast cancer cell line. *Cancer Res.* 65: 4929-4938.

Ramaswamy S. et al. 1999. Regulation of G1 progression by the PTEN tumor suppressor protein is linked to inhibition of phosphatidylinositol 3-kinase/Akt pathway. *Proc. Natl. Acad. Sci.* 96: 2110-2115.

Reinhardt HC. et al. 2011. The p53 network: cellular and systemic DNA damage response in aging and cancer. *Trends Genet.* 28: 128-136.

Rerole AL. et al. 2011. Peptides and aptamers targeting Hsp70: a novel approach for anticancer chemotherapy. *Cancer Res.* 71: 484-495.

Resnier P. et al. 2013. A review of the current status of siRNA nanomedicines in the treatment of cancer. *Biomaterials* 34: 6429-6443.

Riedl SJ. et al. 2004. Molecular mechanisms of caspase regulation during apoptosis. *Nat. Rev. Mol. Cell Biol.* 5: 897-907.

Riedl SJ. et al. 2007. The apoptosome: signaling platform of cell death. *Nat. Rev. Mol. Cell Biol.* 8: 405-413.

Rohde M. et al. 2005. Members of the heat shock protein 70 family promote cancer cell growth by distinct mechanisms. *Genes Dev.* 19: 570-582.

Rogakou EP et al. 1998. DNA double-stranded breaks induce histone H2AX phosphorylation on serine 139. *J. Biol. Chem.* 273: 5858–5868.

Russell JS. et al. 2003. Enhanced cell killing induced by the combination of radiation and the heat shock protein 90 inhibitor 17-allylamino-17-demethoxygeldanamycin: a multitarget approach to radiosensitization. *Clin. Cancer Res.* 9: 3749-3755.

Schilling D. et al. 2011. Radiosensitization of normoxic and hypoxic H1339 lung tumor cells by heat shock protein 90 inhibition is independent of hypoxia inducible factor-1α. *PloS ONE* 7: 1-11.

Seiwert TY. et al. 2007. The concurrent chemoradiation paradigm – general principles. *Nat. Clin. Pract. Oncol.* 4: 86-100.

Seth S. et al. 2012. Delivery and biodistribution of siRNA for cancer therapy: challenges and future prospects. *Ther. Deliv.* 2: 245-261.

Shapiro GI. et al. 2000. The physiology of p16 (INK4A)-mediated G1 proliferative arrest. *Cell Biochem. Biophys.* 33: 189-197.

Sherman M. 2010. Major heat shock protein Hsp72 controls oncogene-induced senescence. *Ann. N. Y. Acad. Sci.* 1197: 152-157.

Sherr CJ. et al. 1999. Cdk inhibitors: positive and negative regulators of G1-phase progression. *Genes Dev.* 13: 1501-1512.

Shintani S. et al. 2006. p53-dependent radiosensitizing effects of Hsp90 inhibitor 17-allylamino-17-demethoxygeldanamycin on human oral squamous cell carcinoma cell lines. *Int. J. Oncol.* 29: 1111-1117.

Smith V. et al. 2005. Comparison of 17-dimethylaminoethylamino-17demethoxygeldanamycin (17-DMAG) and 17-allylamino-17-demethoxygeldanamycin (17-AAG) *in vitro*: effects on Hsp90 and client protein in melanoma models. *Cancer Chemother. Pharmacol.* 56: 126-137.

Solimini NL. et al. 2007 Non-oncogene addiction and the stress phenotype of cancer cells. *Cell* 130: 986-987.

Solit DB. et al. 2007. Phase I trial of 17-allylamino-17-demethoxygeldanamycin in patients with advanced cancer. *Clin. Cancer Res.* 13: 1775-1782.

Sos ML. et al. 2009. Predicting drug susceptibility of non-small cell lung cancers based on genetic lesions. *J. Clin. Invest.* 119: 1727-1740.

Sreedhar AS. et al. 2004. Hsp90 isoforms: functions, expression and clinical importance. *FEBS Lett.* 56: 11-15.

Stangl S. et al. 2011. Targeting membrane heat shock protein 70 (Hsp70) on tumors by cmHsp70.1 antibody. *Proc. Natl. Acad. Sci. U S A* 108: 733-738.

Stankiewicz AR. et al. 2005. Hsp70 inhibits heat-induced apoptosis upstream of mitochondria by preventing Bax translocation. *J. Biol. Chem.* 280: 38729-38739.

Stebbins CE. et al. 1997. Crystal structure of an Hsp90-geldanamycin complex: targeting of a protein chaperone by an antitumor agent. *Cell* 89: 239-250.

Stewart ZA. et al. 2001. p53 signaling and cell cycle checkpoints. *Chem. Res. Toxicol.* 14: 243-263.

Stingl L. et al. 2010. Novel HSP90 inhibitors, NVP-AUY922 and NVP-BEP800, radiosensitize tumour cells through cell-cycle impairment, increased DNA damage and repair protraction. *Br. J. Cancer* 102: 1578-1591.

Stingl L. et al. 2011. Effect of heat shock protein inhibitor KNK437 on the radiotoxicity of tumor cells. *Strahlenther. Onkol.* 187: 121-127 (poster presentation at 17th DEGRO, Wiesbaden, 2011).

Stühmer T. et al. 2008. Signalling profile and antitumour activity of the novel Hsp90 inhibitor NVP-AUY922 in multiple myeloma. *Leukemia* 22: 1604-1612.

Stühmer T. et al. 2009. Anti-myeloma activity of the novel 2-aminothienopyrimidine Hsp90 inhibitor NVP-BEP800. *Br. J. Haematol.* 147: 319-327.

Supko JG. et al. Preclinical pharmacologic evaluation of geldanamycin as an antitumor agent. *Cancer Chemother. Pharmacol.* 1995; 36: 305-315.

Taipale M. et al. 2010. Hsp90 at the hub of protein homeostasis: emerging mechanistic insights. *Nat. Mol. Cell Biol.* 11: 515-528.

Taylor AM. et al. 1975. Ataxia telangiectasia: a human mutation with abnormal radiation sensitivity. *Nature* 258: 427-429.

Taylor WR. et al. 2001. Regulation of the G2/M transition by p53. *Oncogene* 20: 1803-1815.

Toulany M. et al. 2008. Targeting of Akt1 enhances radiation toxicity of human tumor cells by inhibiting DNA-PKcs-dependent DNA double strand repair. *Mol. Cancer Ther.* 7: 1772-1781.

Travers J. et al. 2012. Hsp90 inhibition: two-pronged exploitation of cancer dependencies. *Drug Discov. Today* 17: 242-253.

Trepel J. et al. 2010. Targeting the dynamic Hsp90 complex in cancer. *Nat. Rev. Cancer* 10: 537-549.

Tsutsumi S. et al. 2007. Extracellular heat shock protein 90: a role for a molecular chaperone in cell motility and cancer metastasis. *Cancer Sci.* 98: 1536-1539.

Ward JF. et al. 1975. Radiation-induced strand breakage in DNA. *Basic Life Sci.* 371-472.

Ward JF. et al. 1981. Some biochemical consequences of the spatial distribution of ionizing radiation-produced free radicals. *Radiat. Res.* 86: 185-195.

Weinberg RA. 1995. The retinoblastoma protein and cell cycle control. *Cell* 81: 323-330.

Whitesell L. et al. 2005. Hsp90 and the chaperoning of cancer. *Nat. Rev. Cancer* 5: 761-772.

Wu YC. et al. 2009. Heat shock protein inhibitors, 17-DMAG and KNK437, enhance arsenic trioxide-induced mitotic apoptosis. *Toxicol. Appl. Pharmacol.* 236: 231-238.

Wyman C. et al. 2006. DNA double-strand break repair: all's well that ends well. *Annu. Rev. Genet.* 40: 363-383.

Vakifahmetoglu H. et al. 2008. Death through a tragedy: mitotic catastrophe. *Cell Death Differ.* 15: 1153-1162.

Van Attikum H. et al. 2005. The histone code at DNA breaks: a guide to repair? *Nat. Rev. Mol. Cell Biol.* 6: 757-766.

Van der Schans GP. et al. 1973. Contribution of various types of damage to inactivation of a biologically-active double-stranded circular DNA by gamma-radiation. *Int. J. Radiat. Biol. Relat. Stud. Phys. Chem. Med.* 23: 133-150.

Vermeulen K. et al. 2003. The cell cycle: a review of regulation, deregulation and therapeutic targets in cancer. *Cell Prolif.* 36: 131-149.

Vitiello PF. et al. 2009. p21[Cip1] protects against oxidative stress by suppressing ER-dependent activation of mitochondrial death pathways. *Free Radic. Biol. Med.* 46: 33–41.

Von Sonntag C. et al. 1987. New aspects in the free-radical chemistry of pyrimidine nucleobases. *Free Radic. Res. Commun.* 2: 217-224.

Xu B. et al. 2002. Two molecularly distinct G2/M checkpoints are induced by ionizing irradiation. *Mol. Cell. Biol.* 22: 1049-1059.

Yokota S. et al. 2000. Benzylidene lactam compound, KNK437, a novel inhibitor of acquisition of thermotolerance and heat shock protein induction in human colon carcinoma cells. *Cancer Res.* 60: 2942-2948.

Zhang H. et al. 2004. Targeting multiple signal transduction pathways through inhibition of Hsp90. *J. Mol. Med.* 82: 488-499.

Zhang H. et al. 2010. BIIB021, a synthetic Hsp90 inhibitor, has broad application against tumors with acquired multidrug resistance. *Int. J. Cancer* 126: 1226-1234.

Zhou H. et al. 2000. Akt regulates cell survival and apoptosis at a post-mitochondrial level. *J. Cell Biol.*151: 483-494.

9. Acknowledgements

At this point, I would like to take the opportunity to express my deep gratitude to everyone who has helped me during this doctoral project.

Foremost, I would like to thank Professor Dr. Michael Flentje for giving me the opportunity to complete this thesis at Department of Radiation Oncology. I am also very grateful for kindly finding the time and accepting to act as "Doktorvater". Many thanks for enabling me to gain deeper insight in the interesting field of radiation biology and for supporting my participation in international conferences.

My special gratitude is directed to my supervisor PD Dr. Cholpon S. Djuzenova for attracting me to Würzburg and giving me the opportunity to carry out this work in her group. I am very grateful for the outstanding support, the useful comments, remarks and the engagement throughout all phases of the doctoral studies. Thank you very much for patient reading and correcting my writing.

Furthermore, I would like to thank PD Dr. Vladimir Soukhoroukov for kindly accepting to act as the second reviewer of this work and for the helping to prepare the publications.

Many thanks to Dr. Charles Gould for proofreading of this thesis, and to Philip Hartmann for mediating it. Thank you to Melissa Sadler for controlling every comma and every article of this text. I am also very grateful to Dr. Gisela Wohlleben for the revision of the German part of this manuscript. I would like to acknowledge Dr. Lavinia Stingl, Astrid Katzer and Ines Elsner for support in the lab and friendly cooperation. I want to thank my lab and office mates – Susanne, Eike and Gisela - for professional help, but also for everyday smile and small talks about everything and for cheering me up, particularly during the last phase of writing.

I would like to thank the technical assistants and nurses of the Department of Radiation Oncology working at linear accelerators for allowing us to irradiate the cells between patients.

Susanne, Eike, Sebastian, Gisela, Astrid, Konstanze, Linda, Sarah S, Marlene, Madlen, Ines, Nadine and other past and present members of Labor Strahlentherapie – thank you for introducing me to Würzburg and accepting me as a friend.

Last, but not least, I would like to thank my parents for their continuous love, encouragement and trust. I could never have done this without you. All friends and relatives that kept their fingers crossed for me – thank you very much.

10. Curriculum vitae

Natalia Niewidok

Date and place of birth: 11.09.1985, Warsaw, Poland

Email address: natalia.niewidok@gmail.com

Home address: ul. Storczykowa 16, 64-730 Wielen, Poland

EDUCATION and RESEARCH EXPERIENCE

01.11.2009 01.07.2013	–	Ph. D. thesis at the Department of Radiation Oncology, University Hospital Würzburg, Germany
2007 – 2009		M. Sc. studies biotechnology; Adam Mickiewicz University, Poznań, Poland
July 2008 September 2008	–	Summer Research Project funded by Society for AIDS Research, Institute of Molecular Biology and Preparative Microbiology, Georg-August University, Göttingen, Germany
September 2007 March 2008	–	Longlife Learning Program Erasmus, Institute of Molecular Biology and Preparative Microbiology, Georg-August University, Göttingen, Germany
2004 – 2007		B. Sc. studies biotechnology; Adam Mickiewicz University, Poznań, Poland

PUBLICATIONS

1. <u>Niewidok N</u>, Wack LJ, Schiessl S, Stingl L, Katzer A, Polat B, Sukhorukov VL, Flentje M, Djuzenova CS. Hsp90 inhibitors NVP-AUY922 and NVP-BEP800 may exert a significant radiosensitization on tumor cells along with a cell type-specific cytotoxicity. *Transl. Oncol.* 2012, 5: 356-369.

2. Stingl L, <u>Niewidok N</u>, Müller N, Selle M, Djuzenova CS, Flentje M. Radiosensitizing effect of the novel Hsp90 inhibitor NVP-AUY922 in human tumor cell lines silenced for Hsp90α. *Strahlenther Onkol.* 2012, 188: 507-515.

3. Djuzenova CS, Blassl C, Roloff K, Kuger S, Katzer A, <u>Niewidok N</u>, Günther N, Polat B, Sukhorukov VL, Flentje M. Hsp90 inhibitor NVP-AUY922 enhances radiation sensitivity of tumor cell lines under hypoxia. *Cancer Biol. Ther.* 2012, 13: 425-434.

4. <u>Niewidok N</u>, Staus M, Katzer A, Djuzenova CS, Flentje M. Hsp90 inhibitors NVP-AUY922 and NVP-BEP800 moderately radiosensitize normal human skin fibroblasts [manuscript in preparation].

5. <u>Niewidok N,</u> Schiessl S, Katzer A, Flentje M, Djuzenova CS. Radiosensitizing effect of Hsp90 inhibitor NVP-AUY922 in tumor cell lines pre-silenced for Hsp70 [manuscript in preparation].

PRESENTATIONS and POSTERS

Oral presentation:

1. Niewidok N. et al. NVP-AUY922 and NVP-BEP800 selectively radiosensitize tumor cell lines but not normal skin fibroblasts. 39th Annual Meeting of the European Radiation Research Society, 15-19.10.2012 Vietri sul Mare (Italy) <u>[travel award from ERRS]</u>

Posters:

1. Niewidok N. et al. Hsp90 inhibitors NVP-AUY922 and NVP-BEP800 affect the radiation response of human tumor cell line SNB19, but not of normal fibroblast lines. 6th International Conference on the Hsp90 Chaperone Machine, 19-23.09.2012 Les Diablerets (Switzerland) <u>[travel award from organizers]</u>

2. Niewidok N. et al. Silencing of Hsp70 and Hsc70 with siRNA inhibits tumor cell growth and moderately increases the sensitivity of lung carcinoma A549 and glioblastoma SNB19 cell lines to ionizing radiation.18th DEGRO (German Society for Radiation Oncology), 7-10.06.2012 Wiesbaden (Germany)

3. Niewidok N. et al. Sequence of drug-radiation treatment influences the tumor radiosensitizing properties of the novel Hsp90 inhibitors NVP-AUY922 and NVP-BEP800. 14th International Congress of Radiation Research, 28.08-1.09.2011, Warsaw (Poland) <u>[travel award from IARR]</u>

4. Niewidok N. et al. Partial depletion of Hsp70 and Hsc70 moderately enhances the radiation response of tumor cell lines through impaired DNA repair, cell cycle distortion and apoptosis. 5th International Congress on Stress Responses in Biology and Medicine, 21-25.08.2011 Quebec City (Canada)

5. Niewidok N. et al. Simultaneous radiation and Hsp90 inhibition by NVP-AUY922 or NVP-BEP800 is more efficient in tumor cell killing than drug-first modality followed by irradiation. 17th DEGRO (German Society for Radiation Oncology), 2-5.06.2011 Wiesbaden (Germany)

11.   Affidavit

Affidavit

I hereby declare that my thesis entitled: "Modulation of radiosensitivity of human tumor and normal cells by inhibition of heat shock proteins Hsp90 and Hsp70." is the result of my own work. I did not receive any help or support from commercial consultants. All sources and/or materials applied are listed and specified in the thesis. Furthermore, I verify that this thesis has not yet been submitted as part of another examination process neither in identical nor in similar form.

Würzburg……………………………………………………………………………………
                      Date   Signature

Eidesstattliche Erklärung

Hiermit erkläre ich an Eides statt, die Dissertation "Modulation der Strahlenempfindlichkeit humaner maligner und nicht-maligner Zellen mittels Inhibition der Hitzeschockproteine Hsp90 und Hsp70." eigenständig, d.h. insbesondere selbstständig und ohne Hilfe eines kommerziellen Promotionsberaters, angefertigt und keine anderen als die von mir angegebenen Quellen und Hilfsmittel verwendet zu haben.

Ich erkläre außerdem, dass die Dissertation weder in gleicher noch in ähnlicher Form bereits in einem anderen Prüfungsverfahren vorgelegen hat.

Würzburg……………………………………………………………………………………
                      Datum   Unterschrift